

SLS Reliability Considering Autogenous Self-Sealing in Tension Governed Reinforced Concrete Water Retaining Structures

by

Andrew Christopher Way



Dissertation presented for the degree of

Doctor of Philosophy

in the Faculty of Civil Engineering at Stellenbosch University

Supervisor: Prof. C. Viljoen

March 2021

Declaration

By submitting this dissertation electronically, I declare that the entirety of the work contained therein is my own, original work, that I am the sole author thereof (save to the extent explicitly otherwise stated), that reproduction and publication thereof by Stellenbosch University will not infringe any third party rights and that I have not previously in its entirety or in part submitted it for obtaining any qualification.

Date:

Abstract

This research considers the achieved serviceability limit state (SLS) reliability in tension-governed, reinforced concrete water retaining structures (RC WRS). Currently, the level of achieved SLS reliability in WRS is unknown. Structural codes used to design WRS, such as EN 1992-3 and the *fib* Model Code 2010 (MC 2010), typically specify a 50-year irreversible SLS target reliability index of $\beta = 1.5$. Whether or not this level of reliability is actually achieved, however, has not been determined to date. Due to this, the ability to optimally design these structures to realize cost and material savings is stifled.

The design of RC WRS is governed by the limitation of leakage of the stored liquid to acceptable levels. The limitation of crack widths is used as a critical design parameter in structural codes. All structural codes used to design RC WRS qualitatively mention the beneficial effect that autogenous self-sealing has on the reduction of crack widths and leakage over time in the concrete, however, few attach any quantitative measure to this effect or link it to the specification of target crack widths. This dissertation thus aims to quantify the achieved level of SLS reliability in RC WRS by: 1. Probabilistically characterizing the beneficial effect of autogenous self-sealing on the leakage through a single crack in a RC WRS, 2. Developing a probabilistic analysis that determines the achieved level of SLS reliability in an entire RC WRS considering the effect of self-sealing, 3. Comparing the results to the target reliability in structural design codes, and 4. Making recommendations based on the results and identified trends.

Two experimental databases were compiled to achieve the first aim. The first is for the probabilistic characterization of the initial flow through a tension crack in concrete. For this purpose, a novel initial flow prediction model factor was characterized by a Weibull distribution. The second database is used to probabilistically quantify the effect that self-sealing has on the reduction of leakage flow over time, considering crack width and the ratio of water pressure head to wall thickness, (h_D/h in EN 1992-3). A novel leakage accumulation factor is defined and characterized by a Weibull distribution for this purpose.

A Monte Carlo reliability analysis was used to determine the achieved level of leakage related SLS reliability in a tension governed RC WRS, incorporating the effect of autogenous self-sealing. The analysis uses the MC 2010 crack prediction model for the stabilized cracking phase. The theory of leakage through a single crack in concrete was used to consider the leakage through all cracks in a RC WRS. A SLS reliability limit state was established as the difference between the allowable, and the predicted leakage. A sensitivity analysis was performed on the model using FORM, in order to determine upper and lower reliability limits and to identify which parameters contributed the most uncertainty to the limit state. The limit state was evaluated for 235 combinations of round RC WRS geometries and characteristics, for four leakage regimes, which correspond to commonly used stabilization periods and test times used in the water tightness test of WRS.

Target crack widths were shown to be dependent on the water pressure head to wall thickness ratio, in agreement with EN 1992-3. The target crack widths given by EN 1992-3 were found to be too conservative for three out of the four leakage regimes for an SLS reliability level of $\beta = 1.5$. The MC 2010 recommendation of a target crack width of 0.2 mm resulted in consistently inadequate values of $\beta < 1.5$, and notably so for higher water pressure head to wall thickness ratios. A trend of target crack width vs the ratio of the maximum applied tension to the mean tensile resistance of the wall was identified as a means by which target crack widths may be specified. Recommendations are made for target crack width vs water pressure head to wall thickness ratio, as well as for target crack width vs the ratio of the maximum applied tension to the mean tensile resistance of the wall, to achieve an SLS reliability of $\beta = 1.5$ for the stabilized cracking phase. The novel leakage reliability analysis from this research determines the level of SLS reliability in RC WRS and makes the design- and cost-optimization of tension-governed, RC WRS possible.

Samevatting

Die betroubaarheid van die diensbaarheid limietstaat (DLS) in trekspanning-beheerde, gewapende beton waterhoudende strukture (GB WHS) word ondersoek. Strukturele kodes wat gebruik word om WHS te ontwerp, soos EN 1992-3 en die *fib* Model Code 2010 (MC 2010), spesifiseer gewoonlik 'n 50-jaar onomkeerbare DLS teiken betroubaarheidsindeks van $\beta = 1.5$. Die werklike vlak van betroubaarheid wat bereik word is onbekend, en moeilik om te bepaal. Koste- en materiaalbesparings kan bewerkstellig word deur die optimale betroubaarheidsgebaseerde ontwerp van hierdie strukture.

Die ontwerp van GB WHS is onderworpe aan beperkings met betrekking tot aanvaarbare vlakke van lekkasie van die gestoorde vloeistof. Die beperking van kraakwydtes word as 'n kritieke ontwerp parameter in strukturele kodes gebruik. Alle strukturele kodes wat gebruik word om GB WHS te ontwerp noem die voordelige effek wat outogene self-verseëling op die vermindering van kraakwydtes en lekkasie oor tyd in die beton het, maar min heg egter 'n kwantitatiewe maatstaf hieraan of koppel dit aan die spesifikasie van kraakwydtes. Die doel van hierdie navorsing is dus om die bereikte vlak van DLS-betroubaarheid in GB WHS te kwantifiseer deur: 1. Die waarskynlikheidskarakterisering van die voordelige effek van outogene self-verseëling op die lekkasie deur 'n enkele kraak in 'n GB WHS, 2. 'n waarskynlikheidsanalise te gebruik om die bereikte vlak van DLS betroubaarheid in GB WHS te bepaal, die effek van self-verseëling in ag genome, 3. Om die resultate met die teikenbetroubaarheid in strukturele ontwerpkode te vergelyk, en 4. Om aanbevelings te maak, gebaseer op die resultate en geïdentifiseerde tendense.

Twee eksperimentele databasisse is saamgestel ten einde die eerste doel te bereik. Die eerste databasis is gebruik vir die waarskynlikheidskarakterisering van die aanvanklike vloei deur 'n trekspanningskraak in beton. Hier is gevind dat Weibull verdelings aanvanklike vloei-voorspellingsmodelfaktore karakteriseer. Die tweede databasis is gebruik om 'n waarskynlikheids kwantifisering te maak van die effek wat self-verseëling op die vermindering van lekvloei oor tyd het, met die kraakwydte en die verhouding van waterdrukhoogte tot wanddikte, (h_D/h in EN 1992-3) in ag genome. Vir hierdie doel is 'n lekkasie-oophopingsfaktor gekarakteriseer, wat ook goed beskryf is deur Weibull-verdelings.

'n Monte Carlo-analise is gebruik om die bereikte vlak van lekkasie-verwante DLS-betroubaarheid in 'n trekspanning-beheerde GB WHS te bepaal, wat die effek van outogene self-verseëling insluit. Die analise maak gebruik van die MC 2010-voorspellingsmodel vir krake in die gestabiliseerde kraakfase. Die teorie van lekkasie deur 'n enkele kraak in beton is gebruik vir die beskouing van lekkasie deur alle krake in 'n GB WHS. 'n DLS-betroubaarheid limietstaat is vasgestel as die verskil tussen die toelaatbare en die voorspelde lekkasie. 'n Sensitiwiteitsanalise is op die model uitgevoer met behulp van FORM om die boonste en onderste betroubaarheidsgrense te bepaal en om te identifiseer watter parameters die grootste onsekerheid tot die limietstaat bydra. Die limietstaat is vir 235 kombinasies van ronde GB WHS-geometrieë en eienskappe, met betrekking tot vier lekkasie-regimes geeëvalueer. Die lekkasie-regimes stem ooreen met die algemeen gebruikte stabiliseringstydperke en toetstye wat gebruik word in die waterdigtheidstoets van WHS.

Daar is bevind dat die teikenkraakwydte afhanklik is van die verhouding van die waterdrukhoogte tot die wanddikte, in ooreenstemming met EN 1992-3. Daar is gevind dat die teikenkraakwydte van EN 1992-3 te konserwatief is vir drie uit die vier lekkasie-regimes vir 'n DLS-betroubaarheidsvlak van $\beta = 1.5$. Die MC 2010 teikenkraakwydte van 0.2 mm is onvoldoende om $\beta > 1.5$ te haal, veral vir hoër verhoudings van waterdrukhoogte tot wanddikte. 'n Tendens van teikenkraakwydte teenoor die verhouding van die maksimum toegepaste trekspanning tot die gemiddelde trekweerstand van die muur, is identifiseer as 'n alternatiewe basis vir die spesifisering van teikenkraakwydtes. Aanbevelings word gemaak vir die teikenkraakwydte teen die verhouding van waterdrukhoogte tot wanddikte, sowel

as vir die kraakwydte teenoor die verhouding van die maksimum toegepaste spanning tot die gemiddelde trekweerstand van die muur om 'n DLS-betroubaarheid van $\beta = 1.5$ te bereik vir die gestabiliseerde kraakfase. Die bepaling van die DLS-betroubaarheid in GB WHS uit hierdie navorsing maak verbeterde ontwerp en koste-optimalisering van trekspanning-beheerde GB WHS moontlik.

Acknowledgements

A number of thank-you's are appropriate to those without whom, this research would not likely have even started, let alone come to fruition.

To the Harry Crossley Foundation for its support of this research through an incredible 2-year bursary for PhD studies - thank you so much. Also to the Water Research Commission of South Africa for research grant number K5/2514/1 which also supported this research.

To Prof Celeste Viljoen: Thank you for your guidance and support over the past 3 years. Thank you for encouraging me and shaping this research. Thank you especially that even through this chaotic year, you still found time for meetings, feedback and a sense of humour. I was particularly amused (in hindsight) by some of your review comments, like:

"Sometimes you use way too many words..."

"Check your use of commas. You tend to use too many, inappropriately."

"Find and remove all places in your thesis where you bore the reader with...."

Thanks too, goes to Prof Richard Walls. Thank you for your friendship, mentorship and guidance, whether academic or biblical. Thank you for modelling what a professional, yet caring lecturer should look like.

Thanks to my friends who have kept me sane over the past 3 years. From those at dancing, to those in the office, to those at Church, you've all played a role in my growth and sanity, and I appreciate all of you.

Heartfelt thanks also go to my wonderful parents. I've had the privilege of spending much more time with you two than I would have done through this crazy year and it's been such a blessing. Thank you so much for believing in me, supporting me and loving me, despite hearing about water retaining structures ad-infinitum. Thank you for all that you've done and sacrificed for me; I love you lots.

To my beloved Caitlin. Thank you for the incredible person that you are and all that you mean to me. A year ago, I could never have foreseen what this year would contain and despite all the woe that Covid-19 has brought about, so much good has come from it. I thank God for you every day and pray that He would continue to guide us and use our relationship for His glory, as we do life together. I love you painfully.

Finally, one does not find hope and meaning in degrees, nor achievements, nor career, nor relationships or wealth. *For dust we are, and to dust we shall return.* No, our hope lies in the sacrifice of Christ Jesus, who loved us so much, in that *while we were still sinners Christ died for us.* Do you seek hope and meaning? Have you pursued everything under the sun, from wealth, to wisdom, to pleasure, only to realise that this is: *"Meaningless! Meaningless!" says the Teacher. "Everything is meaningless!"* The answer lies not within yourself, but in the cross of Christ. *Therefore, there is now no condemnation for those who are in Christ Jesus, because through Him, the law of the Spirit who gives life has set you free from the law of sin and death.* Therefore: *seek first His kingdom and His righteousness,* and He will give you hope and meaning.

Now unto Him who is able to do immeasurably more than all we ask or imagine, according to His power that is at work within us, to Him be glory in the church and in Christ Jesus throughout all generations, for ever and ever! Amen.

Contents

Declaration	i
Contents	v
List of Figures	viii
List of Tables	x
List of Acronyms and Symbols	xiii
1 Introduction	1
1.1 Background and motivation	1
1.2 Objectives	2
1.3 Layout of dissertation	3
2 Risk and Reliability Literature Review	4
2.1 Background	4
2.2 Fundamental concepts	5
2.3 Uncertainties in structural engineering	5
2.4 Uncertainties in loading and material resistance	6
2.5 Target reliability	8
2.6 Cost of safety and economic optimization	11
2.7 Reliability analysis methods	13
2.8 Statistical distributions	16
3 Water Retaining Structures Literature Review	19
3.1 Geometry and loading of WRS	19
3.2 Cracking in concrete structures	21
3.3 Crack width calculation models	22
3.4 Comparison of prevalent load-induced crack models	25
3.5 Leakage-related considerations in water retaining structures	30
3.6 Recovery of properties in cracked concrete	33
3.7 Chapter summary	43
4 Experimental Database	45
4.1 Cracking method	45
4.2 Test method	46
4.3 Concrete mix and constituents	47
4.4 Exposure conditions	51
4.5 Uncertainties and bias	51
4.6 Applicability to practical water retaining structures	52
4.7 Database sources	53
4.8 Chapter summary	56

CONTENTS

5	Probabilistic Models	57
5.1	Initial flow prediction model	57
5.2	Leakage prediction model	65
5.3	Total leakage prediction model	78
5.4	Chapter summary	79
6	Prediction of Leakage in a Reservoir	80
6.1	Introduction	80
6.2	Reservoir loading	81
6.3	Load-induced cracking in reservoirs	83
6.4	Stages of cracking in reservoirs	92
6.5	Reliability limit state	94
6.6	Sensitivity analysis	96
6.7	Chapter summary	102
7	Single Reservoir Leakage Simulation	103
7.1	Applicability and assumptions	103
7.2	Analysis using Monte Carlo simulation	104
7.3	Reservoir geometry	104
7.4	Crack arrangement	105
7.5	Reliability limit state	106
7.6	Simulation progression	109
7.7	Results and discussion	113
7.8	Chapter summary	123
8	Multiple Reservoir Leakage Simulation	124
8.1	Simulated reservoir geometry considerations	124
8.2	Simulation progression	125
8.3	Results	125
8.4	Discussion	135
8.5	Chapter summary	146
9	Final Summary and Conclusions	147
9.1	Summary of reviewed literature	147
9.2	Model databases and probabilistic modelling	148
9.3	SLS reliability analyses for leakage in reservoirs	149
9.4	Limitations of the research	152
9.5	Recommendations for future research	152
	Bibliography	154
	Appendices	162
A	Appendix A	163
A.1	Probabilistic distributions	163
B	Appendix B	168
B.1	Hoop tension coefficients	168
C	Appendix C	173
C.1	Table of reinforcing areas	173
D	Appendix D	174
D.1	Values of h^*	174
E	Appendix E	175

CONTENTS

E.1	Recommendations of target crack width	175
F	Appendix F	178
F.1	Initial flow prediction database	178
F.2	Flow reduction database	183
G	Appendix G	194
G.1	Sample of reservoir analyses outputs	194

List of Figures

2.1	Characteristic and design values for variable actions and material strength.	7
2.2	Visualization of FORM and design point in the standardized normal space, adapted [reprinted] from Holický (2009).	15
2.3	Illustration of normal distribution with varying standard deviations.	17
2.4	Illustration of lognormal distribution with varying shape and scale parameters.	18
2.5	Illustration of Weibull distribution with varying shape and scale parameters.	18
3.1	Hydrostatic water load acting on a WRS wall section.	19
3.2	Typical shapes of reinforced concrete water retaining structures.	20
3.3	Illustration of circumferential hoop tension forces in circular WRS from hydrostatic load. Plan view (left) and isometric (right).	20
3.4	Illustration of flexure inducing forces in rectangular WRS from hydrostatic load. Plan view (left) and isometric (right).	21
3.5	Illustration of mechanics involved in the calculation of maximum crack width.	23
3.6	Plan-view illustration of concrete cracking and layout of reinforcing.	24
3.7	Difference in strain distribution assumptions.	26
3.8	Idealized cracking stages, assumed by MC 2010 and EN 1992-1-1.	28
3.9	Illustration of definitions surrounding the recovery of properties in concrete.	34
3.10	Flow rate reduction for dormant and active cracks, reprinted and translated from Edvardsen (1996).	36
3.11	Relationship between water flow and crack width for various water pressure heads, reprinted and translated from Edvardsen (1996).	37
3.12	Initial flow rates as a function of crack width, water acidity and water pressure head (translated) from Ramm and Biscopig (1997), where mW_s is the water pressure head.	38
3.13	Final flow rates as a function of crack width, water acidity and water pressure head (translated) from Ramm and Biscopig (1997).	39
3.14	Recovery of flexural strength of fibre-containing concrete due to self-healing, [reprinted] from Choi <i>et al.</i> (2017)	43
4.1	Typical methods used to form tensile cracks in samples.	46
4.2	Illustration of typical experimental test set up and sample geometry.	47
4.3	Relative shrinkage for a range of aggregate types, [reprinted] from Alexander (2014).	49
4.4	Variation in crack widths in tensile split mortar (top) and concrete (bottom) specimen, from Jin <i>et al.</i> (2017).	52
4.5	Sealing time for dynamic cracks vs. static cracks, [reprinted and translated] from Edvardsen (1996).	53
4.6	Distribution of crack widths in experimental data database ($0 < w \leq 0.4mm$).	55
4.7	Histogram of crack widths in the water flow reduction over time database.	56
5.1	Actual initial flow vs. prediction of initial flow with $\zeta = 0.11$, cut off at $10\ell/\text{min}$ for ease of visualization.	59

LIST OF FIGURES

5.2	Initial flow prediction model uncertainty values as a function of crack width for the entire database.	60
5.3	Histogram of θ_{Q0} values with normal, 2-parameter lognormal and 2-parameter Weibull fits.	61
5.4	Probability plots of the Weibull and lognormal distributions for the θ_{Q0} model uncertainty data.	61
5.5	Distributions of initial flow model factor for various crack width ranges.	62
5.6	Weibull plots for initial flow prediction model uncertainty θ_{Q0} for various crack width ranges.	64
5.7	Mean flow and mean normalized flow vs. time for different crack width ranges.	66
5.8	Example of normalized flow through a database sample and illustrations of θ_{idjd}	67
5.9	Visual illustration of θ_{idjd} leakage regimes.	68
5.10	Histogram of accumulated flow values, θ_{0d7d} with lognormal, Weibull and exponential fits.	69
5.11	Probability plots of the Weibull and lognormal distributions for the θ_{0d7d} data.	69
5.12	Weibull fits to normalized, accumulated leakage at 7 days, with no prior stabilization period, varied by crack width range.	70
5.13	CI's for θ_{0d7d} data for various crack width ranges.	72
5.14	Weibull fits to normalized, accumulated leakage at 8 days, including a 3 day stabilization period, varied by crack width.	73
5.15	CI's for θ_{3d8d} data for various crack width ranges.	74
5.16	Distribution fits to normalized, accumulated leakage at 14 days, including a 7 day stabilization period, θ_{7d14d} , varied by crack width (θ_{14d21d} data similar).	75
5.17	CI's for θ_{7d14d} data for various crack width ranges (θ_{14d21d} similar).	76
5.18	Illustration of the effect of h^*/t ratio on the mean leakage, relative to μ_{tot}	77
6.1	Effect of base restraint on C_t	82
6.2	Comparison of the effect of hinged and fixed base conditions (top free) on C_t for various h^2/Dt ratios.	83
6.3	Illustration of variation in required area of steel for 0.2mm crack width limit, with increasing tension force.	88
6.4	Illustration of applied hoop tension along reservoir wall height, and subsequent crack length prediction.	90
6.5	Lognormal distribution of crack widths.	91
6.6	Illustration example of realistic cracking stages of load-induced cracking in concrete. Probability density function of f_{ct} (top) linked to concrete tensile resistance force (bottom).	93
6.7	Illustration of the simplified reservoir slice analogy for the sensitivity analysis.	97
6.8	Illustration of crack shape and the mean, cubic equivalent and maximum width of crack (exaggerated vertical scale for illustration purposes).	99
7.1	Ideal vs. realistic crack shapes in parallel plate-type and lens shape cracks.	107
7.2	Illustration of individual segments along the length of the unit-length crack, each with respective crack width, w_b (Equation 7.2) and length $\ell_b = 1/n_b$	108
7.3	Illustrative example of using the same quantile value corresponding to, for example, a lower tail probability $q=0.6$, for each crack width range distribution for θ_{0d7d}	108
7.4	Flow chart for the analysis of a single reservoir.	110
7.5	Illustration of f_{ctm} distributions and sampled $f_{ct,a}$ values from analysis. Example of a reservoir specific distribution with $f_{ctm}=2.7 MPa$	111
7.6	Illustration of analysis progression through potential crack points $a, a+1, a+2$ and crack spacing for a section of reservoir (pattern continues around reservoir circumference).	112
7.7	Illustration of output from analysis of reservoir R1, showing the relationship between A_s , w_t and the mean of L_p	114
7.8	Histograms of the strain difference and crack spacing in reservoir R1 for $w_t = 0.2 mm$	114
7.9	Histograms with LN fits of crack widths for a single repetition of reservoir R1 for various target crack widths.	115

7.10	L_p/L_{at} for all repetitions and leakage regimes for reservoir R1 and $w_t = 0.17\text{ mm}$	117
7.11	Recommendations on limitation of crack width based on self-sealing, according to EN 1992-3, Edvardsen (1996), Meichsner (1992) and Lohmeyer (1984).	119
8.1	Histograms of reservoir characteristics from all analysed reservoirs.	126
8.2	Analysis realizations of achieved reliability vs target crack width for all leakage regimes. 10 th percentile, mean and 90 th percentile shown in broken lines.	130
8.3	Mean achieved reliability vs target crack width for all leakage regimes.	130
8.4	Mean achieved reliability vs area of reinforcing for all leakage regimes.	131
8.5	Target crack width vs mean area of reinforcing over all leakage regimes. Note that "kinks" in the graph are caused by increases in bar diameter.	131
8.6	Target crack width for $\beta = 1.5$ vs h^*/t ratio for all leakage regimes. Graphs on the right show box and whisker diagrams of w_t for $\beta = 1.5$ for 5 bins of h^*/t ratio.	133
8.7	Target crack width for $\beta = 1.5$ vs $T_{max}/T_{r,m}$ ratio for all leakage regimes.	135
8.8	Illustration of how mean concrete tensile resistance affects the proportion of cracks that form and leak.	135
8.9	Comparison of recommended target crack width for $\beta = 1.5$ vs h^*/t for $12 \leq h^*/t < 27$ from this research with EN 1992-3 and MC 2010.	136
8.10	Distribution of β achieved for the w_t recommendations from EN 1992-3, MC 2010 and from this research for h^*/t ratio, if applicable, for each reservoir analysed.	138
8.11	Recommended target crack width for $\beta = 1.5$ vs $T_{max}/T_{r,m}$ for the stabilized cracking stage and $12 \leq h^*/t \leq 26$	139
8.12	Distribution of achieved β , based on recommendations of w_t as a function of $T_{max}/T_{r,m}$ from this research.	140
8.13	Illustration of the effect of wall-base connection fixity on the resulting maximum hoop tension force.	142
8.14	Practical, tiered reinforcing layout in a reservoir wall.	145
E.1	Recommended target crack width for $\beta = 1.5$ vs h^*/t for $12 \leq h^*/t < 27$	177

List of Tables

2.1	Relationship between β and p_f (From EN 1990, Table C1)	5
2.2	Proposed standard models of basic variables for time-invariant reliability analyses. (Adapted from Holický (2009))	8
2.3	50-Year return period reliability indices for prominent design codes or standards.	9
2.4	Target reliability indices for a one year return reference period at ULS, using monetary optimization (Adapted from ISO 2394:2014)	10
2.5	Van Nierop (2017) comparison of results of β values for generic vs. case specific cost optimization methods.	13
2.6	Number of repetitions required for p_f convergence, as a function of CoV and p_f , based on Lemaire <i>et al.</i> (2009)	16
3.1	Crack model comparison summary	25
3.2	Model factor (w_{exp}/w_{pred}) mean / CoV for EN 1992-1-1 and MC 2010 from literature.	29

LIST OF TABLES

3.3	Liquid tightness classes to EN 1992-3	30
3.4	Crack width limits of prominent WRS design codes.	31
3.5	Research conducted on autogenous self-sealing in concrete or mortar.	40
4.1	Typical self-sealing environments and characteristics, adapted from Roig-Flores <i>et al.</i> (2015).	51
4.2	Sources of the experimental database for the prediction of initial flow through tension cracked concrete or mortar.	54
4.3	Sources of the experimental database for the reduction of water flow over time.	56
5.1	Flow reduction value, ζ , back-calculated from experimental data collected from different researchers.	58
5.2	Statistical parameters for the initial flow prediction model factor, θ_{Q0} , for crack width ranges.	62
5.3	Reduction of water flow over time database characteristics.	65
5.4	Leakage regimes, C_{idjd} , relating to stabilization period and water tightness test duration for leakage accumulation factor, θ_{idjd}	68
5.5	Characteristics of Weibull fits to crack width ranges for θ_{0d7d} data.	71
5.6	Characteristics of Weibull fits to crack width ranges for θ_{3d8d} data.	73
5.7	Characteristics of Weibull distribution fits to crack width ranges for θ_{7d14d} and θ_{14d21d} data.	75
5.8	Data for the approximation of the effect of h^*/t ratio on self-sealing.	77
5.9	Statistical Weibull distribution parameters for the total leakage model.	78
6.1	MC 2010 model uncertainty (w_{exp}/w_{pred}) characteristics for maximum crack width prediction for short-term tension cracks, from McLeod (2019).	91
6.2	Summary of parameters used in the prediction of leakage.	96
6.3	Circular reservoir geometry constraints for the sensitivity analysis.	98
6.4	Constraint sets for the sensitivity analysis of leakage through a single crack.	100
6.5	Results of sensitivity analysis and α values for SA1-5.	100
6.6	Results of sensitivity analysis for SA6-8 for varied values of θ_{space}	102
7.1	Geometry of reservoirs R1 to R4 used in the reservoir leakage analyses.	105
7.2	Allowable leakage cases evaluated in simulation. Periods given in days, allowable leakage given in $k\ell$	106
7.3	Summary of probabilistic parameters used in the analysis to determine the leakage for an entire reservoir.	109
7.4	Selected analysis output for reservoir R1 for $n = 1000$ repetitions.	113
7.5	Analysis of crack width characteristics, not considering cracks where $T_{max} < T_r$ (uncracked).	116
7.6	Mean, standard deviation and CoV of L_p/L_{al} for selected target crack widths and leakage regimes for reservoir R1.	117
7.7	Probability of failure and execution time of the analysis for C_{7d14d} as a function of target crack width and number of analysis repetitions for reservoir R1.	118
7.8	Reservoir R1 p_f , associated β value and mean L_p/L_{al} , for all leakage regimes and all w_t for which $A_s < 8042 \text{ mm}^2/\text{m}$ (1000 repetitions).	120
7.9	p_f , associated β value and mean L_p/L_{al} , for reservoirs Reservoir R2 to R4 for all leakage regimes and all w_t for which $A_s < 8042 \text{ mm}^2/\text{m}$ (1000 repetitions).	122
8.1	Geometry constraint sets for the reservoir simulations.	124
8.2	Typical, summarized reservoir analysis output. Example of reservoir 57.	128
8.3	Summary and comparison of recommendations of target crack width for round reservoirs in the stabilized cracking stage, from this research, EN 1992-3 and MC 2010.	137
8.4	Achieved reliability for SLS leakage and stabilized cracking using the target crack width recommendations of EN 1992-3, MC 2010 and this research for h^*/t ratio, if applicable.	139
8.5	Recommendations of target crack width for $\beta = 1.5$ as a function of $T_{max}/T_{r,m}$ ratio.	139

LIST OF TABLES

8.6	Achieved reliability for SLS leakage and stabilized cracking using the proposed recommendations of w_t as a function of the $T_{max}/T_{r,m}$ ratio from this research.	140
8.7	Examples of correct and incorrect interpretation of h^*/t (h_D/h) ratio.	144
9.1	Summary of recommendations of target crack widths for round, reinforced concrete reservoirs in the stabilized cracking stage as a function of hydraulic ratio, h^*/t , for $\beta=1.5$. . .	151
9.2	Summary of recommendations of target crack widths for round, reinforced concrete reservoirs in the stabilized cracking stage as a function of $T_{max}/T_{r,m}$ ratio for $\beta=1.5$	151
E.1	Summary of recommendations of target crack widths for round, reinforced concrete reservoirs in the stabilized cracking stage as a function of hydraulic ratio, h^*/t , for $\beta=1.5$. . .	176
E.2	Summary of recommendations of target crack widths for round, reinforced concrete reservoirs in the stabilized cracking stage as a function of $T_{max}/T_{r,m}$ ratio, for $\beta=1.5$	177

List of Acronyms and Symbols

List of Acronyms

AAR	Alkali aggregate reaction
ACI	American Concrete Institute
AS	Australian standard
BS	British Standard
BETA	Beta distribution
CA	Crystalline admixture
CDF	Cumulative density function
CI	Confidence interval
CoV	Coefficient of variation
CSF	Condensed silica fume
EN	European Standard
FA	Fly-ash/pulverized fuel ash
FEM	Finite element method
FORM	First order reliability method
GDP	Gross domestic product
GGBS	Ground granulated blast furnace slag
GU	Gumbel distribution
IS	Indian standard
ISO	International Organization for Standardization
JCSS	Joint committee on Structural Safety
KS	Kolmogorov-Smirnov
LN	Lognormal distribution
LQI	Life quality index
MC 2010	<i>fib</i> Model Code for Concrete Structures 2010
MCS	Monte Carlo simulation
MLE	Maximum likelihood estimate
N	Normal distribution
OPC	Ordinary portland cement
PP	Polypropylene
PVA	Polyvinyl alcohol
PVC	Polyvinyl chloride
SANS	South African National Standard
SAP	Super absorbent polymer
SCM	Supplementary cementitious materials
SLS	Serviceability limit state
SSB	Simply supported beam
ULS	Ultimate limit state
WRS	Water retaining structures

List of Symbols - Greek

α	Significance level of statistical test (chapter 5 only)
α_x	Direction cosines for FORM
α_E	Direction cosine for actions (chapter 2 only)
α_e	Modular ratio between steel and concrete
α_R	Direction cosine for resistances (chapter 2 only)
β	Reliability index
	Empirical integration constant for strain difference in MC 2010 crack prediction model

γ	Shape parameter for Weibull distribution Partial factor (chapter 2 only) Discount rate section 2.6 only
γ_w	Scale parameter for Weibull distribution Unit weight of water
Δp	Water pressure head difference between experimental inlet and outlet
Δw	Change in crack width for active cracks
ϵ_s, ϵ_c	Strain in reinforcing, concrete
$\epsilon_m, \epsilon_{sm}, \epsilon_{cm}$	Mean strain (general), mean strain in reinforcing, concrete
ϵ_{sh}	Free shrinkage strain
ζ	Flow reduction factor to account for crack surface roughness
η	Mean value of conversion factor for material property (chapter 2 only)
η	Dynamic viscosity for initial flow
η_r	Coefficient considering free shrinkage contribution
θ	Model factor / general factor
θ_{cw}	Model factor for MC 2010 crack width prediction model
θ_{HR}	Factor to consider h^*/t ratio
θ_{idjd}	Leakage accumulation factor
θ_{Q0}	Initial flow prediction model factor
θ_{space}	Factor to vary crack spacing between 1 and 2
Λ	Omission sensitivity factor
$\lambda(p)_{SLS}$	Annual failure rate for SLS failures
μ	Mean value
ρ	Ratio of total costs to construction costs (chapter 2 only) Reinforcing ratio
$\rho_{p,eff}$	$= \rho_{s,ef}$ (EN 1992-1-1 nomenclature)
$\rho_{s,ef}$	Effective reinforcing ratio $= A_s/A_{c,ef}$
ρ_w	Density of water
σ	Stress Standard deviation Shape parameter for Lognormal distribution
σ_s	Stress in reinforcing
σ_w	Maximum hydrostatic pressure
τ_{bms}	Mean concrete-steel bond stress (MC 2010)
Φ	Inverse distribution of the standard normal distribution
ϕ, ϕ_b	Reinforcing bar diameter Creep factor
ψ	Accompanying load factor
ω	Obsolescence rate (chapter 2 only)

List of Symbols - English

$A_{c,ef}$	Effective area of concrete in tension
A_s	Area of reinforcing
$A_{s,min}$	Minimum area of reinforcing
$A_{s,req}$	Area of reinforcing required
a_{cr}	Distance from crack point to the surface of the nearest longitudinal bar
C_t	Coefficient to determine maximum hoop tension in round reservoirs
c	Concrete cover
D	Reservoir diameter D-statistic from KS test (chapter 5 only)
d	Sample thickness in direction of flow in Poiseuille Flow and literature review
d_{ave}	Average water depth (BS 8007)
E	Action effect (Reliability)
E	Young's modulus (Modulus of elasticity)
E_c	Young's modulus of concrete

$E_{c,ef}$	Effective Young's modulus of concrete considering creep
E_s	Young's modulus of reinforcing steel
F_{rep}	Representative value for actions
f_b	Mean concrete-steel bond stress (BS 8007)
f_{ck}	Characteristic compression strength of concrete
f_{ct}	Concrete tensile strength
$f_{ct,eff}$	Effective concrete tensile strength at time under consideration = f_{ctm} for $28d < t$
f_{ctm}	Mean concrete tensile strength
$f_{ct,low}$	Lower limit of concrete tensile strength corresponding to one standard deviation below f_{ctm}
$f_{ct,hi}$	Upper limit of concrete tensile strength corresponding to one standard deviation above f_{ctm}
$f_{ct,a}$	Concrete tensile strength at crack point a
f_u	Ultimate strength of steel
f_y	Yield strength of steel
G, Q, W	Permanent, variable, wind load (chapter 2 only)
g	Reliability limit state equation
	Standard acceleration due to gravity
h	Reservoir height
h	Concrete wall thickness (EN 1992-3) = t
h^*	Water pressure head above crack position
h_D	Height of water head above crack point (EN 1992-3) = h^*
I	Hydraulic gradient (Edvardsen) = h^*/t
k_x	Factors used in EN 1992-3 crack prediction model
L_{al}	Allowable leakage for reliability limit state
L_p	Predicted leakage for reliability limit state
ℓ	Length of crack at concrete surface
ℓ_a	Length of crack at crack point a
$\ell_{s,max}, \ell_{s,max}$	Mean and maximum length over which slip between concrete and steel occurs (MC 2010)
m	Scale parameter for the Lognormal distribution
n	Generic "number of"
P	Notation for "probability of"
p	Decision parameter (chapter 2 only)
	Water pressure head
	p-value from KS test (chapter 5 only)
p_f	Probability of failure
Q	Water flow
$Q_{crack,tot,a}$	Total flow through a crack at crack point a between times i and j
Q_{total}	Total flow
Q_0	Initial water flow
$Q_{0,predicted}$	Initial water flow predicted using model
$Q_{0,actual}$	Actual initial water flow from experimental sample
q_0	Poiseuille Initial water flow
R	Resistance effect (Reliability)
r	Reservoir radius
$R_{X,heal}$	Self-healing ratio
$SA1$ to $SA8$	Sensitivity analysis identifiers
$S_{r,max}, S_{rm}, S_{r,max}$	Minimum, mean and maximum crack spacing (EN 1992-3)
T	Applied tension force
T_{max}	Maximum applied tension force
T_r	Tension resistance force of concrete
$T_{r,a}$	Tensile resistance force of concrete at crack point a
$T_{r,m}$	Mean tensile resistance force of concrete
$T_{r,low}, T_{r,hi}$	Lower and upper tensile resistance force of concrete corresponding to $f_{ct,low}$ and $f_{ct,hi}$
U	Direct costs (section 2.6 only)
V	WRS volume
w	Crack width
w_a	Crack width at crack point a

$w_{a,cube}$	Cubic equivalent of crack width at crack point a
$w_{a,max}$	Maximum width of crack at crack point a
$w_{a,mean}$	Mean crack width of crack point a
w_b	Crack width at an individual segment of crack at crack point a
w_{exp}	Crack width from experimental sample
w_k, w_d	Characteristic crack width
w_{mean}	Mean crack width
w_{pred}	Crack width from model prediction
w_t	Target crack width
X	Variable in statistical definitions e.g. $P\{X < X_k\}$
$Z(p)$	and $C(p), I(p), M(p), A(p), D(p), U(P)$ Costs related to decision parameter (chapter 2 only)

1. Introduction

1.1 Background and motivation

This research is concerned with the determination of the achieved level of serviceability limit state (SLS) reliability in tension-governed, reinforced concrete water retaining structures (RC WRS). The primary function of a WRS is to prevent the leakage of the retained water, which is different in function to a typical building structure. Contrary to the design of building structures, which are governed by the ultimate limit state (ULS), the design of WRS is governed by SLS considerations. Specifically, WRS are governed by the need to limit cracks to appropriate widths, in order to ensure that the leakage of the retained liquids is kept to a minimum. Structural design codes provide models and guidelines by which to calculate the reinforcing required to limit the crack widths. The introduction of the Eurocodes and subsequent withdrawal of the British Standard codes ushered in a new era of standardization in design codes across Europe and Britain. As a result of the withdrawal of the British codes, many codes that were based on them are being revised.

For many years, BS 8007 used in conjunction with BS 8110 has served as the de-facto design code for the design of RC WRS in many countries, due to the lack of a local equivalent. The introduction of EN 1992-3 led to the withdrawal of BS 8007 however, many countries have continued to use BS 8007, or a local adoption or adaptation of it. One of the reasons that countries have been slow to adopt EN 1992-3 is due to the concerns expressed with regard to the economic implications of adopting EN 1992-3. Research by McLeod (2013) and Wium (2007) has shown that the amount of reinforcing required to limit cracks to acceptable limits as set out in EN 1992-3 is considerably higher than that required to limit cracks to the limits as set out in BS 8007, especially for cases of pure tension.

The prescription of crack width limits for WRS has been a contentious issue for many years, with widespread disagreement as to the appropriate magnitude of crack width required in order to limit leakage to an acceptable quantity. Further disagreements arise as to whether tension through-cracks should have the same crack width limits as trapezium-shaped flexural cracks. All codes qualitatively state that the phenomenon of autogenous self-sealing in cracked concrete has a significant effect in reducing the leakage of the retained liquid over time, but do not give a quantification of the effect. Self-sealing occurs mainly in the form of precipitated calcium carbonate and the continued hydration and swelling of cement within the cracks, which constricts the available flow area, thus reducing the leakage. Most codes, however, only give a qualitative indication that self-sealing assists in the reduction of leakage and do not comment as to the extent or degree of self-sealing that can be expected. Many codes, such as BS 8007, the *fib* Model Code 2010 and ACI 224-19 have proposed target crack width limits based on satisfactory past performance, acknowledging that self-sealing contributes to this satisfactory performance. EN 1992-3 on the other hand, proposes crack width limits that vary in stringency, based on the hydraulic ratio, h_D/h , defined as the head of water over the wall thickness. The EN 1992-3 re-

commendations of target crack width come directly from research by Edvardsen (1996) that prescribes target crack widths that completely self-seal in 4-10 weeks, with a 90% probability of non exceedance. Though this does give some measure of the effect of autogenous self-sealing, the effect that it has on the leakage-related SLS reliability of WRS is currently unquantified.

While EN 1992-3 and MC 2010 specify irreversible SLS target reliability levels of $\beta = 1.5$, neither provide a means by which to evaluate this level of reliability. Neither code prescribes water tightness test criterion, which is the most common method of evaluating whether a WRS as "water tight" or not, and is standard in almost all reservoir construction project specifications. BS 8007 and ACI 350.1-10 provide water tightness test criterion in the form of an initial stabilization period, where autogenous self-sealing and absorption of water into the concrete take place, followed by a water tightness test of varying duration based on target crack width. The water level is measured over the test period and the quantum of leakage is compared to the code-defined allowable leakage, and thus declared water tight or not. A failed water tightness test leads to costly project delays and remedial work to the concrete to seal the cracks, followed by another water tightness test. Thus, designing to the appropriate crack width to ensure an acceptable degree of leakage is important in the design of WRS.

As the Eurocodes themselves are currently being revised, the Model Code 2010 crack prediction model is to be adopted for use in the revised EN 1992-3 (Caldentey, 2017). Given the reliability basis of MC 2010 and EN 1992-3, the lack of ability to determine whether the target level of reliability is actually achieved or not stifles the potential for being able to cost-optimize the design of WRS. Furthermore, the reliability performance of WRS designed to either code is simply not known.

1.2 Objectives

This research thus aims to determine the achieved level of SLS leakage-related reliability in tension governed RC WRS using the MC 2010 crack prediction model, considering the effect that autogenous self-sealing has on the reduction of leakage over time. It also aims to further the understanding of the effects that various parameters have on the achieved reliability, such as target crack width, stabilization period, water pressure head to wall thickness ratio, applied hoop tension and concrete tensile strength. The aim is split into the following objectives:

1. Determine the effect and extent of self-sealing in reinforced concrete WRS:
 - From the published experimental work of others, compile a set of data that can be used to probabilistically characterize the variation in the prediction of initial flow of water through tension cracked concrete;
 - From the published experimental work of others, compile a set of data that can be used to probabilistically characterize the effect that self-sealing has on the reduction of leakage over time.
2. Develop an analysis to determine the SLS leakage-related reliability of a WRS that considers the effect of self-sealing, using a small set of example WRS geometries:
 - Develop a probabilistic analysis that realistically mimics the loading on, cracking in, and subsequent leakage through, a tension crack governed RC WRS;
 - Incorporate the probabilistic initial leakage flow prediction and self-sealing from objective 1 into the analysis.

3. Evaluate a large set of WRS geometries to confirm the results of achieved level of reliability in objective 2:
 - Compare results to code-specified target reliability;
 - Identify trends in the above-mentioned parameters with the achieved reliability;
 - Make recommendations of parameters to achieve a leakage related SLS reliability of $\beta=1.5$, based on identified trends.

1.3 Layout of dissertation

The dissertation is structured as follows:

Chapter 2: Literature review of risk and reliability and statistical concepts.

Chapter 3: Literature review of water retaining structures, related structural design codes and the current state of research on self-sealing and self-healing in concrete.

Chapter 4: Details of compilation of experimental databases for the initial flow prediction model and leakage prediction model.

Chapter 5: Probabilistic characterization of initial flow prediction model and leakage prediction model and combination of the two for use in the SLS reliability analysis of tension governed RC WRS.

Chapter 6: Detailing of the reliability analysis theory and adaption to a WRS context. Definition of the reliability limit state and a sensitivity analysis of the MC 2010 crack prediction model.

Chapter 7: Monte Carlo reliability analysis of a small set of reservoirs and discussion of results.

Chapter 8: Monte Carlo reliability analysis of a large number of reservoirs and discussion of results. Comparison of results with EN 1992-3 and MC 2010. Recommendation of reliability-based target crack widths.

Chapter 9: Final summary, conclusions and recommendations for future research.

2. Risk and Reliability Literature Review

2.1 Background

As modern day structural design codes continue to develop, the design of structures has advanced from crude methods, that simply over-compensate for worst case loading by applying isolated safety factors, towards reliability-based design methods. In modern design codes, underlying principles based on risk and reliability are a necessity in order to optimize structures in terms of cost and safety, as well as to measure and compare structural performance. The Eurocodes (CEN, 2002) are an example of a set of structural design codes that employ such a philosophy, amongst an increasing number of codes used throughout the world (Holický, 2009).

These design codes, while not employing fully probabilistic methods of design, contain semi-probabilistic methods based on partial factor limit-state design. These methods improve on the isolated safety factor method by assigning unique partial factors to loads and/or resistances to account for the inherent variability and uncertainty. Said methods make use of a target reliability index, β , linked to a probability of failure, p_f , as a measure of the reliability associated with each class of structure, depending on the consequence of failure and relative cost of increasing reliability (ISO, 2014).

The reliability basis of the codes also allow for the potential for reliability based optimization, whereby life cycle costs can be minimized, leading to structures that are more cost-effective. In the Eurocodes, this has been carried out to an extent, depending on the consequence class of the structure under consideration, however, only three classes of structures are defined in the Eurocodes. Furthermore, the majority of structures fall into just one consequence class (labelled CC2 in EN 1990).

This means that widely applicable, blanket-reliability indices are required in order to ensure compliance across a vast array of structures. This single reliability class contains structures of various construction materials and failure modes as well as structures with different environments and functions; all of which are governed by the same reliability index, according to the limit state under consideration, whether ULS or SLS. These respective reliability indices stem from ISO 2394:1998 (though originally from previous research by Rackwitz (2000)) and while the revised ISO 2394:2014 does contain information with which to make a decision of an appropriate reliability index, depending on the consequences of failure and relative cost of safety measures, the majority of designers are not likely to consider structure-specific reliability indices. Most designers will simply use the EN 1990 standard target reliability indices of $\beta_{t,ULS} = 3.8$ for any type of ULS application and $\beta_{t,SLS} = 1.5$ for any type of irreversible SLS failure (for a 50 year reference period). While the standardization of reliability levels is important for structural safety and has many benefits, the one negative is that it can stifle

the potential for further optimization of structures.

This section serves to introduce the concepts of risk and reliability with the view of using the concepts as tools with which to achieve the identified goals in key areas of WRS.

2.2 Fundamental concepts

In structural design, reliability methods were derived to measure and compare the performance of structures, as well as to enable the standardization of structures. During the 1960's and 1970's, research conducted by Cornell (1969), and later refined by Hasofer and Lind (1974) resulted in the introduction of the reliability index, β , as a measure of structural performance related to a specific time-period, where load and resistance distributions are not required to be exclusively normal. The β value is related to a probability of failure for the given period, p_f , as shown in Table 2.1, according to: $\beta = -\Phi^{-1}(p_f)$, where $-\Phi^{-1}(p_f)$ denotes the inverse distribution of a standardized normal distribution.

Table 2.1: Relationship between β and p_f (From EN 1990, Table C1)

p_f	10^{-1}	10^{-2}	10^{-3}	10^{-4}	10^{-5}	10^{-6}	10^{-7}
β	1.28	2.32	3.09	3.72	4.27	4.75	5.20

Further research conducted in the late 1990's as summarized in Rackwitz (2000) greatly contributed to structural optimization, as well as to the standardization of the underlying principles of code making, which form the basis of the Eurocodes. The typical, generalized limit state function, g , of structural reliability problems is given by:

$$g = R - E \quad (2.1)$$

Where R denotes a modelled resistance and E denotes a modelled load effect. Cases where $g \leq 0$ represent a failure for the limit state under consideration. The models of resistance and load incorporate uncertainties; thus the β value is used to give a measure of the reliability of a structure with regard to the limit state(s) incorporated in g .

2.3 Uncertainties in structural engineering

Due to the inherent uncertainty and variability in almost every facet of structural engineering, single-value mean representations of material, load and effect parameters can never completely represent reality. Conversely, it is impossible to incorporate every detail of uncertainty into each calculation due to computational, time and cost constraints. Simplifications therefore need to be made to timeously carry out designs, without compromising the safety thereof. These simplifications may, for example, take the form of using deterministic values for parameters that are not likely to deviate much from these values, or to make assumptions about load behaviour that are not entirely correct, but are sufficient for purposes of design. Uncertainties are generally classified as either being aleatory or epistemic, although most contain elements of both.

Aleatory variability, sometimes termed statistical uncertainty, is the natural randomness that occurs in processes, such as the rolling of dice. Most of the aleatory uncertainty in structural engineering is inherent in nature and thus cannot be reduced or changed, but must be accounted for using probability

density functions.

Epistemic uncertainty, sometimes referred to as systematic uncertainty, is the scientific uncertainty present in the modelling of the process that results from limited data and knowledge. An example of this is in the prediction of deflection in a simply supported beam with a concentrated load at mid-span: The deflection is given by $\delta = WL^3/48EI$, though in reality, should a beam like this be loaded, the deflection will certainly not be exactly what the above formula predicts. This is because the formula is based on the assumptions that the beam material is linearly elastic, that plane sections remain plane and that the stress-strain relationship is the same in tension as it is in compression, some or all of which may not be true. The deflection calculated using the formula is usually close enough to reality for all intents and purposes of design. This type of uncertainty can thus be reduced with increases in data and/or knowledge, if such reductions are worthwhile.

In the Eurocode framework, uncertainty is quantified using partial factors for loads and resistances γ_F and γ_M .

2.4 Uncertainties in loading and material resistance

Similarly to Equation 2.1, the Eurocodes (EN 1990) define a reliable structure as one where the design value of the action effect, E_d , is less than or equal to the design value of the resistance effect, R_d . The action effect is shown in Equation 2.2 and generalized in Equation 2.3:

$$E_d = \gamma_{Ed} E \{ \gamma_g G_k; \gamma_p P; \gamma_q Q_k; \psi_0 Q_k \dots \} \quad (2.2)$$

$$E_d = E \{ \gamma_F F_{rep} \} \quad (2.3)$$

Where:

$G; P; Q$ Are permanent; prestressing; variable actions

ψ_0 Factor allowing reductions in design values of variables as accompanying actions

$\gamma_F = \gamma_{Ed} \cdot \gamma_f =$ Partial factor for actions

F_{rep} Representative value for actions, typically a 98% quantile

The partial factors γ_f and γ_{Ed} are used to take account of the possibility of the action values unfavourably deviating from the representative values and to account for uncertainties in modelling the effects of actions, respectively. Similarly, the resistance effects are shown as Equation 2.4 and generalized by Equation 2.5:

$$R_d = R \{ \eta X_k / \gamma_m \} / \gamma_{Rd} \quad (2.4)$$

$$R_d = R \{ X_k \} / \gamma_M \quad (2.5)$$

Where:

- η Mean value of conversion factor appropriate to the material property
- $\gamma_M = \gamma_{Rd} \cdot \gamma_m =$ Partial factor for resistances
- X_k Representative value for resistances, typically a 5% quantile

The η factor in Equation 2.4 takes into account variations between the conditions in the structure and the conditions under which the characteristic values are determined, though is usually equal to unity. These are sometimes incorporated into the value of X_k (Gulvanessian *et al.*, 2002). The partial factor γ_{Rd} relates to the uncertainty associated with the resistance model and geometric deviations, if not modelled explicitly. Similarly to the actions, γ_m relates to uncertainty in material properties with regard to unfavourable deviations away from characteristic values and to include the "randomness" related to η . The characteristic and design values for variable actions and resistances are illustrated in the probability density functions in Figure 2.1.

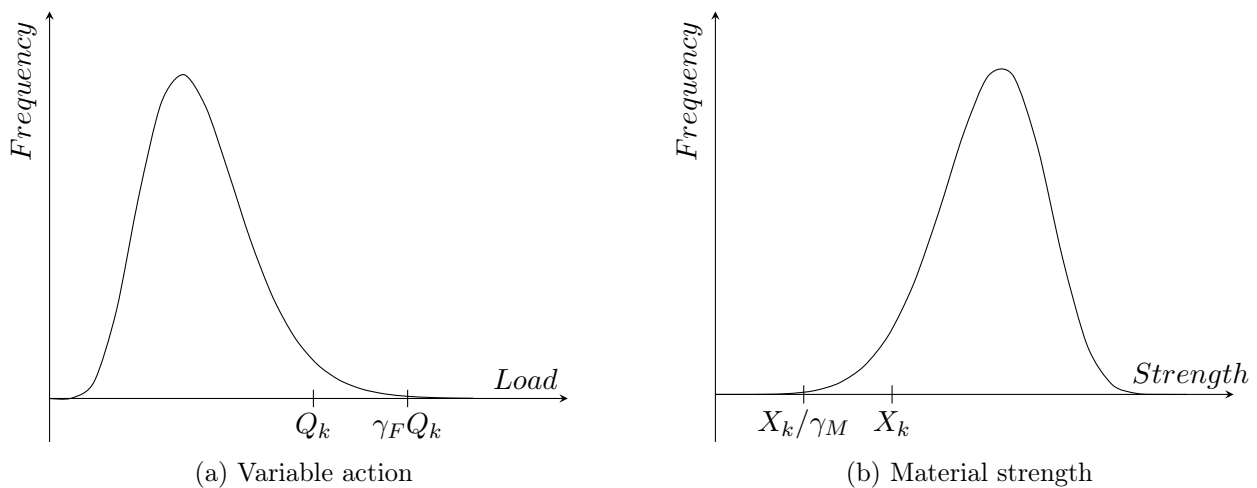


Figure 2.1: Characteristic and design values for variable actions and material strength.

The concept of uncertainty, specifically in the modelling of actions and resistances is commonly referred to as model uncertainty, often denoted by θ . It is usually defined as being a measure of the ability of a model to accurately make predictions of reality. Model uncertainty accounts for random effects not reflected in the models, as well as for assumptions or simplifications made in mathematical models. In the Eurocodes, model uncertainty is usually incorporated into the values of γ_{Rd} and γ_{Ed} . The JCSS Probabilistic Model Code suggests that it is incorporated into probabilistic design as a random variable having a normal or lognormal probability density function with a mean value of unity and a specified coefficient of variation (CoV) of typically between 0.05 and 0.2, but higher values are appropriate in some cases, such as for shear in reinforced concrete beams (Holický *et al.*, 2013), buckling for cold-formed steel structures (West-Russel *et al.*, 2018) and crack widths in reinforced concrete (McLeod *et al.*, 2017).

In probabilistic modelling of structures, standard models of basic variables for load, resistance and model uncertainty having the same background assumptions should be used to determine probabilities of failure so that results can be standardized. EN 1990 partly addresses this in its appendices C and D. Holický (2009) compiled and synthesized a collection of standard model data for time-invariant

reliability analyses, reproduced here as Table 2.2. The data was obtained from the JCSS Probabilistic Model Code¹, Vrouwenvelder (2001)², various CIB reports (CIB, 1989, 1995)^{3,4,5}, Sørensen *et al.* (2001)⁶, Holický and Marková (2000)⁷, Caramelli *et al.* (1997)⁸ and Fajkus *et al.* (1999)⁹. It should be noted that these are reasonable conventional methods, but may not be adequate for out-of-the ordinary situations, such as for wind loads acting on high-rise buildings. Furthermore, the mean values μ_x relate to the characteristic value used in design calculations. The probability that the value of the variable X is less than the characteristic value X_k is given in Table 2.2 as (where Φ_x signifies the distribution function of the basic variable X):

$$P\{X < X_k\} = \Phi_x(X_k) \quad (2.6)$$

The data in Table 2.2 is useful for the standardization of design codes, but more than that, it allows for the definition of a concept of target reliability.

Table 2.2: Proposed standard models of basic variables for time-invariant reliability analyses. (Adapted from Holický (2009))

Variable category	Name of variable	Sym-bol	Dim.	Dist.	Mean μ_x	St. Dev σ_x	Prob. $\Phi_k(\mathbf{X}_k)$	Ref.
Action	Permanent	G	kN/m ²	N	G_k	$0.03 - 0.1\mu_x$	0.5	1,3
	Imposed-5 yr	Q	kN/m ²	GU	$0.2Q_k$	$1.1\mu_x$	0.995	1,4
	Imposed-50 yr	Q	kN/m ²	GU	$0.6Q_k$	$0.35\mu_x$	0.953	1,4
	Wind-1 yr	W	kN/m ²	GU	$0.3W_k$	$0.5\mu_x$	0.999	1,5
	Wind-50 yr	W	kN/m ²	GU	$0.7W_k$	$0.35\mu_x$	0.89	1,5
Material	Steel Yield	f_y	MPa	LN	$f_{yk} + 2\sigma$	$0.07 - 0.1\mu_x$	0.02	1,6-9
	Reinforcement	f_y	MPa	LN	$f_{yk} + 2\sigma$	30MPa	0.02	1,6-9
Strengths	Steel Strength	f_u	MPa	LN	$\kappa\mu_{fy}^*$	$0.5\mu_x$	-	1,6-9
	Concrete	f_c	MPa	LN	$f_{ck} + 2\sigma$	$0.1-0.18\mu_x$	0.02	1,6-9
Geometry (concrete)	X-section	b, h	m	N	b_k, h_k	0.005-0.01	0.5	1
	Cover to reinf	c	m	BETA	c_k	0.005-0.015	0.5	1
	Eccentricity	e	m	N	0	0.003-0.01	-	1
Model	Load effect	θ_E	-	N	1	0.05-0.1	-	1,2
Uncertainty	Resistance	θ_R	-	N	1-1.25	0.05-0.2	-	1,2

* $\kappa = 1.5$ for structural carbon steel. N - Normal distribution ; GU - Gumbel, LN - Lognormal

2.5 Target reliability

Structural reliability performance is measured by a comparison between the achieved reliability level, β , and the target reliability level, β_t . Alternatively, it is often convenient (and easier to conceptualize) to express this as a probability of failure, p_f , versus a target probability of failure, p_t , as illustrated in Table 2.1. Typical target reliability for prominent design codes are given in Table 2.3.

Table 2.3: 50-Year return period reliability indices for prominent design codes or standards.

Design code	ULS - consequence			SLS
	Low	Moderate	Severe	Irreversible
EN 1992-1-1	3.3	3.8	4.3	1.5
MC 2010	3.1	3.8	4.3	1.5
ISO 2394	2.3	3.1	3.8	1.5
JCSS*	3.7	4.2	4.4	1.7

* Values are for a 1 year return period.

Target reliability levels, whether in the form of p_t or β_t , are always related to a reference time period, which is not necessarily the same as the structure's design working life. The target reliability level at ULS for a 50 year return period to EN 1990 (moderate consequence of failure), $\beta_{t,ULS,50} = 3.8$ for example, is equivalent to an annual ULS target reliability level of $\beta_{t,ULS,1} \approx 4.7$. Similarly, a typical target reliability for irreversible SLS failure for a 50 year reference period, $\beta_{t,SLS,50} = 1.5$, is equivalent to $\beta_{t,SLS,25} = 1.84$ for a 25 year return period and $\beta_{t,SLS,1} \approx 3$ for a one year return period.

The target reliability of a structure is dependent on the consequences of failure of the structure and the relative cost of safety measures to reduce the probability of failure, over the lifetime of the structure (Holický *et al.*, 2015). It should be noted that gross human errors in design and construction are not factored directly into probabilistic models. As they are a completely random occurrence and have widely unpredictable effects, they are difficult, if not impossible to incorporate into a probabilistic model in the form of a model factor. Instead, EN 1990 for example, introduces three reliability classes, linked to consequence classes. Structures are categorized into these classes, based on the level of design supervision and design checking, as well as the level of construction quality control. A greater degree of design-checking and quality control allows the use of a reduced target reliability level, due to the reduced probability of a serious error slipping through the design and construction process.

The cost of safety measures vary for each structure, and depend on a number of considerations, for example: the primary construction material, structure geometry, site environment and governing failure modes. Most often, these measures are easy to determine and commonly take the form of quantities of reinforcing in a beam, column or slab or concrete compression strength. The cost of safety measures relative to the total cost of the structure is different for every structure, though for similar structures, the costs should be in the same order of magnitude.

The consequences of failure of a structure are far more difficult to define and quantify. Generally, consequences of failure are categorized into the form of economic loss, loss of human life and effects on the environment. While economic losses may be difficult to quantify, due to losses associated with time-delays and repair costs related to partially collapsed structures, these losses are still quantifiable. Loss of human life, on the other hand, simply cannot be quantified, as a human life is viewed as infinitely valuable. Despite this, a number of approximation methods attempt to either place limits on what is societally acceptable in terms of a loss of human life per time period and/or directly attempt to define a monetary compensation value for a lost life. An example of a limit imposed by what is societally acceptable is the Life Quality Index (LQI) method, developed by Nathwani *et al.* (1997). The LQI method defines a minimum limit, depending on the GDP of the country, life expectancy at birth and a ratio of leisure to working time (Diamantidis *et al.*, 2017).

Various design standards recommend target reliability values for ULS and SLS, however, these are not always in agreement. Most current standards, such as EN 1990, recommend target reliabilities based on a consideration of the consequences of failure. These are generally divided up into qualitative classes of low, medium and high consequences of failure for loss of human life or economic, social or environmental effect. The JCSS probabilistic model code roughly quantifies the consequences of failure into bins using a ratio of total costs (construction costs plus direct failure costs) to construction costs, ρ , as shown below:

$$\rho = \frac{C_{total}}{C_{const}} \quad (2.7)$$

Where:

- $\rho < 2$ Risk to life/economic consequences, given failure, are small/negligible
- $2 < \rho \leq 5$ Risk to life/economic consequences, given failure, are medium/considerable
- $5 < \rho \leq 10$ Risk to life/economic consequences, given failure, are high/significant

Some standards consider the relative cost of providing safety measures in addition to the consequences of failure, such as ISO 2394:1998 and the JCSS Model Code. These relative costs are grouped into qualitative bins of low, moderate and high, resulting in a reliability matrix. Table 2.4 is an example of such a reliability matrix, as found in ISO 2394:2014. The revised ISO 2394:2014 allows for the possibility of economic optimization and gives guidance on acceptance criteria based on the LQI.

Table 2.4: Target reliability indices for a one year return reference period at ULS, using monetary optimization (Adapted from ISO 2394:2014)

Relative cost of safety measure	Failure consequence (classes)		
	Minor (Class 2)	Moderate (Class 3)	Large (Class 4)
Large	$\beta = 3.1 (p_f \approx 10^{-3})$	$\beta = 3.3 (p_f \approx 5 \times 10^{-4})$	$\beta = 3.7 (p_f \approx 10^{-4})$
Medium	$\beta = 3.7 (p_f \approx 10^{-4})$	$\beta = 4.2 (p_f \approx 10^{-5})$	$\beta = 4.4 (p_f \approx 5 \times 10^{-6})$
Small	$\beta = 4.2 (p_f \approx 10^{-5})$	$\beta = 4.4 (p_f \approx 5 \times 10^{-6})$	$\beta = 4.7 (p_f \approx 10^{-6})$

From Table 2.4, the greater the consequences of failure, the higher the target reliability (or the lower the probability of failure) should be. It is also evident that the more costly it is to increase the level of safety, the lower the required target reliability is. In light of this, there need to be absolute minimum reliability values in place so that structures that are deemed "unsafe" by societal standards are not realized.

2.5.1 Achieved SLS reliability relating to crack widths

Little research has been carried out on the achieved level of SLS reliability with respect to crack widths. Research into the probabilistic design and analysis of crack widths in WRS was conducted by Zięba *et al.* (2020). They defined the limit state as the difference between the target crack width (chosen as 0.1 and 0.2mm), and the crack width obtained using the EN 1992-1-1 crack prediction model. A cylindrical, RC WRS was used as the reference case and probabilistic inputs were used for some of the more critical parameters, such as concrete cover, concrete compressive strength and the unit weight

of water. A FORM analysis was used with the area of reinforcing in the wall as the main decision parameter. A FEM model was used to compare the calculated cracks widths to, finding that the EN 1992-1-1 model predicted cracks that are bigger than the FEM output. They reported β values of 2.86 and 2.8 for a 0.1 and 0.2mm target crack width, respectively.

Quan and Gengwei (2002) investigated the SLS reliability of maximum crack widths in RC beams in buildings. They defined the limit state as the difference between the target crack width and the crack width obtained using the crack prediction model in the Chinese code for the design of concrete structures (GB 50010:2002). A model factor was characterized and applied to the crack width predicted using GB 50010. Probabilistic inputs of concrete and reinforcing geometry and concrete tensile strength were used in conjunction with FORM for cases of permanent and variable loading. Their results showed that the SLS reliability ranged from 0-1.8, which is satisfactory for a reversible SLS target reliability of $\beta=0$, according to ISO 2394.

2.6 Cost of safety and economic optimization

From section 2.5, it is clear that the relative cost of safety plays an important role in the determination of target reliability values. This stems from a broader requirement: That the realization of a structure is only feasible when the benefit outweighs the costs or drawbacks thereof for all parties involved. Initial research by Holický *et al.* (2009) indicated that including further elements of probabilistic design into WRS can decrease costs incurred in reinforcing by 25%.

In order to economically optimize a structure, a choice of decision parameter, p , must be made. Changes to the decision parameters almost always incur a cost and in return, increase the level of reliability of the structure (increases in the quantity of tension reinforcing in reinforced concrete beams, for example, decrease the probability of flexural failure, but incur costs in reinforcing steel). As such, said decision parameter should have the most prominent effect on increasing the reliability of the structure and should be most cost-effective. A method proposed by Rackwitz (2000) for the generic economic optimization of structures is detailed in this section. A general function, $Z(p)$, for the determination of the costs of a structure, and for purposes of economic optimization, is given by:

$$Z(p) = B^* - C(p) - I(p) - M(p) - A(p) - D(p) - U(p) \quad (2.8)$$

Where:

$C(p)$ Construction cost

$A(p)$ Obsolescence cost

$U(p)$ Serviceability limit state failure cost

Generally, it is reasonably assumed that the benefit derived from a structure, B^* , is not affected by changes to p . Also, as structural degradation-related failures caused by excessive fatigue or corrosion are uncommon in general structures, the costs related thereto, $M(p)$, are seldom realized. Rackwitz (2000) thus excludes B^* and $M(p)$ from the economic optimization. Costs related to routine inspection and maintenance, $I(p)$, are typically included in the initial cost of construction, $C(p)$. Similarly, the costs associated with SLS failures, $U(p)$, are also excluded by Rackwitz, however, these serviceability failures are of particular interest in this research and will thus be included in the economic

optimization for specific structures that are governed or partially governed by SLS considerations. The costs incurred in the case of ULS failures, $D(p)$, are not of interest, as the design of WRS is governed by the SLS design of limiting crack widths and not by ULS failures (McLeod, 2013; Holický *et al.*, 2009).

Thus the generic, cost function of Equation 2.8 is reduced to a more specific function of SLS-governed failures to be minimized (From Fischer *et al.* (2018), adapted to SLS):

$$\begin{aligned} Z(p) &= C(p) + U(p) + A(p) \\ &= \{C_0 + C_1 \cdot p\} + \left\{ \sum (U_1 + U_2) \frac{p_{f,SLS}(p)}{\gamma} \right\} + \left\{ (C_0 + C_1 \cdot p + A_0) \frac{\omega}{\gamma} \right\} \end{aligned} \quad (2.9)$$

Where:

- C_0 & C_1 Construction costs independent, and dependent on p , respectively
- U_0 & U_1 Indirect, and direct SLS costs, respectively (may also be dependent on p)
- $\frac{p_{f,SLS}(p)}{\gamma}$ Annual probability of SLS failure
- γ Discount rate to convert future costs to current costs
- A_0 Demolition costs
- ω Obsolescence rate

In order to minimize costs, the derivative of the cost function with respect to the decision parameter needs to be determined and then minimized. The point where this function is at a minimum represents the most effective design point, from an economic perspective. It should be noted here that where there is no or negligible risk to human life or considerable environmental consequences in the case of failure (as in most SLS failures), there is no need for any consideration of LQI or a similar minimum threshold and thus optimization is based solely on cost considerations. The derivative of the cost function, with respect to the decision parameter is shown below:

$$\begin{aligned} \frac{dZ(p)}{dp} = 0 &= C_1 + \sum \left(\frac{U_1 + U_2}{\gamma} \right) \frac{dp_{f,SLS}(p)}{dp} + C_1 \left(\frac{\omega}{\gamma} \right) \\ \frac{dp_{f,SLS}(p)}{dp} &= -C_1 \left(1 + \frac{\omega}{\gamma} \right) / \sum \left(\frac{U_1 + U_2}{\gamma} \right) \end{aligned} \quad (2.10)$$

The formulation in Equation 2.10 is broadly comparable to that used in Van Nierop *et al.* (2017), Huaco *et al.* (2012) and Van Coile *et al.* (2017), except focussed on SLS as opposed to ULS failures. Thus it can be seen that the most optimized design point is dependent on a ratio of the costs of increasing safety to the costs of failure, as well as the efficiency of the decision parameter at decreasing the probability of failure $\frac{dp_{f,SLS}(p)}{dp}$.

In WRS, the decision parameter that has the most effect on the SLS reliability state considering leakage through a WRS is the amount of reinforcing used in the walls to limit the crack widths. The choice of target crack width limit thus has a notable influence on the achieved reliability in WRS; this is further discussed in chapter 3. Currently, however, there are no means of determining the achieved level of reliability in WRS and thus cost-optimization can not currently be performed. This is therefore one of the chief aims of this research.

2.6.1 Efficiency parameter

Research conducted by Van Nierop (2017) and later Van Nierop *et al.* (2017) considered the generic structural optimization versus the cost-optimization methods, both proposed by Rackwitz (2000) and applied them to case studies of SLS-governed design. Two WRS (long term, flexural and tension cracking) and a simply supported beam (SSB-deflection) were considered and the optimized β values from the generic versus the cost optimization were compared:

Table 2.5: Van Nierop (2017) comparison of results of β values for generic vs. case specific cost optimization methods.

Case Study	Mechanism	Generic	Unique Cost Optimization	
			Normal	Log-normal
WRS 1	Flexure	1.6	2.2	1.9
	Tension	1.7	2.2	2.1
WRS 2	Flexure	1.5	2.1	1.9
	Tension	1.7	2.3	2.2
SSB	Deflection	1.6	-	2.4

Table 2.5 shows that there is a discrepancy between the values obtained using the generic method and those obtained from a case-specific cost optimization method, and particularly so for the SSB. This led Van Nierop *et al.* (2017) to investigate this further and found that the discrepancy was due to the difference between the assumed efficiency of the generic decision parameter, versus the case specific decision parameter, at reducing the probability of failure, $\frac{dP_{f,SLS}(p)}{dp}$.

Given a highly efficient decision parameter, a higher β value is expected to be appropriate. This is confirmed in the case of the SSB: The decision parameter (height of the beam) has an exponent of the power of 3 and is thus highly effective at changing the probability of failure of the deflection limit state - The SSB has a case specific β value of 2.4, as opposed to a generic value of 1.5.

2.7 Reliability analysis methods

2.7.1 FORM

The First Order Reliability Method (FORM) is perhaps the most accessible, yet efficient and sufficiently accurate reliability analysis method, as confirmed by its use in EN 1990 (Holický, 2009). FORM is particularly useful for the analysis of structural reliability limit states (such as given in Equation 2.1, repeated here for convenience), to determine the probability of failure, measured by the reliability index, β . The action or load effect is the effect that needs to be resisted or withstood by the resistance. A wide range of reliability applications can be considered by the limit state equation, from a ULS case of applied axial load and axial resistance, to the deflection of a beam under SLS loading and the allowable deflection limit, to that of the leakage of water through a WRS and the code-defined allowable leakage. The resistance and action effects are comprised of a number of input parameters such as variable and permanent loads and material yield stresses, which are often modelled as probabilistic distributions.

$$g(X) = R(X) - E(X) \quad (2.11)$$

A FORM analysis makes use of a limit state equation as a method of measuring the level of reliability, by evaluating the limit state equation against pass or fail criterion. The limit state equation, $G(X)$, is defined as the difference between a resistance, $R(X)$, and an action effect, $E(X)$, sometimes denoted as $S(X)$. One, or both, of the resistance and action can be dependent on a number of input parameters $X = x_1, \dots, x_n$. The limit state equation $g(X) = R(X) - E(X)$ defines a safe and failure region, where $g(X)$ is positive ($R(X) > E(X)$) and negative ($R(X) < E(X)$), respectively. The points at which the resistance is equal to the action ($g(X) = 0$) form a curve called the failure plane, which divides the safe and failure regions. The input variables are transformed into standardized normal space $U = u_1, \dots, u_n$, as shown in Equation 2.12. The reliability index, β , is then defined as the shortest distance between the origin and the failure surface in the normalized space, $g(U) = 0$, mathematically given by Equation 2.13 and illustrated by Figure 2.2. The point on the $g(U) = 0$ curve closest to the origin is called the design point, or the most probable point of failure, u^* , and requires an iterative process to obtain convergence. The probability of failure can then be calculated from the β value.

$$u_i = \frac{x_i - \mu_{x_i}}{\sigma_{x_i}} \quad (2.12)$$

$$\beta = -\frac{\{D\}\{u^*\}}{\sqrt{\{D\}^T\{D\}}} \quad (2.13)$$

$$\{\alpha\} = \frac{1}{\beta} \cdot \{u^*\} \quad (2.14)$$

$$\text{with } \{D\} = \begin{Bmatrix} D_i \\ \dots \\ D_n \end{Bmatrix} ; \quad D_i = \frac{\partial G}{\partial X_i} \frac{\partial X_i}{\partial U_i}$$

Once u^* and β have converged, the array of direction cosines, otherwise known as sensitivity factors, $\{\alpha\}$, give an indication of the sensitivity of the model to variations in the input parameters (Equation 2.14). The sign conventions of EN 1990 are such that an increase in a parameter with a negative α value results in a decrease in the overall reliability of the model. Similarly, increases in parameters with positive α values cause an increase in the reliability of the model. In other research, however, the sign convention is sometimes reversed. Each input parameter has its own sensitivity factor ranging from -1 to 1. The closer the sensitivity factor is to 1 or -1, the more sensitive the model is to variation in that factor. Parameters with α values close to 0 have little influence on the model output and can often be replaced with deterministic values, thereby simplifying the model and reducing the computational effort required.

In structural design codes, various simplifications of reliability theory are made in order to be practically applicable, without losing the effect of standardization or comparability of implied reliability. Figure 2.2 illustrates the concept of the design point, for normally distributed action and resistance effects E and R , which has coordinates $(e_d/\sigma_E, r_d/\sigma_R)$ and is situated on the limit state function: $E/\sigma_E = R/\sigma_R$.

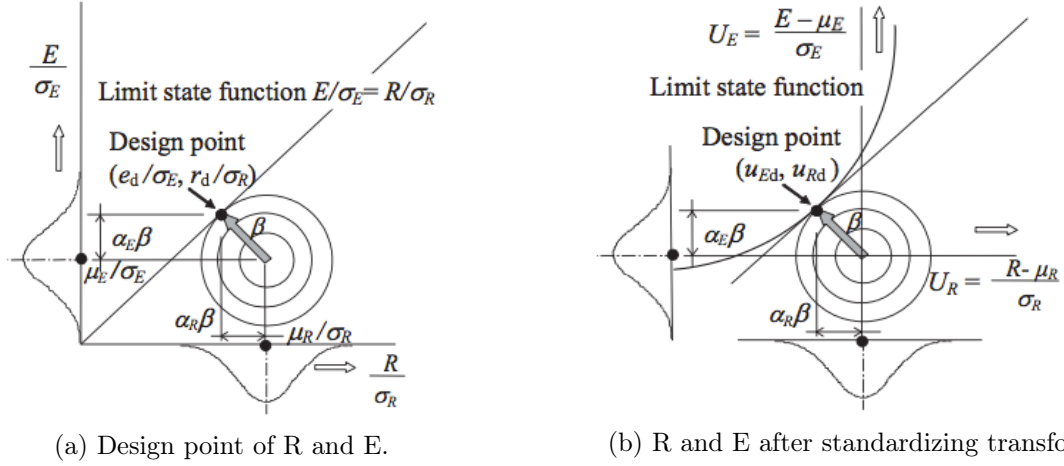


Figure 2.2: Visualization of FORM and design point in the standardized normal space, adapted [re-printed] from Holický (2009).

Further, conservative assumptions are made with regard to the FORM factors in the Eurocodes. Ideally, the sum of the squared α_E and α_R values should be unity but some intentional conservatism is included in the values shown below:

$$\alpha_E = -\sigma_E / \sqrt{\sigma_E^2 + \sigma_R^2} = -0.7 \quad (2.15)$$

$$\alpha_R = \sigma_R / \sqrt{\sigma_E^2 + \sigma_R^2} = 0.8 \quad (2.16)$$

Finally, the design values of E_d and R_d in non-normalized space and the probability of failure are given as:

$$P(E > E_d) = \Phi_U(+\alpha_E\beta) = \Phi_U(-0.7\beta) \quad (2.17)$$

$$P(R < R_d) = \Phi_U(-\alpha_R\beta) = \Phi_U(0.8\beta) \quad (2.18)$$

FORM analyses do have shortcomings, though. For complex limit states or those that consist of large numbers of random variables, convergence is not always guaranteed. Non-convergence can also be a problem where derivatives of the limit state equation approach asymptotic values.

2.7.2 Monte Carlo simulations

A Monte Carlo simulation (MCS) is arguably the simplest form of reliability analysis. Despite its simplicity, it is one of the most robust analysis methods and does not suffer from problems related to non convergence, like FORM analyses. MCS's also use a limit state equation with which to classify realizations as safe or failures. In contrast to FORM analyses, MCS's use a brute-force approach, whereby sample averages stabilize with large numbers of repetitions. Following this approach, a large number of random realizations are sampled from each of the probabilistic distributions in the resistance and action terms and the limit state is evaluated for each of these. The sampling is repeated until some β or p_f convergence criteria is satisfied. Typically though, this requires a considerable number of realizations, which for simple limit states is ideal. If the limit state is complex and requires intensive computational effort, however, the analysis is often very time-consuming. This is usually the case for

FEM applications, for example, where each evaluation of the limit state requires a FEM analysis.

A MCS is attractive because of its simplicity and accessibility, but is less informative than a FORM analysis, as the only output obtained from the analysis is a probability of failure and consequently, a β value. The probability of failure, p_f , of a MCS is simply calculated as the number of repetitions that fail, n_f , as a fraction of the total number of repetitions, n .

$$p_f = \frac{n_f}{n} \quad (2.19)$$

Furthermore, for applications where the probability of failure is very small, such as for ULS applications, the required number of evaluations of the limit state can easily run into the millions. The number of analysis repetitions required in order to achieve convergence in p_f is a debated topic, with no one limiting criterion being applicable to all cases. One approach is to determine the number of repetitions required, based on the the expected p_f and the CoV associated therewith. This has obvious shortcomings in that often, neither the range within which the p_f lies, nor the CoV is known beforehand. Thus, a sample number of repetitions need to be carried out to estimate these parameters. If the initial sample is too small, the required number of iterations can be under or over predicted by several orders of magnitude, especially for large β values. Nevertheless, this approach is useful in situations where the approximate p_f and CoV value is known a-priori. Lemaire *et al.* (2009) estimates the required number of repetitions as shown in Equation 2.20, and Table 2.6.

$$CoV = \sqrt{\frac{1 - p_f}{n \cdot p_f}} \quad (2.20)$$

Table 2.6: Number of repetitions required for p_f convergence, as a function of CoV and p_f , based on Lemaire *et al.* (2009)

CoV	Probability of failure / β value						
	0.5/0	0.3/0.52	0.1/1.28	0.05/1.64	$10^{-2}/2.33$	$10^{-3}/3.09$	$10^{-4}/3.72$
0.05	400	933	3600	7600	39600	399600	4×10^6
0.1	100	233	900	1900	9900	99900	0.99×10^6
0.2	25	58	225	475	2475	24975	0.25×10^6
0.3	11	26	100	211	1100	11100	0.11×10^6
0.5	4	9	36	76	396	3996	39996

Table 2.6 shows the required number of iterations, for various values of CoV and p_f , using Equation 2.20. As the β value increases to ULS-application levels ($3 < \beta$), the number of repetitions required to achieve convergence increases sharply. This is especially so for cases where the CoV is low. A MCS is unlikely to be useful in such cases, unless the limit state is computationally-cheap to evaluate. For SLS cases where the β value is lower ($\beta \approx 2$) and for cases of higher variation, such as concrete cracking, a MCS is an attractive method of reliability analysis.

2.8 Statistical distributions

Due to the focus on risk and reliability in this research, four main statistical distributions are used and are summarized here.

2.8.1 Normal distribution

A normal distribution is a symmetric distribution valid on the interval $-\infty < x < \infty$, which often makes it undesirable for applications where $0 < X$. It is frequently used for self weight loads, geometrical properties and material properties (Holický, 2009). It is symbolically denoted as $X \sim N(\mu, \sigma^2)$, where μ is the mean and σ is the standard deviation. The probability density function is given by Equation 2.21 and illustrated in Figure 2.3.

$$f(x) = \frac{1}{\sigma\sqrt{2\pi}} \cdot \exp\left[-\frac{1}{2}\left(\frac{x-\mu}{\sigma}\right)^2\right] \quad (2.21)$$

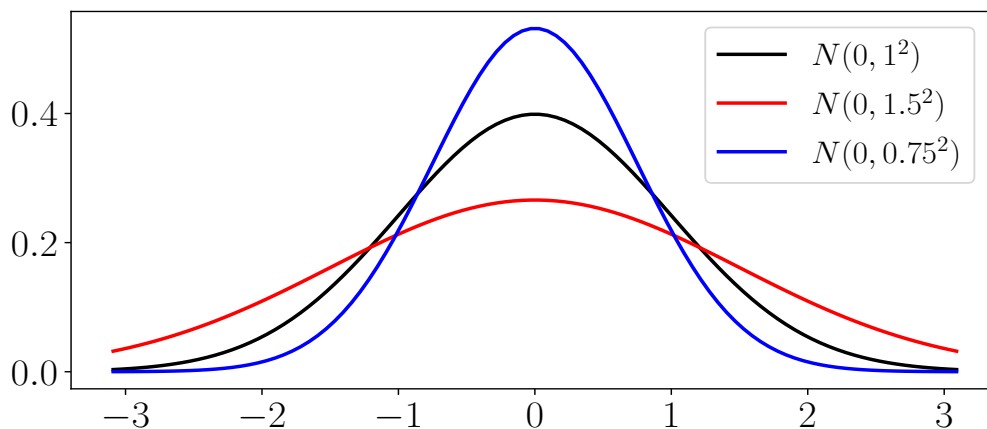


Figure 2.3: Illustration of normal distribution with varying standard deviations.

2.8.2 Lognormal distribution

A 2-parameter lognormal distribution is an asymmetrical distribution valid for the interval $0 < x < \infty$ and is thus useful for cases where a parameter cannot be a negative number, such as material strengths and model factors. It is denoted by $X \sim LN(\mu, \sigma^2)$, where μ and σ are the mean and standard deviation of the logarithm of X . The probability density function is given by Equation 2.22, where σ and m are shape (and standard deviation of the log of the distribution) and scale parameters, respectively, and illustrated in Figure 2.4.

$$f(x) = \frac{1}{x\sigma\sqrt{2\pi}} \cdot \exp\left[-\frac{1}{2}\left(\frac{(\ln(x/m))^2}{\sigma^2}\right)\right] \quad (2.22)$$

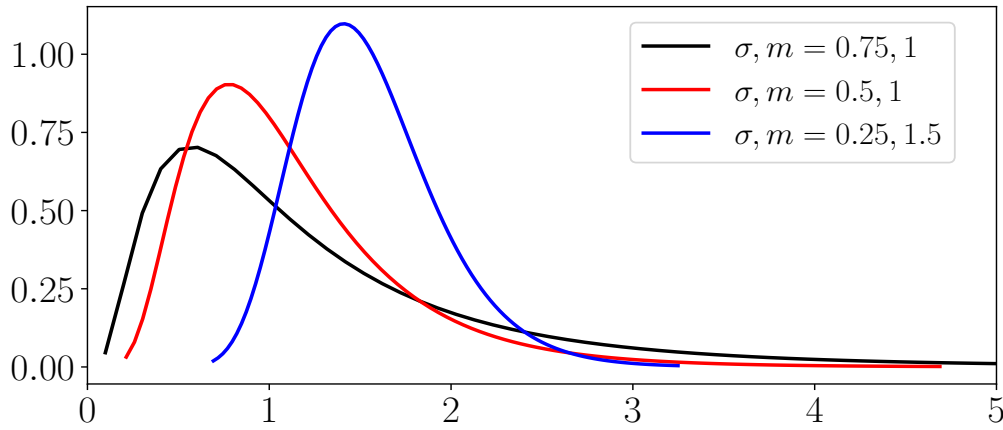


Figure 2.4: Illustration of lognormal distribution with varying shape and scale parameters.

2.8.3 Weibull distribution

The 2-parameter Weibull distribution is also an asymmetrical distribution and is highly versatile. A Weibull distribution is typically used for extreme loading, but is often used for other phenomenon, due to its flexibility. The probability density function is given as shown in Equation 2.23, where β and γ are the shape and scale parameters, respectively. Note that a number of different parametrizations of the Weibull distribution exist.

$$f(x, \gamma, \beta) = \frac{\beta}{\gamma} \left(\frac{x}{\gamma}\right)^{\beta-1} \cdot \exp \left[-\left(\frac{x}{\gamma}\right)^{\beta} \right] \quad (2.23)$$

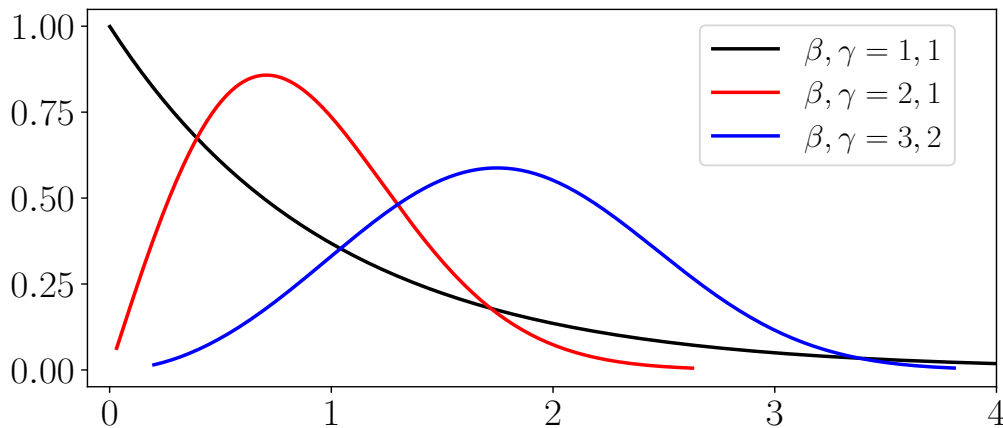


Figure 2.5: Illustration of Weibull distribution with varying shape and scale parameters.

2.8.4 Continuous uniform distribution

A continuous uniform distribution is used when each point on an interval $i \leq x \leq j$ has an equal probability density. It thus has a constant probability density function given as $f(x) = 1/(j - i)$

3. Water Retaining Structures

Literature Review

The design of RC WRS is governed by SLS considerations, particularly designing to limit cracking to acceptable levels. While the occurrence of cracking is undesirable aesthetically and practically (in the case of WRS to prevent leakage), it is usually inevitable. The degree and extent to which a structure cracks, in terms of the spacing and width of cracks, can be controlled through proper design (Pillai and Menon, 2003). Cracking in concrete is usually classified as being either mechanically load-induced or restraint induced. The extent of load-induced cracking is dependent on the applied moments and forces that a structure experiences. Restraint cracking on the other hand, is caused by the restraint conditions present in the structure, combined with thermal and temperature fluctuations. This research is specifically concerned with load-induced cracking in non-prestressed, reinforced concrete, but will include the strain effects of free shrinkage on crack widths.

3.1 Geometry and loading of WRS

The loading on WRS is relatively simple in comparison to most other structures where uncertain, variable loads dominate. The main loading is naturally due to the height of retained water, as shown in Figure 3.1, assuming no external earth pressure. The triangular, hydrostatic loading is predictable with a high level of certainty, being dependent only on the height and unit weight of the retained water as a variable. The height of water is physically constrained by the height of the walls. This leads to the consideration of the water load as being quasi-static; It is easily predicted with little variation in intensity, as the water weight, γ_w , is constant.

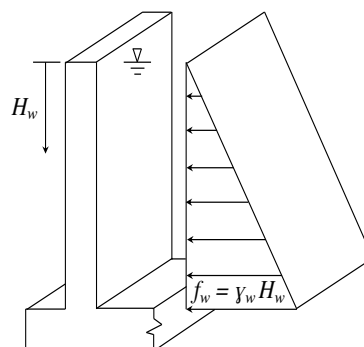


Figure 3.1: Hydrostatic water load acting on a WRS wall section.

Containment structures for liquids are usually rectangular, square or cylindrical in shape as shown in Figure 3.2, sometimes with roofs, in the case of water reservoirs and sometimes without, as in the case of aerating tanks in water treatment plants. Cylindrical geometries are usually preferred, as they make

the most efficient use of materials (Alfanda and Farouk, 2017), though rectangular WRS are often used in cases where site geometry prevents the use of cylindrical shapes or where the WRS are required to be compartmentalized. The behaviour of these two structural shapes are notably different from one another.

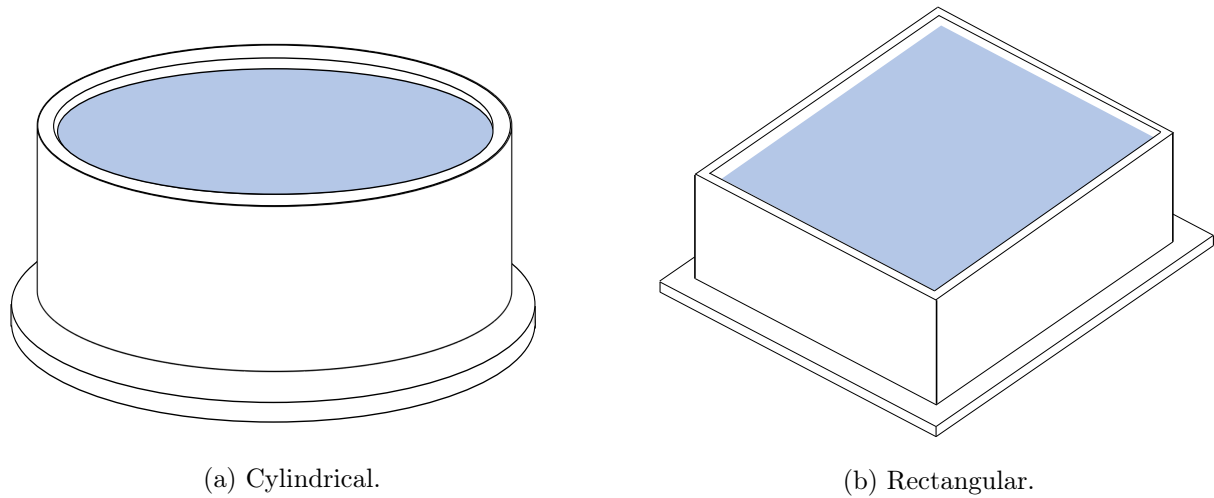


Figure 3.2: Typical shapes of reinforced concrete water retaining structures.

Round or cylindrical WRS are governed by circumferential hoop-tension forces, caused by the hydrostatic load acting on the height of the wall, throughout the circular form of the structure, as shown in Figure 3.3. Flexural stresses develop along the height of the wall, depending on the type of base restraint, but these are secondary and are less onerous than the circumferential tension stresses. Consequently, this type of retaining structure relies predominantly on the tensile resistance of the reinforced concrete to withstand the forces created by the hydrostatic load. The main reinforcing is placed in a radial direction and the secondary reinforcing placed in a vertical plane. Although the analysis of a cylindrical WRS is initially more complex than that of a rectangular one, the wall cross-section is usually uniform across its circumference and thus one cross section is designed and is used throughout the structure.

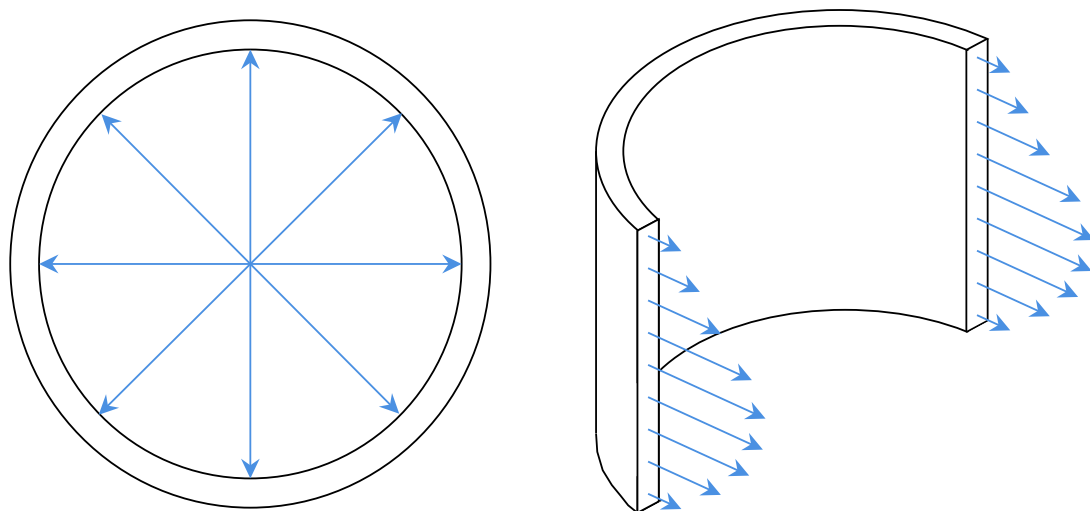


Figure 3.3: Illustration of circumferential hoop tension forces in circular WRS from hydrostatic load. Plan view (left) and isometric (right).

Rectangular WRS on the other hand (Figure 3.4), are usually based on a combination of cantilever retaining wall and two-way spanning slab design, whereby flexural stresses primarily govern the design. The walls are typically thicker than those in cylindrical WRS and often taper off from being thicker at the base, where the applied moment is at a maximum, to being thinner at the top of the wall. Secondary, longitudinal tension forces develop in the walls at mid span and at corners. Shear at the wall base and at corners should also be considered. As flexure is the governing action, the main reinforcing is placed in a vertical plane and the secondary reinforcing is placed longitudinally. Rectangular WRS design is usually more laborious than a cylindrical equivalent, as a number of wall sections need to be designed and detailed (corner sections, mid-span sections etc.).

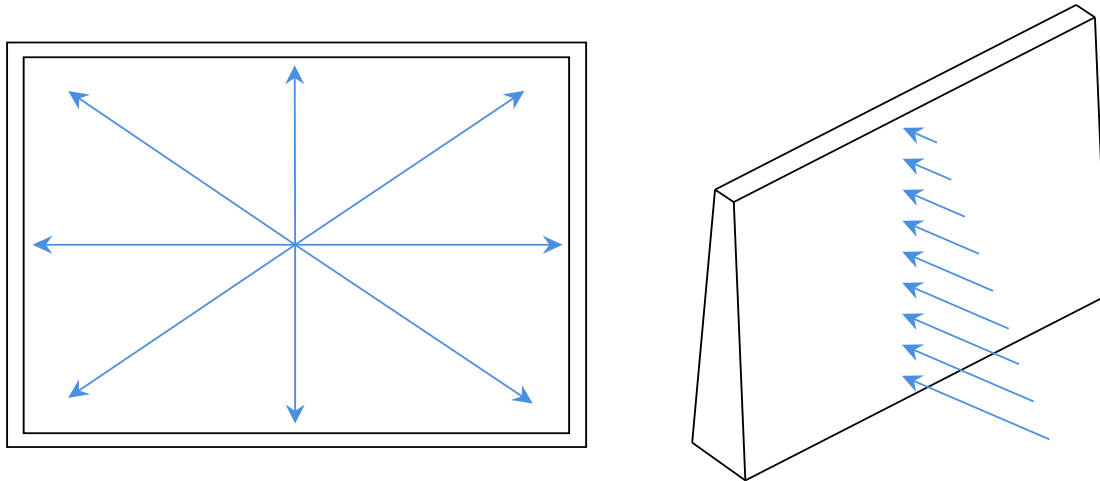


Figure 3.4: Illustration of flexure inducing forces in rectangular WRS from hydrostatic load. Plan view (left) and isometric (right).

Three different base restraint conditions are typically used in cylindrical WRS; fixed, pinned or sliding, although sliding bases are usually only used for prestressed concrete designs. Pinned bases are used more frequently than fixed bases, as the reinforcing layout required for a fixed base is more material, labour and time intensive. The elasticity of the soil underlying the foundation also allows a degree of rotation, except when the bases are founded on rock, or are piled. Typical reinforcing details do provide a measure of restraint against wall rotation, but not enough to be considered fixed, indicating that in reality, base restraint conditions are in between the fixed and pinned cases. Due to the thinner walls and thus narrower interface between the base and walls in cylindrical WRS, the base restraint is typically closer to pinned than fixed. Base restraint in rectangular WRS can only be fixed or pinned. As the walls are typically thicker at the base, the reinforcing layout is such that a greater degree of fixity against wall rotation is realized than in cylindrical WRS. The base restraint affects the distribution of flexural and tensile stress along the height of the wall (Anchor, 1992), as will be discussed in further detail in chapter 6.

3.2 Cracking in concrete structures

Cracking in reinforced concrete results as a consequence of the comparatively low tensile strength of concrete, compared to its compressive strength (usually around 10%). Reinforcing steel is therefore embedded in the concrete, however, the reinforcing only starts to carry significant tensile load once the concrete has started to crack. Design codes usually prescribe guidelines for the calculation and

limitation of crack widths, depending on a number of variables such as applied moment, tensile stress, element geometry and environment, amongst others.

In general structures, the limiting of design crack width, w , to below a specified crack width limit, w_{lim} , is desirable for one of three reasons:

- To prevent the onset of corrosion and subsequent damage to the reinforcing and concrete;
- To prevent the unsightly staining of concrete faces or
- To prevent or limit leakage through cracks.

Crack width limits in the design of WRS specifically are primarily aimed at ensuring water tightness and to protect the aesthetic appearance of the concrete faces from unsightly staining. There seems to be little consensus among researchers around whether the limiting of crack widths also functions as a corrosion protection measure or not. A comprehensive review of the effect of cracking on reinforcing corrosion by Shaikh (2011) confirms that over the years, a number of research projects have considered the topic in WRS. A fairly equal number of researchers for and against the notion exist but for cracking transverse to loading "*It can also be seen that in a broader scale no relationships between the crack widths and corrosion can be established*". This research therefore only considers the effect of crack width limits on water tightness.

3.3 Crack width calculation models

Design codes vary in their depth of detail when considering the calculation of crack widths. Three different models of load-induced cracking are considered in the following section, namely those used in EN 1992-1-1/EN 1992-3, BS 8007 and the *fib* Model Code 2010. The theory between various crack prediction models differ on certain points, however, the underlying basis is largely the same and especially so for EN 1992-1-1 and MC 2010. With reference to Figure 3.5, the general form of the calculation of crack widths is given by Equation 3.1. The crack width is given by the difference in strain between the steel and the concrete (black and blue lines in Figure 3.5, respectively), integrated over the transmission length, l_0 , on either side of the crack.

$$w = \int_{-l_0}^{l_0} (\epsilon_s - \epsilon_c) dl \quad (3.1)$$

From this general form, a simplification is made in EN 1992-1- and MC 2010 to use the average steel and concrete strain (ϵ_{sm} and ϵ_{cm} , respectively), to avoid the integration over the complex shape of the steel and concrete strains. In addition, assuming a maximum spacing of $S_{r,max}$ (EN 1992-1-1 or $2l_{s,max}$ in MC 2010) occurs between cracks in the stabilized cracking stage, the maximum design crack width will be realised, and is given by:

$$w_{max} = \int_{-s_{mean}}^{s_{mean}} (\epsilon_{sm} - \epsilon_{cm}) dl \quad (3.2)$$

$$= S_{r,max} \cdot (\epsilon_{sm} - \epsilon_{cm}) \quad (3.3)$$

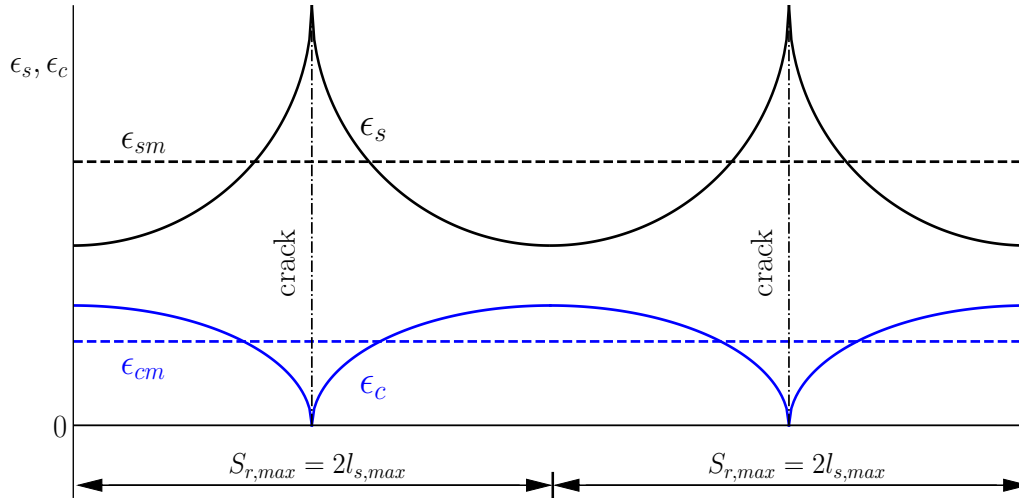


Figure 3.5: Illustration of mechanics involved in the calculation of maximum crack width.

Most crack prediction models stem from this general form. The following subsections detail the specifics of each model.

3.3.1 EN 1992-1-1/1992-3 Crack model

The EN 1992-1-1 crack model is based on a combination of slip and no-slip theory. EN 1992-1-1 differentiates between cracking due to pure tension and flexure related load-induced cracking through the k_2 factor in the formulation of the crack spacing. The EN 1992-1-1 calculation of crack width, w_k , is shown in Equation 3.4. The crack width is dependent on the maximum crack spacing, $S_{r,max}$. Assuming that the reinforcement spacing is relatively close ($\leq 5(c + \frac{\phi}{2})$), where c is the concrete cover and ϕ is the reinforcing bar diameter (assuming only one diameter of bar is used), $S_{r,max}$ is calculated from Equation 3.5.

$$w_k = S_{r,max}(\epsilon_{sm} - \epsilon_{cm}) \quad (3.4)$$

$$S_{r,max} = k_3c + k_1k_2k_4\phi/\rho_{p,eff} \quad (3.5)$$

Where:

- $\epsilon_{sm} - \epsilon_{cm}$ Difference between mean reinforcing- and concrete strain

$$= \frac{\sigma_s - k_t \frac{f_{ct,eff}}{\rho_{p,eff}} (1 + \alpha_e \rho_{p,eff})}{E_s} \geq 0.6 \sigma_s / E_s$$
- σ_s Stress in tension reinforcing assuming a cracked section
 k_t Factor depending on duration of load: 0.6 for short term ; 0.4 for long term
 $f_{ct,eff}$ Tensile strength of concrete at time of first crack = f_{ctm} for $28d < t$
 f_{ctm} Mean concrete tensile resistance
 $\rho_{p,eff}$ Reinforcing ratio = $A_s / A_{c,eff}$
 $A_s ; A_{c,eff}$ Effective area of reinforcing ; concrete in tension
 α_e Modular ratio of reinforcing to concrete = E_s / E_{cm}
 k_3 & k_4 Coefficients from National Annexes = (3.4 and 0.425), respectively
 k_1 Coefficient that takes into account the bond properties of the reinforcement
 = 0.8 for high bond bars ; 0.6 for plain surfaced bars
 k_2 Coefficient for the strain distribution = 0.5 for bending ; 1.0 for pure tension

A plan-view illustration of the reinforcing layout in a typical concrete member subjected to pure tension is shown in Figure 3.6. In the stabilized cracking phase, as assumed by both EN 1992-3 and MC 2010, the maximum crack spacing between any two cracks in a member is given by $S_{r,max}$ (or $2l_{s,max}$, as defined in MC 2010). A more detailed discussion of concrete cracking is given in section 6.3. In the case of a tension-governed RC WRS, the longitudinal (or circumferential) reinforcing bridges the cracks, whereas the vertical reinforcing bridges the cracks in a retaining wall-style, flexure-governed structure.

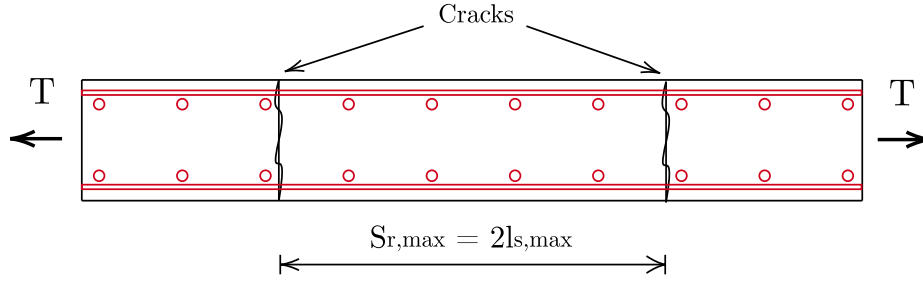


Figure 3.6: Plan-view illustration of concrete cracking and layout of reinforcing.

3.3.2 *fib* Model Code 2010 crack model

The *fib* Model Code 2010 (MC 2010) is a state-of-the-art code created by the International Federation for Structural Concrete (Fédération internationale du béton - *fib*). Many of the principles in MC 2010 are similar to EN 1992-1-1 as the predecessor of MC 2010, Model Code 1990, was used as a basis for parts of EN 1992-1-1. As such, the design crack width formulation of MC 2010 is also based on bond-slip theory and has a similar form to that of EN 1992-1-1. MC 2010 differentiates between cracking in the short and long term, similarly to EN 1992-1-1 but it also differentiates between different stages of cracking (formation and stabilized). The formulation below has been rearranged for the purpose of comparison with the formulation in EN 1992-1-1. The design crack width is given by Equation 3.6. The crack width calculation is also dependent on the length over which slip between concrete and steel occurs, $l_{s,max}$. Note that $\rho_{s,ef} = \rho_{p,eff}$.

$$w_d = 2l_{s,max} (\epsilon_{sm} - \epsilon_{cm} - \epsilon_{sh}) \quad (3.6)$$

$$l_{s,max} = kc + \frac{1}{4} \frac{f_{ctm}}{\tau_{bms}} \frac{\phi_s}{\rho_{s,ef}} \quad (3.7)$$

Where:

$$\epsilon_{sm} - \epsilon_{cm} - \epsilon_{sh} = \text{Mean steel strain} - \text{mean concrete strain} - \text{free shrinkage strain}$$

$$= \frac{\sigma_s - \beta \frac{f_{ctm}}{\rho_{s,ef}} (1 + \alpha_e \rho_{s,ef})}{E_s} + \eta_r \epsilon_{sh}$$

k Empirical parameter to incorporate the effect of the concrete cover = 1

τ_{bms} Bond stress between concrete and steel reinforcing

β Empirical coefficient to assess the mean strain over $l_{s,max}$

η_r Coefficient to consider the contribution of shrinkage

3.3.3 BS 8007 crack model

BS 8007 is a (now dated) British code, first published in 1987. Despite its considerable age, it is still widely used in particularly third world and emerging third-world countries. The crack model is based on slip theory, but is also empirical in nature. The design crack width (w) and spacing (s_{max}) are calculated as shown below. Note that $\rho = \rho_{s,ef}$, $f_{ct} = f_{ctm}$ and $f_b = \tau_{bms}$.

$$w = \frac{3 a_{cr} \epsilon_m}{1 + 2 \left(\frac{a_{cr} - c}{h - x} \right)} \quad \text{in flexure} \quad (3.8)$$

$$w = 3 a_{cr} \epsilon_m \quad \text{in pure tension} \quad (3.9)$$

$$s_{max} = \frac{f_{ct}}{f_b} \cdot \frac{\phi}{2\rho} \quad (3.10)$$

Where:

$$\begin{aligned} \epsilon_m &= \epsilon_1 - \epsilon_2 \\ &= \text{Strain at crack, less the tension-stiffening effect of concrete} \\ a_{cr} &= \text{Furthest distance from crack to nearest reinforcing bar surface} \end{aligned}$$

3.4 Comparison of prevalent load-induced crack models

The assessment of prevalent load-induced crack models requires consideration of the nuances of each model and the differences between them. For the purposes of comparison, the three models are summarized in Table 3.1.

Table 3.1: Crack model comparison summary

	BS 8007	EN 1992-1-1	MC 2010
Crack width	$w = \left[\frac{3 a_{cr} \epsilon_m}{1 + 2 \left(\frac{a_{cr} - c}{h - x} \right)} \right]^*$	$w_k = S_{r,max} (\epsilon_{sm} - \epsilon_{cm})$	$w_d = 2l_{s,max} (\epsilon_{sm} - \epsilon_{cm} - \epsilon_{sh})$
Crack Spacing	$s_{max} = \frac{f_{ct}}{f_b} \cdot \frac{\phi}{2\rho}$	$S_{r,max} = k_3 c + k_1 k_2 k_4 \frac{\phi}{\rho_{p,eff}}$	$2l_{s,max} = 2 \left[kC + \frac{1}{4} \frac{f_{ctm}}{\tau_{bms}} \cdot \frac{\phi_s}{\rho_{s,ef}} \right]$
Strain	$\epsilon_m = \epsilon_1 - \epsilon_2 = \frac{(h-x)}{E_s(d-x)} \left[f_s - \frac{b_t(h-x)}{3A_s} \right]^\dagger$	$\epsilon_{sm} - \epsilon_{cm} = \left[\frac{\sigma_s - k_t \frac{f_{ct,eff}}{\rho_{p,eff}} (1 + \alpha_e \rho_{p,eff})}{E_s} \right]^\ddagger$	$\epsilon_{sm} - \epsilon_{cm} - \epsilon_{sh} = \frac{\sigma_s - \beta \frac{f_{ctm}}{\rho_{s,ef}} (1 + \alpha_e \rho_{s,ef})}{E_s} + \eta_r \epsilon_{sh}$

* Only for flexure case

† Only for flexure case for $w_{lim} = 0.2\text{mm}$

‡ Must be $\geq 0.6 \frac{\sigma_s}{E_s}$

3.4.1 Differentiation between flexure and tension

One of the more contested topics around crack width models is whether or not the same formulation can be used to describe both tension and flexure-induced cracking. Both BS 8007 and EN 1992-1-1 differentiate between the two and have a factor of 2 differentiating between tension and flexure. This

stems from the definition of the distribution of strain.

The assumption made in the derivation of the BS 8007 and EN 1992-1-1 formulations is that due to the nature of flexure - with reference to Figure 3.7 (a), the force that needs to be transmitted to the concrete through bond (in order to produce a new crack) for flexure is half of that for tension (Caldentey, 2017). This is reflected in the k_2 factor in the crack spacing equation of EN 1992-1-1 (varied between 0.5 and 1 for flexure and tension, respectively) and similarly for the tension-stiffening terms for flexure and tension in BS 8007.

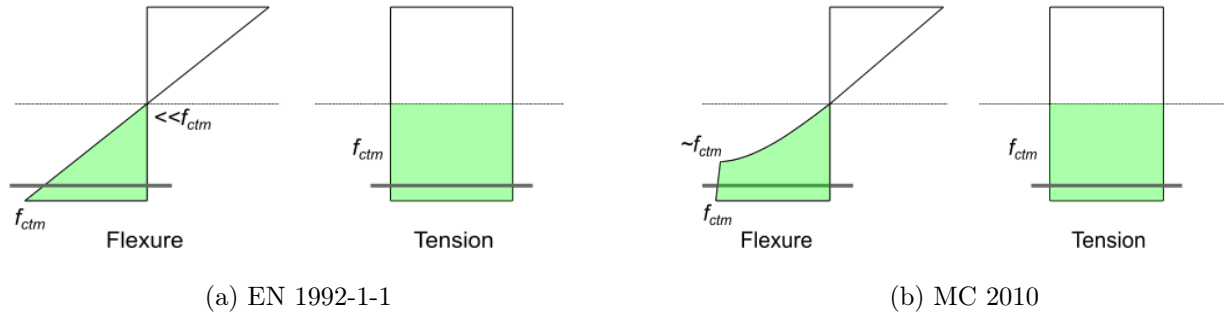


Figure 3.7: Difference in strain distribution assumptions.

A different assumption is made in MC 2010; irrespective of whether the section is in flexure or tension. An area of concrete forms directly around the reinforcing bars, within which there is minimal variation in concrete stress and thus little difference between flexure and tension with reference to Figure 3.7 (b) (Caldentey, 2017). Thus in the MC 2010 formulation, there is no differentiation between flexural and tension induced cracking. Results from research by McLeod (2019) indicate that the MC 2010 assumption produces better predictions of crack width, when compared to experimental results.

3.4.2 Prediction of crack spacing

The base assumptions in the mechanics of crack spacing are fairly similar for all three codes. Both EN 1992-1-1 and MC 2010 are based on slip theory, but include a facet of no-slip theory, whereas BS 8007 is based exclusively on slip theory. All assume that, from slip theory, once the loading has increased to a point where the bond strength between the concrete and the reinforcing is exceeded, a "slip" occurs and the first crack forms. This assumes that plane sections remain plane and that the crack faces remain parallel to one another.

At this point, the strain in the concrete is relieved and completely transferred to the reinforcement. The tensile stress is transferred from the reinforcing to the concrete through bond stress (τ_{bms}) away from the crack. At a distance L_0 ("transfer length"), away from the initial crack, the concrete strain is unaffected by the crack (Hendy and Smith, 2013). Another crack can then form at any distance $> L_0$ away from the first crack. The maximum spacing is given as $2L_0$, as a spacing greater than $2L_0$ will allow the formation of another crack in between. This pattern continues until the maximum spacing of all cracks is less than $2L_0$, after which further increases in load will not cause any more cracks to occur. This is commonly referred to as the stabilized cracking stage. The transfer length according to slip theory (L_{slip}) is defined by Equation 3.11, where f_b is the bond stress between concrete and steel, equivalent to τ_{bms} in Equation 3.7. Equation 3.11 appears in the crack spacing equation of all three codes, with slightly different notation. BS 8007 uses this directly and assumes a maximum spacing of

$2L_{slip}$, as seen in Table 3.1. MC 2010 uses this term directly in conjunction with a contribution from no-slip theory, as detailed below, as does EN 1992-1-1. In EN 1992-1-1, the $f_{ct}/4f_b$ term is accounted for within factors k_1 and k_4 .

$$L_{slip} = \frac{f_{ct}}{f_b} \frac{\phi}{4\rho} \quad (3.11)$$

Other researchers believe that the transfer length is based solely on no-slip theory. According to this theory, no physical slip occurs and that cracks are caused by elastic shear deformation (sometimes called "shear lag") in the concrete, i.e that plane sections do not remain plane in the concrete area adjacent to a crack (Tan *et al.*, 2018). The transfer length is thus solely a function of the concrete cover. The inclusion of a term from no-slip theory was originally suggested in a research report on crack control characteristics of reinforcing bars by Base *et al.* (1966). Equation 3.12 gives the general form and implies that crack widths vary through the cover, being widest at the concrete surface and smallest at the interface between the concrete and reinforcing. Both EN 1992-1-1 and MC 2010 include an effect of concrete cover on the transfer length that can be calibrated, adding a semi-empirical element to the formulations, as can be seen in Equation 3.12.

$$L_{noslip} = kc \quad (3.12)$$

The general combination of slip and no-slip theory to describe the transfer length is shown in Equation 3.13. The inclusion of the cover term is used as a compromise between slip and no-slip theory to more accurately predict transfer length (Tan *et al.*, 2017). This seemingly incompatible mix of two opposite theories is perhaps "unscientific", however, it is widely accepted in predicting the transfer length better than either slip or no slip theory alone (Balázs and Borosnyói, 2005).

$$L_{combined} = kc + \frac{f_{ct}}{f_b} \frac{\phi}{4\rho} \quad (3.13)$$

By comparison of Equations 3.13, 3.7 and 3.6 it is clear that MC 2010 uses this formulation directly and defines the maximum crack spacing as double the combined-theory transfer length. The k value defined in MC 2010 is an empirical parameter that can be calibrated but will more than likely be taken as unity as a simplification, as suggested in MC 2010. EN 1992-1-1 uses a similar formulation, except that it defines the mean crack spacing (S_{rm}) as being 1.5 times the minimum crack spacing ($S_{r,min}$ - equivalent to the transfer length, using slip-theory, L_s), although many researchers have proposed different values (Balázs and Borosnyói, 2005). The maximum is then defined as crack spacing having a 5% probability of exceedance (Beeby and Narayanan, 2009). It was found experimentally that the maximum crack width is obtained by multiplying the mean value by ≈ 1.7 , thus achieving the 95% fractile. This is commonly assumed to be because crack widths are normally distributed and that the conversion from a mean value to a 95th percentile is ≈ 1.65 . This is uncertain, however, as crack widths were experimentally found to be lognormally distributed (Balázs and Borosnyói, 2005). This is investigated further in this research. EN 1992-1-1 places more of an emphasis on the effect that the cover term plays in the crack spacing and as such, defines that $k = 2$. From this, the factors defined in the EN 1992-1-1 crack spacing formulation (Equation 3.5) are realised.

3.4.3 Idealized approximation of cracking stages

In concrete, three distinct stages of cracking exist, depending on the magnitude of the loading: the uncracked, crack formation and stabilized cracking stages. It is important to distinguish which state the concrete is in, as the calculation of strain difference differs for each stage. Consider the *idealized* assumption of concrete cracking due to a tension force from the theory in MC 2010 and EN 1992-1-1, as illustrated in Figure 3.8 (Comparable to Figure 7.6-2 in MC 2010). The mean tensile resistance of the concrete section, $T_{r,m}$, is calculated using the mean value of concrete tensile strength, f_{ctm} , as per Equation 3.14. When the applied tension, T , is below $T_{r,m}$ the concrete is in the uncracked stage, and no cracks form. When tension is exactly equal to the $T_{r,m}$ value, the concrete enters the crack formation stage, shown by the horizontal line (2) in Figure 3.8. Here, cracks form rapidly and at random along the concrete element, but do not widen. When the tension is greater than $T_{r,m}$, the concrete enters the stabilized cracking stage. In this stage, and the spacing between any two cracks is less than $2l_{s,max}$ and no more cracks form, but the existing cracks widen as the load increases. This idealization thus assumes piecewise behaviour in that the concrete is either in the uncracked or stabilized cracking phase.

$$T_r = A_{c,ef} \cdot f_{ct}(1 + \alpha_e \rho_{s,ef}) \quad (3.14)$$

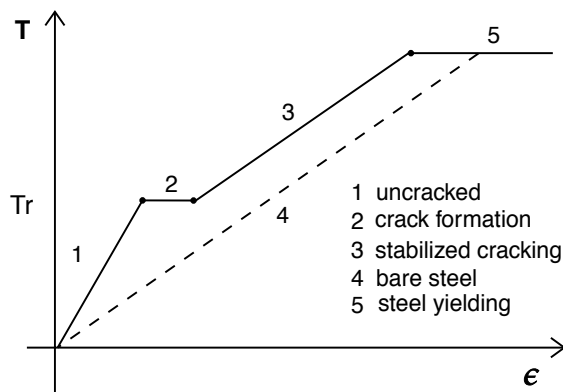


Figure 3.8: Idealized cracking stages, assumed by MC 2010 and EN 1992-1-1.

3.4.4 Model uncertainty of crack prediction models

Every theory-based model used to predict real-life phenomenon contains a measure of uncertainty, whether aleatory, epistemic or a combination of both. The models used to predict crack widths are no different. The uncertainty in these models is predominantly due to the considerable aleatory uncertainty present in reinforcing concrete cracking applications. Thus, a model uncertainty factor is used to account for the variation in the prediction of the crack widths using the models.

Little research has been conducted into characterizing model factors for crack width prediction models for EN 1992-1-1 and MC 2010. The need to effectively analyse the short and long term for both flexure and tension requires a large number of test samples, which has limited research in this regard. The case of the prediction of long term cracking has received particularly little attention, due to the requirement of both a large number of samples and a long test duration.

McLeod (2019) conducted research into the model uncertainty of various crack-prediction models, including MC 2010 and EN 1992-1-1. McLeod investigated the experimental vs predicted crack width (w_{exp}/w_{pred}). In effect, the research describes how well the crack prediction model predict a crack width, given typical input parameters. McLeod removed forms of bias in the crack prediction equations, so as to get an indication of the accuracy of the prediction of values of maximum crack width. Research by Lapi *et al.* (2018), investigated the same. Both researchers compiled a database of experimental samples tested by other researchers and used the databases to evaluate the predictions of both crack models. McLeod considered both long and short term crack prediction for cases of tension and flexure, whereas Lapi *et al.* only considered short term cracking, for a combination of tension and flexure. Tan *et al.* (2018) cast a smaller set of experimental samples and also investigated both formulations. The results of their research are summarized in Table 3.2.

Table 3.2: Model factor (w_{exp}/w_{pred}) mean / CoV for EN 1992-1-1 and MC 2010 from literature.

		Author		
		McLeod (2019)	Lapi <i>et al.</i> (2018)	Tan <i>et al.</i> (2018)
EN 1992-1-1	Flexure St	1.11 / 0.38	1.04 / 0.31	-
	Tension St	0.74 / 0.25		0.54 / 0.32
	Flexure Lt	1.44 / 0.33	-	-
	Tension Lt	0.89 / 0.25	-	-
MC 2010	Flexure St	1.05 / 0.38	1.06 / 0.32	-
	Tension St	0.98 / 0.32		0.93 / 0.40
	Flexure Lt	1.13 / 0.38	-	-
	Tension Lt	0.99 / 0.22	-	-

The results from Lapi *et al.* were defined as the inverse of McLeod which, when redefined as w_{exp}/w_{pred} , found a mean and CoV for short term cracking to EN 1992-1-1 of 1.04 and 0.31, respectively. McLeod found a notable difference between short term flexure and tension to EN 1992-1-1, in that cracks in flexure were slightly under-predicted and that cracks in tension were over-predicted, albeit with less variation than for flexure. The results from Tan *et al.* for tension in the short term are in agreement with McLeod (2019) in that the EN 1992-1-1 model notably over-predicts tension in the short term. Considering long term cracking, McLeod found that EN 1992-1-1 under-predicted flexural cracks and slightly over-predicted tension cracks.

For MC 2010, Lapi *et al.* found an almost identical mean and CoV to that of EN 1992-1-1. Tan *et al.*'s results for MC 2010 showed agreement with results from McLeod. The CoV of around 0.3 is comparable to that of concrete shear applications, where CoV values range from 0.2-0.3 (Holický *et al.*, 2016). McLeod's results showed a more consistent prediction across the entire cracking spectrum using the MC 2010 model, though with a slightly higher variation than EN 1992-1-1.

The inconsistency in the prediction of long term cracking in EN 1992-1-1 comes as a result of the crack model not considering the free shrinkage strain in concrete that consists of autogenous and drying shrinkage. As a result of this, the revision of EN 1992-1-1 that is currently in progress will be adopting the MC 2010 crack prediction model with a few minor adjustments (Caldentey, 2017).

3.5 Leakage-related considerations in water retaining structures

3.5.1 Leakage

The main function of water retaining structures is to retain water. As will be discussed later in section 3.5.2, ensuring absolutely no leakage is unreasonably expensive, if at all possible without employing the use of waterproofing membranes or prestressing. Thus and due to the potential for self-sealing of cracks as discussed later in section 3.6.1, it is often more preferable to allow an initial degree of leakage, as long as the leakage is not excessive and that it stops or reduces to insignificant levels within a reasonable time-period.

In light of this, most water retaining structure design codes define liquid tightness classes, with an associated prescription of crack width limit. An example of such tightness classes, from EN 1992-3, is shown in Table 3.3. Most WRS in practice fall into Class 1 (or the code equivalent of Class 1), with a small number falling in Class 2 or 3 when aesthetics or environmental implications of leakage are of importance.

Table 3.3: Liquid tightness classes to EN 1992-3

Tightness Class	Degree of leakage allowed
0	Some degree of leakage acceptable, or leakage of fluids irrelevant.
1	Leakage to be limited to a small amount. Some surface staining or damp patches acceptable.
2	Leakage to be minimal. Appearance not to be impaired by staining.
3	No leakage permitted

Even with design code liquid tightness classes similar to Table 3.3, the prescribed leakage limitations are qualitative and vague. What quantifies "some degree of leakage", or to be "limited to a small amount" is subjective. These open-ended limits often lead to conflict between consultants, clients and contractors when there is a degree of leakage. In light of this, a number of code committees have adopted quantitative methods of defining what acceptable leakage is and what periods of leakage are acceptable:

BS 8007 recommends that the structure be filled to the normal maximum level and maintained for a "stabilizing" period, in order to allow for water absorption and autogenous healing to take place. The stabilizing period is to be 7 days for a design crack width of 0.1mm and 21 days (or greater) for a crack width of 0.2mm. Thereafter, the water level is to be recorded at 24-hour intervals over a test period of 7 days. The maximum allowable drop in water level at the end of the 7 day test period is either $d_{ave}/500$, where d_{ave} is the average depth of water at the normal maximum depth, 10mm or another accepted value. Even if the structure passes the acceptance test, any seepage of the retained liquid must be evaluated against the requirements and if deemed unacceptable, remedial work shall be undertaken to stop the flow. In the event that the structure fails the test, remedial work is to be done and another 7 day test period is to be carried out. **AS 3735-2001** adopts identical criterion for checking water tightness.

ACI 350.1-10 prescribes that for standard reinforced concrete tanks, in the event that water tightness criterion are not specified, a maximum loss of 0.05% of the total volume of the tank is allowable per

day. Similarly to BS 8007, a water-filled "stabilizing" period of at least three days is prescribed, though longer periods are suggested for more stringent tightness levels. The test period must be long enough for the water level to drop a theoretical amount of 10mm at the maximum allowable loss per day, but need not be longer than 5 days. Both codes require that for open tanks, the effects of precipitation and evaporation are taken into account.

3.5.2 Crack width limits

The philosophy behind the limiting of crack widths is to design for cracks that (depending on structural or aesthetic requirements) may initially leak, but that self-heal within an acceptable period of time. The specification of how much initial leakage is allowed and how long the cracks take to seal varies for different design codes. Thus, there is no general consensus among researchers with regard to a basis for the evaluation for crack widths and as a result, crack width limits are largely based on practical experience and semi-empirical formulae (Beeby and Narayanan, 2009; Holický *et al.*, 2009).

Most design codes specify a target crack width, depending on the exposure conditions, structure type (reinforced concrete or prestressed concrete), appearance and aesthetic considerations and structural function. For general construction, where water tightness is not a consideration, a crack width of 0.3 or 0.4 mm is generally accepted as being sufficient to avoid any durability or aesthetic problems. Most codes implement this by prescribing minimum reinforcing areas and maximum spacing of reinforcement. This promotes smaller spacings between cracks and thus a greater number of cracks of lesser crack width, as opposed to fewer cracks spaced further apart with greater crack widths.

Code-imposed target crack widths are typically in the range of 0.05 – 0.3 mm, depending on design code. A summary of selected design code crack width limits is shown in Table 3.4. EN 1992-3 is one of the few codes that differentiates between pure tension (through-cracks) and flexure cracks, by assigning a stricter crack width limit to tension cracking. This philosophy is based on the notion that cracks relating to flexure seldom pass through the entire height of the section, due to the compression-tension mechanism. Conversely, cracks that form as a result of pure tension (e.g due to hoop-stress in round reservoirs), by nature pass through the entire section and are notably more prone to leakage. Furthermore, the increasing stringency on crack width stems from the research by Edvardsen (1999) and is dependent on the ratio between the pressure head of water above the crack and the thickness of the section under consideration.

Table 3.4: Crack width limits of prominent WRS design codes.

Code	Target crack width (mm)	
	Pure Tension	Flexure
BS 8007	0.2	0.2
EN 1992-3	for $h_D/h \leq 5$: 0.2 for $h_D/h \geq 35$: 0.05	0.3*
MC 2010	0.2	0.2
ACI 224-19	0.1	0.1

* Assumes cracks do not pass through the full section. h_D is the water pressure head and h is the concrete section thickness.

Table 3.4 shows the variation in crack width limits for various codes, which at first glance may not seem particularly significant. The increase in steel reinforcing required to limit crack widths to 0.05 mm compared with that required to limit widths to 0.2 mm for tension, however, is in the order of 2-3 times more (for EN 1992-3) and so the specification of a crack width has a considerable effect on the cost of WRS, especially for those subject to pure tension (McLeod, 2013). The recommendations for BS 8007 and MC 2010 in Table 3.4 are given for the case when a small amount of leakage is acceptable. When leakage is unacceptable, a limit of 0.1 mm is suggested.

The design of WRS to SLS crack width requirements and crack width prediction is by no means an exact science. Cracking in reinforced concrete is highly variable, due to a number of factors, including but not limited to: mix deviation from specifications, aggregate distribution, in-situ vibration, compaction and site environment, placing temperature, reinforcing distribution, cover and nature and magnitude of loading. As a consequence, there is usually considerable variation between the predicted and measured values of crack width, as was shown in section 3.4.4.

Furthermore, codified crack width limits (e.g. as in Table 3.4) are not guaranteed to ensure that unacceptable leakage will not occur. These limits have been set over time, mainly as a result of practical experience in that, when designed to, WRS on average tend to have an acceptable degree of leakage. EN 1992-3 is an exception in that the limits were based on specific research, notably that of Edvardsen (1999) (see section 3.6). The deemed-to-satisfy limits seem to have served the WRS industry fairly well over the years, but they present a notable challenge to the reliability assessment of WRS.

3.5.3 Flow through cracks

In order to consider the leakage through cracks, the initial flow through cracked concrete needs to be considered. Numerous studies have been undertaken to, amongst other aims, predict the flow rate of fluids through cracks in concrete (Edvardsen (1999); Ramm and Biscopig (1998); Ripphausen (1989); Meichsner (1992); Roig-Flores *et al.* (2016)). These projects all base their prediction of initial flow rate on the principles of flow through parallel-plates. Often referred to as Poiseuille Flow, this theory is appropriate for incompressible fluids that flow through smooth, parallel-faced surfaces and is adjusted by a reduction factor to account for the roughness of the surface of typical crack faces. The initial flow is predicted by Equation 3.15:

$$q_0 = \frac{\Delta p \ell w^3}{12 \eta d} \cdot \zeta \quad (3.15)$$

Where:

- q_0 Initial flow through crack faces
- Δp Fluid pressure between inlet and outlet
- ℓ Length of visible crack at concrete surface
- w Crack width
- ζ Flow reduction factor to account for crack surface roughness
- η Dynamic (absolute) viscosity
- d Thickness of concrete element in direction of flow

The notable uncertainties within the prediction made by Equation 3.15 are the crack width and flow reduction factor. There is widespread debate as to what the most appropriate crack width value should

be, considering the notable variation in width, both along the length of the crack and through the depth of the element - this is discussed later in section 4.5. The flow reduction factor also has considerable variation, as reported in literature.

The flow reduction factor (ζ) is as a result of the surface roughness (tortuosity) of the concrete crack faces, which cause friction and turbulence and thus retards the flow of water. The tortuosity is affected by the constituents of the concrete, but the ζ value also changes with variations in crack width, water pressure head and other flow conditions in the same concrete sample, as shown by Bozorgzadeh (2012). Ramm and Biscopig (1998) analysed ζ values of between 0.03 and 0.1 (when using the average surface crack width) with a mean-optimized value of ≈ 0.04 , though with considerable scatter. Edvardsen (1999) reported optimized values over her numerous samples of 0.25. Van Mullem *et al.* (2019) found that an average ζ value of 0.043 was most appropriate for their data. Esgandani (2017) measured ζ values of ranging 0.0025 to 0.14 for crack widths of 0.1 to 0.4mm. He reported that the ζ values increased with increasing crack width (i.e the actual flow tends more towards the theoretical flow) likely due to the fact that as cracks widen, the effect of the surface roughness reduces. Other researchers contend this though, reporting no link between crack width and ζ value.

3.6 Recovery of properties in cracked concrete

Due to fast-evolving research into the field of recovery of properties in cracked concrete, distinctions need to be made related to terms of reference. Firstly, a distinction needs to be made between *self-sealing* and *self-healing* in cracked concrete. Both refer to the self-filling of cracks in concrete without physical external interference (i.e repair), but for different purposes. Self-sealing specifically refers to self-filling of cracks with the purpose of the recovery of **durability** properties in cracked concrete (the reduction of fluid- or gas-permeability or the retarding of chloride ingress). Self-healing, on the other hand, refers specifically to the self-filling of cracks with the purpose of the recovery of **material or mechanical properties** such as the tensile or compressive resistance, stiffness (Young's modulus) or flexural strength, for example. It should also be noted, particularly in the earlier literature that was reviewed, that these definitions were not necessarily adhered to and so research should be carefully considered when determining whether it actually refers to self-sealing or self-healing.

Furthermore, a distinction has to be made between *autogenous* and *autonomous* means. Autogenous healing refers to the recovery or improvement of performance of properties in cracked concrete, due to healing mechanisms that are brought about by properties inherent to "ordinary" concrete mixes (typically used classes of cements, slag, silica fume and fly-ash) (de Rooij *et al.*, 2013). Conversely, autonomous healing refers to the recovery of properties or improvement of performance as a result of healing caused by constituents other than those in "ordinary concrete" that are specifically added to promote the recovery of certain properties (Super-absorbent polymers, epoxies, shape memory polymers etc.). It should be noted here though, that both self-sealing and self-healing behaviour can be brought about by either autogenous or autonomous means. This is further clarified in Figure 3.9:

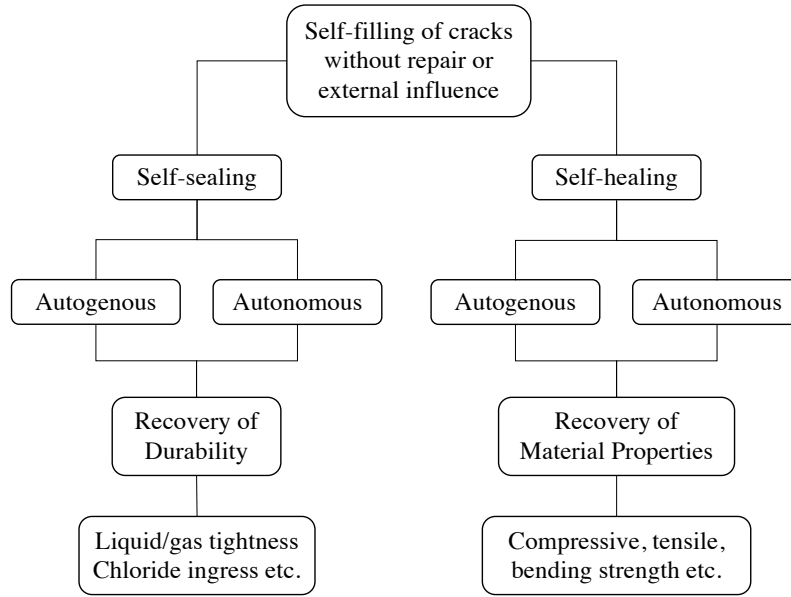


Figure 3.9: Illustration of definitions surrounding the recovery of properties in concrete.

These definitions were necessitated during a review of literature on the subject of the recovery of "performance" in cracked concrete, where the definition of the "performance" differs for each project and its specific research goal.

3.6.1 Self-sealing in concrete

One of the most important recovery mechanisms in cracked concrete is its ability to self-seal cracks, as mentioned in section 3.5. This phenomenon is especially useful in WRS, where extended periods of leakage are undesirable. The self-sealing of cracks considerably reduces the permeability of the cracked concrete and can sometimes stop the flow of liquids through the concrete entirely, depending on crack width, water pressure head, duration of sealing time, sealing environment, presence of sealing agents, composition of the permeant (potable water, effluent, salt water etc.) and whether autogenous or autonomous methods are employed. A common measure of the degree to which cracks self-seal themselves and the degree to which water flow reduces as a result of self-sealing are: The sealing ratio, $R_{w,seal}$, (sometimes called the sealing or crack sealing index) and flow reduction ratio, $R_{Q,red}$ and are defined in Eq 3.16 and Eq 3.17, respectively (Roig-Flores *et al.*, 2015):

$$R_{w,seal} = 1 - \frac{w_f}{w_i} \quad (3.16)$$

$$R_{Q,red} = 1 - \frac{Q_f}{Q_i} \quad (3.17)$$

Where:

w_f Crack width after self-sealing

w_i Crack width before self-sealing

Q_f Flow rate through cracks after self-sealing

Q_i Flow rate through cracks before self-sealing

Ratios of 1 indicate complete sealing of cracks or the reduction of water flow, whereas ratios of 0 indicate no sealing or reduction of water flow. Note though that, following from Eq 3.15, a decrease

in crack width does not imply an equivalent decrease in water flow, but rather a three-fold decrease, theoretically. Similarly, by theory, a $R_{w,seal}$ value of 0.5, does not imply a $R_{Q,red}$ value of 0.5, but rather, 0.125. In reality, however, the cubic relationship between crack width and water flow is not always valid, as the reduction of the crack widths at the point(s) of measurement may not be reflective of the sealing over the entire crack surfaces.

3.6.1.1 Autogenous self-sealing

Typically, the two main contributors to the autogenous self-sealing process are: primarily, the precipitation of calcium carbonate ($CaCO_3$) within the crack faces and; further hydration and swelling of the cement within the cracks as a lesser, secondary mechanism (Teal, 2016). Other mechanisms are suggested to aid in the sealing of cracks by clogging, whereby materials transported through the cracks by water accumulate within the crack and effectively block the water from flowing through the crack. These mechanisms contribute to a lesser extent though, especially in the presence of higher water pressure heads (Edvardsen, 1996; Ramm and Biscopig, 1997). The following research projects, which focussed on autogenous self-sealing, were reviewed:

Edvardsen (1999)

A summary of one of the most notable research projects into the self-sealing of cracks, conducted by Edvardsen (1996), partly focused on the relationship between crack width and the flow of retained water through tension cracks. Edvardsen investigated the effect of varying the following parameters on the autogenous self-sealing of the cracks:

- Crack width ($w = 0.1, 0.2$ and $0.3mm$)
- Cement type (portland, slag, sulfate-resistant cement)
- Cement extenders (limestone dust, fly-ash)
- Aggregate (granite, limestone, basalt)
- Active vs. dormant cracks
- Water $CaCO_3$ concentration
- Element thickness ($d = 200, 300$ and $400mm$)
- Water pressure head ($p = 2.5$ to $20m$)
- Hydraulic gradient ($I = \frac{p}{d} = 6.25$ to 50)

Edvardsen tension-cracked a number of $200 \times 200 \times (200/400) mm$ concrete prisms, by using a wedge-splitting apparatus. The apparatus was effective at varying the crack width wider and narrower, which enabled the testing of self-sealing in concrete with dynamic cracks. The apparatus had two drawbacks: Firstly, during the varying of the crack width, the crack faces were not able to be perfectly realigned, which may have allowed the crack walls to be ground down, smoothing the faces somewhat. Secondly, the crack widths were not able to be controlled to strict tolerances, which lead to the crack ranges:

$$\text{For } w = 0.1mm : \quad 0.07 \leq w \leq 0.13mm$$

$$\text{For } w = 0.2mm : \quad 0.17 \leq w \leq 0.23mm$$

$$\text{For } w = 0.3mm : \quad 0.27 \leq w \leq 0.33mm$$

Upon initial inspection, these do not seem to be particularly notable ranges, however, when considering Equation 3.15, the cubic effect of these tolerances can lead to a six-fold difference in initial flow, from $120 ml/min$ for $w = 0.07 mm$ to $771 ml/min$ for $w = 0.13 mm$. The accurate replication of tight-tolerance concrete crack widths in a laboratory testing environment is a common problem, echoed by most researchers in the field of self-sealing or self-healing concrete.

Edvardsen tested in excess of 80 cube samples, varying the above-mentioned parameters for static cracks, to study the effects they have on the self-sealing of cracks. The cracked samples were exposed to a pressure head of water on the inlet side, which permeated through the cracks and was measured on the outlet side. This was repeated at regular intervals, in order to measure the reduction in water flow due to self-sealing in the samples. A similar methodology was followed for 10 samples with dynamic cracks. The crack widths were varied by $\Delta w = 10, 30$ and 50% of the base static crack width depending on the sample under consideration, as illustrated by Figure 3.10.

A number of important conclusions were drawn from Edvardsen's research. Both active and static cracks subjected to water pressure heads are able to self-seal in the presence of water, though static cracks seal quicker, as can be seen from Figure 3.10. Figure 3.11 shows that the initial leakage through a crack is exponentially increased by increasing crack width. Additionally, it shows that increases in the water pressure head increase leakage for the same crack width. Both of these effects have a negative influence on the probability that the cracks self-seal.

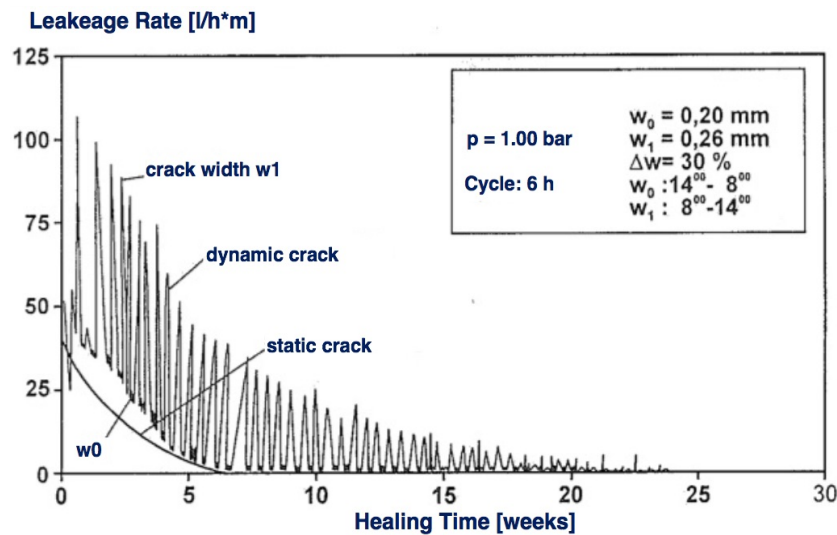


Figure 3.10: Flow rate reduction for dormant and active cracks, reprinted and translated from Edvardsen (1996).

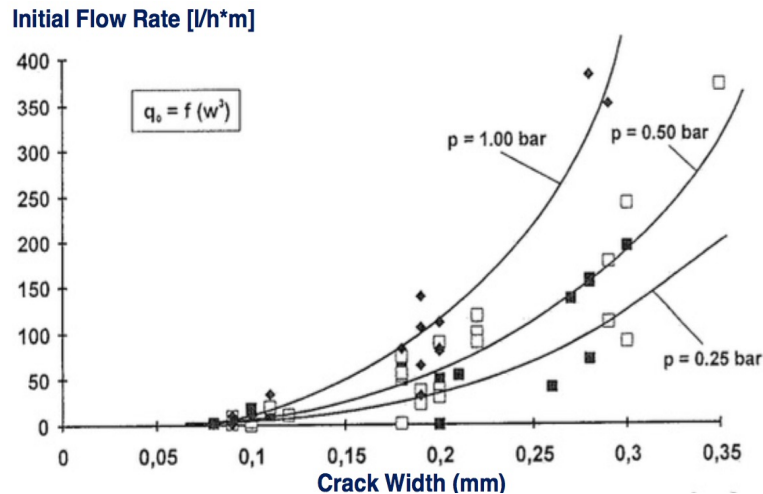


Figure 3.11: Relationship between water flow and crack width for various water pressure heads, reprinted and translated from Edvardsen (1996).

Furthermore, Edvardsen reports that the precipitation of $CaCO_3$ is almost entirely responsible for the self-sealing of cracks. A similar study, by van Tittelboom and De Belie (2013) challenged this, suggesting that in young concrete, continuing hydration is the main mechanism due to the abundance of unhydrated cement particles. As time goes on and as the concentration of unhydrated cement particles diminishes, the precipitation of $CaCO_3$ becomes the main contributor. It was found that the cement type, fine and coarse aggregate type and water hardness had a negligible influence on the formation of $CaCO_3$, and thus self-sealing. Thus, Edvardsen concluded that the potential for the self-sealing of cracks is dependent on crack width, water pressure head, element thickness and crack activity, whereas it is negligibly dependent or independent of cement and aggregate type and water $CaCO_3$ concentration.

Ramm and Biscopig (1997)

This research investigated on the reduction in the flow rate of water through tension-cracked concrete over an extended time period. The thickness of concrete in the direction of flow was varied ($d = 180, 300$ and 600 mm), as was the acidity of the permeant water (pH of 5.2, 6.1 and 7.0), the width of cracks ($w = 0.1, 0.2, 0.3$ and 0.4 mm), the water head ($p = 2.5$ and 12 m) and thereby the hydraulic gradient ($I = \frac{p}{d}$).

The resulting flow rates through the cracks were normalized to an equivalent of litres of flow per meter of crack, for the selected crack widths. Initially, the flow rate through the cracks was considerable, and agreed with the findings of Edvardsen, in that the crack width has a cubic effect on the flow rate (Figure 3.12). Additionally, it was found that increases in concrete thickness yielded lower initial flow rates. After a two-year period, the water flow through the concrete had reduced to an insignificant fraction of the original flow rate, as can be seen in Figure 3.13.

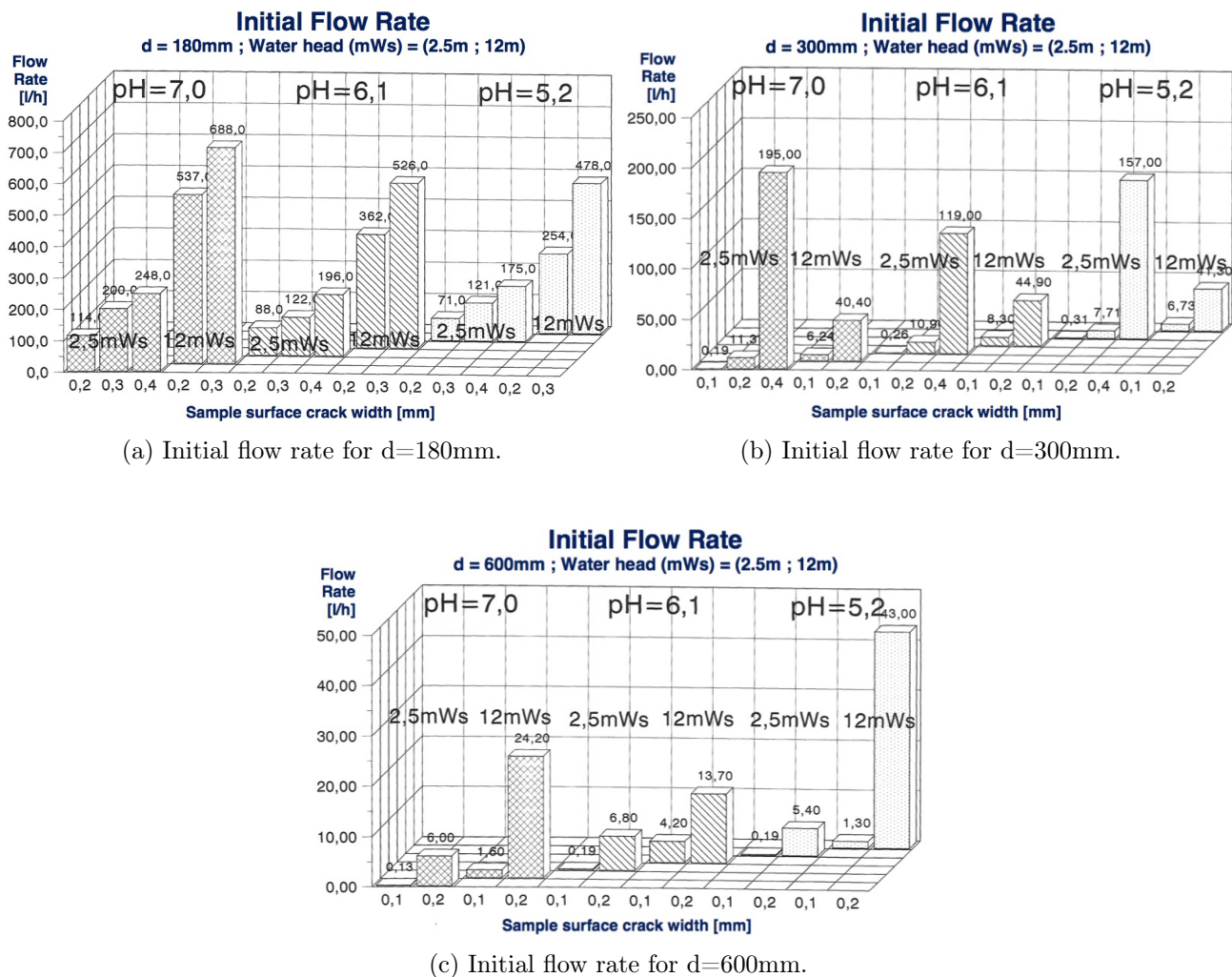
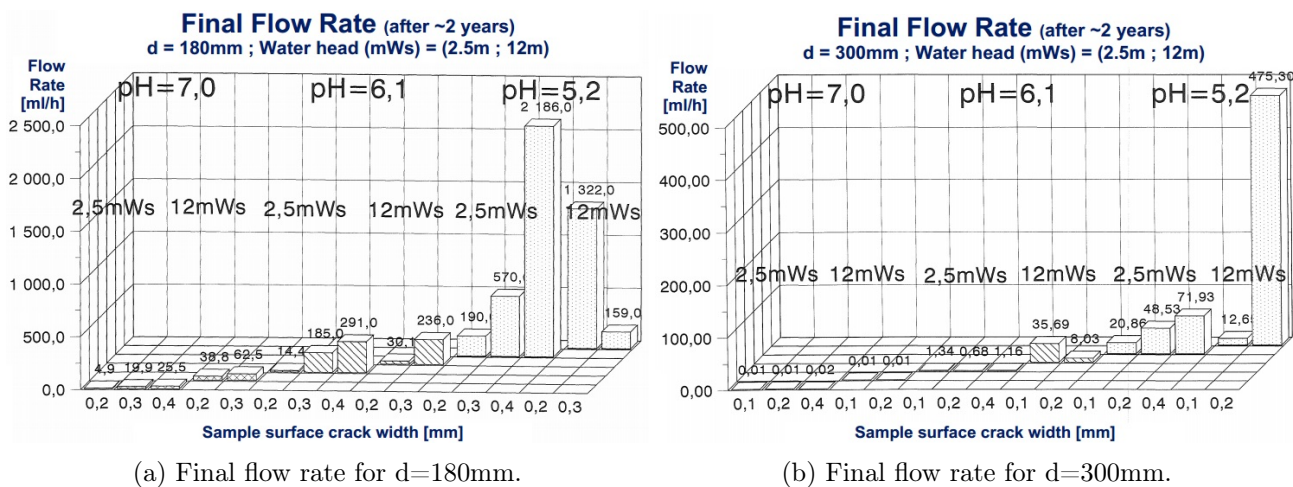
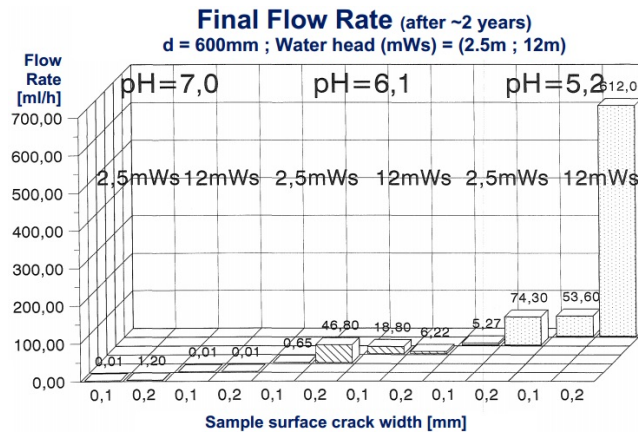


Figure 3.12: Initial flow rates as a function of crack width, water acidity and water pressure head (translated) from Ramm and Biscopig (1997), where mWs is the water pressure head.





(c) Final flow rate for d=600mm.

Figure 3.13: Final flow rates as a function of crack width, water acidity and water pressure head (translated) from Ramm and Biscopig (1997).

Additionally, it was noted that the flow rate of all the samples with the lower water pressure head of 2.5m reduced to below 50% of the initial flow within the first 6 hours. A notable decrease was also seen in the samples with a water pressure head of 12m, although not of the same magnitude. This report of a rapid decrease in flow within the first few hours is a phenomenon that is echoed by other researchers (van Tittelboom *et al.*, 2012; Ratnayake and Nanayakkara, 2018; Nanayakkara and Elakneshwaran, 2005; Edvardsen, 1999).

This rapid, initial reduction in water flow was studied in-depth by Ikoma *et al.* (2015). This phenomenon is argued to be attributed to the entrapment of air bubbles that restrict the flow of water, and not to self-sealing. Air bubbles are generated by water permeating into the concrete, displacing the air in the pores, and dissolved air in the stored water. This was confirmed by short-term, cracked-concrete permeability testing that experienced the same 60-80% reduction in flow over the first 24 hours. This would necessitate a crack width reduction of ~30%, however, only a ~5% reduction in crack width was measured, with almost no precipitation of self-sealing products found on the crack surfaces. This was further illustrated by the use of de-aerated water in an identical test, which found that the short term water flow rate was not reduced by the same, or even near to the same degree as the test with normal water. Similar arguments were made by Meichsner and Röhling (2015), in that water flows in irregular, jagged channels within the cracks.

Nanayakkara and Elakneshwaran (2005); Ratnayake and Nanayakkara (2018)

These two research projects investigated the effects of Portland limestone cement and fly-ash on self sealing, respectively. The crack width was varied, while the water pressure head was kept constant. Greater crack widths resulted in longer sealing times. It was found that varying the quantity of limestone in the concrete mix had an insignificant effect on the duration and extent of sealing. The research indicated that a moderate percentage of fly ash (20 – 30%) may increase the potential for self-sealing, but not enough samples were tested to be able to confirm this or quantify the effect.

A number of other research projects were carried out to investigate the effect of mix design, admixtures, supplementary cementitious materials typically incorporated in "ordinary concrete" used in water retaining structures, and other factors affecting self-sealing. Such cementitious materials include ground granulated blast furnace slag (GGBS), fly ash or silica fume and other factors that may affect self-

sealing include curing environment, pH levels of permeating water and temperature, for example. A summary of the reviewed literature and the focus of each project is given in Table 3.5 below:

Table 3.5: Research conducted on autogenous self-sealing in concrete or mortar.

Authors	Autogenous self-sealing research focus
Ramm and Biscopig (1997)	Effect of water pressure head, water pH and element thickness on reduction of water flow.
Aldea <i>et al.</i> (2000)	Reduction of permeability coefficient.
Reinhardt and Jooss (2003)	Effect of temperature on reduction of water flow.
Nanayakkara (2003)	Effect of water pressure head on reduction of water flow.
Edvardsen (1999)	Effect of water pressure head and element thickness on reduction of water flow.
Li and Yang (2007)	Reduction of water flow in mortar containing steel fibres .
van Tittelboom <i>et al.</i> (2012)	Effect of mix composition (OPC, GGBS, fly ash) on reduction of water flow and crack closure.
Roig-Flores <i>et al.</i> (2015)	Effect of healing environment on water flow reduction and crack sealing cement containing steel fibres.
Sisomphon and Copuroglu (2011)	Reduction of crack widths.
Sisomphon <i>et al.</i> (2011)	Reduction of crack widths.
Hosoda <i>et al.</i> (2008)	Effect of submerged vs. water flowing through cracks; and crack widths on the reduction of water flow and the sealing of crack widths.
Maes (2015)	Combined effect of chlorides and sulphates in marine environments.
Sahmaran <i>et al.</i> (2013)	Effect of supplementary cementitious materials and healing environment on self-sealing of cracks.
Nanayakkara and Elakneshwaran (2005)	Reduction of crack widths and water flow in Portland limestone concrete.
Ratnayake and Nanayakkara (2018)	Effect of fly ash on reduction of water flow.
Ikoma <i>et al.</i> (2015)	Effect of air bubble formation and agglomeration on rapid reduction of water flow through concrete cracks regarded as self-sealing phenomenon.
Jaroenratanapirom and Sahamitmongkol (2011)	Effect of different additives on reduction of crack widths.
Suleiman and Nehdi (2013)	Effect of healing environment on reduction of crack widths.
Ferrara <i>et al.</i> (2018)	Effect of repeated cracking-healing cycles on the reduction of crack widths.
Van Mullem <i>et al.</i> (2019)	Effect of crack width control techniques to reduce the variation on water permeability results.
Borg <i>et al.</i> (2018)	Effect of supplementary cementitious materials and chloride-rich environments.
Cuenca <i>et al.</i> (2018)	Effect of repeated cracking-healing cycles and healing environment on the reduction of crack area.
Azarsa <i>et al.</i> (2018)	Reduction of permeability coefficient and flow rate.

Despite the considerable number of research projects aimed at determining the effect of various factors on the self-sealing capability of "ordinary" concrete, there is still widespread variation in recommendations as to what width of crack is deemed "sealable" within a given time period. Even when a recommendation of "sealable" crack width is made, there is very seldom any indication of a probability of exceedance or confidence interval associated with the recommended limit.

3.6.1.2 Autonomous self-sealing

In the engineered, autonomous self-sealing of cracks, a number of different mechanisms and materials are employed to close or block the cracks in concrete. A selection of the myriad of methods that have

been investigated is given below.

Crystalline admixtures

One of the most common forms of autonomous self-sealing is in the form of hydrophilic crystalline admixtures (CA) that are added into the concrete mix. Its popularity stems from the ease of use, in that it can simply be added to the concrete mix, usually in a liquid or powder form. Slight adjustments need to be made to the concrete mix to ensure workability and the concrete tends to harden faster than ordinary concrete but other than these minor adjustments, the resulting concrete is reported to have lower permeability and crack self-healing ability is increased. Roig-Flores *et al.* (2015), Sisomphon *et al.* (2011) and Jaroenratanapirom and Sahamitmongkol (2011) all tested the effect of different crystalline admixtures on the self-sealing of cracks in concrete or mortar. Generally, it seems that CA's nominally increase the self-sealing ability of the concrete but most importantly, it noted that CA's improve the consistency of the self-sealing, i.e with less variation in flow reduction ratios between different samples. Also it noted that CA's were able to sometimes facilitate the sealing of greater crack widths, that would not likely seal in OPC cement.

Super-absorbent Polymers (SAP's)

Numerous studies have been undertaken into the usefulness of SAP's as water flow reducing agents (Snoeck *et al.*, 2012; Lee *et al.*, 2010; Gwon *et al.*, 2019). Also called hydrogels, SAP's are polymers that absorb water and swell up to form insoluble gels. SAP's are mixed in with the other concrete constituents and absorb water when the concrete is mixed. The SAP's absorb less water during the highly alkaline concrete mixing stage than in the in-service stage, as the swelling ability reduces with increases in the alkalinity of the absorbed water. When the concrete hardens, devoid of water, the SAP's shrink back to their original size, leaving small pores in the concrete. These pores serve as a path-of-least-resistance for propagating cracks and get rehydrated by the ingressing water, swelling to block the flow of water. Additionally, when the concrete dries out again, the SAP's release the stored water, which allows the opportunity for autogenous healing in the cracked area (van Tittelboom and De Belie, 2013). These pore-voids do have setbacks, as they lead to reduced strength of the concrete.

Bacteria-based self-sealing concrete

One of the most innovative autonomous sealing phenomena is that of bacteria-based concrete. These bacteria (most commonly of the genus *Bacillus*) precipitate expansive minerals when exposed to moisture. In order to circumvent the bacteria germinating during casting, one particular research project (Jonkers, 2011) used alkali-resistant bacteria that activated once the alkalinity of the concrete reduced sufficiently (after casting). This method was later refined, as it was found that the bacteria only survived for a period of around two months when exposed to the bare concrete. Subsequently though, clay pellets have typically been used to embed the bacteria and its "food" in. The bacteria then lie dormant within these pellets until moisture ingresses, prompting the activation of the bacteria (Gautam, 2018).

Capsule- and vascular-based self-healing

Yet other methods employ capsule-based healing mechanisms, whereby a healing agent is encapsulated in some form of protective shell (usually cylindrical or spherical). When these shells rupture, most commonly brought about by cracking, they release the encapsulated healing agent which, depending on the type of agent and when it comes into contact with the reaction catalyst (moisture, air, temperature or other phenomenon), seals or blocks the cracks, stopping or reducing the flow of water. Vascular systems work much the same, except that the healing agent is contained within a vascular network of tubes. Some of the healing agents that have been investigated are: methyl methacrylate, various

epoxies, cyanoacrylate (Dry, 2000), tung oil, $\text{Ca}(\text{OH})_2$ solution (Cailleux and Pollet, 2009). These have been encapsulated or encased in: glass, gelatin, wax, clay and silica gel, to name but a few (van Tittelboom *et al.*, 2012).

Currently, many of the autonomous methods show promise in a controlled laboratory environment, however, a number of challenges exist before they can be effectively applied in practice (Teal, 2016). The main problem with the use of most of the autonomous healing methods in real-life structures is that of ensuring an even distribution of healing agent (or capsules containing the agent) throughout the concrete. Generally, those that are included within the concrete mix in powder or liquid form are preferable, as these have the best probability of being spread equally throughout the concrete mix. Capsules, pellets and tubes are not ideal, as the probability of the cracks intercepting them is not likely, unless there are an excessive number of them, which would cause problems with workability, strength reduction and the like. Two particular projects (Lv *et al.*, 2011; Zemskov *et al.*, 2011) were aimed at modelling the probability that a crack intercepted a capsule in a concrete element, as starting points toward determining whether capsule-based self-sealing is a viable option or not.

Two other parameters also fall under the durability umbrella, namely: gas-permeability and chloride penetration. Gas-impermeability is not a common requirement for concrete structures, except in specialist cases, such as hazardous material storage. Typically though, gas-permeability follows a similar trend to fluid-permeability in terms of recovery due to self-healing. Chloride-penetration, in comparison, has received considerable attention, given that it leads to corrosion. The long term costs associated with corrosion repair are considerable, especially for structures that have long design lives and do not frequently become obsolete or get re-purposed, as in the case of water retaining structures.

3.6.2 Self-healing in cracked concrete

Even though the reduction of crack widths and water flow is arguably the most useful self-regenerative phenomenon for cracked concrete in water retaining structures, the regeneration of mechanical properties in concrete have also been investigated, for other applications in structural engineering. Self-healing refers to this recovery of mechanical properties in concrete after cracking has reduced them from uncracked, "virgin" values, often characterized by the self-healing ratio (Eq 3.18). As previously mentioned, self-healing can be brought about by either autogenous or autonomous means.

$$R_{X,heal} = 1 - \frac{X_f}{X_i} \quad (3.18)$$

Where:

X_f Measure of generic mechanical property after self-healing

X_i Measure of generic mechanical property before self-healing

In contrast to the degree of reduction of water flow possible through autogenous self-sealing, autogenous self-healing is not very effective in the recovery of mechanical properties. This is generally due to the fact that the precipitated CaCO_3 , that makes up the bulk of the self-sealing mechanism, is not a strong material, especially when it is randomly deposited on crack surfaces, as is the case here.

Engineered, autonomous healing, conversely, has a considerably higher capacity for the recovery of material properties. Although many autonomous methods have been explored to self-heal various mechanical properties, few of them experience the complete regain of said property. One of the aims of a project by Choi *et al.* (2017), for example, explores the recovery of flexural resistance in concrete

exposed to freeze and thaw effects. The self-healing is brought about autonomously, through the inclusion of various doses (% by volume) of polypropylene (PP) and polyvinyl-alcohol (PVA) fibres. The recovery is shown in Figure 3.14(a) and 3.14(b), where Step E refers to the uncracked state, Step F is after 300 freeze and thaw cycles and Step G is after self-healing has taken place.

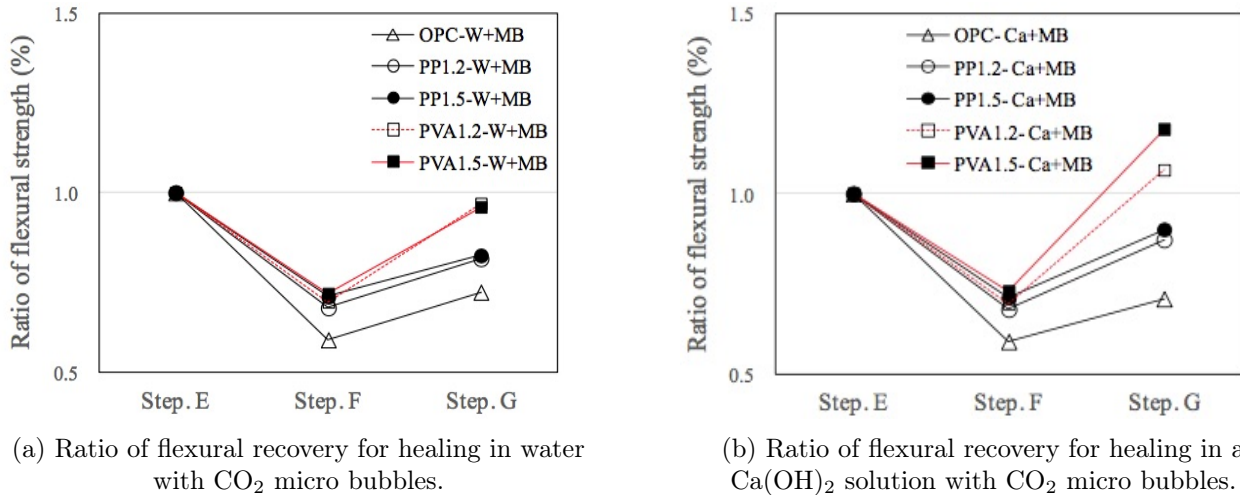


Figure 3.14: Recovery of flexural strength of fibre-containing concrete due to self-healing, [reprinted] from Choi *et al.* (2017)

One can see from the Figure that the control mix (OPC-W+MB) exhibits the least recovery of flexural strength, further illustrating that autogenous healing is not very effective in the recovery of material properties. Notably, Figure 3.14(b) shows that a dosage of 1.5% PVA fibres combined with saturation in a Ca(OH)₂ solution with CO₂ micro bubbles results in a flexural strength recovery ratio of ~1.2 with respect to the uncracked state, i.e. the concrete is actually stronger after healing than it was before it was cracked.

3.7 Chapter summary

This chapter summarizes a selection of the research on the topic of water retaining structures, particularly with regard to cracking in concrete and the prospects of the recovery of properties in concrete. Focus was specifically placed on the increased liquid-permeability of cracked concrete and the ability of concrete to autogenously self-seal cracks, so as to reduce the leakage of the stored liquids. The consideration of target crack widths and the various models used to predict them is shown to be a critical aspect with regard to the design, cost and achieved SLS reliability in WRS.

From the reviewed literature, it is clear that the effect of autogenous self-sealing in cracked concrete contributes notably to the reduction of crack widths, and thus leakage, in WRS. A focus is placed on autogenous self-sealing specifically, as the vast majority of WRS currently designed in practice do not employ autonomous means to promote self-sealing, with the exception of a few crystalline admixtures. Furthermore, self-healing is not particularly useful in tension cracked WRS, as the recovery of mechanical properties is not helpful in reducing leakage of the stored water. The extent of the effect autogenous self-sealing, however, has not been probabilistically quantified and thus it remains a qualitatively-considered element in many WRS design codes. Furthermore, it is clear that the design

code target SLS reliability in WRS has not been verified to any appreciable extent and that the achieved reliability in WRS simply deems to satisfy. From a code-reliability perspective, this stifles the possibility for optimization.

This rest of this research thus focusses on the quantification of the effect that autogenous self-sealing has on the reduction of leakage in cracked concrete. It subsequently investigates how autogenous self-sealing and the specification of target crack width affects the achieved SLS reliability level in WRS.

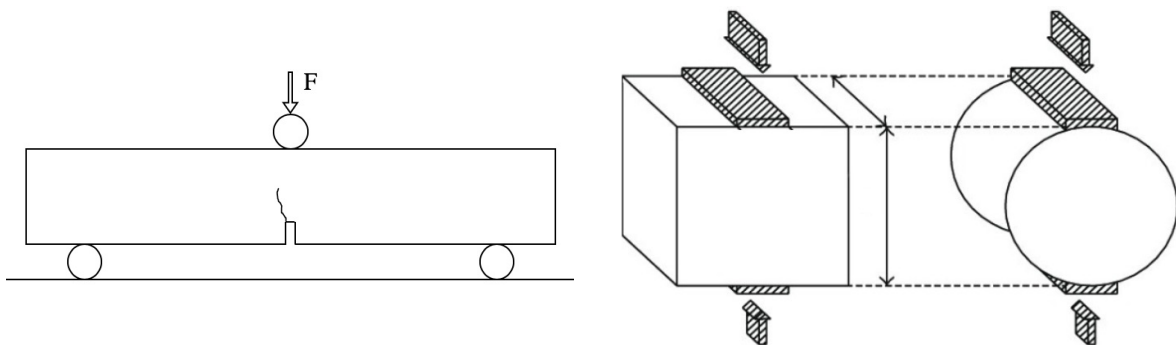
4. Experimental Database

Given the findings of the literature reviews, chapter 4 and 5 investigate the effect that autogenous self-sealing has on the reduction of leakage over time. Thus, this experimental database was compiled in order to investigate the initial flow of water through, and self-sealing in, tension-cracked concrete. The experimental data was collected from a number of researchers within the academic field of self-sealing in concrete. The data was collected from research projects ranging from 1996 to 2019, from around the world, by researchers of varying levels of experience and facility availability, differing hypotheses and different aims of research output. Much of the data was sourced by contacting the researchers personally, or by manually extracting the data from articles or theses. As such, the following subsections aim to identify the nature and methodology of each data source, to determine how the data can be sensibly used.

4.1 Cracking method

As mentioned in section 3.4.1, a notable distinction is made between tension and flexure cracks. In this research, crack self-sealing in flexure-type concrete walls for WRS is not considered. The reason for this stems from the compression-tension zone behaviour in flexure, where the crack propagates from the tension side towards the neutral axis. In almost all cases of flexure in WRS, the compression zone limits the crack from penetrating through the entire wall section, thus making it highly improbable that flexure cracks will leak. Tension through-cracks on the other hand, by nature, go right through the entire section depth, creating a direct path for the retained water to leak through. This type of crack usually results in the most severe leakage.

Nevertheless, a few research projects testing rectangular concrete prisms employ a 3- or 4-point bending test method, see Figure 4.1(a), as a way of producing a through crack, the geometry of which is not dissimilar to that of a tension-type through crack. Bending tests are reported to be able to control the width of a crack better than tensile splitting tests, when used in conjunction with reinforcing bars or wires (Van Mullem *et al.*, 2019). In some cases therefore, initial flow and flow reduction data obtained from samples with flexure cracks can be used in conjunction with tension-cracked sample data.



(a) Typical 3-point bending test to split sample. (b) Typical tensile splitting test to split sample.

Figure 4.1: Typical methods used to form tensile cracks in samples.

Most of the considered research employs some variation of a tensile-splitting technique to crack the samples, see Figure 4.1(b). Often, a notch is sawn into the section to control where the crack forms - alternatively, a void former is sometimes cast into the specimen to form the notch. To avoid imprecise crack widths, a section is occasionally split through and then reattached using some mechanism to provide a specific crack width. This method is not preferred, however, as the perfect realignment of the two separated sections is impossible to achieve and often leads to the grinding down of the crack faces. Sample data that employs this cracking-and-reattaching method is scrutinized for outlier-behaviour. Thus the data is classified, according to cracking method.

4.2 Test method

The samples are then subjected to the water permeability test method. A number of test methods are employed in literature depending on the parameter or phenomenon being investigated. Most of the test methods output the same data in the form of a series of water flow values per unit time. Particular attention was given to the units of the output data (typically in millilitres per minute, per meter of crack) to be able to appropriately compare data.

Samples were generally clamped in place to avoid any further deformation. The sides are then sealed with epoxy, silicone or a similar product in order to prevent any leakage occurring through non-crack-related paths. One side of the crack is exposed to pressurized water and some form of container receives the leaked water and is measured by weight or volume, as shown in Figure 4.2. Some projects elect to employ a different method (Van Mullem *et al.*, 2019) whereby a smooth, greased steel rod is inserted into the center of the concrete sample during casting. Once the concrete has hardened the rod is removed, leaving a rod-shaped hole through the length of the sample. The sample is then cracked in the middle using a 3-point beam bending test. The hole through the sample is then sealed at one end, allowing for pressurized water to be fed in through the other end (with a seal preventing leakage around the inlet). The entire cracked section is then sealed except at the bottom, allowing for water to run through the crack.

In the case of research investigating the effect of a parameter on the self-sealing ability, an initial water flow measurement is taken after which a series of measurements over time are taken in order to monitor the reduction in flow resulting from self-sealing as time progresses. In the case of research that aims at predicting the initial flow through cracked concrete, only an initial measurement is taken.

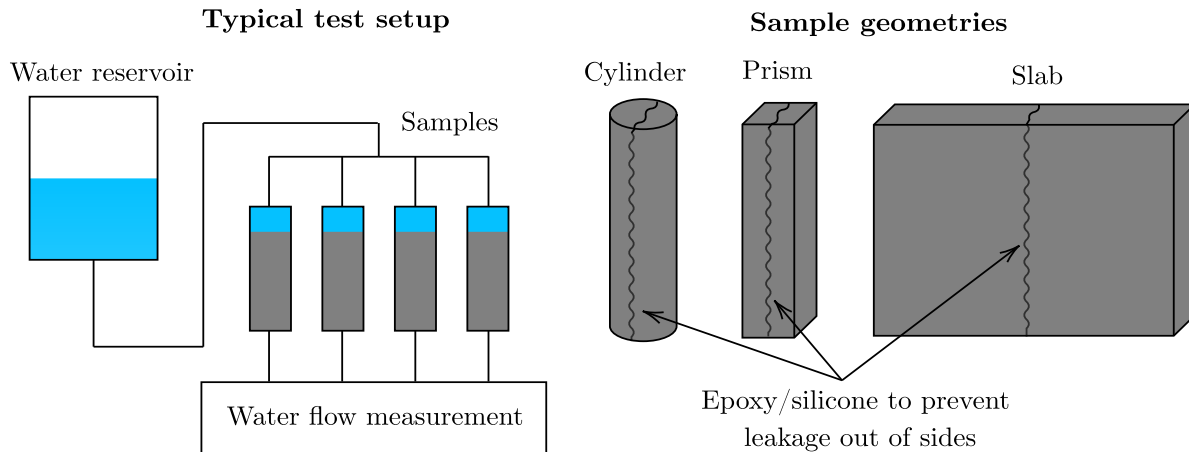


Figure 4.2: Illustration of typical experimental test set up and sample geometry.

4.3 Concrete mix and constituents

From the extensive literature review, it was clear that the effects of individual constituents on self-sealing in typical concrete mixes can not be practically isolated. The quantitative effect that each has on self-sealing in WRS could not be realised due to one of the following reasons:

- The parameter has an insignificant effect on self-sealing or;
- The considerable inherent variability of self-sealing in cracked concrete overshadows the change in self-sealing brought about by the parameter or;
- The sheer number of samples required to come to a decisive conclusion, given the notable variation, is more than most research projects can warrant or;
- Different research projects report conflicting findings.

In spite of this, limits are still set in place with regard to concrete mix designs and constituents allowed in the experimental data set for this research. The application of this research is specific to practical WRS; the mix design should thus not be dissimilar to, or should not behave differently from, one used for a typical WRS.

4.3.1 Cement and grade

No specific limitations are set in terms of cement type, as mix designs can make successful use of most CEM I to V cements. In non-pre stressed WRS, BS 8007 specifies concrete grade C35A as standard. As a considerable number of countries still use BS 8007 as their standard and that EN 1992-3 was also influenced by BS 8007, most WRS designs specify C35/45 concrete. A range of C25/30 to C40/50 is considered appropriate for use in WRS. Concrete grades lower than C25/30 would not be advisable, due to the low resulting compression and tensile strengths. Concrete grades higher than C40/50 should generally be avoided, due to the amount of CEM I required to achieve this strength, which leads to a higher heat of hydration and the potential for restraint cracking. Thus, any experimental samples with concrete cylinder/cube strength in the range of 25-45/30-55 MPa are included in the dataset.

4.3.2 Supplementary cementitious materials

In the design of WRS it is common practice to use Supplementary Cementitious Materials (SCM's), which are typically waste by-products of other industries, in the concrete mix. Three of the most commonly used are Ground Granulated Blast furnace Slag (GGBS), Fly-Ash (FA, sometimes referred to as pulverized fuel ash) and Condensed Silica Fume (CSF), which are by-products from the smelting of iron ore, the burning of coal in coal-fired power stations and from the manufacture of silicon or ferro-silicon alloys, respectively (Juenger *et al.*, 2012).

The replacement of some of the cement content with SCM's is beneficial for a number of reasons. SCM's typically react with some component of the cement, in order to bring about beneficial characteristics or behaviour, among these are improved durability, workability and particularly, reduced heat of hydration. Given that these SCM's are semi-waste by-products of other industries, they are generally fairly cheap in comparison to ordinary Portland cement, as well as being more environmentally friendly. The hydration of cement is one of the biggest contributors to the release of CO_2 into the atmosphere, so the use of SCM's reduces this too.

Due to its ability to reduce the heat of hydration, increase water impermeability and improve workability, the use of GGBS in WRS is common (25-65% replacement of cement content, by weight). For a typical case, a replacement of 50% of a South African CEM I cement with GGBS results in a design T1 temperature reduction in the order of $10^\circ C$ (Viljoen and Retief, 2017), thereby considerably reducing the probability of thermal-restraint cracking. The excessive replacement of OPC with GGBS is cautioned, as this often leads to extended setting time and reduced compressive strength.

FA is often used in WRS in concrete replacement percentages normally ranging from 10-40%. FA allows for a slight reduction in water requirement to produce concrete with the same workability as a concrete without FA, attributed to the particle shape of FA. The spherical particle shape of FA allows it to act in a ball-bearing type manner, which makes the inclusion of FA appealing for pump-mix concrete. For replacement percentages in excess of 30-40%, however, both setting time and strength gain are delayed considerably. Also, in cases where the aesthetics of concrete are of concern, the visual performance of concrete can be compromised by excess FA, due to inconsistencies in colour and patching of darker or lighter coloured concrete.

CSF is only used in smaller cement replacement quantities (up to $\sim 10\%$), due to the extremely fine particle size, which is in the order of 100 times finer than cement. The use thereof increases strength, significantly promotes concrete durability and impermeability and reduces the amount of bleed water to practically zero. Replacement quantities in excess of 10% lead to "sticky" concrete that is practically unworkable.

Given the above, the following restrictions are posed on SCM's, in terms of % of binder content, by weight:

$$\begin{aligned} \text{GGBS} &\leq 65\% \\ \text{FA} &\leq 40\% \\ \text{CSF} &\leq 10\% \end{aligned}$$

4.3.3 Aggregate

The inclusion of aggregate in concrete mixes for WRS is essential for reasons of economy, durability and water tightness. No-aggregate concrete with its excessive use of CEM I, is unnecessarily expensive due to the cost of the cement, but also because of the measures that would need to be put in place to combat the effects of the additional heat of hydration. The increased heat of hydration causes considerable thermal contraction of the concrete paste, which (without a notably increased quantity of reinforcing) leads to a higher probability of restraint cracking.

Both fine and coarse aggregate are therefore added to the concrete mix. In order to reduce the shrinkage of the concrete, a greater ratio of coarse-to-fine aggregate is preferable. For sizeable WRS projects, a pumped concrete mix is often employed to expedite the concrete pouring and compacting processes. Pumped concrete requires more flowability and workability than ordinary mixes so that it can be effectively pumped into place. To make this possible, such mixes usually have a higher water and cement paste content, a greater ratio of fine aggregate and make use of super plasticizers.

Coarse aggregate is usually graded between 5 and 25 mm for use in WRS. Stiffer aggregates like dolomite and granite with E-moduli higher than that of the paste are preferable in WRS, as they exhibit lower shrinkage and in turn, provide restraint against paste movement, thereby reducing the effect of shrinkage in the concrete (Alexander, 2014), as illustrated by Figure 4.3.

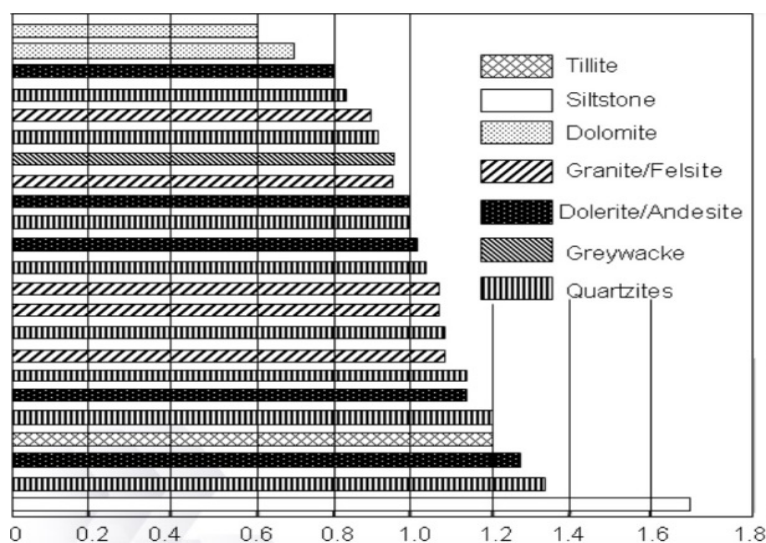


Figure 4.3: Relative shrinkage for a range of aggregate types, [reprinted] from Alexander (2014).

Furthermore, another consideration for aggregates is the potential for Alkali Aggregate Reaction (AAR). AAR is a chemical reaction whereby the alkali's within the cement matrix and the reactive components of the aggregates react to form a gel. Where sufficient moisture allows, this gel swells within the concrete, causing internal strains that cause cracking and spalling of the concrete (Blight and Alexander, 2011). In order to avoid AAR-related problems in concrete, the quantity of reactive silica in the (mainly coarse) aggregate and within the binder needs to be limited to acceptable levels.

The experimental database contains a number of samples from research projects that made use of concrete mortar, i.e. do not contain coarse aggregates. This is assumed to be mainly due to the small size of the samples tested, so that any large aggregate would not adversely affect the geometry and/or

behaviour of the samples. The effect of the lack of aggregate on the self-sealing potential is debatable. Due to the abundance of cement paste and a greater fraction of unhydrated cement particles in a pure mortar sample, a greater degree of self-sealing is expected. In contrast to this, Edvardsen (1996) notes that changes in binder content had negligible to no effect on the healing potential of the samples, although she did not test samples with binder content as high as that found in mortar samples. The data from the mortar samples is thus carefully considered to confirm that the behaviour of mortar samples is comparable to that of the concrete samples.

Given that both conventional and pumped mixes are used in WRS construction, any typical coarse aggregate not exceeding 20 mm is acceptable, with due consideration given to the effect of mortar mixes.

4.3.4 Additives

Water reducing agents, such as super plasticizers are frequently used in WRS construction, especially for pump mixes, to increase the flowability and workability of the concrete, while keeping the water content low. Thus, such additives are acceptable in the database. It should be emphasized that no additives (that are not already in typical WRS concrete mixes) that promote self-healing or self-sealing are included in the *flow-reduction* part of the experimental database. In the initial flow-prediction section, however, such additives are included, but only for the express purpose of predicting the initial flow. For the initial flow measurement, the sealing-promoting agent would not have had time to take effect and will thus not affect the initial flow.

In the section for initial flow-prediction, a number of the research projects made use of fibre reinforcement in the concrete to more accurately control crack widths and thus reduce the variation in the actual vs. target crack width, given that the crack width has a cubic effect on the flow. The fibres provide a way of bridging cracks and thereby ensure that the concrete does not split apart completely when it cracks. If used in excess, the fibres may obstruct the flow path of the water through the crack, thereby reducing the effective crack width, as well as creating eddies and vortices, which may further reduce the flow. In the database, however, only low percentages of steel fibre were added which was assumed not to produce the above-mentioned effects.

4.3.5 W/b ratio and minimum binder content

The ratio of water to binder in a concrete mix (w/b) has a direct effect on a number of characteristics. Increasing w/b ratios lead to concretes with lower compressive strengths and less durability, but greater workability and flowability. Conversely, lower w/b ratios increase the compressive strength and durability, but may cause unworkable concrete (Angelucci *et al.*, 2017). A lower w/b ratio also reduces the shrinkage strain experienced by the concrete, so a lower ratio is preferred for WRS construction. As WRS concretes do not need particularly high compressive strengths (given that the predominant failure mechanisms are all tension or flexure related), the target strength is not often the factor that governs the concrete mix design. W/b ratios between 0.3 and 0.5 are typical for WRS, though sometimes higher w/b ratios are allowed. Given the importance of the w/b ratio, and the relative unimportance of concrete strength in WRS, strict adherence to a specified minimum binder content, which is typically specified in WRS design specifications, is not enforced here.

4.4 Exposure conditions

The exposure conditions present during the self-sealing period have a pronounced effect on the efficiency of the sealing. Exposure conditions are usually classified categorically into low relative humidity, medium to high relative humidity, wet and dry cycles, water contact on one side and full immersion. Table 4.1 illustrates the various healing environments and their effectivity, based on research by Roig-Flores *et al.* (2015).

Table 4.1: Typical self-sealing environments and characteristics, adapted from Roig-Flores *et al.* (2015).

Exposure	Characteristics	Crack sealing effectivity
Low humidity	Relative humidity 20-60% - Dry, semi-desert environments	Least
Med-high humidity	Relative humidity 60-100% - Humid, tropical environments	Increasing
Water contact	Continuous water contact on one side - Reservoir, waste water treatment	
Water Immersion	Continuous water immersion - Underwater and marine	Most

As eluded to in Table 4.1, the vast majority of WRS fall into the "Water contact" section, categorised by the presence of water on one side of the cracked section (inside) and the other being open to air contact (outside). This situation is such that there is always an abundance of water available to flow through the cracks to provide the transportation and materials necessary to facilitate self-sealing. Due to the focus of this research and due to the limited number of test samples, the only sealing environment that will be considered for the reduction of water flow is the "Water contact" environment, as it most accurately simulates the conditions of a typical reservoir.

4.5 Uncertainties and bias

Experimental research will always have some degree of uncertainty and bias. Although unavoidable, these need to be incorporated into the results of the research, to give as accurate a representation of what would actually happen in practice as possible. Research into cracked concrete is associated with considerable aleatory uncertainty. The structure of the concrete matrix itself is such that, being made up of a number of different materials, the behaviour of concrete is never exactly repeatable and is difficult to predict. In addition, researchers and laboratories using different experimental set-ups will get different results, not only because of the aleatory uncertainty, but also due to the epistemic uncertainty associated to their chosen methods, measuring tools, machinery and so forth.

The reported crack width contributes the most to the combined epistemic and aleatory uncertainty within the database. Given that the crack width has such a pronounced effect on the flow of water through the crack, with reference to Equation 3.15, it stands to reason that any inaccuracy within the reported crack width will be compounded by the cubic influence of the crack width on the flow. Figure 4.4 illustrates how the crack can vary over the crack length on both a mortar and concrete specimen. The same variation is present through the depth or thickness of the element. Actual crack widths can

therefore vary considerably from reported crack widths, which introduces notable uncertainty into the prediction of initial water flow through a crack.



Figure 4.4: Variation in crack widths in tensile split mortar (top) and concrete (bottom) specimen, from Jin *et al.* (2017).

Given that the crack width limits the flow, the narrowest part of the crack likely controls the flow, however, using only the narrowest part of the crack will grossly under-predict the flow for the other parts of the crack that are wider. Similarly, using the maximum crack width will over-predict the flow. A few researchers have tried to better calculate an effective crack width (Bomhard, 1986; Akhavan *et al.*, 2012) with limited success, mainly due to the impractical number of crack measurements that need to be taken on the sample. Thus most researchers prefer to simply use the mean of a number of crack measurements at different positions on the sample. This approximation becomes more accurate as more crack measurements are taken but accurately measuring the crack width on the surface still does not guarantee an accurate representation of the crack widths throughout the thickness of the sample.

Similarly, the flow reduction factor, ζ , varies considerably. The main source of uncertainty within the ζ value is linked to the uncertainty in the measurement of the effective crack width, as is further discussed in section 5.1.1. This is because researchers back-calculate the ζ value for an experimental sample with an initial flow rate. Thus the ζ value that gets back-calculated is actually representative of the uncertainty associated with both the crack width and the tortuosity of the crack faces. Due to the inseparability of the crack width and the ζ value, the uncertainty of the crack width will be incorporated into the ζ value in this research.

4.6 Applicability to practical water retaining structures

The parameters and limitations set forth in this experimental database are such that the database attempts to be representative of the majority of tension-cracked water retaining structures experienced in practice.

One specific facet of the direct applicability of this research is the question of the effect of static cracks versus dynamic (active) cracks on the water flow reduction and rate. In practice, fluctuations in water level from the filling and discharge of the WRS during operation cause cracks to open and close with the application and relief of load, causing a dynamic crack. This dynamic behaviour can vary in frequency, fluctuating daily, weekly, monthly etc. depending on the operational function and circumstances of the WRS. As mentioned previously, the self-sealing ability of the concrete is mainly through the formation of $CaCO_3$ crystals, which are of lower stiffness and compressive strength than the concrete. A cyclic load could therefore destroy some of the formed $CaCO_3$ on the crack faces, retarding the self-sealing process.

Only one of the sets of data (Edvardsen, 1996) considers the effect of dynamic cracks and of this data, only nine samples were subjected to daily-varying cyclic loading, as shown in Figure 4.5. These cyclic load tests showed that the shape of the normalized sealing curve followed the same hyperbolically-decaying shape as those of the static cracks (refer to Figure 3.10). It is apparent that the magnitude of the variation in crack width also affects the self-sealing rate, showing that crack widths that vary considerably ($\Delta w = 50\%$) take even longer to seal than those that vary only slightly ($\Delta w = 10\%$). Due to the lack of available data, the effect of cyclic loading is not further considered in this research. Furthermore, this research is primarily concerned with the state of the WRS at water tightness test stage, before any cyclic loading has occurred.

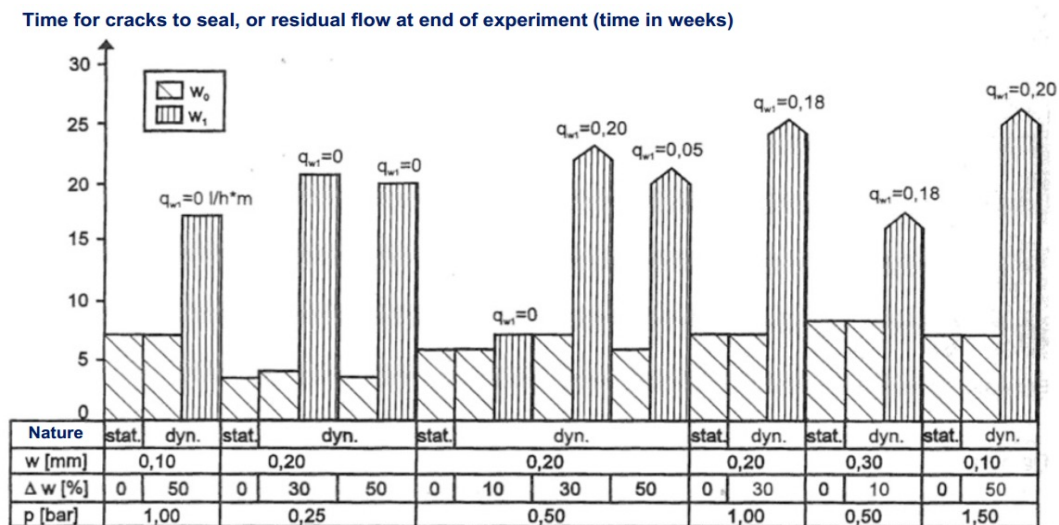


Figure 4.5: Sealing time for dynamic cracks vs. static cracks, [reprinted and translated] from Edvardsen (1996).

4.7 Database sources

The database is split into two sections, one for the prediction of the initial flow and the other for the prediction of leakage over time, considering the effect of self-sealing.

4.7.1 Initial flow prediction

Table 4.2 shows the sources and details of contributions to the experimental database for the initial flow prediction. Figure 4.6 shows the distribution of crack widths in the initial flow prediction database.

In the table, the following should be noted:

- Water head is given in meters;
- Crack width, w , given in millimeters;
- A mortar sample is indicated by M and a concrete one denoted by C;
- Blast furnace slag (GGBS) and Fly Ash (FA) values are given as percentages of total binder content, by weight;
- Cracking method is indicated by either T.S (Tensile Splitting) or 3 Pnt (controlled 3-Point Bending);
- Samples by Roig-Flores *et al.* (2015) contain steel fibres.

Table 4.2: Sources of the experimental database for the prediction of initial flow through tension cracked concrete or mortar.

Author	w/b ratio	f_{cu}	Water head	w	Samples	Mort. /Conc.	GGBS	FA	Crack Method
Roig-Flores <i>et al.</i> (2016)	0.45, 0.6	C30/37, C45/55	20	0.07-0.51	165	C-CEM II/A-L R	-	-	T.S
Van Mullem <i>et al.</i> (2019).	0.5	Not given	0.5	0.15-0.32	24	M-CEM I N	-	-	3 Pnt
Ramm and Biscopig (1997)	0.55	C30/35	2.5, 12	0.1-0.4	42	C-CEM II/A-V R*	-	15%	T.S
Palin <i>et al.</i> (2015)	0.5	Not given	1	0.2, 0.4	16	M-CEM I N	-	-	T.S
Palin <i>et al.</i> (2017)	0.5	Not given	1	0.4	8	M-CEM III/B N LH	65%	-	T.S
Azarsa <i>et al.</i> (2018)	0.53	C30/35	1.5	0.2-0.3	6	C-CEM I N	-	-	T.S
Bozorgzadeh (2012)	Not given	C35/45	2.3, 4.5, 7.2	0.05-0.32	42**	C	-	-	T.S
Esgandani (2017)	0.5	C30/35	40	0.09-0.41	23	C-CEM II/A-V N	-	20%	T.S
Edwardsen (1996)	0.6	C30/35	2.5-15	0.1, 0.2, 0.3	58	C-CEM III/A*	65%	-	T.S
						C-CEM I R*	-	-	T.S
Total					384				

*Modern day equivalent of concrete used. Ramm & Biscopig - PZ 35 F, Edwardsen - HOZ 35 L, PZ 35 F.

**Only two sample slabs, but varied crack widths and pressure heads.

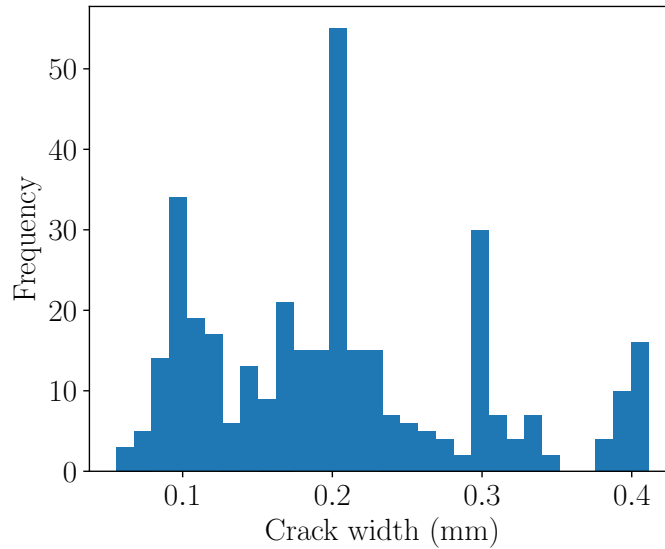


Figure 4.6: Distribution of crack widths in experimental data database ($0 < w \leq 0.4mm$).

4.7.2 Water flow reduction

The database for the reduction of leakage through tension cracks over time due to self-sealing contains fewer samples than that of the initial flow database. The duration of time, effort and laboratory resources required for these tests are such that few research projects can warrant them. The distribution of crack widths in the samples is shown in Figure 4.7. The sources and details of the sample data are shown in Table 4.3. In the table, the following should be noted:

- Water head is given in meters;
- Crack width, w , given in millimeters;
- All samples are concrete;
- GGBS and FA values are given as percentages of total binder content, by weight;
- All samples are cracked using a tensile splitting technique

Table 4.3: Sources of the experimental database for the reduction of water flow over time.

Author(s)	w/b ratio	f_{cu}	Water head	w	Samples	Concrete type	GGBS	FA
Nanayakkara and Elakneshwaran (2005)	0.44	C45/55	2.0	0.07-0.14	8	CEM I, CEM II/A-L	-	-
Ratnayake and Nanayakkara (2018)	0.5	C35/45	2.0	0.10-0.24	10	CEM I, CEM II/A&B-V	-	0-40%
Ramm and Biscopig (1997)	0.55	C30/35	2.5, 12	0.10-0.40	36	CEM II/A-V 42.5 R* (PZ 35 F)	-	15%
Edwardsen (1996)**	0.6	C30/35	2.5-15	0.10-0.30	19	CEM III/A* (HOZ 35 L)	65%	-
						CEM I 42.5 R* (PZ 35 F)	-	-
Total					73			

*Modern day equivalent of concrete used. Ramm & Biscopig - PZ 35 F, Edwardsen - HOZ 35 L, PZ 35 F.

**Edwardsen's research contains near 80 samples, but only some are detailed in full.

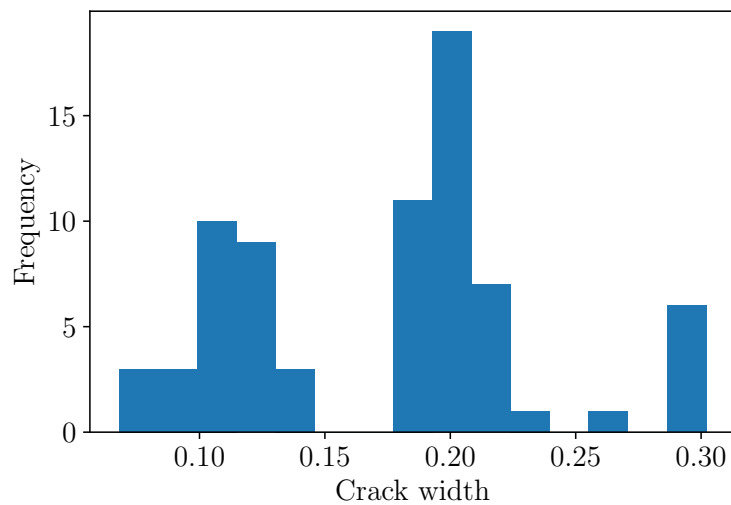


Figure 4.7: Histogram of crack widths in the water flow reduction over time database.

4.8 Chapter summary

This chapter details the compilation of two databases from experimental tests conducted by other researchers. The two databases contain experimental samples for which the initial leakage is measured, and for which the leakage (and reduction of leakage due to self-sealing) is measured over time, respectively, for tension cracked concrete or mortar. Requirements for the inclusion of samples in the database are given in terms of the cracking and test method, concrete mix constituents and exposure conditions. The two datasets are shown in Appendix F.

5. Probabilistic Models

The main aim of this research is to determine the leakage-related SLS reliability in tension-governed WRS. In order to achieve this aim, the leakage that transpires through cracks in WRS needs to be predicted. Autogenous self-sealing reduces the width of these cracks and the leakage through them, over time. The effect that the self-sealing has on the reduction of leakage over time is therefore quantitatively considered in this chapter.

This chapter details the derivation of probabilistic models to describe:

1. The prediction of the initial flow of water flow through a tension crack in concrete (Initial flow prediction model);
2. The prediction of leakage volume through a tension crack in concrete and the effect that self-sealing has on the reduction of leakage over time (Leakage prediction model).

The initial flow prediction model predicts the initial flow through a tension crack and the leakage prediction model predicts the volume of water that subsequently leaks through the crack over time, considering self-sealing. The two databases compiled in chapter 4 are used here to probabilistically characterize the models. The models characterized in this chapter will later be used in a reliability analysis to predict whether unacceptable leakage is likely to occur through all cracks in a reservoir at the time of water tightness testing. Both models are specifically applicable to round, tension-cracked, RC WRS as described in chapter 4.

5.1 Initial flow prediction model

The initial flow prediction model aims to predict the initial leakage through a single tension crack in concrete with a measure of uncertainty, given certain input parameters. This section describes the choice of flow reduction factor, ζ and the characterization of a flow prediction model factor, θ_{Q0} , for use in the initial flow prediction model.

The initial flow prediction model is based on the modified equation for Poiseuille flow between two frictionless, parallel plates given by Equation 3.15, repeated here as Equation 5.1. The flow reduction factor, ζ , is introduced to take cognizance of the friction from the roughness of the concrete surface and the effect it has on the reduction of flow from ideal, frictionless flow, as discussed in section 3.5.3. Each sample in the experimental dataset reports parameters of initial water flow, water pressure head, crack length, crack width, and crack depth or section thickness (q_0 , Δp , ℓ , w and d , respectively). The dynamic viscosity of water, η , is assumed constant in this research as $8.9 \times 10^{-4} \text{ N s/m}^2$. The only undefined parameter in Equation 5.1 is the flow reduction factor, ζ , which is discussed below.

$$q_0 = \frac{\Delta p \ell w^3}{12 \eta d} \cdot \zeta \quad (5.1)$$

5.1.1 Flow reduction factor - ζ

The range of ζ values reported in literature vary considerably, as discussed in section 3.5.3. The flow reduction factor is generally back-calculated using the actual initial flow from experimental samples, as per Equation 5.2. For this reason, the uncertainty contained within the calculated flow reduction factor is actually representative of the uncertainty in flow reduction factor *combined* with the uncertainty in crack width (the other parameters do not contribute notable uncertainty). The uncertainty introduced by the crack width includes that from the method of measurement, the averaging of the crack width along its length, as well as the variation in crack width through the thickness of the sample.

$$\zeta = \frac{12 q_0 \eta d}{\Delta p \ell w^3} \quad (5.2)$$

In order to determine an appropriate value of ζ for use in the initial flow prediction model, the ζ value is back-calculated from the actual initial flow for each sample in the experimental database using Equation 5.2. The results are presented for the sample data from each researcher in Table 5.1. The ζ values in Table 5.1 contain uncertainty from the variation in w , as well as that from ζ . It can be seen from the CoV that the flow reduction factors for the experimental dataset also vary considerably.

Table 5.1: Flow reduction value, ζ , back-calculated from experimental data collected from different researchers.

Author	Mean μ	Std. dev. σ	CoV	Samples
Roig-Flores <i>et al.</i> (2015)	0.119	0.080	0.671	165
Van Mullem <i>et al.</i> (2019)	0.037	0.006	0.160	24
Ramm and Biscopig (1997)	0.079	0.075	0.952	42
Palin <i>et al.</i> (2015, 2017)	0.114	0.064	0.559	24
Azarsa <i>et al.</i> (2018)	0.097	0.037	0.381	6
Esgandani (2017)	0.052	0.048	0.931	23
Bozorgzadeh (2012)	0.090	0.068	0.758	42
Edvardsen (1996)	0.163	0.109	0.669	58
Overall ζ^*	0.113	0.086	0.76	360

*Note that samples by Van Mullem *et al.* were not included in the overall characterization - See discussion below.

There is notably less variation in the samples tested by Van Mullem *et al.* (2019) in comparison to the rest. In their project, a novel active crack control method was developed to crack the samples. This, combined with a concerted effort to meticulously measure the crack widths resulted in a much lower CoV. This is an indication that the bulk of the variation in the flow reduction factor is actually attributed to the variation in crack width measurement and not to the surface roughness of the concrete. The data from Van Mullem *et al.* (2019) was not included in the overall choice of ζ factor, however, as the project used a bending test set-up to crack the samples, leading to trapezium-shaped cracks.

Irrespective of whether the crack width or the surface roughness contributes the most uncertainty to the prediction of initial flow through cracks, the separate quantification of the variation contribution from each is not practical. As such, a deterministic value was used for ζ based on the results of the back-calculation of the ζ value from the data in the database. From Table 5.1 a mean value of $\zeta = \mu_0 = 0.11$ was adopted. This was checked for statistical validity, using a two-sided t-test.

$$T_0 = \frac{\bar{X} - \mu_0}{S/\sqrt{n}} \quad (5.3)$$

Where:

- H_0 : $\mu = \mu_0$ (*Null hypothesis*)
- \bar{X} *Sample mean*
- μ_0 *Hypothesized mean*
- S *Sample standard deviation*
- n *Number of samples*

The null hypothesis is $H_0 : \mu_0 = 0.11$ which yields $p = 0.514 > 0.05$, for which the null hypothesis cannot be rejected. Thus, a deterministic mean value of $\zeta = 0.11$ will be used in this research. Contrary to findings by Esgandani (2017), there does not appear to be any correlation between crack width and the ζ value, for the range of crack widths considered here. The actual initial flow from the database samples is shown in Figure 5.1, along with the initial flow predicted using Equation 5.1 with $\zeta = 0.11$, as a function of crack width.

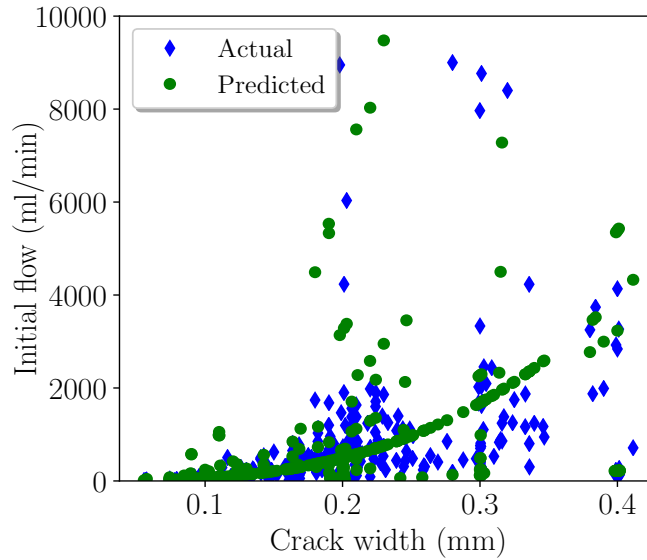


Figure 5.1: Actual initial flow vs. prediction of initial flow with $\zeta = 0.11$, cut off at $10\ell/\text{min}$ for ease of visualization.

Following the choice of $\zeta = 0.11$, the variation contained in the initial flow prediction model using Equation 5.1 is introduced through an initial flow prediction model factor, θ_{Q_0} , which is detailed in the following section.

5.1.2 θ_{Q_0} Model factor characterization

In order to consider the variation in the prediction of initial flow using Equation 5.1 with $\zeta = 0.11$, a novel initial flow prediction model factor is introduced. The initial flow prediction model factor is defined as the actual initial flow over the predicted initial flow, as shown in Equation 5.4, where $Q_{0,\text{predicted}}$ is Equation 5.1 with $\zeta = 0.11$.

$$\theta_{Q_0} = \frac{Q_{0,actual}}{Q_{0,predicted}} \quad (5.4)$$

$$= Q_{0,actual} \cdot \frac{12 \eta d}{0.11 \Delta p \ell w^3} \quad (5.5)$$

Where:

- θ_{Q_0} Initial flow prediction model uncertainty
 $Q_{0,predicted}$ Predicted initial flow
 $Q_{0,actual}$ Experimentally determined initial flow

The model uncertainty factor needs to characterize the uncertainty in the performance of the model across all relevant crack widths. In this case, the crack width range considered for the database samples was limited to an upper limit of 0.4 mm, as crack widths greater than 0.4 mm are outside the range typically found in WRS. The θ_{Q_0} model factor is characterized using Equation 5.5 for all samples in the database. The distribution of θ_{Q_0} values with respect to crack width for the whole dataset is shown in Figure 5.2. As can be seen from Figure 5.2, the model contains less variation and thus predicts the initial flow more consistently at wider crack widths, indicated by the clusters of sample points around $\theta_{Q_0} = 1$. This is due to the magnitude of the error in prediction caused by even small errors in effective crack widths at narrower crack widths.

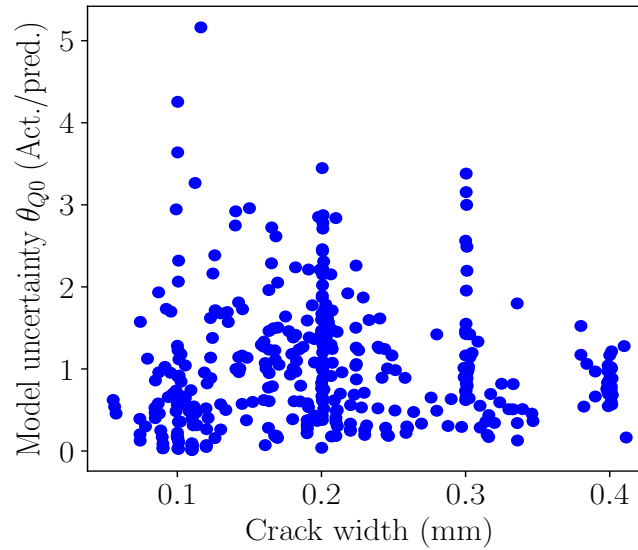


Figure 5.2: Initial flow prediction model uncertainty values as a function of crack width for the entire database.

In order to characterize the θ_{Q_0} model factor, a histogram of the values is shown in Figure 5.3. Typically, model factors follow either a normal or lognormal distribution, following JCSS recommendations. A fit was performed for a normal, 2-parameter lognormal (location=0) and a 2-parameter Weibull distribution (location=0). From Figure 5.3, it can be seen that a normal distribution does not characterize the data well. Other than the fact that the shape does not fit the data well, a normal distribution allows for the realization of negative values. From the definition of the model factor in Equation 5.4 the realization of a negative value is not possible.

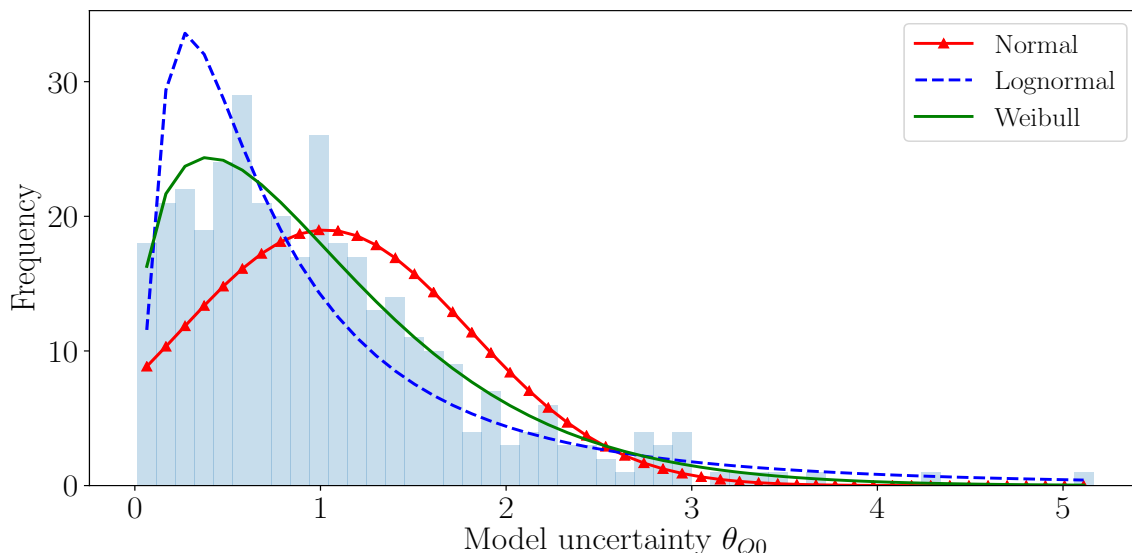


Figure 5.3: Histogram of θ_{Q0} values with normal, 2-parameter lognormal and 2-parameter Weibull fits.

Thus either a lognormal or Weibull distribution would be most applicable to characterizing the model uncertainty, as neither can realize negative values. In order to test the agreement between the data and the proposed distributions, probability plots were generated for both and are shown in Figure 5.4. The shape and scale parameters (location=0) are determined using Maximum Likelihood Estimates (MLE) and are shown from top to bottom, respectively. Probability plots are a graphical method of measuring how well a proposed theoretical distribution matches the distribution of a given set of data (Montgomery and Runger, 2003). A straight line indicates the ideal, in that there is no difference between the data and the proposed theoretical distribution. Notable deviations from the straight line indicate that the proposed theoretical distribution does not adequately describe the distribution of the data. A probability plot compares the Cumulative Distribution Function (CDF) of the proposed theoretical distribution with the actual distribution of the sample data.

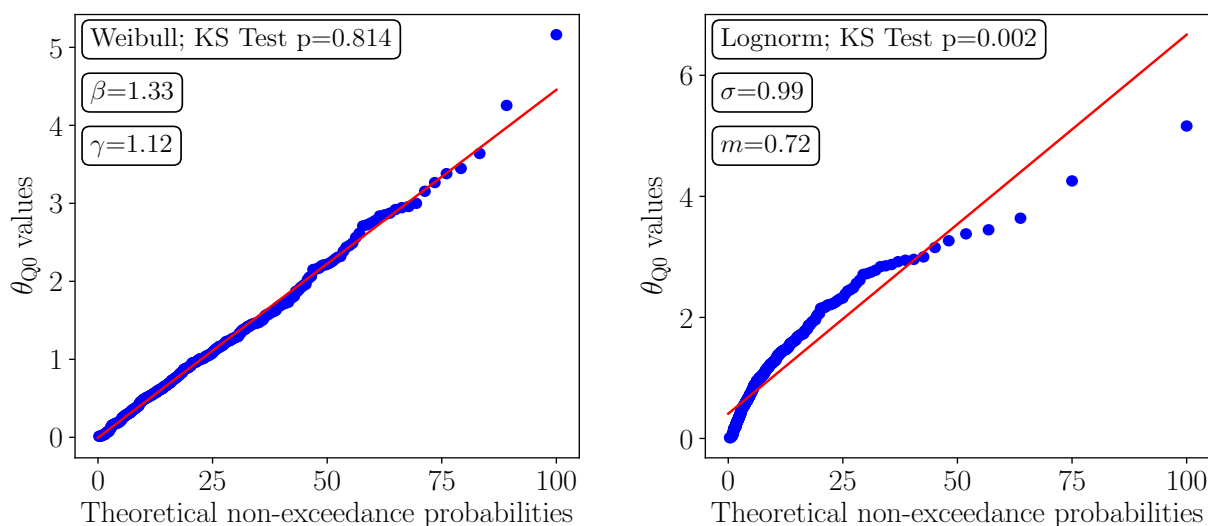


Figure 5.4: Probability plots of the Weibull and lognormal distributions for the θ_{Q0} model uncertainty data.

Figure 5.4 additionally shows the p-value that results from a Kolmogorov-Smirnov (KS) test, which indicates goodness of fit for data and a given distribution. A higher p-value indicates greater statist-

ical support for the non-rejection of the null hypothesis (i.e that the data is, in fact, characterized by the given distribution). Considering the two sets of figures, the plots and KS test results both indicate that a lognormal distribution is not a good fit for the data. Conversely, the Weibull distribution well-characterizes the data throughout the percentile ranges, supported by the high KS p-value of 0.814.

As Figure 5.2 alludes to reduced variation for greater crack widths, the θ_{Q0} model factor data is split into three crack width ranges and is characterized according to these ranges in the following section.

5.1.3 θ_{Q0} Model factor characterization for crack width ranges

The number of samples available for the parametrization of the initial prediction model uncertainty allow the model factor to be characterized for various crack width ranges. The initial flow prediction data was separated into three crack width ranges and distributions were fit accordingly. As the full dataset is well-characterized by a Weibull distribution, a Weibull distribution was used to characterize the sub-sets of the data, though lognormal and exponential distributions were also considered. Figure 5.5 shows the fitted Weibull distributions, with statistical parameters as detailed in Table 5.2.

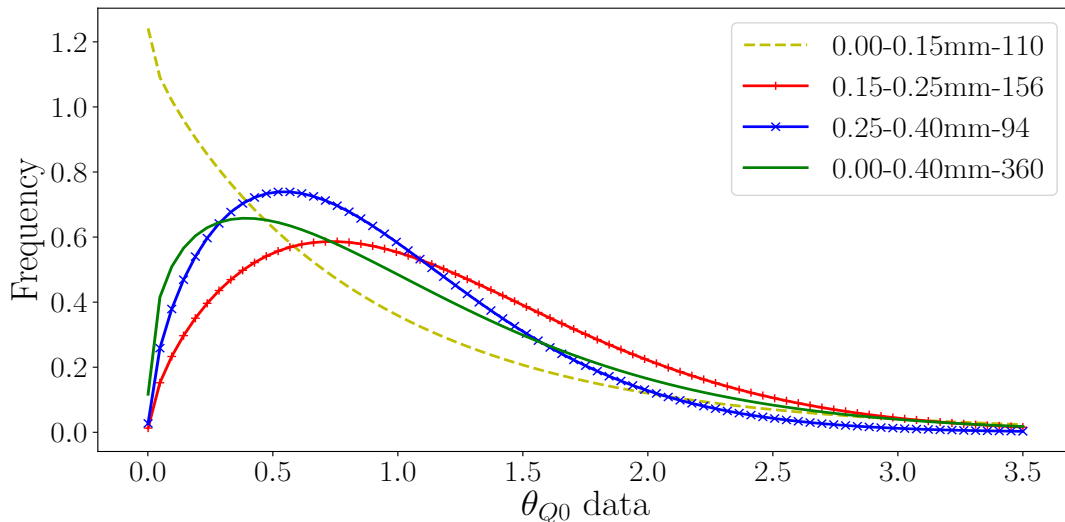


Figure 5.5: Distributions of initial flow model factor for various crack width ranges.

Table 5.2: Statistical parameters for the initial flow prediction model factor, θ_{Q0} , for crack width ranges.

Crack width range	Sample size	Weibull shape/scale	KS Test p	Mean	Std. Dev	CoV
0.00-0.15mm	110	0.98 / 0.90	0.74	0.90	0.92	1.02
0.15-0.25mm	156	1.64 / 1.31	0.68	1.17	0.73	0.62
0.25-0.40mm	94	1.58 / 1.03	0.26	0.91	0.63	0.69
0.0-0.40mm	360	1.33 / 1.12	0.81	1.03	0.78	0.76

Figure 5.5 illustrates that each of the crack width ranges have slightly different distribution shapes. The legend indicates the crack width range and number of samples in the range. In the lower and upper crack width range, the model factor is less than one, indicating that the model slightly over-predicts at lower and upper crack widths, but under-predicts in the middle range. The CoV of the 0.00-0.15 range is also notably higher than the other ranges, and the shape is distinctly different. This is attributed

to the difficulty in accurately measuring crack widths at narrower crack widths, as discussed in section 5.1.2. The two other crack width ranges have a lower CoV and a similar shape to one another and to the overall distribution. The p-values indicate that a Weibull distribution fits the data well. A lognormal distribution fits the 0.25-0.40mm range slightly better than a Weibull, but for consistency in statistical uncertainty, a Weibull distribution was used for all ranges.

5.1.4 Consideration of potential outliers and distribution validation

The left hand side of Figure 5.4 alludes to a section towards the upper third of the data where the values do not seem to fit into the distribution of the rest of the data as well, which leads to the consideration of the points as outliers. Outliers have the ability to unhelpfully skew data and are therefore often quickly discarded, without due consideration of whether the points are actually true outliers or not. Outliers should, as far as possible, be discarded on the grounds of practical reason, rather than on statistics. A negative value obtained for initial flow, for example, is a physical impossibility and is a clear case of a data input or measurement error. An initial flow value that is 4 standard deviations away from the mean could be a measurement error but it could also be an indication that there is high variation within the data. The removal of the "outlier" in the latter case could result in a misrepresentation of the actual variation of the data and would not be advised.

When investigating potential outliers in normally-distributed data, a quick gauge of data can be obtained through the use of the Z-score. For non-normal distributions, due to their non-symmetric nature, the Z-score is not as readily usable. Instead, Weibull plots of the data are generated, to determine whether the data can be considered as outliers or not, and to check the validity of the shape (β) and scale (γ) parameters. A Weibull plot is created by changing the form of the CDF (or unreliability) from:

$$y = P(x) = 1 - \exp^{-\left(\frac{x}{\gamma}\right)^\beta} \quad (5.6)$$

into the linear form of:

$$y = \ln\left(\ln\left(\frac{1}{1 - P(x)}\right)\right) \quad (5.7)$$

The unreliability is based on the $P(x)$ function, which needs to be estimated. These "unreliability estimates" are obtained through the use of median ranks. The rank is calculated as shown in Equation 5.8, and the median rank is the solution to Z in Equation 5.8 for the j^{th} element of a sample of N elements, with $P = 0.5$ (median value). This is often simplified using an approximation derived by Benard and Bosi-Levenbach (1953), given by Equation 5.9, where j is the failure order number. The transformation leaves the horizontal axis in the form of $\ln(\theta_{Q0})$. The resulting Weibull plots for each crack width range are shown in Figure 5.6.

$$P = \sum_{k=j}^N \binom{N}{k} Z^k (1 - Z)^{N-k} \quad (5.8)$$

$$P(x_j) = \frac{j - 0.3}{N + 0.4} \quad (5.9)$$

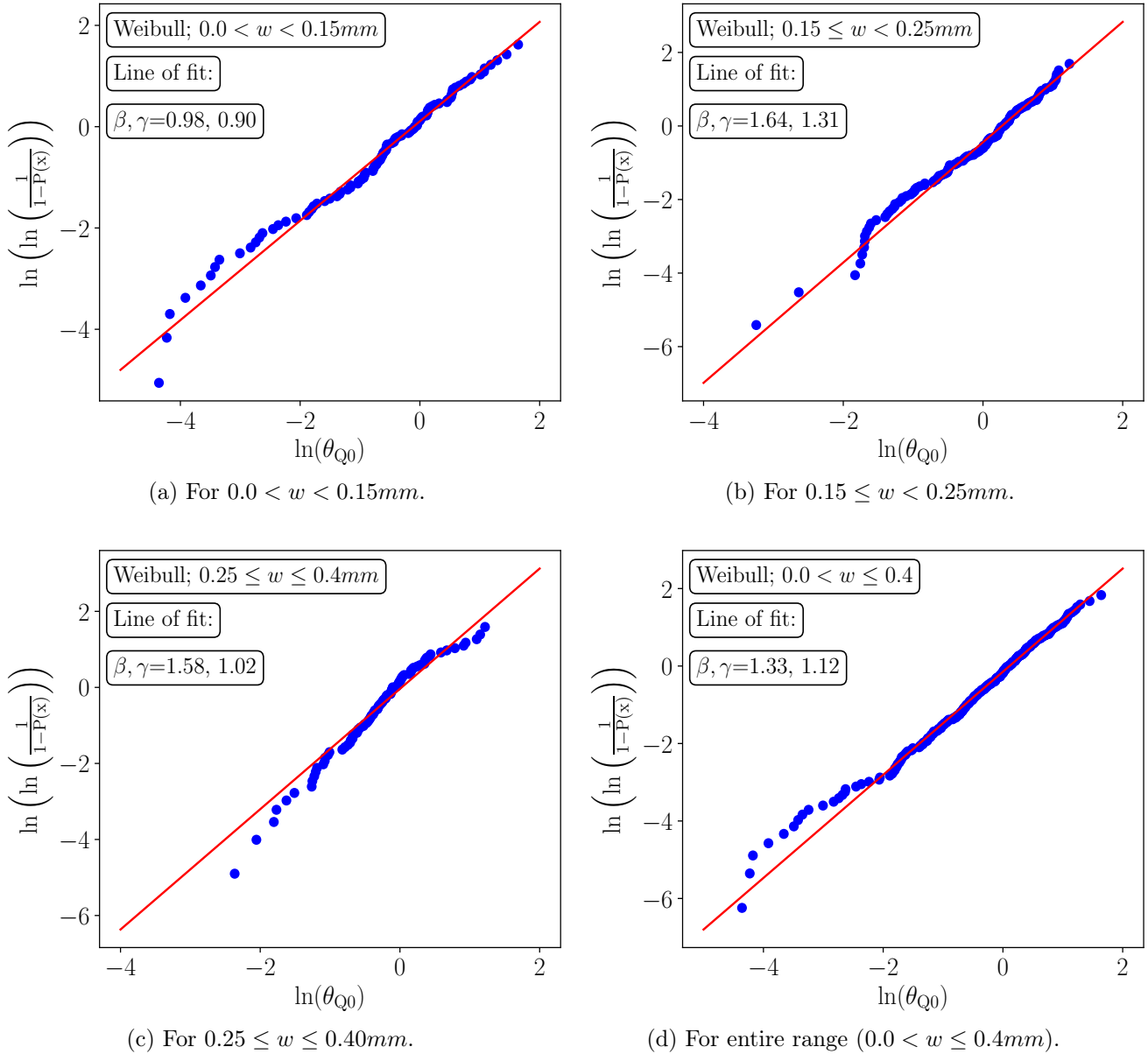


Figure 5.6: Weibull plots for initial flow prediction model uncertainty θ_{Q0} for various crack width ranges.

The red, linear lines were plotted using the shape and scale parameters obtained from the MLE in Table 5.2, and indicate that the parameters predicted using MLE are appropriate. From Figure 5.6, it can be seen that the lower tail of the data contains potential outliers, more so than the upper tail; these represent cases where the prediction is higher than the actual (experimental) value. These points, however, do not notably deviate from the Weibull fit and are not an indication of a separate mechanism, warranting a separate distribution. Additionally, there are no indications from the individual research projects as to why these points should be considered erroneous outliers. As such, the potential outliers are retained.

Thus it is concluded that a 2-parameter Weibull fit, with shape and scale parameters as shown in Figure 5.6, adequately describes the distribution of the initial flow model uncertainty factor as a whole, as well

as within the discrete crack width ranges. The initial flow prediction model is thus given by Equation 5.10.

$$Q_0 = \theta_{Q_0} \cdot \frac{0.11 \Delta p \ell w^3}{12 \eta d} \quad (5.10)$$

5.2 Leakage prediction model

The initial flow prediction model is used to predict the initial flow of water through a tension crack. The leakage prediction model is subsequently used to probabilistically consider the leakage over time that results from such a tension crack, with a predicted initial flow of Q_0 (kl/hr). The leakage prediction model uses the water flow reduction database to model the reduction in flow over time, as a consequence of self-sealing. For this purpose, a novel leakage accumulation factor, θ_{idd} , is characterized using the data in the flow reduction database. The following subsections consider the effect of crack width range and hydraulic ratio on the leakage accumulation factor.

5.2.1 Crack width ranges

From the reviewed literature, it is clear that the leakage and self-sealing experienced in cracked concrete is highly dependent on the crack width, with greater crack widths being less likely to self-seal and taking longer to do so. The leakage prediction model thus considers the leakage depending on the range in which the crack width falls. As additional statistical uncertainty may be introduced when characterizing a distribution to an inadequate number of sample points, the distribution for each crack width range is fit and analysed to determine the confidence in the suitability of the fits. Distributions are fit for each of the following crack width ranges: $0.05 < w \leq 0.15$ mm, $0.15 < w \leq 0.25$ mm and $0.25 < w \leq 0.35$ mm.

5.2.2 Hydraulic ratio

The database contains samples with varying water pressure head and specimen thickness and thus varying hydraulic ratios (water head to section thickness, h^*/t or h_D/h in EN 1992-3). In consideration of practical WRS, it is important to note that the hydraulic pressure present at a crack is only developed by the head of water *above* the crack position. Additionally, the position of maximum tension (and most likely place for the maximum crack width to occur) in non-prestressed circular concrete WRS is generally at 0.4 to 0.7 of the height, down from the top of the wall, depending on the base fixity. In light of this, hydraulic ratios for circular WRS are typically in the range of 12.5-25. Table 5.3 gives more detailed characteristics of the sample geometry and hydraulic ratios of the database sources. The effect of the hydraulic ratio on the leakage and self-sealing is considered in section 5.2.8.

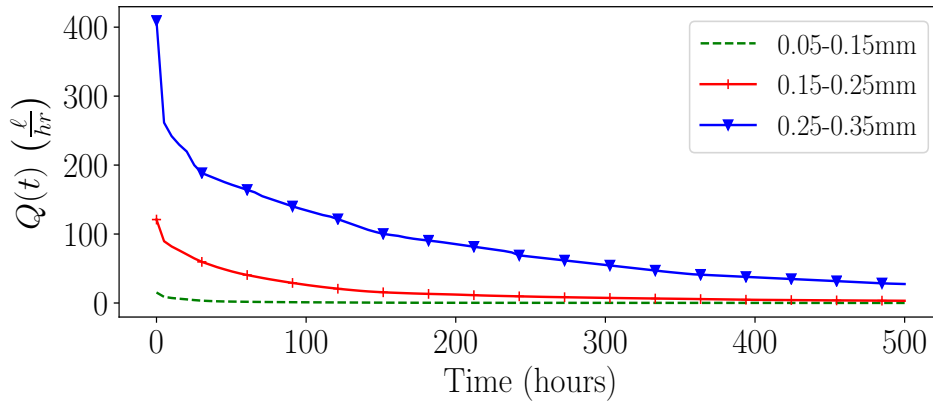
Table 5.3: Reduction of water flow over time database characteristics.

Author(s)	Sample Geometry ($\ell \times b \times h$)	Water head	h^*/t	Samples
Nanayakkara and Elakneshwaran (2005)	P150x150x200	2m	10	8
Ratnayake and Nanayakkara (2018)	C ϕ 150x200	2m	10	10
Ramm and Biscop (1997)	P300x600x180/300/600	2.5, 12m	4.2 - 67	36
Edvardsen (1996)	P200x200x200/400	2.5 - 10m	6.3 - 25	19

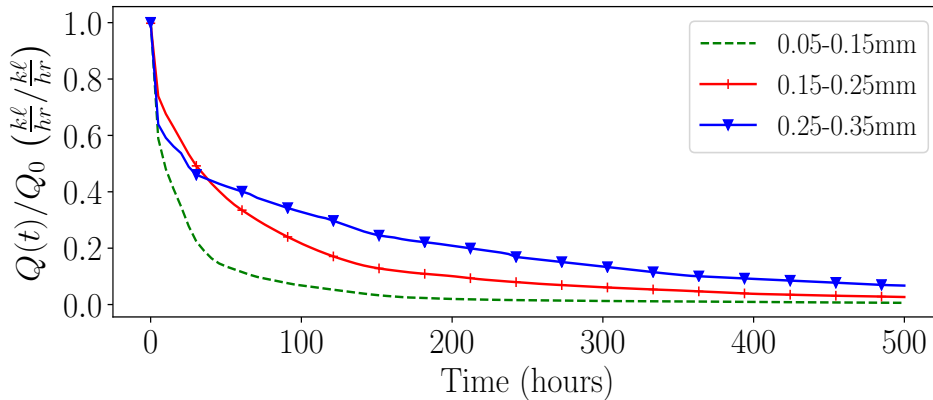
P - Prismatic, rectangular geometry; C - Cylindrical geometry

5.2.3 Leakage accumulation factor definition - θ_{idjd}

The flow through a crack is typically illustrated as flow over time, as shown in Figure 5.7(a). Here, however, the flow data from samples in the database are converted to normalized flow over time, in order to compare the data on the same basis for varying crack widths, h^*/t ratios etc., as can be seen in Figure 5.7(b). The normalized flow begins at 100% of the initial flow (Q_0) and decreases with time; quickly at first, likely due to the entrapment of air bubbles as identified by Ikoma *et al.* (2015), and then at a slower pace as the $CaCO_3$ precipitates form and as the other sealing mechanisms develop. An appreciation of the greater initial flow as a consequence of greater crack widths can be seen in Figure 5.7(a).



(a) Mean flow through cracks vs. time for different crack width ranges.



(b) Mean normalized flow through cracks vs. time for different crack width ranges.

Figure 5.7: Mean flow and mean normalized flow vs. time for different crack width ranges.

The total predicted leakage through a crack, Q_{total} , is determined by the probabilistically-predicted initial leakage, Q_0 (kl/hr), and a measure of the leakage over time considering self-sealing. A novel leakage accumulation factor, θ_{idjd} , is therefore introduced and characterized here as a means of probabilistically predicting the leakage through a tension crack between times t_i and t_j . The leakage accumulation factor is given as a function of Q_0 and can be interpreted as the accumulated, normalized leakage between times t_i and t_j in hours, as shown in Equation 5.11. The total flow through the crack between t_i and t_j is given by Equation 5.12.

$$\theta_{idjd} = \int_{t_i}^{t_j} \frac{Q(t)}{Q_0} dt \quad (\text{in hours}) \quad (5.11)$$

$$Q_{total,ij} = Q_0 \cdot \theta_{idjd} \quad (\text{in } kl) \quad (5.12)$$

An illustration of θ_{idjd} is shown in Figure 5.8 for a single sample from the database. The total accumulated flow through the crack from day 0 to 7 days is 84.8 hours worth of Q_0 flow, which equates to 73% of the total flow through the crack (73% of the total area under the curve, including the area to the right of the green section). Similarly, the total accumulated flow through the crack from day 0 to 14 days is 112.4 hours worth of Q_0 flow (97% of the total flow). The accumulated flow between time $t_i = 0$ days and $t_j = 7$ days is thus $\theta_{0d7d} = 84.8$ hours, illustrated as the red area under the curve in Figure 5.8. The accumulated flow between time $t_i = 7$ days and $t_j = 14$ days is therefore $\theta_{7d14d} = 27.6$ hours, illustrated as the green area under the curve in Figure 5.8.

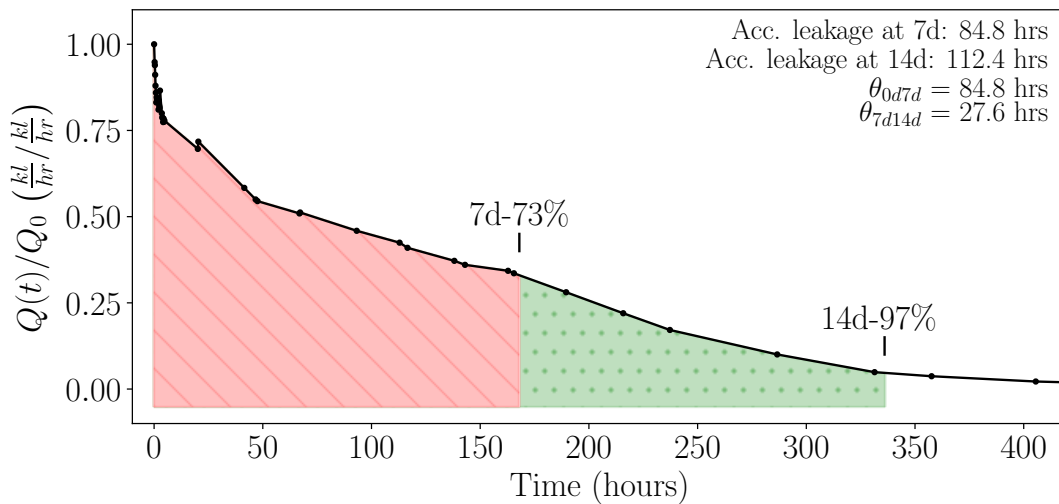


Figure 5.8: Example of normalized flow through a database sample and illustrations of θ_{idjd} .

Figure 5.8 shows an illustration of θ_{idjd} for a single sample. This process is followed for all samples in the database, by crack width range as discussed in section 5.2.1. The normalized, accumulated flow is then calculated at various combinations of start and end times for all samples, creating a distribution of values at each considered time combination, as discussed below.

5.2.4 Leakage regimes considered

The θ_{idjd} factor will be used as part of determining the leakage from a WRS in the context of a water tightness test. The combinations of start and end times at which to consider the leakage are therefore based on the recommended stabilization periods and water tightness test periods from prominent WRS design codes, as discussed in section 3.5.1. BS 8007 specifies a stabilization period of 7 days for a 0.1 mm target crack width and 21 days or more for a 0.2 mm crack width, which is followed by a water tightness test duration of 7 days. ACI 350.1-10 specifies a 3 day stabilization period, followed by a 5 day water tightness test, given a target crack width of 0.1 mm. From this, the following leakage regimes are considered:

Table 5.4: Leakage regimes, C_{idjd} , relating to stabilization period and water tightness test duration for leakage accumulation factor, θ_{idjd} .

Leakage regime	Leak. accum. factor	Stab. period start	Stab. period end	Water test start	Water test end	Code
C_{0d7d}	θ_{0d7d}	-	-	0	7	-
C_{3d8d}	θ_{3d8d}	0	3	3	8	ACI
C_{7d14d}	θ_{7d14d}	0	7	7	14	BS 8007
C_{14d21d}	θ_{14d21d}	0	14	14	21	BS 8007

Figure 5.9 gives a visual representation of the various leakage regimes. The leakage accumulation factor for C_{0d7d} , θ_{0d7d} , is shown by the combination of the orange and red areas under the curve; θ_{3d8d} is given by the combination of the red and blue area; θ_{7d14d} is given by the green and blue area and the θ_{14d21d} is given by the cyan area. The leakage that takes place during the stabilization period is discarded from the total leakage for the respective regimes.

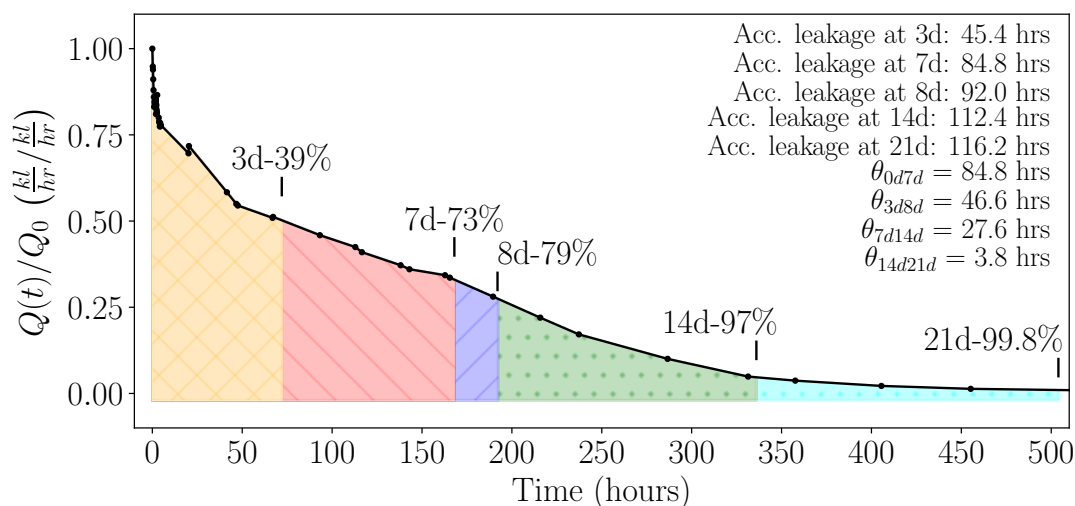


Figure 5.9: Visual illustration of θ_{idjd} leakage regimes.

The following sections discuss the distribution of the θ_{idjd} data and the characterization thereof, for each of the leakage regimes.

5.2.5 Characterization of θ_{0d7d}

Figure 5.10 shows a histogram of the accumulated relative flow at 7 days with no stabilization period, θ_{0d7d} . Units are in hours of leakage at the Q_0 rate, with fits for lognormal, exponential and 2-parameter Weibull distributions. The assumption of normality was ruled out a-priori, due to the same concerns as for the initial flow model uncertainty. Instead, an exponential distribution was tested, though with limited suitability of fit, being notably unrepresentative near the origin. The Weibull and lognormal distributions show the most potential as being representative of the data.

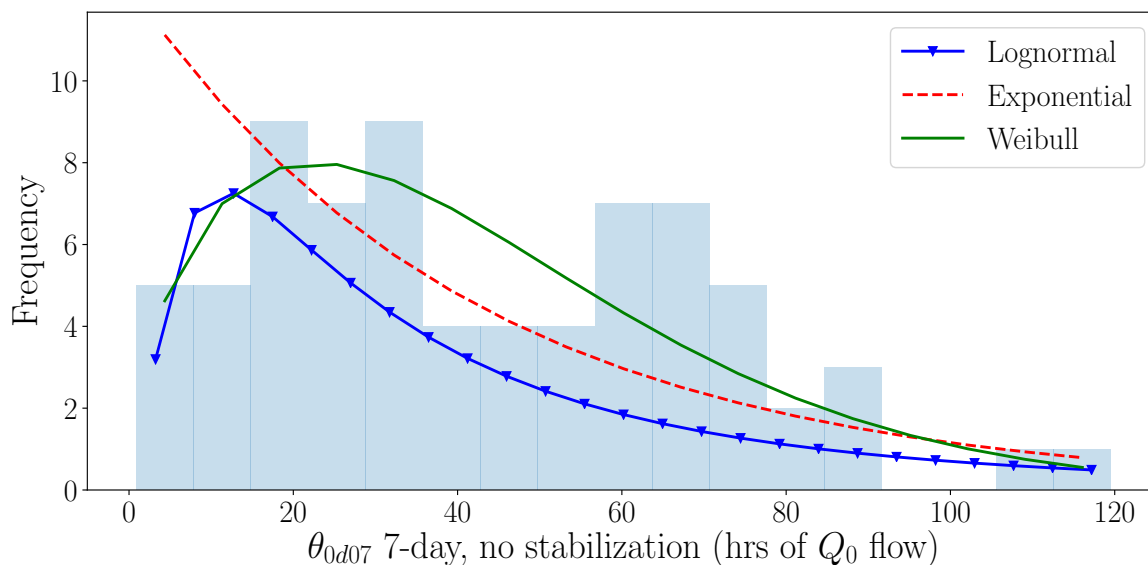


Figure 5.10: Histogram of accumulated flow values, θ_{0d7d} with lognormal, Weibull and exponential fits.

By inspection, the Weibull distribution seems to characterize the data better than the lognormal distribution. Probability plots of Weibull and lognormal fits to the θ_{0d7d} data are shown in comparison to the theoretical Weibull and lognormal probabilities with fitted shape and scale parameters as shown in Figure 5.11.

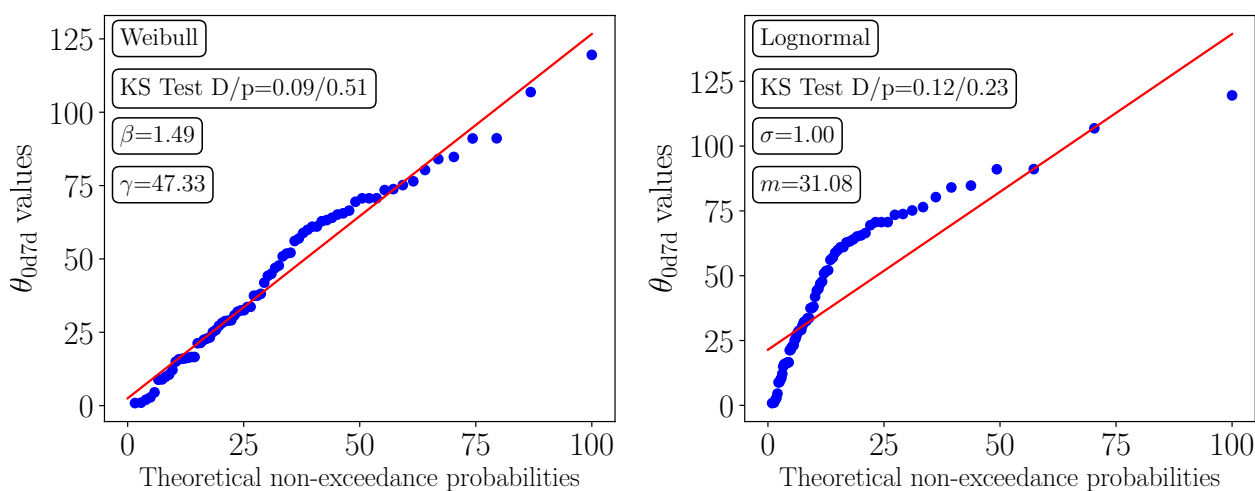


Figure 5.11: Probability plots of the Weibull and lognormal distributions for the θ_{0d7d} data.

As can be seen from the p-values from the KS test results in Figure 5.11, the fitted distributions are less representative of the data than for the model factor of the initial flow prediction. The number of samples in the current data is fewer than for the initial flow prediction (73 samples, in comparison to 360). In light of this, the KS test p-value and D-statistic are to be adjusted to account for the reduced number of samples, as the confidence in the fitted distribution reduces with fewer samples. The sample D-statistic in this case is required to be lower than $1.36/\sqrt{n} = 0.159$ (for sample size > 35 at a significance level $\alpha = 0.05$) to confirm that the null hypothesis cannot be rejected. Both fitted distributions fall below this threshold, so neither can be outright rejected but it is clear that the

Weibull characterizes the data better than the lognormal. A further verification of the suitability of the Weibull fits can be seen in Figure 5.13 in the following section.

5.2.5.1 Characterization of θ_{0d7d} by crack width range

In this section, the θ_{0d7d} data is separated into the three crack width ranges, similarly to the initial flow prediction model factor. A distribution is fit to each range and statistical suitability tests are performed thereon. In agreement with the findings of Edvardsen (1996), greater crack widths were found to lead to reduced self-sealing and thus greater relative leakage over time, in addition to greater initial leakage. Figure 5.12 and Table 5.5 illustrate the effect that increases in crack width have on the degree and extent of leakage at 7 days, with no stabilization period. Figure 5.12 shows Weibull fits to the θ_{0d7d} data for each crack width range.

As the crack width increases, the mean of the data shifts further to the right, as illustrated in Figure 5.12 and as numerically shown in Table 5.5, indicating greater leakage. For the first range (0.05-0.15mm), the leakage is concentrated towards the origin. As the crack width increases, the shapes flatten out, changing more towards that of a Weibull or lognormal shape and eventually nearing a normal-type shape in the 0.25-0.35mm range. Over the entire crack width range, the fit appears to be more typical of a Weibull distribution. The final column of Table 5.5 shows the mean fraction of the total leakage (from $t=0$ to t_{end} , when the crack stops leaking entirely), that has already transpired by 7 days. Narrower cracks are shown to have experienced most of their total leakage within 7 days, whereas wider cracks have only realised two-thirds of the total leakage by 7 days.

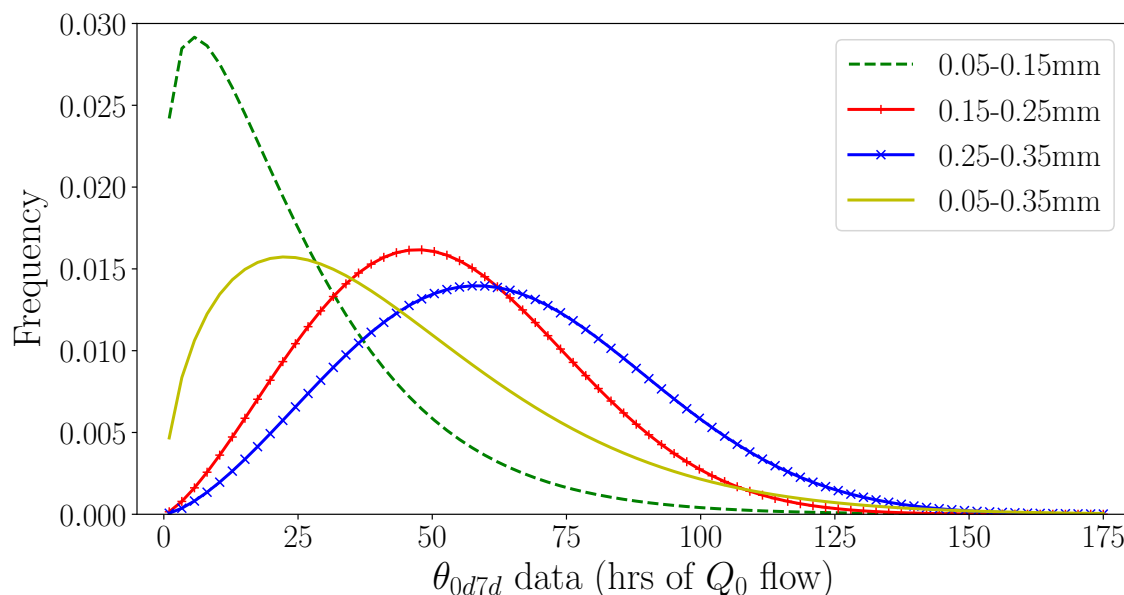


Figure 5.12: Weibull fits to normalized, accumulated leakage at 7 days, with no prior stabilization period, varied by crack width range.

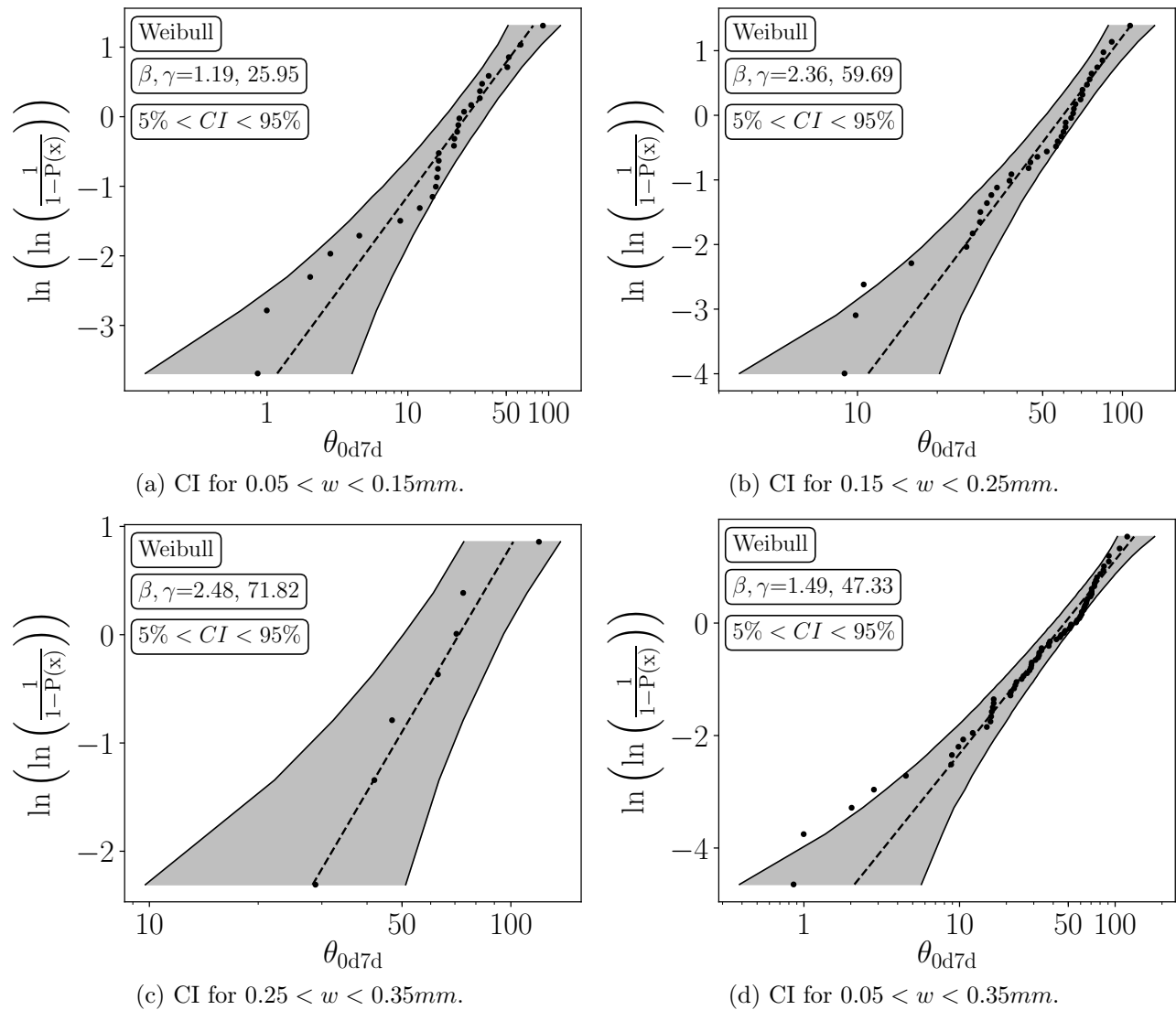
Table 5.5: Characteristics of Weibull fits to crack width ranges for θ_{0d7d} data.

Crack width range	Sample size	Weibull shape/scale	Mean	KS Test D/p	Rejection D level	Validity	Leakage frac.
0.05-0.15mm	28	1.19 / 25.95	24.5	0.15 / 0.48	0.25	Accept	93%
0.15-0.25mm	38	2.36 / 59.69	53.0	0.13 / 0.50	0.22	Accept	74%
0.25-0.35mm	7	2.48 / 71.82	63.5	0.20 / 0.94	0.48	Accept*	65%
0.05-0.35mm	73	1.49 / 47.33	43.1	0.09 / 0.51	0.16	Accept	80%

*Due to the limited sample size, this distribution is statistically acceptable, but will only be used indicatively.

Table 5.5 illustrates the sample size of each of the crack width ranges and gives an indication of the confidence in the associated fitted Weibull distributions through KS D-statistics/p values. The table also lists threshold D-statistic values, for rejection of the null hypothesis that the data is represented by the fitted distribution. The first, second and overall crack width ranges are shown to have acceptable agreement with the fitted Weibull distributions. The statistics related to the third crack width range, however, are misleading. According to the KS test p value, the data is well represented by the distribution fit. Similarly, the D-statistic of the data seems to be well below the rejection level, but both of these are of limited use. Due to the limited data in this crack range (7 samples), there is not enough data to reject the null hypothesis, except if the data is notably misrepresented by the distribution fit. Thus, the distribution of the crack width range of 0.25-0.35mm will be used as being indicative of the true distribution. Considering the progression of the distributions for the other crack width ranges, the proposed distribution seems to follow the trend.

Visual representations of the uncertainty associated with the number of samples, and the distribution fits related thereto, are shown in Figure 5.13 in the form of approximate confidence intervals (CI's) overlaying Weibull plots of the θ_{0d7d} data. The two-sided CI's exclude the bottom and top 5%, giving a CI of 90%. The CI's were generated using Monte-Carlo simulation, by repeatedly sampling the same number of points as the original data (refer to Table 5.5) from the proposed Weibull distributions, for each crack width range. The wide CI for the $0.25 < w < 0.35$ mm crack width range is indicative of the greater uncertainty associated with the limited sample size. By comparison, the CI's of the other crack width ranges are narrower, illustrating the relationship between sample size and statistical confidence in distribution fits. The original θ_{0d7d} data can be seen as the black dots around the fit line in the figures, a further indication that the Weibull characterizes the data well. The close proximity of the points to the fit line also gives confidence in the distribution fit for the $0.25 < w < 0.35$ mm crack width range.

Figure 5.13: CI's for θ_{0d7d} data for various crack width ranges.

5.2.6 Characterization of θ_{3d8d}

The same process to that of characterizing the θ_{0d7d} leakage was followed for the θ_{3d8d} leakage for each crack width range. The θ_{3d8d} data represents a 3 day stabilization period followed by a 5 day water tightness test, corresponding to ACI water tightness test requirements.

5.2.6.1 Characterization of θ_{3d8d} by crack width range

Figure 5.14 shows the Weibull distribution fits to the θ_{3d8d} data for each of the crack width ranges, with characteristics as shown in Table 5.6. In comparison to Figure 5.12, the θ_{3d8d} distributions are more positively skewed and are flatter, indicating greater variation in the data albeit with a lesser magnitude of values, due to the stabilization period. The considerable reduction in magnitude can be seen from the *Mean* column of Table 5.6, in comparison to that of Table 5.5. The $0.05 - 0.15\text{mm}$ range can be seen to be approaching an exponential-decaying shape, however, a Weibull distribution was still found to be more representative of the data and was retained as the distribution of choice. The KS tests confirm that the distributions are appropriate and that the null hypotheses cannot be rejected,

although the concerns surrounding the $0.25 < w < 0.35$ mm crack width range for the θ_{0d7d} data are also noted here.

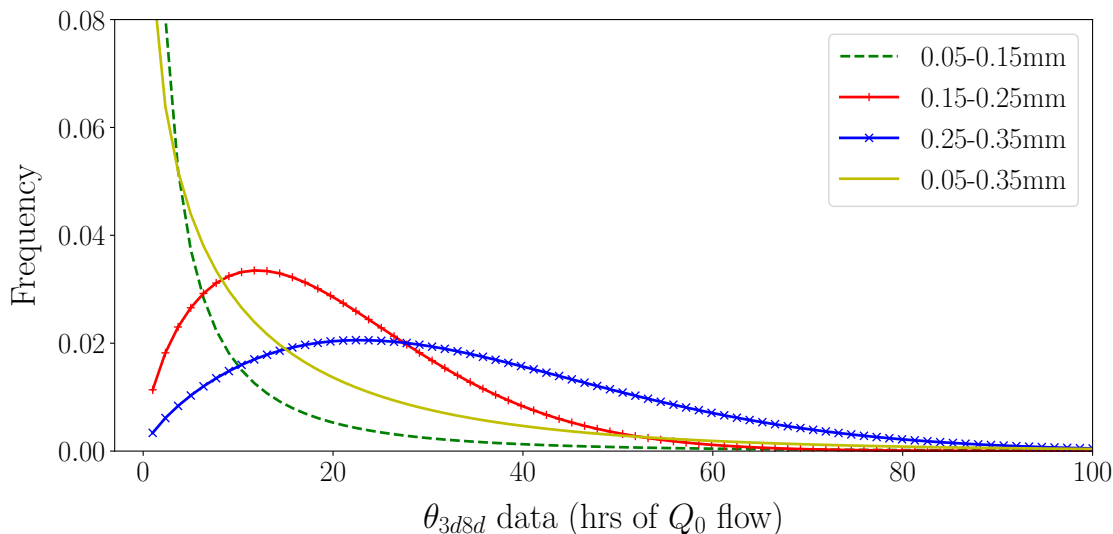


Figure 5.14: Weibull fits to normalized, accumulated leakage at 8 days, including a 3 day stabilization period, varied by crack width.

Table 5.6: Characteristics of Weibull fits to crack width ranges for θ_{3d8d} data.

Crack width range	Sample size	Weibull shape/scale	Mean	KS Test D/p	Rejection D level	Validity	Leakage frac.
0.05-0.15mm	28	0.52 / 3.40	5.9	0.14 / 0.57	0.25	Accept	94.0%
0.15-0.25mm	38	1.58 / 22.6	20.3	0.12 / 0.63	0.22	Accept	77.2%
0.25-0.35mm	7	1.71 / 38.1	33.9	0.19 / 0.97	0.48	Accept*	69.0%
0.05-0.35mm	73	0.77 / 14.25	16.1	0.11 / 0.31	0.16	Accept	83.0%

*Due to the limited sample size, this distribution is statistically acceptable, but will only be used indicatively.

Figure 5.15 shows Weibull plots of each of the crack width ranges overlain by approximate 90% CI's for the θ_{3d8d} data. The data is shown to be well-characterized by a Weibull distribution and the CI's indicate that there is reasonable confidence in the distributions, despite the limited number of samples (with the exception of the $0.25 < w < 0.35$ mm range).

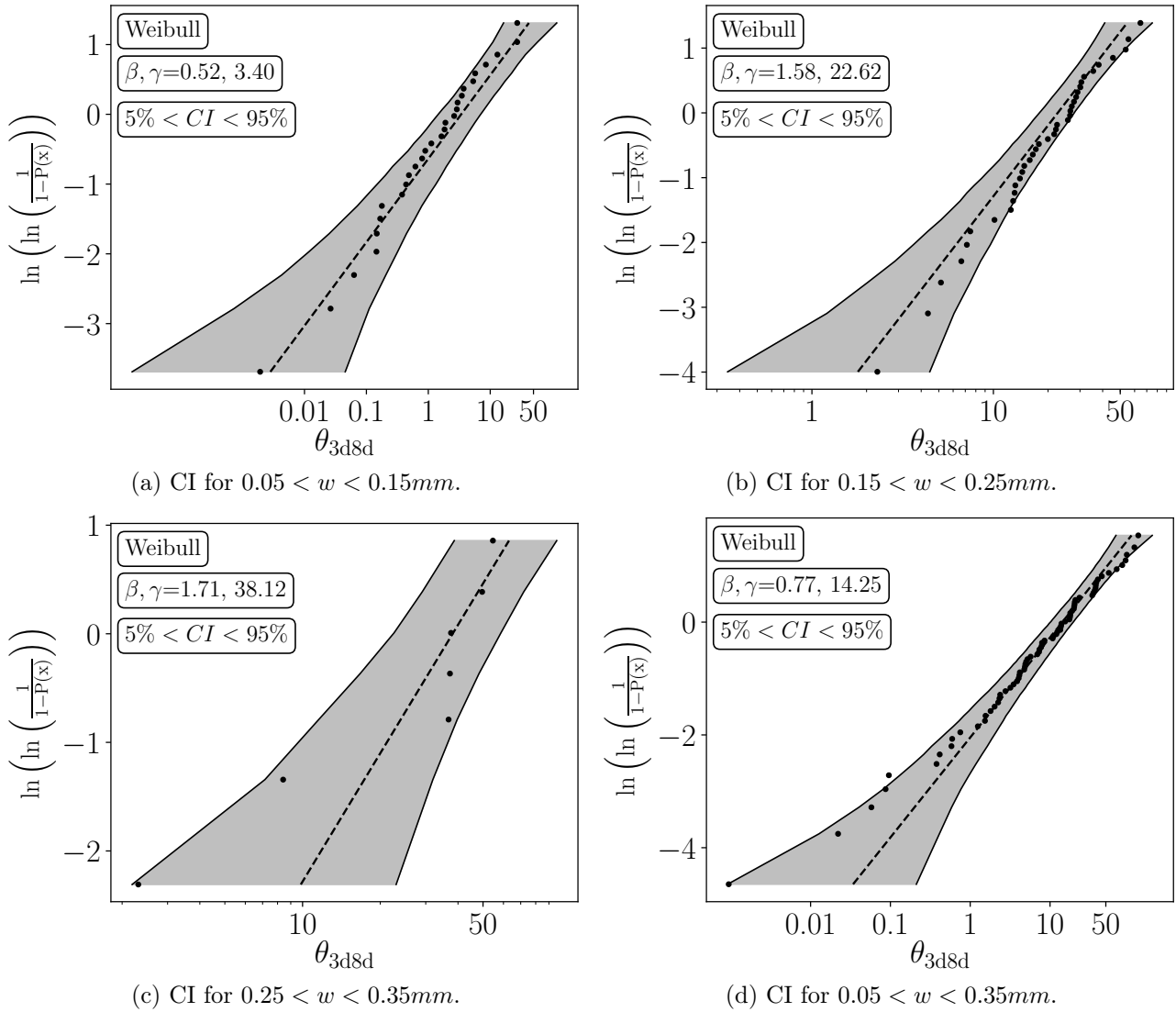


Figure 5.15: CI's for θ_{3d8d} data for various crack width ranges.

5.2.7 Characterization of θ_{7d14d} and θ_{14d21d}

The results from the θ_{7d14d} and θ_{14d21d} are grouped together due to their similarity in behaviour. Both exhibit considerably less leakage than the previous leakage regimes, due to the increasing stabilization periods. The two regimes are considered by crack width range as before.

5.2.7.1 Characterization of θ_{7d14d} and θ_{14d21d} by crack width range

A histogram of the distribution fits to the θ_{7d14d} data is shown in Figure 5.16; the θ_{14d21d} histograms are similar and are not shown, to avoid unnecessary repetition. One can see the shift towards the left, showing that the leakage is considerably reduced from previous leakage regimes. It is so much reduced that the distributions now closely resemble exponential distributions.

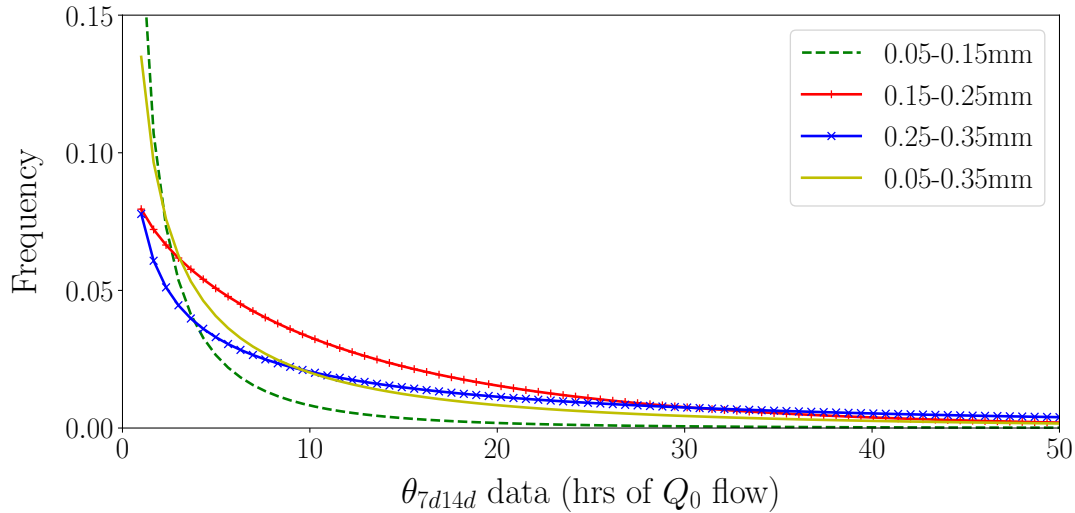


Figure 5.16: Distribution fits to normalized, accumulated leakage at 14 days, including a 7 day stabilization period, θ_{7d14d} , varied by crack width (θ_{14d21d} data similar).

Table 5.7 shows the distribution parameters and descriptive statistics for the θ_{7d14d} and θ_{14d21d} data. Despite the exponentially decaying shape of the data, the inflexibility of the exponential distribution meant that a Weibull distribution was again most representative of the data. In both cases for the 0.25–0.35 mm range, however, the KS test results from Weibull and exponential distribution fits were similar, with no clear indication of which is more appropriate, especially given the limited confidence in the KS results from the small sample size. In order to keep the statistical uncertainty consistent, Weibull distributions were used for both, as before. The fraction of the total leakage is shown to be further advanced than the previous regimes, and so much so for the θ_{14d21d} regime, that considering leakage times after 21 days would make little difference to the resulting leakage. From Table 5.7, the mean leakage from the 0.25–0.35 mm range is in the vicinity of ≈ 9 times the mean leakage of the 0.05–0.15 mm range for both regimes, compared to ≈ 6 and ≈ 3 times for the θ_{3d8d} and θ_{0d7d} regimes, respectively. This shows that the relative leakage (and self-sealing) is more sensitive to crack width with increasing time and stabilization period.

Table 5.7: Characteristics of Weibull distribution fits to crack width ranges for θ_{7d14d} and θ_{14d21d} data.

Crack width range	Sample size	Dist. parameters	Mean	KS Test D/p	Reject. D level	Validity	Leakage frac.
θ_{7d14d} data							
0.05-0.15mm	28	0.49 / 1.20	2.7	0.15 / 0.54	0.25	Accept	98%
0.15-0.25mm	38	0.92 / 12.91	13.3	0.17 / 0.18	0.22	Accept	88%
0.25-0.35mm	7	0.62 / 22.51	28.4	0.28 / 0.57	0.48	Accept*	81%
0.05-0.35mm	73	0.56 / 6.93	10.7	0.13 / 0.14	0.16	Accept	92%
θ_{14d21d} data							
0.05-0.15mm	28	0.46 / 0.46	1.47	0.17 / 0.38	0.25	Accept	99.6%
0.15-0.25mm	38	0.70 / 5.02	6.24	0.09 / 0.91	0.22	Accept	95.5%
0.25-0.35mm	7	0.56 / 10.01	14.55	0.31 / 0.43	0.48	Accept*	91.4%
0.05-0.35mm	73	0.48 / 2.54	5.20	0.11 / 0.30	0.16	Accept	96.7%

*Due to the limited sample size, this distribution is statistically acceptable, but will only be used indicatively.
Weibull dist. parameters - shape/scale, loc=0

The CI's for each distribution for the θ_{7d14d} data are shown in Figure 5.17; the CI's for the θ_{14d21d} are similar, and are therefore not shown. As before, the first two crack width ranges are well-characterized by a Weibull distribution and form narrow confidence bands. The Weibull probability plot shown for the 0.25–0.35 mm range, with a similar 90% confidence band, shows notable uncertainty as before.

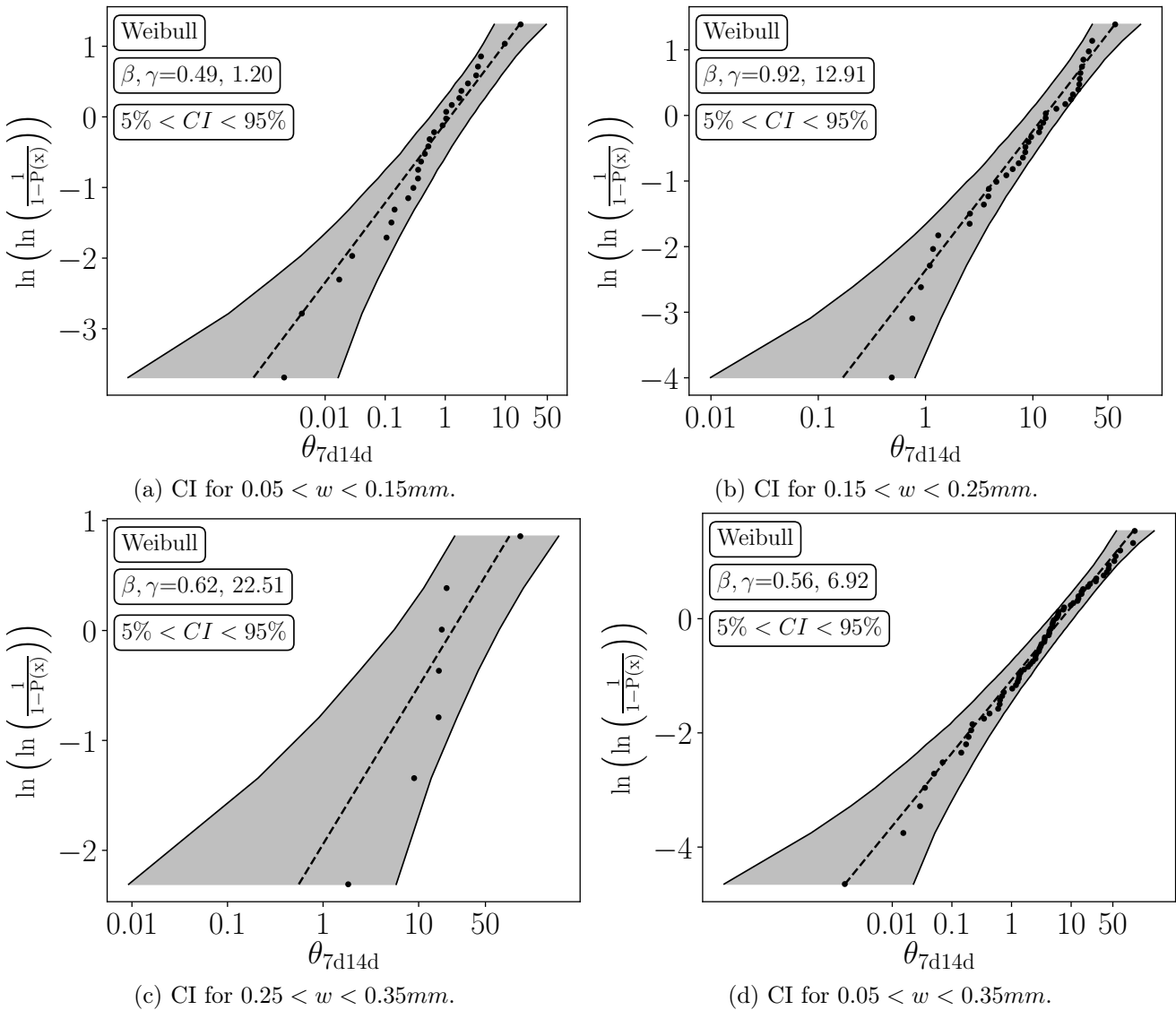


Figure 5.17: CI's for θ_{7d14d} data for various crack width ranges (θ_{14d21d} similar).

5.2.8 Consideration of hydraulic ratio

As Edvardsen (1996) and Ramm and Biscopig (1997) note, increasing hydraulic ratios delay the self-sealing efficiency and extent. Due to the relatively decreasing section thickness to increasing water pressure, the increased speed of the water flowing through the cracks is detrimental to the formation of the calcite crystals. An increased hydraulic ratio retards the self-sealing ability, though to a lesser extent than increases in crack width. Due to the limited number of samples and spread of hydraulic ratios, a full probabilistic quantification of the effect of increases in hydraulic ratio on the duration of leakage could not be made. A semi-probabilistic approximation is therefore used for two broad ranges of $h^*/t < 20$ and $20 \leq h^*/t$.

Each leakage regime was broken up into two crack width ranges, 0–0.15 mm and 0.15–0.25 mm (range 0.25–0.35 mm had too few samples to be separated into two groups). Each crack width range was then separated into the two groups for which $h^*/t < 20$ (low) and $20 \leq h^*/t$ (high), respectively. The mean accumulated leakage value for the whole h^*/t range, μ_{tot} , is then compared to the means for the two separate h^*/t ranges, μ_{low} and μ_{high} , in order to gauge the effect that the h^*/t ratio has on the resultant leakage. The results are shown in Table 5.8 and Figure 5.18.

Table 5.8: Data for the approximation of the effect of h^*/t ratio on self-sealing.

	w range (mm)		h^*/t range	h^*/t mean
	0.05–0.15	0.15–0.25		
Samples in μ_{low}	22	11	4-19	9.4
Samples in μ_{high}	6	27	20-67	34.4
Samples in μ_{tot}	28	38	4-67	20

Factor	w range	μ_{low} (hrs)	μ_{tot} (hrs)	μ_{high} (hrs)	μ_{low}/μ_{tot}	μ_{high}/μ_{tot}
θ_{0d7d}	0.05-0.15	19.30	24.50	43.60	0.79	1.78
	0.15-0.25	32.60	53.03	61.36	0.61	1.16
θ_{3d8d}	0.05-0.15	3.12	5.90	16.10	0.53	2.73
	0.15-0.25	13.47	20.32	23.11	0.66	1.14
θ_{7d14d}	0.05-0.15	1.52	2.74	7.24	0.55	2.64
	0.15-0.25	8.98	13.30	15.09	0.68	1.13
θ_{14d21d}	0.05-0.15	0.80	1.47	4.00	0.54	2.72
	0.15-0.25	3.56	6.24	7.30	0.57	1.17
Mean ratio					0.62	1.81

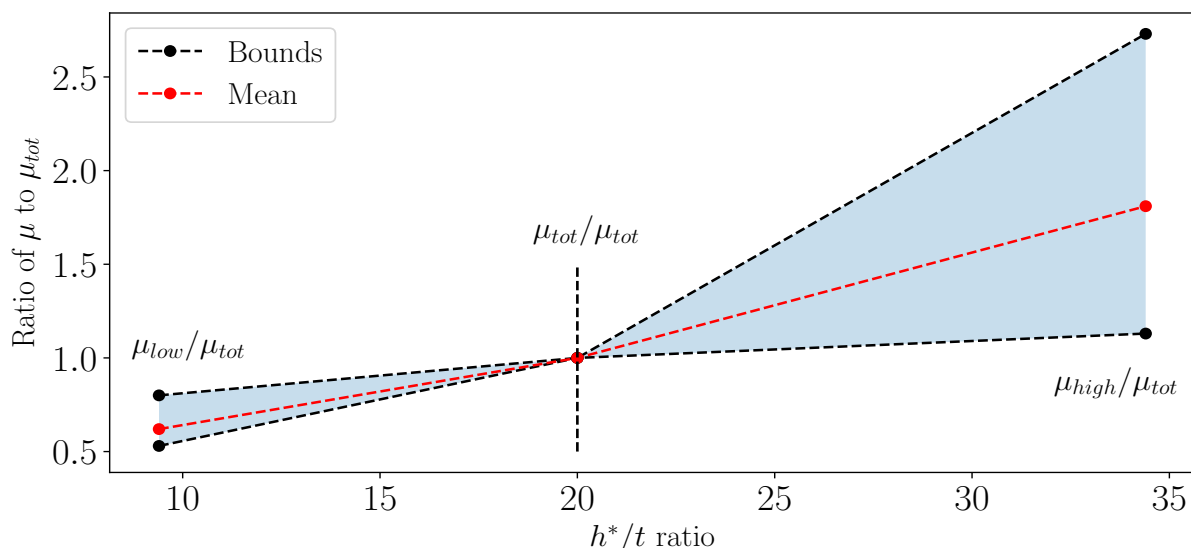


Figure 5.18: Illustration of the effect of h^*/t ratio on the mean leakage, relative to μ_{tot} .

From Figure 5.18 (red line) and Table 5.8 it can be seen that the mean value of accumulated leakage for samples in the lower h^*/t range (μ_{low}) is 0.62 times the mean accumulated leakage of the whole h^*/t range (μ_{tot}). The mean accumulated leakage of the samples in the upper range (μ_{high}) is shown

to be 1.81 times μ_{tot} . The mean h^*/t ratios of the lower and upper ranges are at $h^*/t = 9.4$ and $h^*/t = 34.4$, respectively.

The effect of the h^*/t ratio is included in the leakage prediction model through the use of a hydraulic ratio factor, θ_{HR} , calculated as per Equations 5.13 and 5.14. The θ_{HR} factor is illustrated by the red line in Figure 5.18, and is interpolated for h^*/t ratios between $9.4 \leq h^*/t < 20$ and $20 \leq h^*/t < 34.4$. The leakage accumulation factor is multiplied by the hydraulic ratio factor to incorporate a measure of the effect of hydraulic ratio on self-sealing, as shown in Equation 5.15.

$$\text{for } h^*/t < 20 \quad \theta_{HR} = 0.62 + 0.0358 \cdot (h^*/t - 9.4) \quad (5.13)$$

$$\text{for } 20 \leq h^*/t \quad \theta_{HR} = 1 + 0.0563 \cdot (h^*/t - 20) \quad (5.14)$$

5.3 Total leakage prediction model

Combining the initial flow prediction and leakage prediction models, the total probabilistically-predicted leakage through a crack in a tension-cracked, reinforced concrete element between time i and j and a given h^*/t ratio is given as:

$$\begin{aligned} Q_{total,ij} &= Q_0 \cdot \theta_{ijd} \cdot \theta_{HR} \\ &= \theta_{Q0} \cdot \frac{0.11 \Delta p \ell w^3}{12 \eta d} \cdot \theta_{ijd} \cdot \theta_{HR} \end{aligned} \quad (5.15)$$

Where:

Q_0 Predicted initial flow in kl/hr

θ_{Q0} Initial flow prediction model uncertainty

θ_{ijd} Normalized, accumulated leakage between time i and j , in hrs of Q_0 flow

θ_{HR} Hydraulic ratio factor

Table 5.9: Statistical Weibull distribution parameters for the total leakage model.

Parameter	Shape/Scale	Parameter	Shape/Scale
θ_{Q0} for $0.05 < w \leq 0.15mm$	0.98 / 0.90	θ_{7d14d} for $0.05 < w \leq 0.15mm$	0.49 / 1.20
for $0.15 < w \leq 0.25mm$	1.64 / 1.31	for $0.15 < w \leq 0.25mm$	0.92 / 12.91
*for $0.25 < w \leq 0.35mm$	1.58 / 1.03	*for $0.25 < w \leq 0.35mm$	0.62 / 22.51
for $0.05 < w \leq 0.35mm$	1.33 / 1.12	for $0.05 < w \leq 0.35mm$	0.56 / 6.93
θ_{0d7d} for $0.05 < w \leq 0.15mm$	1.19 / 25.95	θ_{14d21d} for $0.05 < w \leq 0.15mm$	0.46 / 0.46
for $0.15 < w \leq 0.25mm$	2.36 / 59.69	for $0.15 < w \leq 0.25mm$	0.70 / 5.02
*for $0.25 < w \leq 0.35mm$	2.48 / 71.82	*for $0.25 < w \leq 0.35mm$	0.56 / 10.01
for $0.05 < w \leq 0.35mm$	1.49 / 47.33	for $0.05 < w \leq 0.35mm$	0.48 / 2.54
θ_{3d8d} for $0.05 < w \leq 0.15mm$	0.52 / 3.40		
for $0.15 < w \leq 0.25mm$	1.58 / 22.60		
*for $0.25 < w \leq 0.35mm$	1.71 / 38.10		
for $0.05 < w \leq 0.35mm$	0.77 / 14.25		

*Distribution only indicative due to limited sample size.

5.3.1 Discussion on model use

The probabilistic leakage prediction model is envisaged to be used within the context of a typical circular WRS. Specifically, it is used to probabilistically predict the level of reliability resulting from the leakage vs allowable leakage in the SLS design of WRS with regard to the chosen design crack width.

The effect of the hydraulic ratio is implemented here in a simplified form, due to the limited number of samples and distribution of h^*/t ratios. Furthermore, the effect of the cyclic nature of cracking in WRS is not taken into account in this research as there is not enough experimental data to be able to characterize the effect of dynamic cracks. Additionally, at water tightness testing stage the structure will be filled with water and left in such a state. Thus there is no cyclic action, as the water level is kept constant until the end of the test. Consideration of the behaviour of the WRS after water tightness testing stage is beyond the scope of this research.

5.4 Chapter summary

Chapter 5 details the development of the probabilistic models for the prediction of initial flow through a crack in WRS, as well as for the prediction of leakage through the same for four different leakage regimes. The two models are then combined to create a probabilistic model for the prediction of the total leakage through a crack in an ordinary, tension-cracked concrete WRS. The definition of this model is the first step towards being able to predict the total leakage outflow from a WRS, given a design value of crack width.

6. Prediction of Leakage in a Reservoir

6.1 Introduction

Concepts of reliability are used to create a uniformity and consistency in the design of structures to ensure that structures are designed considering the costs, associated risks and consequences of failure. Due to the potential for catastrophic failure and loss of human life associated with ULS failures, a vast degree of research into the optimization of ULS-governed structures has been conducted to date. Comparatively little research effort has been dedicated to SLS-governed structures (Beeby and Narayanan, 2009). As such, WRS in general, have received little reliability-related consideration.

The design of a WRS (interchangeably called a reservoir), is different to typical reinforced concrete structures. In design, most reinforced concrete structures are governed by the resistance of members against typical ULS failures, such as failure in flexure due to a moment or crushing of the concrete, due to axial loads or shear. Comparatively, reservoirs are governed by resistance against SLS failures and not strength requirements. Specifically, the primary requirement of a reservoir is to retain water. The leakage of the retained water is to be limited to an acceptable level, which is accomplished by designing the structure to keep the cracks below a certain threshold crack width. The reinforcing steel required to limit the crack widths to values smaller than the threshold limits (typically 0.05-0.3mm) is greater than that required for ULS purposes in practically all cases (McLeod, 2013; Holický *et al.*, 2009). The limitation of crack widths to below the code-specified values then generally results in the leakage being below the allowable leakage limits.

The crack width limits are therefore considered deemed-to-satisfy criterion, and are based on previous experience of satisfactory performance over a number of decades. The achieved level of reliability (β value) associated with these deemed-to-satisfy requirements, however, remains unknown. Qualitatively, decreases in design crack width result in smaller cracks that leak less and have a greater probability of self-sealing, and will thus increase the level of reliability. However, there is currently no *quantitative* measurement of how adjustments to design crack width affect the SLS reliability performance of the structure. This makes the structural optimization of WRS difficult, if not impossible.

Given the above, this chapter aims at presenting and further developing the necessary theory and background to be able to use the total leakage model developed in chapter 5 to predict the achieved SLS level of reliability of a reservoir, based on considerations of acceptable leakage. In chapter 5, the total leakage model was developed to predict the leakage through a single tension crack in reinforced concrete. This chapter now applies the model to the case of a reservoir, in order to predict the leakage that transpires, considering the effect of self-sealing. The leakage is predicted using the probabilistic total leakage model and is evaluated against the code-defined allowable leakage, in order to determine the achieved level of reliability. In order to determine the leakage that transpires from a reservoir, the

reservoir structure, geometry and environment need to be considered. This chapter discusses these details, in terms of the loading on, and design of the structure and cracking in tension-governed reservoirs in general.

As a first step towards determining the effect that self-sealing has on the level of SLS reliability in a whole reservoir, a probabilistic sensitivity analysis is performed on the total leakage prediction model. A sensitivity analysis is typically performed on a model to determine how variation in the input parameters affect the model output (Holický, 2009). As such, a sensitivity analysis is performed on the total leakage prediction model to get an indication of which parameters contribute the most uncertainty to the prediction of the total leakage. The results from the sensitivity analysis are then used to reduce the complexity of the model by replacing the probabilistic parameters that contribute little uncertainty to the total leakage with deterministic mean value equivalents. Another aim of the sensitivity analysis is to investigate the behaviour of the total leakage prediction model. The sensitivity analysis is performed on a simplified "slice" of a reservoir, corresponding to the leakage through a single crack. The slice model is then expanded and incorporated into an analysis of a complete reservoir in chapter 7.

The following sections detail the development of the reservoir-environment, to be able to evaluate the predicted leakage against the allowable leakage.

6.2 Reservoir loading

In this research, only above-ground, circular, reinforced concrete reservoirs with a simply supported roof (or no roof) and with no backfill against the walls are considered. As such, the only load considered to act on the walls is the hydrostatic load from the retained water. The triangular hydrostatic load acting on the reservoir walls is dependent on the height and unit weight of the retained water, $\gamma_w = \rho_w \cdot g$. The maximum hydrostatic pressure, σ_w , for a height of retained water, h , is given by Equation 6.1.

$$\sigma_w = h \cdot \gamma_w \quad (6.1)$$

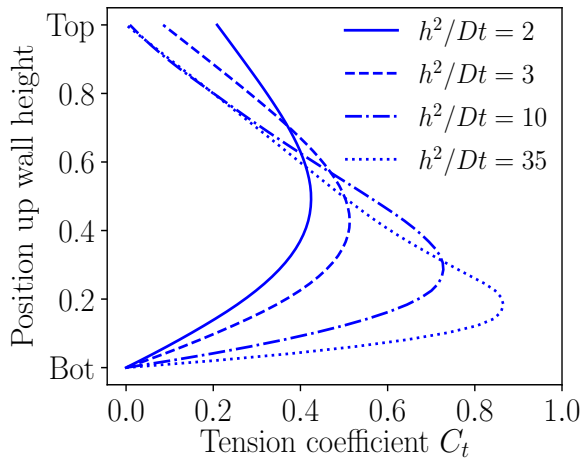
Due to the cylindrical shape of the structure, the hydrostatic load causes hoop tension forces in the walls that act in the plane of the walls. The radius of the reservoir, $r = D/2$, affects the magnitude of the hoop tension. In the case of a sliding base, i.e. where there is no restraint of movement perpendicular to the wall, the maximum hoop tension develops at the bottom of the wall, where the hydrostatic load is at a maximum, and is given by Equation 6.2, with a tension coefficient, C_t equal to 1. Given that sliding bases are only used for prestressed circular concrete reservoirs, the effect of the base restraint, which restrains movement perpendicular to the wall, whether it be hinged or fixed, must also be taken into account. From force equilibrium in a thin-walled pressure vessel, the equation for the hoop tension developed in the wall, T , is given by Equation 6.2.

$$T = \gamma_w \cdot h \cdot \frac{D}{2} \cdot C_t \quad (6.2)$$

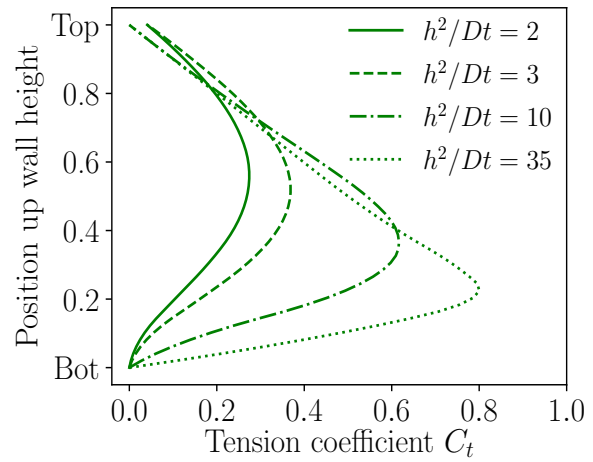
The tension coefficient, C_t , considers the effect of the reservoir geometry, as well as the base restraint conditions and is determined as a function of the h^2/Dt ratio, where t is the wall thickness (this assumes that the wall height and the height of retained water are synonymous). In effect, C_t is a fraction of the absolute maximum hoop tension that would be experienced by a reservoir with a sliding base, as is illustrated by Equation 6.2, with $C_t = 1$. This coefficient simplifies the design considerably, as the derivation of the tension force in the wall from first principles is both complex and time consuming. The C_t coefficients were initially made popular through a publication by the Portland Cement

Association in the USA (PCA, 1943). This design method has been adapted and is still used in water retaining design codes today, such as in IS 3370-4:1967 (R2004). Tables of C_t values for fixed and pinned (hinged) base conditions are given in Appendix B.

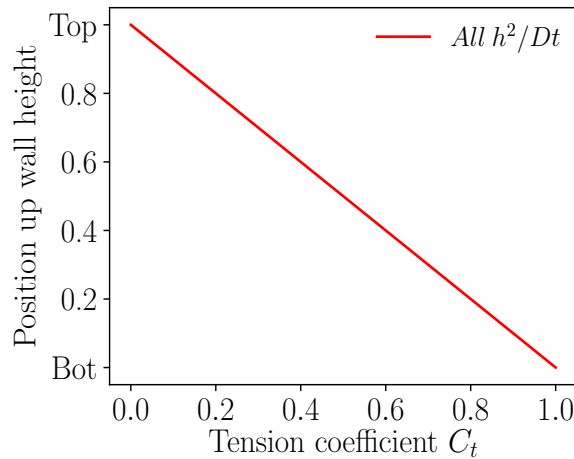
The tabled C_t values are given as a function of the distance from the top of the wall and are derived from a differential equation typically used for a beam on elastic foundation. Figure 6.1 illustrates the difference that the base restraint condition makes to the shape of the distribution up the height of the wall and also the magnitude of the tension coefficient. Figure 6.2 further illustrates the comparison between the fixed and pinned base restraints for various h^2/Dt ratios. The lower h^2/Dt ratios in Figure 6.2 illustrate the case of a relatively shorter reservoir with a large diameter and a thick wall section, for which it can be seen that the C_t value is more uniform across the height of the wall. The higher h^2/Dt ratios represent relatively taller reservoirs with small diameter and wall thickness, which have a higher tension load concentrated lower down on the wall. The maximum tension force is developed at the point along the wall height where C_t is at a maximum.



(a) Base restraint condition hinged, top free.



(b) Base restraint condition fixed, top free.



(c) Base restraint condition sliding, top free.

Figure 6.1: Effect of base restraint on C_t .

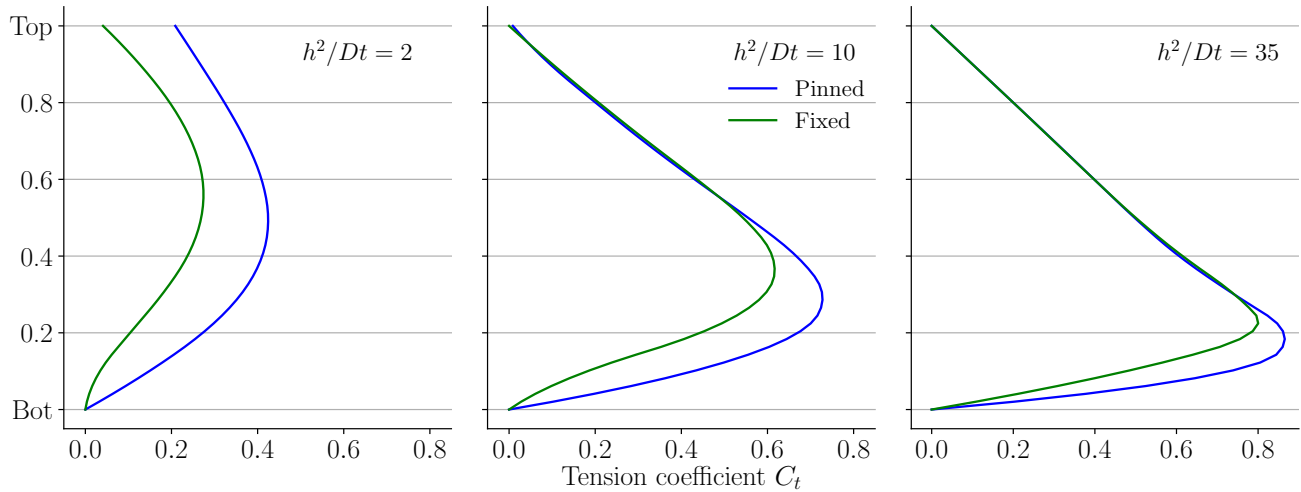


Figure 6.2: Comparison of the effect of hinged and fixed base conditions (top free) on C_t for various h^2/Dt ratios.

Equation 6.2 is used in this and subsequent chapters to determine the hoop tension forces, $T(h)$, as a function of the height down from the top of the wall. It is also used to determine the point at which the tension force is at a maximum, T_{max} .

6.3 Load-induced cracking in reservoirs

In order to determine the level of reliability in a reservoir, both the leakage and allowable leakage need to be probabilistically determined. A reliability limit state (g) is defined as the difference between the allowable leakage and the predicted leakage, as shown in Equation 6.3. Acceptable leakage performance is defined by $0 \leq g$ and unacceptable leakage by $g < 0$. This section develops the theory of the predicted leakage (L_{al}) part of the limit state equation.

$$g = L_{al} - L_p \quad (6.3)$$

L_{al} = Allowable leakage

L_p = Predicted leakage

In order to realistically predict the leakage that results from tension cracks in reservoirs, the crack generation mechanism caused by the applied loading must first be considered. It is imperative that the development of tension cracks follows the cracking mechanism that would actually occur in reality. This section builds on from section 3.3 and 3.4. The MC 2010 crack width model is used as the model of choice for this research. This stems from the discussion in section 3.4.4, whereby MC 2010 was found to predict crack widths most consistently over the spectrum of cracking, due to its consideration of shrinkage strains in the concrete. Additionally, it is to be used instead of the current EN 1992-1-1 crack prediction model in the future revision of EN 1992-1-1.

Around the reservoir, the hoop tension force is developed due to the hydrostatic water load, which increases the strain in the concrete and steel (ϵ_s and ϵ_c , respectively). With reference to Figure 3.5, assuming that the strain contribution from shrinkage in the concrete, $\eta \epsilon_{sh}$, is independent of applied load, the general form of the calculation of crack widths is given by Equation 3.1. From this general form, a simplification is made in MC 2010 to use the average steel and concrete strain (ϵ_{sm} and ϵ_{cm} , respectively), to avoid the integration over the complex shape of the steel and concrete strains. In

addition, following from MC 2010, assuming a maximum spacing of $2l_{s,max}$ occurs between cracks in the stabilized cracking stage, the maximum design crack width will be realised, and is given by Equation 6.6. Parameters are described in section 3.3 and discussed in depth later in this section.

$$w_{max} = \int_{-l_{s,max}}^{l_{s,max}} (\epsilon_{sm} - \epsilon_{cm} - \eta \epsilon_{sh}) dl \quad (6.4)$$

$$= 2l_{s,max} \cdot (\epsilon_{sm} - \epsilon_{cm} - \eta \epsilon_{sh}) \quad (6.5)$$

$$= 2 \left(kc + \frac{1}{4} \frac{f_{ctm}}{\tau_{bms}} \cdot \frac{\phi_s}{\rho_{s,ef}} \right) \cdot \left(\frac{\sigma_s - \beta \frac{f_{ctm}}{\rho_{s,ef}} (1 + \alpha_e \rho_{s,ef})}{E_s} + \eta_r \epsilon_{sh} \right) \quad (6.6)$$

Where:

- k Empirical parameter to incorporate the effect of the concrete cover, taken as 1
- $A_s, A_{c,ef}$ Area of steel reinforcing, effective area of concrete in one concrete face
- $A_{c,ef} = \min(2.5(c + \phi_s/2); t/2)$
- t Concrete section thickness
- β Integration constant to assess mean strain over the transfer length

In order to estimate the level of reliability achieved by WRS, the reservoirs need to be designed using the same assumptions that would be used in practice. As such, the area of reinforcing required to achieve the target crack widths is calculated according to the deterministic procedure in MC 2010 (Equation 6.6), considering long term effects and a design period of 50 years. The reservoir analysis is subsequently carried out using the deterministically-calculated A_s value, but with a probabilistic approach, to be able to determine a spectrum of crack widths, not just the maximum. Moreover, the probabilistic analysis is carried out at water-tightness test stage i.e. the short term, at ≈ 28 days.

As it stands, the formulation in Equation 6.6 is designed to calculate the maximum crack width (95% probability of non-exceedance). This is appropriate for use in a design situation, in order to increase the SLS reliability to an acceptable level, and will be used as-is to calculate the required A_s . In order to probabilistically evaluate the resulting leakage and level of reliability, the formulation in Equation 6.6 needs to be adjusted, in order to remove the conservative bias, making it appropriate for probabilistically predicting crack widths (McLeod, 2019).

The following subsections discuss the MC 2010 crack width formulation parameters in Equation 6.6 and how they are adjusted in order to determine a spectrum of crack widths, for use in the limit state equation. The terms *deterministic design* and *probabilistic analysis* are used to differentiate between the initial, long-term, deterministic design used to calculate A_s and the subsequent short-term, probabilistic analysis of the leakage and achieved level of reliability of the reservoir, respectively.

6.3.1 Crack spacing

The spacing of cracks in a reservoir combined with the widths of the cracks and the rate of self-sealing determines the amount of leakage that a reservoir experiences. Adequate reinforcement at smaller center-to-center spacings ensures that a greater number of cracks form at regular, close spacings with small to moderate crack widths which can self-seal quickly. When insufficient reinforcing is provided or the bars are spaced too far apart, larger cracks form that are spaced further apart, which leads to

excessive leakage.

At a crack, all the stress is transferred from the concrete to the reinforcing, that is, the strain in the concrete is zero, as can be seen from Figure 3.5. Away from the crack, the bond stress between the concrete and the reinforcing increases and transfers some of the stress (and strain) from the reinforcing back to the concrete. This is illustrated by the progression from the crack to halfway between the two cracks in Figure 3.5. This transfer length is denoted as $l_{s,max}$. In MC 2010, the deterministic maximum crack spacing is given as $2l_{s,max}$, and represents a 95th non-exceedance percentile value (Balázs and Borosnyói, 2005):

$$2l_{s,max} = 2 \left(kc + \frac{1}{4} \frac{f_{ctm}}{\tau_{bms}} \cdot \frac{\phi_s}{\rho_{s,ef}} \right) \quad (6.7)$$

Equation 6.7 is similar to the EN 1992-1-1 equation for maximum crack spacing, $S_{r,max}$, both of which are derived according to the semi-empirical combination of slip and no-slip theory presented in section 3.4.2. In order to be used in the analysis, a probabilistic distribution of the crack spacing needs to be used, instead of a 95th percentile characteristic value. A more in-depth consideration is given to the various parameters involved in the development of crack spacing in the following subsections.

6.3.1.1 Probabilistic consideration of crack spacing parameters

c - Concrete cover

The concrete cover from the outer edge of the reinforcing bar to the outside concrete face is a parameter for which the variation varies, depending on the on-site quality control. The JCSS probabilistic model code suggests standard deviations of between 5 and 15 mm, depending on the level of quality control. Due to the importance of the concrete cover for concerns over corrosion and the limiting crack widths in reservoirs, an emphasis is usually placed on the checking of cover. Additionally, cover-blocks are frequently used in reservoirs to help limit the variation in cover. The quality control is therefore typically better than for conventional structures, which leads to the adoption of a standard deviation of 5 mm. Although many studies simply use a normal distribution to describe the concrete cover, the JCSS notes that the concrete cover tends to not be normally distributed, and that the data tends to be more spread out, than focussed around the mean. McLeod (2013) notes however, that the concrete cover contributes little to the total uncertainty. As such, a uniform distribution is initially used, for simplicity. If the cover is shown to have a notable influence on the limit state, a Beta distribution will be considered. Typical cover for reservoirs is 40 mm, and thus a uniform distribution ranging from 31.5 mm to 48.5 mm achieves a standard deviation of 5 mm.

ϕ_s - Reinforcing bar diameter

The properties of reinforcing bars are usually considerably less variant than those of concrete, due to the homogeneity of steel and the automated manufacturing thereof in quality-controlled environments. The diameter of reinforcing bars thus has a low variation. Tat (1991) conducted research into the statistical properties of reinforcing steel, including the variation in gross area. It was found that, from the variation in gross area, the diameter varied 1 mm at most, for bar diameters ranging from 10 to 32 mm. Thus, the bar diameter was modelled as being normally distributed, as suggested by Holický (2009), with a value of $CoV=1/20=0.05$, assuming a mean bar diameter of 20 mm.

$\rho_{s,ef}$ - Effective reinforcing ratio

The effective reinforcing ratio is dependent on A_s and $A_{c,ef}$. The uncertainty in A_s has already been

considered in ϕ_s . $A_{c,ef}$ is defined as the effective area of concrete in tension which, as shown below Equation 6.6, is the lesser of two values (for cases of pure tension). The value for $A_{c,ef}$ is an empirically-determined one with no apparent probabilistic basis or bias. It is thus used without adjustment for bias.

f_{ctm} - Mean concrete tensile strength

It should be noted that in a deterministic formulation, the mean value of concrete tensile strength, f_{ctm} , is used, whereas in a probabilistic approach, a distribution of tensile strengths are used. As such, and for clarity, the mean of the f_{ct} distribution is denoted as f_{ctm} here. The tensile strength of the concrete is one of the primary variables under consideration in the analysis. Given that each realization of reservoir has a different mix design, concrete supplier etc., the distribution of f_{ct} values will be different for each reservoir. The tensile strength can also vary within the same reservoir, as every concrete lift comes from a different batch of concrete. Even within the same batch of concrete, spatial variations in f_{ct} will occur due to the aleatory uncertainty inherent in concrete, caused by the complex matrix of materials that make up the concrete.

In section 6.4, it will be noted that variations in the concrete tensile resistance force, T_r are caused by variations in f_{ct} . In reality, further variation in T_r will occur due to random geometrical imperfections, spatial variations in compaction and curing, as well as other construction-related defects. This research does not consider the effect of construction-related defects on T_r . Thus, the variation in T_r around the reservoir is assumed to only be due to the variation in f_{ct} .

In their research on the consideration of SLS reliability indices for maximum crack width, Quan and Gengwei (2002) modelled the mean concrete tensile strength lognormally, with a mean of f_{ctm} and a CoV of 0.14. MC 2010 notes that the lower and upper bound characteristic tensile strengths are given by $0.7 f_{ctm}$ and $1.3 f_{ctm}$, respectively, indicating a CoV of ≈ 0.175 , assuming a normal distribution. Tran and Graubner (2018) investigated a model factor of experimental tensile strength vs predicted mean concrete tensile strength ($\theta = f_{ct,exp}/f_{ct,pred}$). Their mean tensile strength prediction equation used the same form as those used in MC 2010 and EN 1992-1-1 (based on characteristic compression strength). They found that, when calculated based on compression strength, from a large number of samples, the CoV of f_{ctm} was ≈ 0.15 for concrete compression strengths less than 68 MPa (cylinder). This is within the range recommended by Holický (2009): CoV between 0.10 – 0.18, for concrete strengths. The model investigated by Tran and Graubner (2018) was found to under predict slightly, with a mean of $\mu_{f_{ct}} \approx 1.05$. In this research, the mean tensile strength of the concrete is modelled as in Tran and Graubner (2018), with a lognormally-distributed random variable for each reservoir simulation, with a mean value of $f_{ctm} = 1.05 \cdot 0.3 \cdot f_{ck,cyl}^{2/3} = 3 \text{ MPa}$ (for $f_{ck} = 30 \text{ MPa}$) and a CoV of 0.15. The deterministic design takes on the value according to MC 2010: $f_{ctm} = 0.3 \cdot f_{ck,cyl}^{2/3} = 2.9 \text{ MPa}$

τ_{bms} - Mean bond strength between steel and concrete

It is widely accepted that the mean bond stress between the concrete and the reinforcing steel is dependent on the tensile resistance of the concrete. MC 2010 and EN 1992-1-1 adopt simplified values of $\tau_{bms} = 1.8 f_{ctm}$ and $1.25 f_{ctm}$, respectively, which couples the mean bond stress solely to the mean concrete tensile resistance. These deterministic values, however, are mean values representative of a range of reinforcing bar diameters, reinforcing ratios and concrete strengths. Thus, in reality, the value of τ_{bms} is not deterministic but varies depending on these parameters, as well as due to statistical uncertainty. Debernardi and Taliano (2015) investigated the τ_{bms}/f_{ctm} ratio for various bar diameters, reinforcing ratios and concrete strengths. From their research, for typical reinforcing bar diameters of 16 – 25 mm, concrete strengths of 30 – 50 MPa and reinforcing ratios of 1 – 3%,

the ratio is in the range of $1.25 < \tau_{bms}/f_{ctm} < 1.8$. As such, and without other detailed information related to a specific distribution of τ_{bms} , it was uniformly distributed between $1.25f_{ctm}$ and $1.8f_{ctm}$. The distribution characteristics are summarized in Table 6.2, in the chapter summary. The deterministic design uses a long term value of $\tau_{bms} = 1.8f_{ctm}$ for the stabilized cracking stage, as per MC 2010.

θ_{space} - Factor for crack spacing

With reference to Equation 6.7, the development of the formulation for maximum crack spacing uses a multiple of two times the transfer length, $l_{s,max}$. This maximum represents a crack spacing with a 95% probability of non-exceedance. The multiplication of the transfer length by 2 is used in the deterministic design to obtain A_s for the target crack width. For the probabilistic analysis, however, from the discussion in section 3.4.2, the mean crack spacing, $l_{s,mean}$, is between 1 and 2 times the transfer length. The mean is generally assumed to be 1.5 times the transfer length (Beeby and Narayanan, 2009; Balázs, 1993). The crack spacing factor, θ_{space} is therefore introduced to vary the crack spacing between 1 and 2, with a mean value of 1.5. As such, it is defined as being uniformly distributed between 1 and 2. This leads to the equation for the mean spacing between cracks in a reservoir of $\theta_{space} \cdot l_{s,mean}$, shown in Equation 6.8. The spacing between cracks is probabilistically varied due to the variation in θ_{space} and f_{ctm} .

$$\theta_{space} \cdot l_{s,mean} = \theta_{space} \cdot \left(c + \frac{1}{4} \frac{f_{ctm}}{\tau_{bms}} \cdot \frac{\phi_s}{\rho_{s,ef}} \right) \quad (6.8)$$

6.3.2 Crack strain

From Equation 6.6, the width of the cracks that occur in reservoirs is dependent on the crack spacing and the strain difference between the reinforcing steel and concrete from loading, as well as the strain from shrinkage in concrete. The greater the spacing between cracks, the greater the crack width. Similarly, the greater the difference in strain between the reinforcing and the concrete, the greater the crack width. Equation 6.9 gives insight into the strain-related part of the calculation of a crack width in the stabilized cracking stage:

$$\epsilon_{sm} - \epsilon_{cm} - \epsilon_{sh} = \frac{\sigma_s - \beta \frac{f_{ctm}}{\rho_{s,ef}} (1 + \alpha_e \rho_{s,ef})}{E_s} + \eta_r \epsilon_{sh} \quad (6.9)$$

The σ_s term relates to the stress in the reinforcing steel, whereas the second term beginning with β represents the tension-stiffening effect that occurs in the concrete (blue ϵ_c line in Figure 3.5). The final term considers the additional strain present in the concrete due to shrinkage in the concrete. As before, the individual parameters of the crack strain equation are considered in a probabilistic light.

6.3.2.1 Probabilistic consideration of crack strain parameters

σ_s - Stress in reinforcing

The stress in the reinforcing, $\sigma_s = T/(2A_s)$, is dependent on the applied hoop-tension force acting on the whole section, T , and the area of steel reinforcing per concrete face, A_s . In practice, the tension force profile with respect to the height of the reservoir is considered and the reinforcing is varied and reduced stepwise, away from the point of maximum tension. Figure 6.3 illustrates this, showing the increase in reinforcing steel required to obtain a target crack width of $w_t = 0.2 \text{ mm}$ as T increases, for a typical reservoir with a hinged base. In the upper part, where the tension force is relatively low, minimum reinforcing governs. In this research, a simplification is made whereby the amount of

steel reinforcing is kept constant up the height of the reservoir, as shown by the broken line. The amount of reinforcing required to limit the crack width to the specified crack width limit, at the point of maximum tension, is applied throughout the whole reservoir.

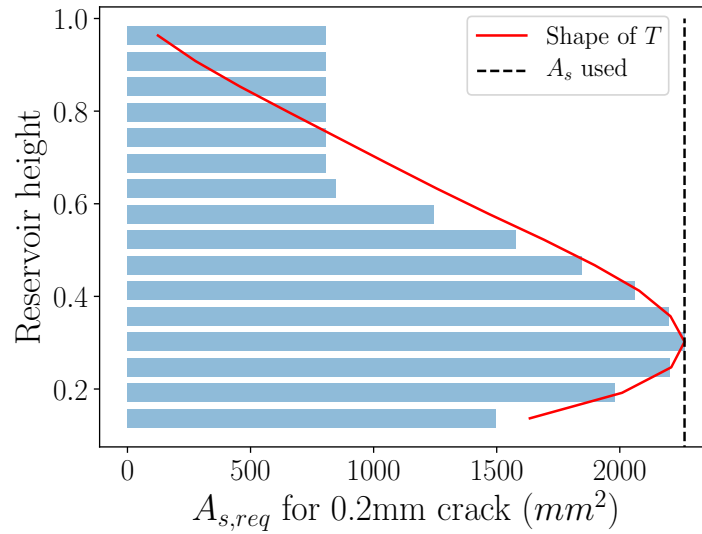


Figure 6.3: Illustration of variation in required area of steel for 0.2mm crack width limit, with increasing tension force.

β - Empirical constant to evaluate mean strain

The empirical constant, β , is used to evaluate the mean strain over the transmission length, effectively converting the shape from the parabolic form in Figure 3.5, to an equivalent-area of mean strain, thereby simplifying the strains in Equation 3.1 to mean strains in Equation 6.4. For the stabilized cracking phase, β takes on deterministic values of 0.6 and 0.4 for long and short term applications, respectively.

α_e - Modular ratio between steel and concrete

The modular ratio α_e is a ratio of two mean values of E-moduli. The modular ratio α_e is to be used considering whether the design is for the short-term or long-term. The long-term effects of creep on the reduction of the E-modulus of concrete, in line with MC 2010, EN 1992-1-1 and CIRIA C660 (Bamforth, 2007) are incorporated in the design by using an effective concrete modulus $E_{c,ef}$, as shown in Equation 6.10. The creep coefficient, ϕ , is dependent on the design time under consideration and the type of loading, amongst other things. For a design period of 50 years, and tension loading on a reservoir wall, an appropriate value for ϕ was calculated as 1.75.

$$E_{c,ef} = \frac{E_c}{1 + \phi} \quad (6.10)$$

This leads to a long-term value of $E_{c,ef} = 12.3 \text{ GPa}$ for a typical C30/37 concrete. A short-term 28-day value for a C30/37 concrete of $E_c = 33 \text{ GPa}$ will be used, as no long-term deterioration will have taken place by the time the water tightness test is conducted. This gives values of $\alpha_e = 200/33 \approx 6$ and $\alpha_e = 200/12.3 \approx 16$ for short- and long-term modular ratios, respectively. Previous research indicates that variations in E_c contribute little uncertainty in the calculation of crack widths (Mlčoch *et al.*, 2017) and it has typically been used deterministically in similar research (McLeod, 2019; Zięba *et al.*, 2020; Quan and Gengwei, 2002). The variation in E_s is small due to the quality control in steel mills, and it is usually modelled deterministically. The α_e ratio is therefore modelled as being deterministic

in this research.

$\eta \epsilon_{sh}$ - Contribution of shrinkage strain

The free shrinkage strain, ϵ_{sh} , also contributes to the strain difference, and is comprised of autogenous and drying shrinkage. When considering crack widths at an early stage (≈ 3 days), a small degree of autogenous and very little, if any drying shrinkage has occurred. It is therefore not considered as contributing to the strain ($\eta = 0$) in the immediate short-term. Conversely, in the long-term, shrinkage contributes a notable amount of strain (particularly drying shrinkage) and $\eta = 1$. The water tightness test is often conducted as soon as the concrete has reached its full 28 day strength, where a large proportion of the autogenous shrinkage and some of the drying shrinkage has taken place. The short-term free shrinkage strain used in the probabilistic analysis is a mean value for 28 day old concrete, which has been cured for 7 days, calculated as recommended by EN 1992-1-1 and MC 2010, $\epsilon_{sh} = 70 \mu m$ with $\eta = 1$. The long-term value to be used in the deterministic design for A_s is a mean value for 50 years, $\epsilon_{sh} = 250 \mu m$ with $\eta = 1$.

6.3.3 Crack length

In a circular reservoir, the crack lengths run in a vertical direction and are dependent on the distribution of the applied tension force up the height of the reservoir. Considering the reinforcing along the height of the reservoir wall as constant; the $\rho_{s,ef}$, α_e , β , η_{sh} and E_s parameters are also constant. The highest strain state in the reservoir wall, as a result of hydrostatic loading, will then be where σ_s is the highest, from Equation 6.9. This means that, at the height where T_{max} occurs, as shown in Figure 6.3, the strain in the reservoir due to loading will be at maximum. Given the brittle nature and random matrix of materials in concrete, the cracks do not repeat the same pattern, nor do they run in a completely straight line. Rather, they follow a jagged zig-zag pattern, running approximately vertically, between individual pieces of coarse aggregate. In this research a simplification is made in that the cracks are assumed to run in a vertical line up the wall, as illustrated later in Figure 6.7, with a length as discussed below.

The tensile resistance of a concrete section is given by Equation 6.11. In a reservoir, each crack point, a , around the circumference will have its own value of concrete tensile resistance force, $T_{r,a}$, which will vary, depending on the variation in the value of concrete tensile strength $f_{ct,a}$ (other factors in Equation 6.11 remain constant). Assuming that a crack does in fact, occur at a potential crack point, the applied hoop tension exceeds the concrete tensile resistance force at all points along the crack ($T_{r,a} < T$). Figure 6.4 illustrates the concrete tensile resistance force up the wall height for two different values of h^2/Dt ratio. From this, there are two points for which T is exactly equal to $T_{r,a}$, where the concrete will be right on the verge of cracking. The length of wall between the two points for which $T = T_{r,a}$ is taken as the length of the crack.

$$T_r = A_{c,ef} \cdot f_{ct,a}(1 + \alpha_e \rho_{s,ef}) \quad (6.11)$$

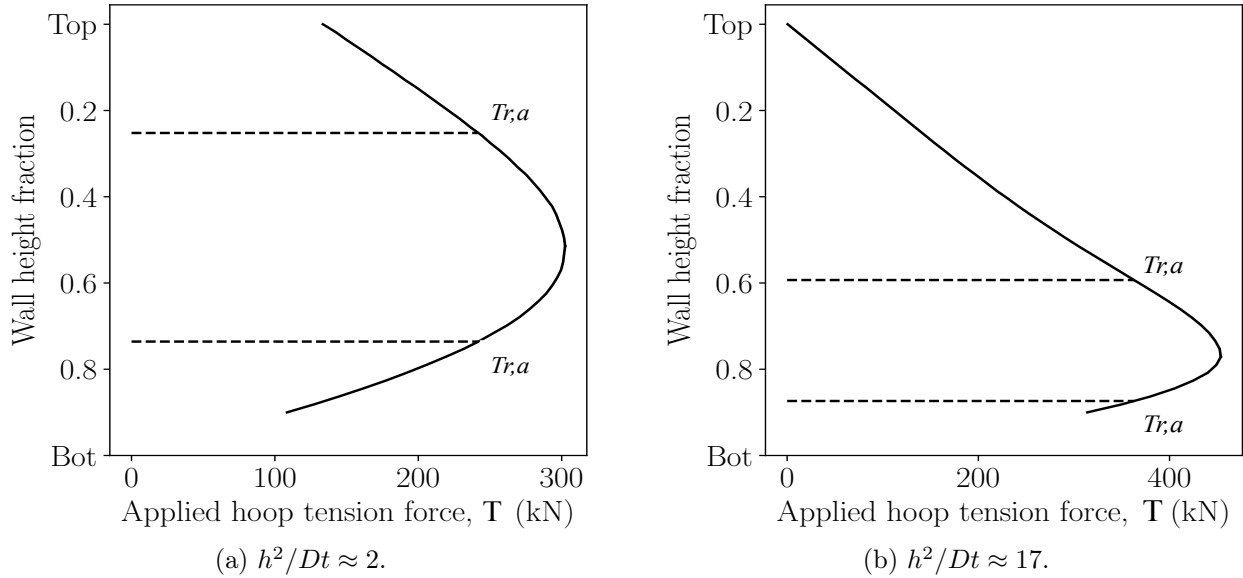


Figure 6.4: Illustration of applied hoop tension along reservoir wall height, and subsequent crack length prediction.

6.3.4 Crack widths

The f_{ctm} value is the common link between the strain and crack spacing. A lower value of f_{ctm} results in a lower bond strength between the concrete and the reinforcing. A lower bond strength results in a slower rate of stress transfer from the reinforcing to the concrete, leading to a greater strain difference between the reinforcing and the concrete. This subsequently leads to greater crack widths, with reference to Equation 6.9.

Following from the calculation of crack lengths, the modelling of the crack widths across the crack length also needs to be considered. The crack width varies, from being widest at the point of maximum tension force, to being zero at the points where the concrete is uncracked again. Considering Figure 6.4, the parameter that drives the width of the crack is the applied hoop tension, assuming that the wall section thickness and amount of reinforcing are constant over the length of the crack. The crack shape is approximated by a lens-type shape, as shown later in Figure 6.8.

As discussed in section 3.4.4, the development of a crack width prediction model is generally based on a combination of slip and no-slip theory, thus being semi-empirical. As such, and while the models are calibrated to be as representative of reality as possible, model predictions are never entirely accurate, especially in the case of predicting concrete-cracking related phenomenon. The crack width prediction equation of MC 2010 is no exception. A number of researchers have undertaken the task of attempting to quantify the model uncertainty associated with the MC 2010 crack width prediction equation, as discussed in section 3.4.4.

The crack spacing and strain difference affect the distribution of crack widths. The biggest crack widths occur when the strain difference between the reinforcing and concrete is highest and where the crack spacing is greatest. With reference to the discussion of θ_{space} towards the end of section 6.3.1.1, the maximum crack width is defined as a crack width with a 95% non-exceedance probability, which occurs at the maximum crack spacing, $2l_{s,mean}$. The mean crack width is commonly assumed to be at

a spacing of $1.5 l_{s,mean}$. In this research, a spectrum of crack widths is required, hence the variation of θ_{space} between 1 and 2 times $l_{s,mean}$, as illustrated by Figure 6.5.

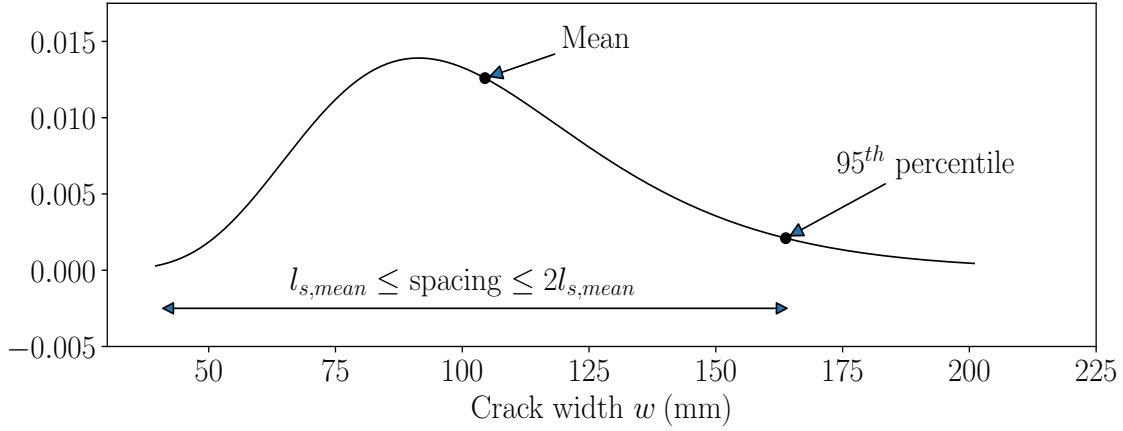


Figure 6.5: Lognormal distribution of crack widths.

Given the relative agreement on model factor mean and CoV of the three research projects in section 3.4.4, the results from McLeod (2019) in Table 6.1 will be used in this research. This is used in order to quantify the uncertainty of, and variability in the prediction of crack widths resulting from the use of the MC 2010 crack width prediction equation. The predictions of crack widths will thus be probabilistically modelled through the use of the crack width prediction model factor, θ_{cw} , as defined in Table 6.2. It should be noted that McLeod's model uncertainty factor was developed in terms of the prediction of *maximum* crack width, whereas this research aims at predicting a spectrum of crack widths. The assumption is made that the model uncertainty in the prediction of mean crack widths follows the same probabilistic behaviour as the model uncertainty in the prediction of maximum crack widths.

Table 6.1: MC 2010 model uncertainty (w_{exp}/w_{pred}) characteristics for maximum crack width prediction for short-term tension cracks, from McLeod (2019).

Statistic	Value	Statistic	Value
Mean	0.984	Kurtosis	-0.486
Standard Deviation	0.319	Skewness	0.49
CoV	0.324	Minimum	0.416
Median	0.897	Maximum	1.824
Number of tests	82		

6.3.5 Probabilistic formulation of total leakage prediction model

Having considered the loading on the reservoir and the probabilistic formulation of the crack width, strain and length, the total leakage prediction model from chapter 5 needs to be considered in the context of a reservoir. The total leakage prediction model is repeated here for convenience and is further developed to be used in the context of leakage in a reservoir.

$$Q_{total,ij} = \theta_{Q0} \cdot \frac{0.11 \Delta p \ell w^3}{12 \eta t} \cdot \theta_{idjd} \cdot \theta_{HR} \quad (5.15)$$

The parameters in Equation 5.15 need to be defined for the context of the leakage through a crack in a reservoir. The pressure head Δp is the water pressure caused by the weight of water above the

the crack. As the tension cracks in a reservoir are in a vertical plane, the head of water above the centre of the crack (the point where the tension force is at a maximum), h^* , is used to determine Δp as $\Delta p = \rho_w g h^*$ (N/m^2). The reservoir wall thickness, d , is denoted here and further on as t (m), and η is the dynamic viscosity of water (Ns/m^2). The length of the crack, ℓ_a , is as defined in section 6.3.3. The initial leakage prediction model factor, θ_{Q0} , the leakage accumulation factor, θ_{idd} , and the hydraulic ratio factor, θ_{HR} are then defined as per section 5.3. The crack width, w , then stems from the MC 2010 formulation for the calculation of maximum design crack widths, adjusted to probabilistically predict the mean crack width, from sections 6.3.1 and 6.3.2.

$$w = w_{mean} = \theta_{cw} \cdot \theta_{space} \cdot \left(c + \frac{1}{4} \frac{f_{ctm}}{\tau_{bms}} \cdot \frac{\phi_s}{\rho_{s,ef}} \right) \cdot \left(\frac{\sigma_s - \beta \frac{f_{ctm}}{\rho_{s,ef}} (1 + \alpha_e \rho_{s,ef})}{E_s} + \eta_r \epsilon_{sh} \right) \quad (6.12)$$

6.4 Stages of cracking in reservoirs

As discussed in section 3.4.3, three distinct stages of cracking exist for tension-loading, depending on the magnitude of the loading: the uncracked, crack formation and stabilized cracking stages. For the case of cracking in concrete reservoirs, two theories are considered: an idealized design approximation according to MC 2010 and EN 1992-1-1 from section 3.4.3 and a realistic, probabilistic consideration. The idealization of cracking stages in section 3.4.3 is appropriate for the design model in MC 2010 and EN 1992-1-1, however, for the purposes of a reliability analysis, a more realistic consideration is required.

6.4.1 Realistic cracking stages

Consider a more realistic view of the stages of cracking, from commentary in MC 2010 and Balázs (2013). This view introduces a probabilistic consideration of a range of values for f_{ct} and not just a mean value. When the applied tension force is low, the reservoir is in the uncracked stage. In this stage, the applied hoop tension force, T , in the section is notably less than the mean tensile cracking force of the section ($T \ll T_{r,m}$). As the water level increases, the stress in the section increases until the first crack forms at the point where the concrete tensile resistance force is the lowest. This can be due to construction defects, such as a geometric imperfection, bad compaction etc., affecting $A_{c,ef}$ and $\rho_{s,ef}$, and/or a lower value of concrete tensile stress, f_{ct} (aleatory variation due to the concrete material matrix). At this point, it enters the crack formation stage, shown in Figure 6.6. Here, cracks form rapidly and at random around the reservoir, with increasing tension force. As the applied tension force increases, enough cracks form so that the spacing between all cracks is less than $2\ell_{s,max}$ and the reservoir enters the stabilized cracking stage, where no more cracks form and existing cracks widen.

The difference between the theory developed for the calculation of crack widths for the crack formation and stabilized cracking stages stems from the difference in the calculation of strains. In the crack formation stage, where the strain due to load is relatively low, the strain difference between the concrete and reinforcing is zero at the end of the transfer length, between two cracks (strain compatibility). In the stabilized cracking phase, where the strain due to load is higher, the strain difference is not zero, as seen in Figure 3.5 (strain incompatibility). As the cracking stage transitions from formation to stabilized, the two crack strain formulation theories overlap in a zone around the mean concrete tensile resistance force, $T_{r,m}$, where both theories will be approximately valid. Therefore, in contrast to the idealized approximation where a piecewise border separates the crack formation stage from the stabilized cracking stage (when $f_{ct} = f_{ctm}$), the concept of a "transition" zone is adopted.

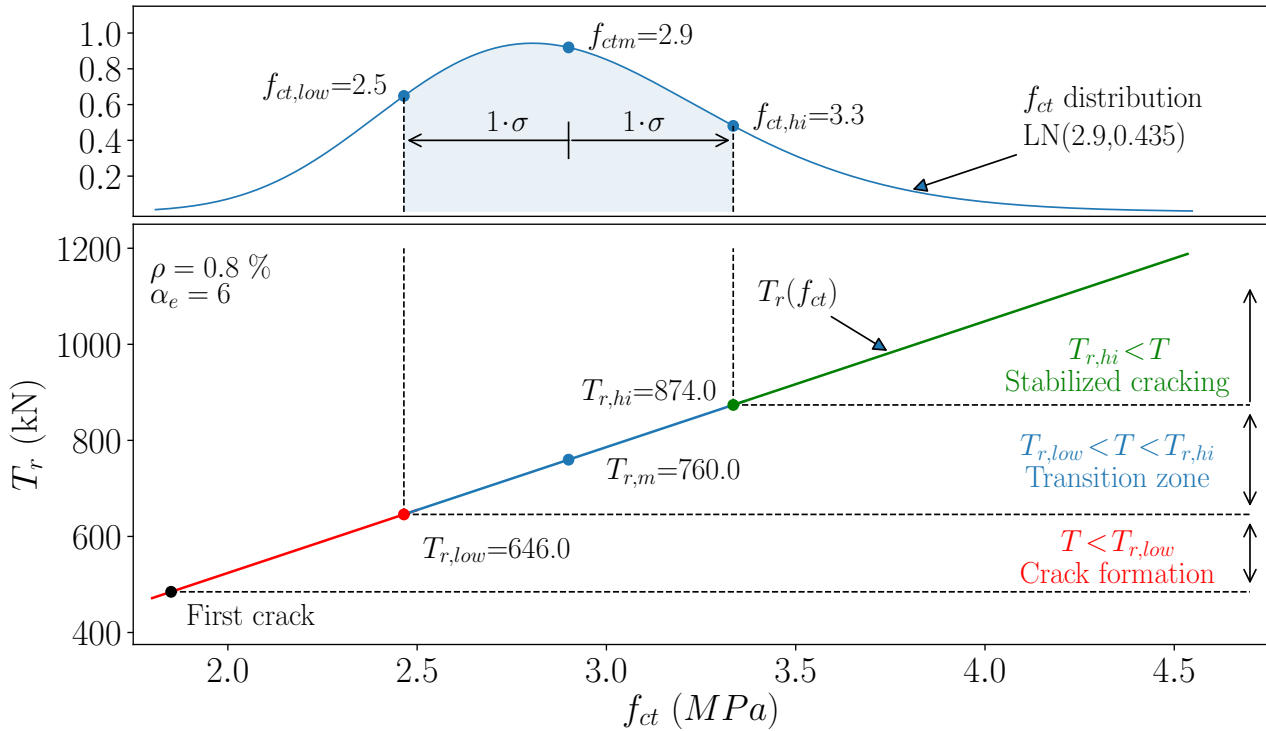


Figure 6.6: Illustration example of realistic cracking stages of load-induced cracking in concrete. Probability density function of f_{ct} (top) linked to concrete tensile resistance force (bottom).

The transition zone is used to introduce a more realistic transition from the crack formation stage to the stabilized cracking stage. In this zone, some sections along the circumference of the reservoir will be in a stage of crack formation, while others will be in a stabilized cracking stage, due to the variation in the concrete tensile resistance force. Figure 6.6 illustrates the variation in the concrete tensile resistance force (bottom), based on the variation in the concrete tensile strength (top). Bounds to the transition zone are introduced based on the concrete tensile strength. In this research, bounds are introduced one standard deviation either side of f_{ctm} ($f_{ct,low}$ and $f_{ct,hi}$ which correspond to $T_{r,low}$ and $T_{r,hi}$ respectively) as shown in Figure 6.6. Furthermore, in this research, the theory of stabilized cracking is assumed to be valid if the maximum applied tension is greater than $T_{r,low}$, where $T_{r,low}$ corresponds to a value of f_{ct} one standard deviation below f_{ctm} (using $CoV = 0.15$). This does introduce an element of conservatism in that for cracks in the transition zone closer to the crack formation zone, the strain difference will be slightly over-estimated using stabilized cracking theory. Finally, this research only considers the leakage from reservoirs that are in the adjusted stabilized cracking stage (where $T_{r,low} < T_{max}$).

When the reservoir has been filled to the design level and the maximum load has been reached, no further cracking or widening of cracks occurs. It is in this state that the water tightness test takes place. Changes in the stress and strain state of the concrete will be affected by fluctuating water levels and creep and shrinkage during normal operation of the reservoir over time, however, this research only considers the state of the reservoir at the end of the water tightness test. The leakage and predicted leakage are determined at this stage and the achieved level of SLS reliability is determined.

6.5 Reliability limit state

The SLS design of a reservoir is typically done first, whereby the requirements for limiting crack widths are met, in order to limit leakage to an acceptable level. The ULS requirements are then checked after the SLS design has been carried out, and are typically more-than-satisfied. Though it is noted that there are cases where the ULS may govern, such as in cases of uplift or earthquakes, this research focuses exclusively on the SLS design. Furthermore, this research is concerned with the specific SLS case where the reservoir leakage is evaluated against allowable leakage criterion at the water tightness test stage.

The leakage through the cracks is evaluated against the SLS code-defined allowable leakage. If the reservoir leaks more than the allowable leakage for the reservoir, it is classified as a failure, and a pass otherwise. The limit state equation is therefore defined as the difference between the allowable leakage, L_{al} , and the predicted leakage, L_p . The limit state equation, g , is discussed in detail in the sections that follow.

6.5.1 Predicted leakage - L_p

The predicted leakage part of the limit state equation in a reservoir is the total leakage that results from cracks in the concrete. The total leakage prediction model is used to predict this leakage. The total leakage prediction given by the combination of Equation 5.15 and 6.12 is that for a single tension crack. It should be noted that the A_s value contained within the reinforcing ratio, $\rho_{s,ef}$, is calculated to the long term deterministic design approach according to MC 2010. The leakage for the entire reservoir is the summation of the leakage over all cracks in the reservoir, $a = 1, a + 1, \dots, a = n_a$. The leakage for the entire reservoir is thus given by Equation 6.13.

$$\begin{aligned}
 L_p &= \sum_{a=1}^{a=n_a} \theta_{Q0,a} \cdot \frac{0.11 \Delta p \ell_a w_a^3}{12 \eta t} \cdot \theta_{idjd,a} \cdot \theta_{HR} \quad \text{in } k\ell \\
 &= \sum_{a=1}^{a=n_a} \theta_{Q0,a} \cdot \frac{0.11 \Delta p \ell_a}{12 \eta t} \cdot \theta_{idjd,a} \cdot \theta_{HR} \cdot \\
 &\quad \left(\theta_{cw,a} \cdot \theta_{space,a} \left(c_a + \frac{1}{4} \frac{f_{ctm,a} \phi_s}{\tau_{bms,a} \rho_{s,ef}} \right) \cdot \left(\frac{\sigma_s - \beta \frac{f_{ctm,a}}{\rho_{s,ef}} (1 + \alpha_e \rho_{s,ef})}{E_s} + \eta_r \epsilon_{sh} \right) \right)^3 \quad (6.13)
 \end{aligned}$$

Equation 6.13 is the prediction of the initial flow, taking into account the loading on, and geometry of, the structure and specific crack, which is then multiplied by the initial flow prediction model factor, leakage accumulation factor and hydraulic ratio factor to obtain the total leakage that transpires from the reservoir, in $k\ell$.

6.5.2 Allowable leakage - L_{al}

The allowable leakage part of the limit state equation is based on the code-defined allowable leakage. Four separate variants will be used; two from BS 8007, one from ACI 350.1-10 and one as a purely academic base variant.

Most design codes define the water tightness test as having two stages. The first stage is a "stabilization period", whereby the reservoir is filled and left for a time period, allowing for the concrete to absorb water and for the process of autogenous self-sealing to take place. The leakage during this

stage is ignored. The second stage, and actual leakage test, commences at the end of the stabilization period; the water level is measured for a specified period and the drop in water level is measured. From a self-sealing perspective, the longer the reservoir has to self-heal, before the water tightness test begins, the lower the probability will be that the reservoir fails the water tightness test. This can be seen from the difference between the *Mean* columns for the various leakage regimes in Tables 5.5, 5.6 and 5.7.

When a stabilization period is specified, a large volume of the total leakage will already have taken place by the end of the period. Hence, the difference between the leakage at the end of the total period, and the leakage at the end of the stabilization period will be significantly less than the total period leakage if there were no stabilization period. In practice, contractors often prefer to specify shorter stabilization periods. This is to reduce the likelihood of having to pay penalty costs associated with the delay of project completion as well as overheads, in the event of the reservoir failing the water tightness test. Considerable delays can result from a water tightness test failure, as the reservoir has to be emptied, cracks sealed and the test performed again. There is thus a trade-off between a longer stabilization period and a lower probability of failure, and a shorter stabilization period with a higher probability of failure, considering the delays and costs associated with failure.

From the discussion of stabilization and water tightness test times in section 3.5.1, as well as here and the leakage regimes chosen in chapter 5, the following leakage regimes are specified in terms of allowable leakage. Two variants of BS 8007 are used: A 7 day stabilization period followed by a 7 day test; and a 14 day stabilization period, followed by a 7 day test. One variant from ACI 350.1-10 is used, in a 3 day stabilization period, followed by a 5 day water tightness test. The academic variant uses no stabilization period, followed by a 7 day water tightness test. Assuming no stabilization period is not practical and thus the last regime will not likely be used in practice but it will provide insight as an academic reference case.

The acceptable drop in water level at the end of the water tightness test in this research follows from the BS 8007 recommendation. A drop in water level of $(1/500) \cdot h = 0.2\%$ of the volume of retained water. Note that in this research, the height of the reservoir is synonymous with the height of the retained water, i.e. there is no freeboard. The allowable leakage for the entire reservoir is given by Equation 6.14.

$$L_{al} = 0.002 \cdot \pi r^2 h \quad \text{for all leakage regimes} \quad (6.14)$$

6.5.3 Limit state equation

The difference between the allowable leakage and predicted leakage is defined as the limit state equation, g , where L_{al} and L_p are given by Equations 6.14 and 6.13. This represents the case of an entire reservoir, as shown below. Table 6.2 summarizes the probabilistic parameters to be used in the prediction of leakage in a reservoir, as well as the deterministic design values used to determine A_s according to the design method in MC 2010. Visualizations of the distributions are shown in Appendix A.

$$g = L_{al} - L_p \quad (\text{in } kl) \quad (6.15)$$

Table 6.2: Summary of parameters used in the prediction of leakage.

Parameter	Symbol	Unit	Dist.	28d - Probabilistic		50yr - Design
				Mean	CoV	
Concrete mean tensile strength	f_{ctm}	MPa	LN	3.0	0.15	2.9
Conc-reinf bond strength	τ_{bms}	MPa	Uni	$(1.25 - 1.8) \cdot f_{ctm}$		$1.8 f_{ctm}$
Concrete cover	c	mm	Uni	31.5 - 48.5		40
Steel bar diameter	ϕ_s	mm	N	20	1	20
Crack width prediction MF	θ_{cw}		LN	0.984	0.324	-
Crack spacing factor	θ_{space}		Uni	1 - 2		2
Initial flow prediction MF	θ_{Q0}		W	Table 5.2		-
Leakage accumulation factor	θ_{idjd}	hrs	W	Tables 5.5, 5.6, 5.7		-
Hydraulic ratio factor	θ_{HR}		Det	$h^*/t < 20: 0.62 + 0.0358 \cdot (h^*/t - 9.4)$ $20 \leq h^*/t: 1 + 0.0563 \cdot (h^*/t - 20)$		
Area of reinforcing	A_s	mm^2	Det	Follows from design		
Shrinkage strain	ϵ_{sh}	$10^{-6}m/m$	Det	75		250
Modular ratio	α_e		Det	6		16
Empirical integration constant	β		Det	0.6		0.4

LN - Lognormal Uni - Uniform N - Normal Det - Deterministic W - Weibull

6.6 Sensitivity analysis

Before a leakage prediction analysis is performed on an entire reservoir, a sensitivity analysis is performed on a single crack. The sensitivity analysis is used to identify how sensitive the limit state equation is to each of the probabilistic parameters. In any computational analysis, there is a trade-off between simplicity and accuracy. The simpler an analysis becomes, the faster it can be executed, but the less reflective of reality (and less useful) it becomes. Thus, the aim is to simplify the analysis as much as possible without detracting from its usefulness. The sensitivity analysis is therefore used to identify parameters that contribute little uncertainty to the limit state. These are then replaced by deterministic, mean-value-equivalents, which simplify the analysis and reduce the computational time and effort required.

Another use of the sensitivity analysis is to gain a better understanding of the behaviour of the total leakage model and to build confidence in the use thereof, as it will later be expanded and used to determine the leakage from an entire reservoir, comprised of a large number of cracks. Furthermore, the sensitivity analysis will give indication of an upper and lower bound of reliability, corresponding to a crack spacing of $\ell_{s,mean} = 1$ and $\ell_{s,mean} = 2$, respectively. This section details the sensitivity analysis performed on the total leakage prediction model, using a simplified reservoir geometry.

6.6.1 Method of analysis - FORM

The reliability method chosen for the probabilistic sensitivity analysis is the First Order Reliability Method (FORM) with adjustments by Hasofer and Lind (1974). For the sake of brevity, the method is only briefly reviewed here, following on from the overview of FORM in section 2.7.1. A more detailed description can be found in Holický (2009) with guidance from Manoj (2016). The Python Reliability (PyRe) module (Hackl, 2018) was used to perform the FORM analyses.

Following from the general description of the FORM process in section 2.7.1, one of the useful outputs of the FORM analysis is the vector of direction cosines normal to the failure boundary at the design point (sensitivity factors), $\{\alpha\}$. Each of the probabilistic parameters have an associated α value, the sum of squares of which add up to 1. The square of each parameters' α value constitutes a fraction of the the total uncertainty in the limit state (see Equation 6.6.3) that is attributed to that parameter. Parameters with α values close to zero contribute insignificant uncertainty towards the limit state and can be replaced with deterministic mean value equivalents, without much effect on the determined reliability. From this, those parameters from Table 6.2 that have little influence on the uncertainty can be identified and replaced, if warranted.

In addition to the scrutiny of the probabilistic parameters, the sensitivity analysis is also used to get an indication of how the variation in parameters affect the level of reliability. As FORM is limited by its inability to evaluate non-linear limit states with conditional decision making, a number of sensitivity analyses are carried out, varying different parameters in each.

6.6.2 Simplified reservoir geometry

In order to understand the model behaviour and the role that the individual parameters play in it, a simplified WRS geometry is used. A "slice" of a reservoir is used in the sensitivity analysis to avoid unnecessary complexity. The slice of reservoir contains only a single vertical crack, as shown in Figure 6.7, and has an allowable leakage that is apportioned based on the circumferential length of the slice as a fraction of the total reservoir circumference. For the sensitivity analysis, the geometrical reservoir parameters (height, diameter, wall thickness) are kept deterministic.

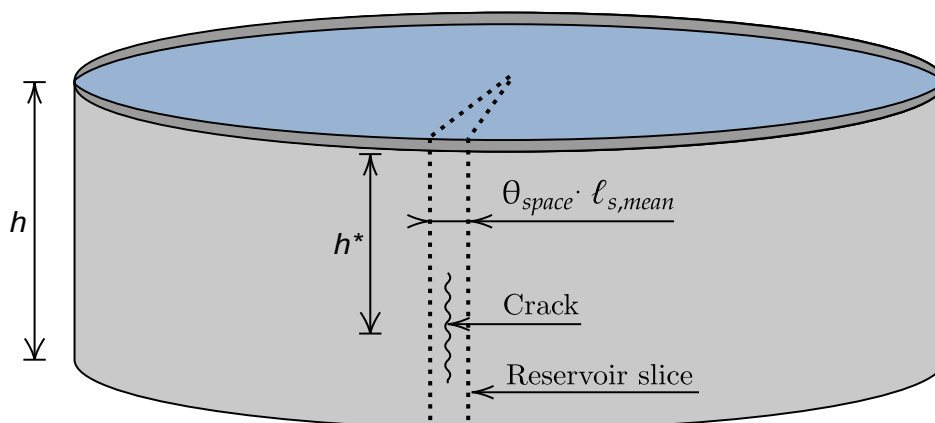


Figure 6.7: Illustration of the simplified reservoir slice analogy for the sensitivity analysis.

The circular reservoir geometry and other deterministic parameters are shown in Table 6.3. The geometric parameters chosen are for a slightly larger-than-average reservoir. The remainder of the deterministic parameters have been calculated based on the geometric design parameters as discussed in sections 6.2 and 6.3.

Table 6.3: Circular reservoir geometry constraints for the sensitivity analysis.

Parameter/ratio	Symbol (unit)	Value
Height of retained water	h (m)	8.5
Reservoir diameter	D (m)	34
Wall thickness	t (m)	0.25
Distance to w_{max} from top of wall	h^* (m)	5.93
Hydraulic ratio	h^*/t	23.7
Hydraulic ratio factor	θ_{HR}	1.13
Dimensionless parameter ratio	h^2/Dt	9
Reservoir volume	V (Mℓ)	7.7
Crack length	ℓ (m)	Varies
Maximum tension force	T_{max} (kN)	997
Water pressure above crack	Δ_p (N/m ²)	58 200
Base restraint		Hinged
Top of wall restraint		Free

*Note that this is the height of water above the point where the maximum crack is likely to occur (position of T_{max}).

6.6.3 Limit state equation

In the simplified sensitivity analysis, the leakage from the single crack will be evaluated against the SLS code-defined allowable leakage. If the crack leaks more than the allowable leakage for that section of the reservoir, it gets classified as a failure, and a pass otherwise. The limit state equation from section 6.5.3 is therefore amended, to be applicable to the slice encapsulating one crack, a :

$$g_{slice} = L_{al,slice} - L_{p,slice} \quad (\text{in } k\ell)$$

$$L_{al,slice} = 0.002 \cdot \pi r^2 \cdot \frac{\theta_{space} \ell_{s,mean}}{2\pi r} = 0.001 \cdot r \cdot \theta_{space,a} \cdot \left(c + \frac{1}{4} \frac{f_{ctm,a} \phi_s}{\tau_{bms,a} \rho_{s,ef}} \right) \quad (6.16)$$

$$L_{p,slice} = \theta_{Q0,a} \cdot \frac{0.11 \Delta_p \ell_a}{12 \eta t} \cdot \theta_{idjd,a} \cdot \theta_{HR} \cdot \quad (6.17)$$

$$0.7 \cdot \left(\theta_{space,a} \left(c + \frac{1}{4} \frac{f_{ctm,a} \phi_s}{\tau_{bms,a} \rho_{s,ef}} \right) \cdot \left(\frac{\sigma_s - \beta \frac{f_{ctm,a}}{\rho_{s,ef}} (1 + \alpha_e \rho_{s,ef})}{E_s} + \eta_r \epsilon_{sh} \right) \cdot \theta_{cw,a} \right)^3$$

Calculating the initial flow at a number of points along the length of the lens shaped crack, as illustrated in Figure 6.8, was made difficult by the limitations of the FORM analysis, due to the need to conditionally-assign different probabilistic distributions to the θ_{Q0} and θ_{idjd} parameters, as discussed in the following paragraphs. Due to the lens-shape of the crack, using the width of the crack at its widest point, $w_{a,max}$, would be too conservative and using a mean value, $w_{a,mean}$, would under-predict the leakage, due to the cubic effect of crack width on flow. Instead, a simplified method of approximating the effective crack width was used for the purposes of the sensitivity analysis. A crack width that is cubically representative of the entire crack was used, as determined by Equation 6.18. Crack a is sub-divided into a number of segments, $b_1, b_2 \dots b_n$, each with their own crack width, w_b . The resulting cubically-representative factor is $\approx 0.7 \cdot w_{a,max}$. The crack width part of Equation 6.17, is thus multiplied by the value of 0.7 to account for the lens shape of the crack, for the purposes of the sensitivity analysis.

$$w_{a,cube} = \sqrt[3]{\frac{\sum_{b=1}^{b=n_b} w_b^3}{n}} \approx 0.7 \cdot w_{a,max} \quad (6.18)$$

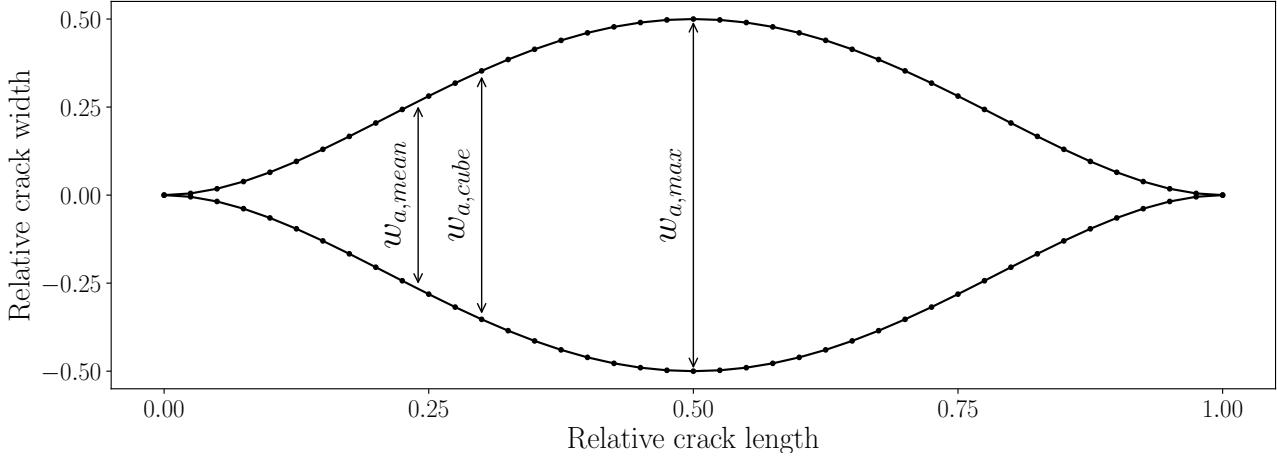


Figure 6.8: Illustration of crack shape and the mean, cubic equivalent and maximum width of crack (exaggerated vertical scale for illustration purposes).

In the sensitivity analysis, the BS 8007 variant of a 7 day stabilization period followed by a 7 day test was chosen as the leakage regime ($\theta_{idjd} = \theta_{7d14d}$). The allowable leakage is then 0.2% of the total volume. However, as only the leakage through a single crack is considered, the allowable leakage criterion for the whole reservoir is adjusted to that for the slice, by including the ratio of the arc slice length to the total circumference, $\theta_{space} \ell_{s,mean}/2\pi r$, as seen in Equation 6.16 and illustrated in Figure 6.7. The predicted leakage term is also adjusted to that of a single crack, rather than a summation over all cracks.

As the FORM method uses partial differentials of the limit state function to be able to determine the sensitivity factors, α , the limit state equation cannot contain any forms of conditional decision-making, such as the case where the effective area of concrete in tension, $A_{c,ef}$, is defined as the minimum of two values: $2.5(c + \phi_s/2)$ or $t/2$. Similarly, it cannot contain the conditional assignment of different distributions to parameters, depending on the crack width range, as is required for the θ_{Q0} and θ_{idjd} parameters.

As such, a number of separate sensitivity analyses are conducted; one for each set of constraints which are grouped according to purpose. SA1 and SA2 are used to consider the difference made by the definition of $A_{c,ef}$; SA3 to SA5 are used to consider the effect of changes in design crack width range on the sensitivity factors and reliability level and; SA6 to SA8 are used to investigate the effect of values of interest for the crack spacing, θ_{space} , in order to obtain upper and lower bound reliabilities. The constraint sets are shown in Table 6.4. Unless otherwise mentioned, the probabilistic parameters are modelled as per Table 6.2

Table 6.4: Constraint sets for the sensitivity analysis of leakage through a single crack.

Analysis Designation	Variation	Crack length
	With θ_{Q0} and θ_{7d14d} for $0 < w \leq 0.15mm$	
SA1	$A_{c,ef} = 2.5 (c + \phi_s/2)$	2.25 m
SA2	$A_{c,ef} = t/2$	2.25 m
	With $A_{c,ef} = t/2$	
SA3	θ_{Q0} and θ_{7d14d} for $0 < w \leq 0.15mm$	1.85 m
SA4	θ_{Q0} and θ_{7d14d} for $0.15 < w \leq 0.25mm$	2.7 m
SA5	θ_{Q0} and θ_{7d14d} for $0.25 < w \leq 0.35mm$	3.0 m
	With $A_{c,ef} = t/2$; θ_{Q0} and θ_{7d14d} for $0 < w \leq 0.15mm$	
SA6	$\theta_{space} = 1$	2.25 m
SA7	$\theta_{space} = 1.5$	2.25 m
SA8	$\theta_{space} = 2$	2.25 m

6.6.4 Results and discussion

The sensitivity analysis was performed on each of the constraint sets from Table 6.4. The results for analysis sets SA1 through SA5 are shown in Table 6.5, in terms of the α sensitivity factors and β reliability indices.

Table 6.5: Results of sensitivity analysis and α values for SA1-5.

Parameter	Symbol	SA1	SA2	SA3	SA4	SA5
Crack length (m)	ℓ	2.25	2.25	1.85	2.7	3
Area of reinforcing (mm^2)	A_s	3300	3300	3900	1800	1300
Target crack width (mm)	w_t	0.12	0.12	0.1	0.2	0.3
Cover	α_c	0.015	-0.035	-0.044	-0.02	-0.011
Mean conc. tens. strength	$\alpha_{f_{ctm}}$	0.178	0.178	0.19	0.183	0.12
Bar diameter	α_{ϕ_s}	-0.029	-0.033	-0.033	-0.034	-0.024
Steel-conc. bond strength	$\alpha_{\tau_{bms}}$	0.096	0.095	0.097	0.095	0.068
Crack width MF	$\alpha_{\theta_{cw}}$	-0.41	-0.41	-0.441	-0.381	-0.261
Initial flow MF	$\alpha_{\theta_{Q0}}$	-0.43	-0.429	-0.43	-0.343	-0.231
Leakage factor	$\alpha_{\theta_{7d14d}}$	-0.749	-0.748	-0.725	-0.802	-0.914
Crack spacing	$\alpha_{\theta_{space}}$	-0.211	-0.211	-0.214	-0.223	-0.153
Reliability index /Prob. failure	β/p_f	1.06/0.14	1.06/0.14	1.47/0.07	-1.60/0.94	-1.78/0.96

The α values give an indication of how much each parameter contributes to the total uncertainty in the resultant leakage ($L_{al,slice} - L_{p,slice}$), as well as whether increases in the parameter result in greater (positive values) or reduced (negative values) reliability. From Table 6.5, the change of sign in the α values for the cover, from SA1 to the rest is due to the cover term being included in, and then subsequently excluded from, the $A_{c,ef}$ definition. The mean concrete tensile strength and mean concrete-reinforcing bond strength are shown to increase, whereas the rest of the parameters decrease, the level of reliability.

SA1 and SA2 used a target crack width of $w_t = 0.12 \text{ mm}$, which required an area of steel of $A_s = 3300 \text{ mm}^2/\text{m}$ to satisfy. This resulted in a crack length of 2.25 m , calculated based on section 6.3.3, using T_r and T . A comparison between the analyses for SA1 and SA2 from Table 6.5, reveal practically-identical α values. An additional analysis was conducted using a wall section thickness of $t = 0.3 \text{ m}$ (not shown here), which confirmed that the change in definition of $A_{c,ef}$ makes no practical difference to the α values. From this, the definition of $A_{c,ef}$ was kept as $A_{c,ef} = t/2$ for the rest of the sensitivity analyses.

SA3, SA4 and SA5 are used to consider the difference that results from cracks in different crack width ranges. As expected, decreases in A_s lead to decreased β values. A decrease in β value with increasing crack width range is observed, as one progresses from the $0 < w \leq 0.15 \text{ mm}$ range (SA3) to the $0.25 < w \leq 0.35 \text{ mm}$ range (SA5), in Table 6.5. This is due to the reduced area of reinforcing required to satisfy the less-stringent target crack width, which in turn reduces the T_r value of the concrete. This leads to a greater crack length. Additionally, a greater crack width leads to greater Q_0 flow (also a greater magnitude of θ_{Q_0} value) and increased magnitudes of accumulated leakage over time factor (θ_{idjd}). All of this leads to a sharply increasing probability of failure with increasing target crack width.

The magnitude of the α values show which parameters contribute the most uncertainty towards the difference between the allowable leakage and the predicted leakage. Those with α values closer to 1 or -1 contribute greater uncertainty to the resultant leakage. The β value is affected by the square of the α values and thus values smaller than 0.15 have little effect on the uncertainty. From this, it is clear that the cover, bar diameter and mean concrete-reinforcing bond strength contribute little to the total uncertainty in the resultant leakage, across the spectrum. The mean concrete tensile strength, crack width MF, Initial flow MF and crack spacing factor have a moderate contribution and the leakage accumulation factor has the biggest contribution towards the total uncertainty in the resultant leakage.

An omission sensitivity factor, Λ , given by Madsen and Egeland (1989), can be used to approximate the relative error in β , when replacing a probabilistic parameter with a deterministic value. A value of $\Lambda = 1$ indicates no error, whereas values greater than one indicate errors in the calculation of β . From this, using deterministic values for c , ϕ_s and τ_{bms} result in combined relative errors in β of 1 percent, at most. As such, the actual specified cover and bar diameter will be used as deterministic values. The mean concrete-reinforcing bond strength will be used at a value in the middle of the considered range $\tau_{bms} = (1.25 + 1.8)/2 = 1.525 f_{ctm}$. The parameters are thus replaced with deterministic mean values in the following chapters.

$$\Lambda = \frac{1}{\sqrt{1 - \alpha^2}} \quad (6.19)$$

In analyses SA6 through SA8, the effect of the crack spacing was investigated as being one of three deterministic values ($\theta_{space} = 1, 1.5$ or 2) instead of being uniformly distributed between 1 and 2, as it was for the previous analyses. The crack spacing contributes to the width of the cracks, with greater crack spacings being associated with wider cracks. The crack spacing has a minimum value of $1 \ell_{s,max}$, from bond-slip theory, as discussed in section 3.4.2. In the MC 2010 formulation, a crack spacing of $2 \ell_{s,max}$ is used to calculate the design crack width, whereas EN 1992-1-1 uses a less conservative value of $1.7 S_{r,max}$. This does not directly translate into EN 1992-1-1 having a proportionately-lower level of reliability than MC 2010, due to differences in the contribution of the c term and the value of τ_{bms} . The mean crack width is commonly taken to be $1.5 \ell_{s,max}$. These three cases of $1 \ell_{s,max}$, $1.5 \ell_{s,max}$, and $2 \ell_{s,max}$ therefore represent upper, mid and lower bound reliability

levels with regard to crack spacing. In SA6 to 8, the reinforcing was kept constant; the resulting crack length is also constant. The resulting crack widths and β/p_f values for SA6, 7 and 8 are shown in Table 6.6.

Table 6.6: Results of sensitivity analysis for SA6-8 for varied values of θ_{space} .

Parameter	Symbol	SA6	SA7	SA8
		$\theta_{space} = 1$	$\theta_{space} = 1.5$	$\theta_{space} = 2$
Crack length (m)	ℓ	2.25	2.25	2.25
Area of reinforcing (mm^2/m)	A_s	3300	3300	3300
Achieved crack width (mm)	w	0.08	0.111	0.141
Probability of failure	p_f	0.073	0.138	0.200
Reliability index	β	1.46	1.09	0.84

Varying the θ_{space} value has a notable effect on the p_f , almost tripling the p_f from the upper to the lower bound case. This is due to the effect that the crack spacing has on the achieved crack widths, with increasing crack widths resulting from increasing θ_{space} values. This shows that more, closely-spaced cracks with smaller crack widths lead to less leakage and thus greater reliability than fewer cracks spaced further apart with bigger crack widths. The probabilistic variation of θ_{space} is important to be able to obtain a realistic distribution of crack spacings, and thereby crack widths, for the total leakage model. As previously mentioned, MC 2010 intentionally uses the value of $\theta_{space} = 2$ as a way of introducing a conservative design value instead of a mean value. This conservatism can be seen by comparison of the results from SA7 ($\theta_{space} = 1.5$, mean value) with SA8 ($\theta_{space} = 2$, design value).

6.7 Chapter summary

This chapter developed the theory of hydrostatic loading and the effect of reservoir geometry and base restraint condition on the resultant tension forces experience in a reservoir wall. Furthermore, cracking in reinforced concrete subject to tension load, and the associated probabilistic parameters, was investigated. The total leakage prediction model was then adapted and used to determine the leakage resulting from a reservoir, by the specification of a limit state equation considering the allowable leakage and predicted leakage.

A probabilistic sensitivity analysis was conducted on the difference between the allowable leakage and predicted leakage through a single crack within a simplified slice of reservoir. This gave insight into the use of the total leakage model by investigating the effect of a number of parameters on the resultant leakage and associated uncertainty. The sensitivity analysis also served to identify the probabilistic parameters that contribute little uncertainty toward the total uncertainty in the resultant leakage. The cover, bar diameter and mean concrete-reinforcing bond strength (c , ϕ_s and τ_{bms}) were identified as being in this category and are therefore replaced by deterministic mean values in subsequent chapters. Notable changes in β/p_f values result from variation in the θ_{space} parameter, giving an indication of an upper and lower bound of reliability for the considered reservoir slice.

7. Single Reservoir Leakage Simulation

The probabilistic models derived in chapter 5, as well as the theory developed in chapter 6 are used in a novel probabilistic leakage analysis of an entire reservoir in this chapter. The sensitivity analysis performed in chapter 6 served to reduce the complexity of the prediction of SLS leakage through a single crack. This chapter now further develops the theory required to analyse an entire reservoir, rather than the slice analysed in chapter 6. Analyses of four entire reservoirs are then performed to predict the leakage that results from tension-cracks, incorporating the beneficial effect of self-sealing. The distribution of the predicted leakage will be compared to design code permissible leakage for each reservoir to determine the achieved level of reliability.

7.1 Applicability and assumptions

In order to be practically useful in addition to being theoretically sound, the following assumptions are made with regard to the simulated reservoirs.

- The simulations are only applicable to round, tension-governed reinforced concrete structures that retain water or liquids of a nature that are able to facilitate self-sealing in the concrete (e.g. water storage reservoirs, waste water treatment settlement or aeration tanks etc.). Furthermore, the simulations focus on load-induced cracking and related leakage, and do not consider heat of hydration, temperature or restraint effects, although the reinforcing required to control cracking in these cases is important to consider.
- The simulations do not consider the effect of dynamic cracks, nor do they consider the state of the reservoir past the water tightness test stage.
- Due to the unlikelihood of flexural cracks experiencing leakage, the secondary horizontal cracks that may occur due to the flexural retaining wall-type action are not considered in the simulation. Additionally, the design of the roof (if applicable) and floor slab, which are also flexure-governed, are not considered.
- The support condition at the top of the walls is assumed to be free. Roofs, when present, are most often simply supported on a bearing pad or layers of PVC sheeting and thus provide little restraint against lateral movement (axial forces in the wall are not considered).
- The dominating load case is assumed to be due to the hydrostatic pressure on the inside of the reservoir from the retained liquid i.e. the beneficial effect of soil backfill on the outside walls is not considered. This is common practice, as the walls are not usually backfilled until such time as the reservoir has passed the water tightness test. The water tightness test requires a visual inspection of the outside surface of the walls, which is not possible if the reservoir has been backfilled.

- Sources of leakage other than through tension cracks in the walls are not considered. This includes leakage through joints, at pipe penetrations through the wall, evaporation etc.

7.2 Analysis using Monte Carlo simulation

A simulation of the entire reservoir is developed in Python. The code from the FORM analysis is used and extended to be applicable to an entire reservoir. A Monte Carlo simulation (MCS) is used for the analysis of the entire reservoir instead of FORM. This is partly because the sensitivity factors from a FORM analysis are no longer required. More importantly, due to the large number of conditional statements required for parameter assignment and decision-making, using FORM is not appropriate, for reasons similar to those given in section 6.6.3. The MCS uses the same input parameters and probabilistic distributions as the FORM analysis, with the exception of the c , ϕ_s and τ_{bms} parameters, which are replaced with deterministic mean value equivalents, as deemed acceptable by the results from the sensitivity analysis. Unlike FORM, a MCS simply outputs a probability of failure and a subsequent value for the achieved β . The probability of failure, p_f , is the number of realizations that fail, n_f , divided by the total number of realizations, n :

$$p_f = \frac{n_f}{n} \quad (7.1)$$

As previously mentioned in section 2.7.2, the number of repetitions required to produce reasonable output from a MCS is a debated topic. Some applications require that millions of realizations are necessary before convergence is reached, whereas other applications may only require a few hundred. This is especially poignant, given the notable uncertainty associated with leakage through cracked concrete. This is further investigated in section 7.7.3

7.3 Reservoir geometry

Reservoir $R1$ will be used as the reference reservoir for the simulation. At the end of the chapter, an analysis will be carried out on other reservoirs, $R2$ to $R4$, to be able to gauge the effect different geometries have on the leakage and reliability. Importantly, the reservoir geometry must be such that the tension forces in the wall exceeds the threshold concrete tensile resistance, $T_{r,low}$, or the reservoir will not reach the stabilized cracking phase. The geometries of the four reservoirs reflect this and are detailed in Table 7.1.

Table 7.1: Geometry of reservoirs R1 to R4 used in the reservoir leakage analyses.

Parameter/ratio	Symbol (unit)	R1	R2	R3	R4
Height of retained water	h (m)	7.5	8	7	9
Reservoir diameter	D (m)	30	24	40	36
Wall thickness	t (m)	0.25	0.225	0.275	0.30
Mean concrete tensile strength	f_{ctm} (MPa)	2.58	2.53	2.72	2.39
Distance to w_{max} from top of wall	h^* (m)	5.10	5.87	4.24	6.12
Hydraulic ratio	h^*/t	20.4	26.1	15.4	20.4
Hydraulic ratio factor	θ_{HR}	1.02	1.34	0.84	1.02
Dimensionless parameter ratio	h^2/Dt	7.5	11.9	4.5	7.5
Reservoir volume	V (Mℓ)	5.3	3.6	8.8	9.2
Maximum tension force	T_{max} (kN)	754	707	812	1086
Water pressure above crack	Δ_p (N/m ²)	49 930	57 500	41 460	59 920
Base restraint			Hinged		
Top of wall restraint			Free		

*height of water above the point where the maximum crack is likely to occur (position of T_{max}).

7.4 Crack arrangement

Due to the notable effect they have on the resulting leakage and reliability, the behaviour and interaction between the crack width, crack spacing and the number of cracks that form around a reservoir need to be realistically simulated. The crack strain and spacing play an important role in determining both the width, as well the number of cracks that occur around the circumference of the reservoir. When adequate reinforcing is provided at regular, closely spaced intervals, cracks are spaced closer together with smaller crack widths. This is reflected in the formulation for both the mean crack spacing and the mean strain, as shown in the $\rho_{s,ef}$ terms in Equation 7.6. The mean crack spacing can be seen to be inversely proportional to the reinforcing ratio, $\rho_{s,ef} = A_s/A_{c,ef}$. Given that increasing crack width cubically affects the initial leakage, reduces both the efficiency and efficacy of self-sealing, and increases the length of the crack that forms, the specification of adequate reinforcing at regular intervals is crucial to reducing the total leakage that transpires from a reservoir.

A realistic crack arrangement is therefore developed, which extends the single crack theory in the reservoir slice analogy to apply to numerous cracks around an entire reservoir. Once the hoop tension force in a reservoir exceeds the tension resistance of the concrete, cracks form rapidly at random, until all crack spacings are less than $2\ell_{s,max}$ for design purposes. Here though, the entire range of crack spacing is of interest, not just maximum values. Capturing this behaviour is important to analyse a reservoir in a manner that is reflective of reality. The θ_{space} value is used in conjunction with the mean transfer length, $\ell_{s,mean}$, to effectively model this random crack spacing behaviour.

Considering the arrangement of cracks around the reservoir; in the analysis, c , ϕ_s , A_s and τ_{bms} remain constant for a single reservoir. The crack arrangement and spacing around the reservoir is then driven by the variation in the f_{ct} and θ_{space} parameters. A pair of realizations of $f_{ct,a}$ and $\theta_{space,a}$ are generated at a crack position, a , in the reservoir, whereby a crack spacing is also generated. Thereafter, another independent pair, $f_{ct,a+1}$ and $\theta_{space,a+1}$, is generated at a subsequent crack position $a+1$, which

generates another crack spacing and so on, as illustrated later in Figure 7.6. This continues until the entire reservoir circumference has been covered with potential crack positions.

7.5 Reliability limit state

The limit state equation builds on that developed for the single crack in section 6.5. Additional developments are introduced here, to adapt the theory from the leakage through a single crack to that through an entire reservoir.

7.5.1 Reservoir allowable leakage - L_{al}

The allowable leakage for each reservoir follows from the discussion in section 6.5.2 and is summarized in Table 7.2. The leakage accumulation factor distribution associated with each case is shown, as well as the allowable leakage for each of the four reservoirs.

Table 7.2: Allowable leakage cases evaluated in simulation. Periods given in days, allowable leakage given in $k\ell$.

Leak. regime	Design code	Stabiliz. period	Test period	Total period	Allowable leakage	R1	R2	R3	R4
C_{0d7d}	-	0	7	7					
C_{3d8d}	ACI 350.1	3	5	8	0.2% Vol	10.6	7.2	17.6	18.3
C_{7d14d}	BS 8007	7	7	14					
C_{14d21d}	BS 8007	14	7	21					

7.5.2 Reservoir predicted leakage - L_p

This section further develops the predicted leakage side of the limit state equation, from sections 6.5.1 and 6.6.3. In section 6.6.3, an approximation of an effective crack width was made for purposes of the sensitivity analysis, given the lens-type shape of the cracks. For the entire reservoir analysis, however, the effective crack width needs to be developed further. The calculation of the predicted initial flow through a concrete crack, given by Equation 5.10 is repeated here for convenience (note that the experimental concrete sample element thickness, d , is replaced with the reservoir wall thickness, t).

$$Q_{0,actual} = \theta_{Q0} \cdot \frac{0.11 \Delta p \ell w^3}{12 \eta t} \quad (5.10)$$

The value of 0.11 is the mean value determined for ζ from section 5.1.1. This factor takes cognizance of the deviations of the actual w values (averaged crack width) from an ideal, parallel-plate situation, as illustrated by Figure 7.1(a). It also takes into account the effect of the tortuosity of the cracks, through the thickness of the element. The specimens that the database researchers considered were all cracked using a tensile splitting technique, whereby the cracks extend to the ends of the specimen, similar to that of parallel plates, except with jagged edges (Figure 7.1(a)). In a reservoir, however, the shape of a vertical, tension-crack is more lens-like, having two end points where the crack width is zero, and increasing to the maximum crack width at approximately halfway between the two (Figure 7.1(b)). The equation for the geometry of a lens-shaped crack with a maximum width of w and unit length is given by Equation 7.2 and is used as a standard model of a crack for use in the analyses; see

Figure 7.2. The maximum width of the crack at the midpoint, w , is calculated as per Equation 7.6. The crack width at the midpoint of each segment is then denoted by w_b .

$$w_b = \pm 8 \cdot w \cdot x^2(1-x)^2 \quad \text{for } x \in [0, 1] \quad (7.2)$$

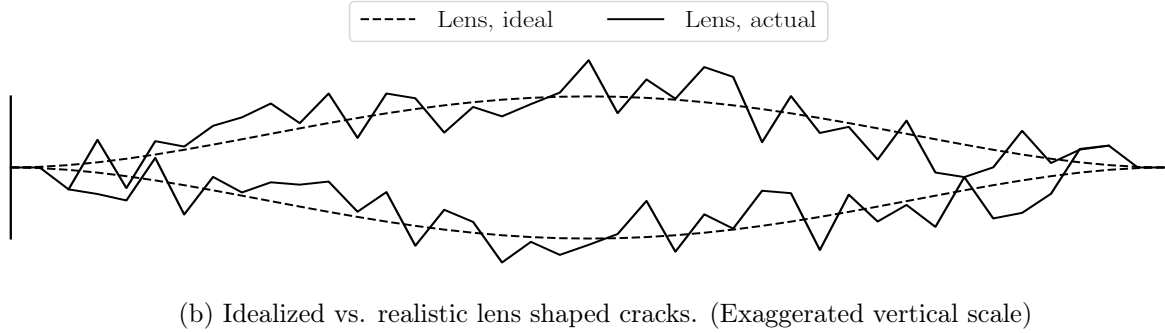
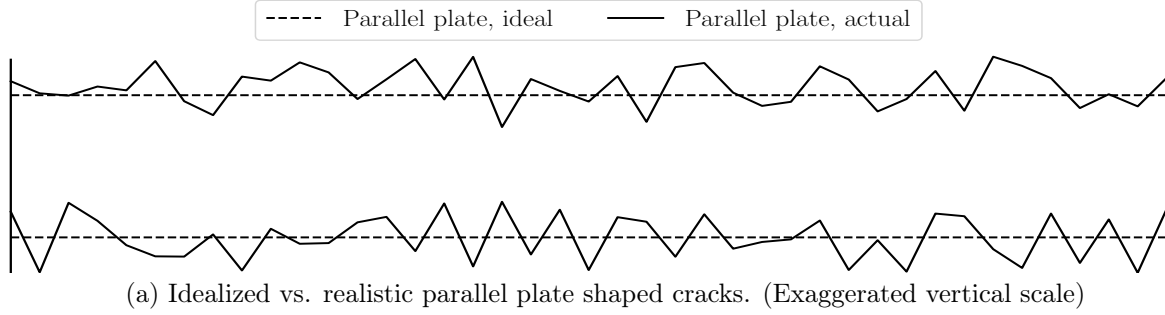


Figure 7.1: Ideal vs. realistic crack shapes in parallel plate-type and lens shape cracks.

The findings of section 5.1.1 showed that the ζ value was found to be independent of crack width for the range of cracks under consideration in this research. The ζ factor is therefore unlikely to change with the shape of the crack. As neither a lengthwise-averaged, nor a single value approximation to the effective crack width are appropriate, the leakage is predicted by breaking up the lens shape into a number (n_b) of individual segments, each with its own crack width w_b , and length, ℓ_b , as illustrated in Figure 7.2. For the sake of avoiding confusion regarding indices, each crack is denoted by a subscript a , whereas each individual crack segment within a crack, is denoted by a subscript b . Those parameters without a subscript are assumed constant for the whole reservoir. The leakage of each segment b in crack a is calculated and summed to get the total leakage through a crack, as per Equation 7.3. Given that a number of the terms are constant for each crack, they are removed from the summation. Furthermore the summation is done over a crack of length ℓ_a with segments of length $\ell_b = \ell_a/n_b$, resulting in Equation 7.4. Equation 7.4 reflects the fact that θ_{Q0} and θ_{idjd} have separate distributions, depending on the w_b of that segment.

$$Q_{crack,tot,a} = \sum_{b=1}^{b=n_b} \frac{0.11 \Delta p \ell_b w_b^3}{12 \eta t} \cdot \theta_{idjd,b} \cdot \theta_{Q0,b} \cdot \theta_{HR} \quad (7.3)$$

$$= \frac{0.11 \Delta p \theta_{HR}}{12 \eta t} \cdot \sum_{b=1}^{b=n_b} (\theta_{idjd,b} \cdot w_b^3 \cdot \theta_{Q0,b} \cdot \ell_b) \quad (7.4)$$

$$L_p = \sum_{a=1}^{a=n_a} Q_{crack,tot,a} \quad (7.5)$$

Where:

$$w_b = \text{Width for an individual segment of a crack with maximum crack width } w$$

$$w = \theta_{cw,a} \cdot \theta_{space,a} \left(c + \frac{1}{4} \frac{f_{ct,a}}{\tau_{bms}} \cdot \frac{\phi_s}{\rho_{s,ef}} \right) \cdot \left(\frac{\sigma_s - \beta \frac{f_{ct,a}}{\rho_{s,ef}} (1 + \alpha_e \rho_{s,ef})}{E_s} + \eta_r \epsilon_{sh} \right) \quad (7.6)$$

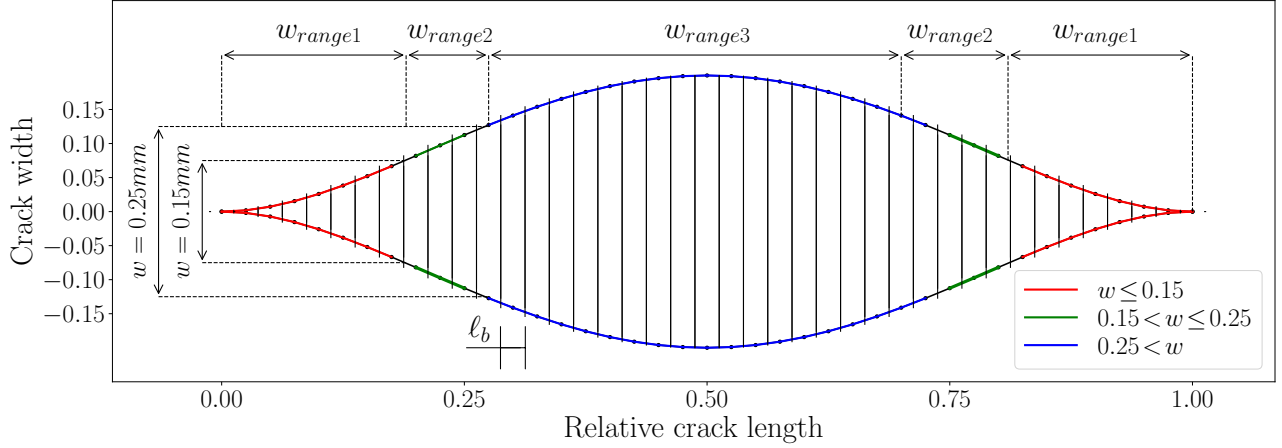


Figure 7.2: Illustration of individual segments along the length of the unit-length crack, each with respective crack width, w_b (Equation 7.2) and length $\ell_b = 1/n_b$.

Figure 7.2 illustrates the individual crack width segments and the three crack width ranges that they fall into. The red segments of the crack are assigned a realization from the θ_{Q0} and θ_{idjd} distributions for $w_b \leq 0.15$ mm, and similarly for the green ($0.15 < w_b \leq 0.25$ mm) and blue ($0.25 < w_b$) sections. Within the same crack, the concrete roughness and ζ -related friction will be similar. Similarly, the factors that affect the leakage over time and extent of self-sealing will be similar throughout the same crack. As such, the Monte Carlo generated realizations from the various distributions (θ_{Q0} , θ_{0d7d} , θ_{3d8d} , θ_{7d14d} and θ_{14d21d}) are taken from the same quantile value in each of their respective crack width ranges, as illustrated by the θ_{0d7d} distributions in Figure 7.3. The flow is then summed over all cracks to give the leakage through the entire reservoir, L_p , as shown by Equation 7.5.

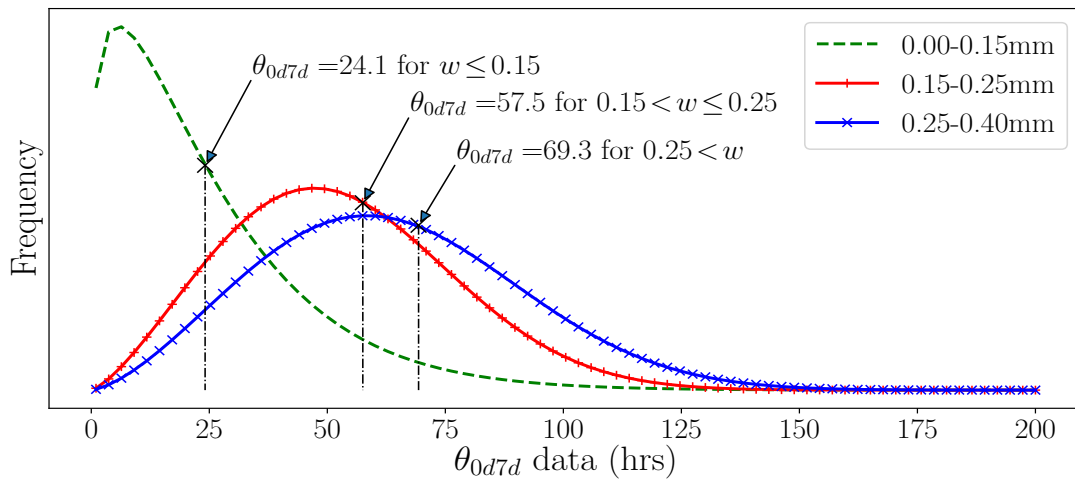


Figure 7.3: Illustrative example of using the same quantile value corresponding to, for example, a lower tail probability $q=0.6$, for each crack width range distribution for θ_{0d7d} .

7.5.3 Limit state equation

The limit state is summarized below, with probabilistic parameters as shown in Table 7.3, along with the deterministic design parameters used to obtain A_s .

$$g = L_{al} - L_p \quad \text{in } k\ell \quad (7.7)$$

$$L_{al} = 0.002 \cdot \pi r^2 h \quad \text{for all leakage regimes} \quad (7.8)$$

$$L_p \quad \text{As per Equation 7.5}$$

Table 7.3: Summary of probabilistic parameters used in the analysis to determine the leakage for an entire reservoir.

Parameter	Symbol	Unit	Dist.	28d Probabilistic		50-yr Design
				Mean	CoV	
Mean concrete tensile strength	f_{ctm}	<i>MPa</i>	LN	3.0	0.15	2.9
Mean conc-reinf bond strength	τ_{bms}	<i>MPa</i>	Det	$1.525 \cdot f_{ctm}$		$1.8 f_{ctm}$
Concrete cover	c	<i>mm</i>	Det	40		40
Steel bar diameter	ϕ_s	<i>mm</i>	Det	$\phi_s (12 - 32 \text{ mm})$		
Crack width prediction MF	θ_{cw}		LN	0.984	0.324	-
Crack spacing factor	θ_{space}		Uni	1 – 2		2
Initial flow prediction MF	θ_{Q0}		W	Table 5.2		-
Leakage accumulation factor	θ_{idjd}	<i>hrs</i>	W	Tables 5.5, 5.6 and 5.7		-
Area of reinforcing	A_s	<i>mm</i> ²	Det	Follows from design		
Shrinkage strain	ϵ_{sh}	10^{-6} m/m	Det	75		250
Modular ratio	α_e		Det	6		16
Empirical integration constant	β		Det	0.6		0.4

LN - Lognormal Uni - Uniform W - Weibull Det - Deterministic.

7.6 Simulation progression

The steps of the simulation are illustrated by the flow chart in Figure 7.4. The various chart elements implement the theory presented in this and the previous chapter. The simulation begins with the generation of the primary parameters for the reservoir. The diameter (D) and height (h) are selected and a mean concrete tensile strength (f_{ctm}) for the reservoir is sampled from the distribution from Table 7.3 ($\mu=3$, $\sigma=0.15 \cdot 3=0.45$, as illustrated later in Figure 7.5). The reservoir wall thickness (t) is then chosen depending on the reservoir height, on grounds of shear resistance, ease of reinforcement fixing and minimum distance to allow aggregate to easily pass between layers of reinforcing. The h^2/Dt ratio is then calculated and used to determine the tension force profile along the height of the wall, the maximum tension force (T_{max}), as well as the height at which it acts from the top of the wall (h^*). The most likely position that the cracks will be at their widest is at the point of T_{max} , given the simplification of a constant area and spacing of reinforcing throughout the reservoir. The h^* parameter is then used to determine the water pressure that acts at the midpoint of the crack. The volume and allowable leakage are also determined here.

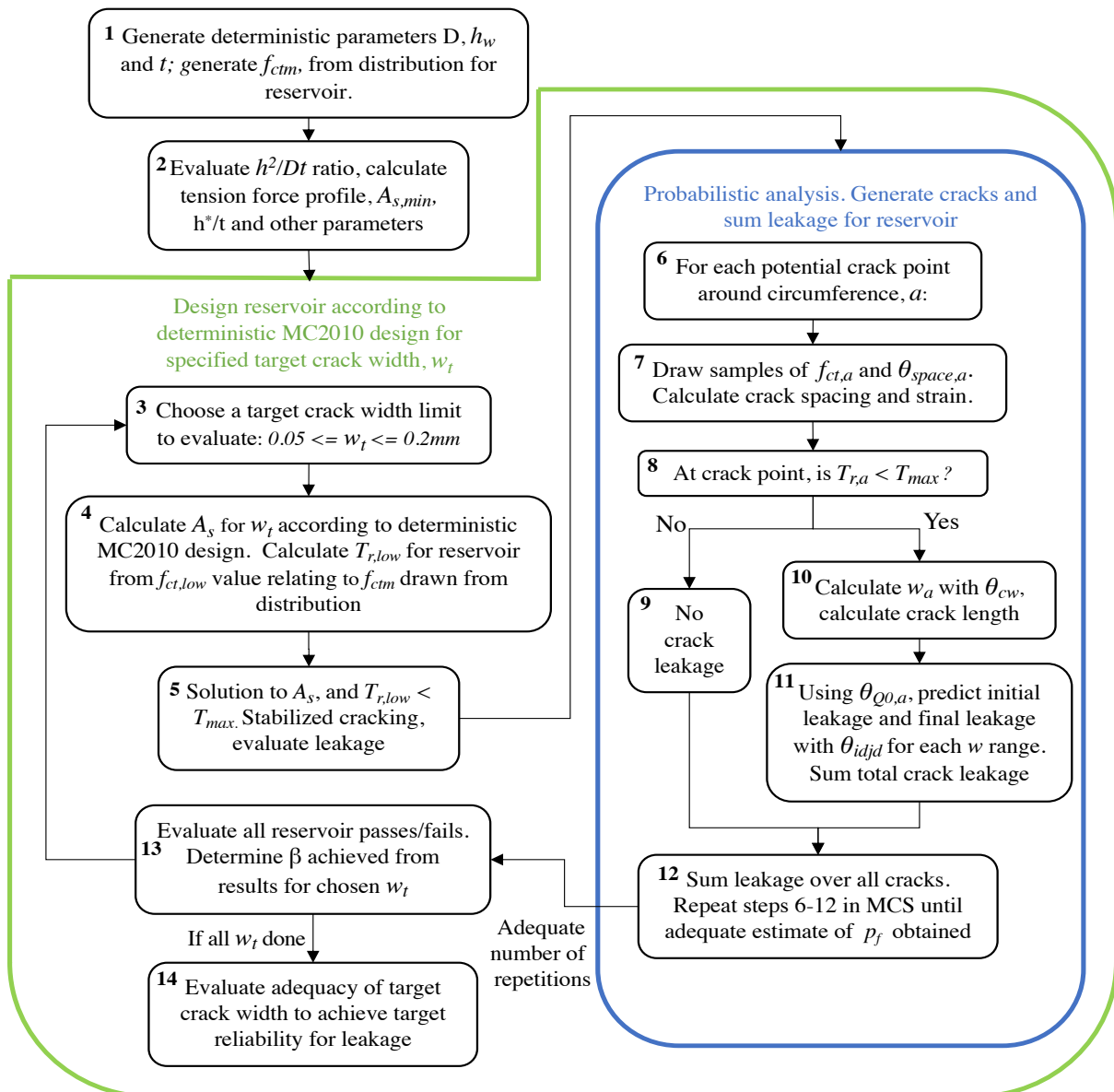


Figure 7.4: Flow chart for the analysis of a single reservoir.

The simulation then enters a loop which iterates through the same reservoir for each target crack width, w_t , as shown by the enveloping green loop in Figure 7.4. This begins with the deterministic design process according to MC 2010. Values of w_t are varied in decrements from the upper limit for tension cracks, 0.2 mm from BS 8007, EN 1992-3 and MC 2010, to the 0.05 mm lower limit of EN 1992-3, for cases of $35 < h^*/t$. For each iteration of w_t , the reinforcing required to achieve w_t , A_s , is calculated according to the deterministic MC 2010 formulation. Equation 6.6 is used with the deterministic, long term values, as shown in the *Design* column of Table 7.3. If necessary, the bar diameter, ϕ_s , is adjusted to an appropriate value, depending on A_s . A minimum and maximum bar diameter of 12 and 32 mm , and a minimum and maximum centre-to-centre bar spacing of 100 and 200 mm are used. Reinforcing areas greater than $8024\text{ mm}^2/\text{m}$ (32 mm bars spaced at 100 mm c/c) are impractical and are not considered in the analysis.

If	$A_{s,min} < A_s < 1130 \text{ mm}^2/m$:	$\phi_s = 12 \text{ mm}$
If	$1130 \leq A_s < 2010 \text{ mm}^2/m$:	$\phi_s = 16 \text{ mm}$
If	$2010 \leq A_s < 3140 \text{ mm}^2/m$:	$\phi_s = 20 \text{ mm}$
If	$3140 \leq A_s < 4910 \text{ mm}^2/m$:	$\phi_s = 25 \text{ mm}$
If	$4910 < A_s < 8042 \text{ mm}^2/m$:	$\phi_s = 32 \text{ mm}$
If	$8042 \text{ mm}^2/m < A_s$:	Not considered

In the event that a rational solution of A_s to the equation is not found, the strain difference in the section is too low to cause significant cracking and the reservoir is discarded from the analysis. If a rational solution for A_s is found, the lower-bound tensile force resistance of the concrete, $T_{r,low}$, for the transition zone is calculated for the reservoir (using $f_{ct,low}$ from the reservoir f_{ctm} value - refer to section 6.4.1) and compared to T_{max} . If the lower-bound concrete tensile resistance is greater than the maximum applied tension ($T_{max} < T_{r,low}$), the reservoir is in the crack formation phase and is discarded. If the reservoir does enter the stabilized cracking phase, the analysis proceeds.

The analysis then enters a second loop that performs a MCS analysis on the leakage of the designed reservoir using the design A_s value, as shown by the blue loop in Figure 7.4. Due to the variation in the total leakage prediction model, a number of iterations of the analysis are required to get an accurate representation of the reliability level. The required number of iterations is discussed in section 7.7.3. At the first potential crack point around the circumference of the reservoir, a , a value of $f_{ct,a}$ and $\theta_{space,a}$ are generated from their probabilistic models. Note that the $f_{ct,a}$ value is sampled from the reservoir-specific f_{ctm} distribution, as shown in Figure 7.5. Figure 7.5 illustrates a reservoir-specific distribution with an f_{ctm} value of 2.7 MPa and CoV of $0.15 \cdot 2.7 = 0.4$, for example.

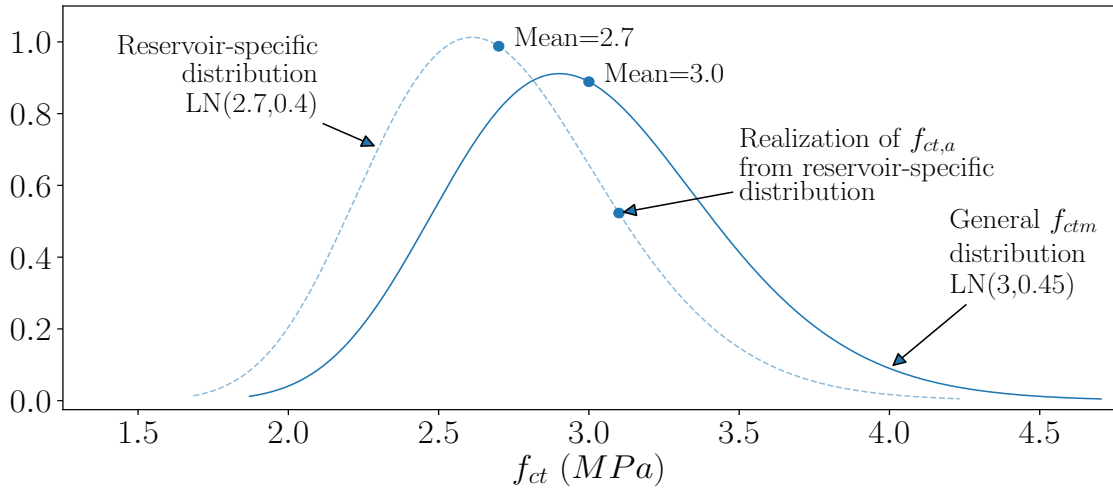
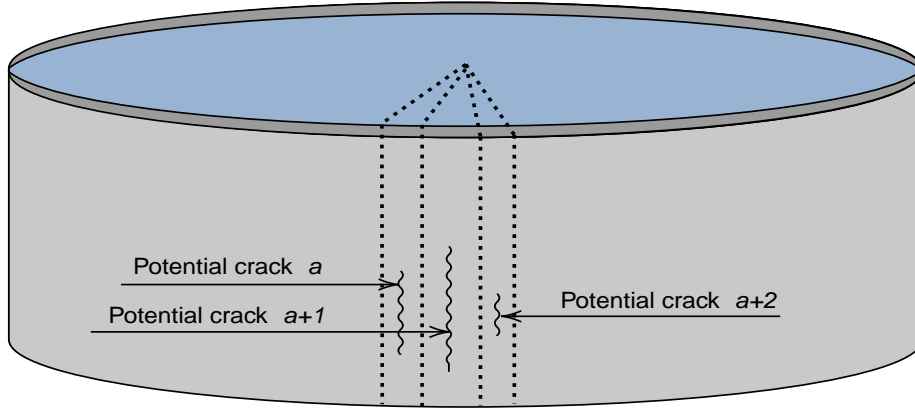


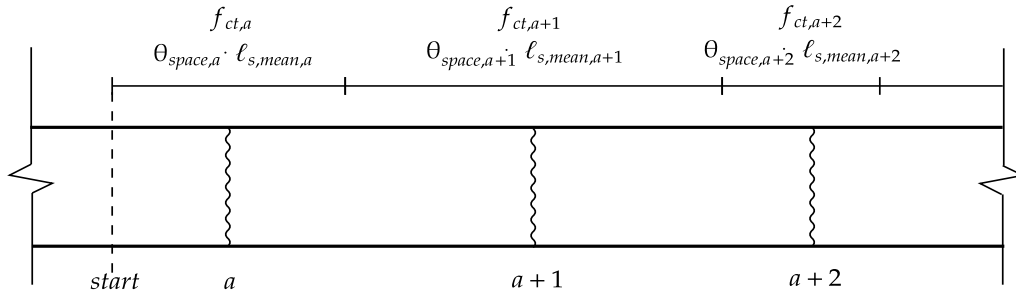
Figure 7.5: Illustration of f_{ctm} distributions and sampled $f_{ct,a}$ values from analysis. Example of a reservoir specific distribution with $f_{ctm} = 2.7 \text{ MPa}$

From this, the crack spacing and mean strain are calculated, from Equation 7.6. Potential crack position a is situated at a distance $\theta_{space,a} \cdot \ell_{s,mean,a}/2$ from the "start" position. The concrete tensile resistance, $T_{r,a}$, is calculated at point a , using $f_{ct,a}$. A check is performed to determine whether a crack forms at point a or not. If $T_{max} \leq T_{r,a}$, due to the realization of a higher $f_{ct,a}$ value from the

distribution, then no crack forms at point a and the analysis moves onto the next potential crack point, $a+1$, as illustrated in Figure 7.6.



(a) Reservoir with potential crack points $a, a+1$ and $a+2$



(b) Plan view of reservoir wall with potential crack points $a, a+1$ and $a+2$ (wall curvature omitted).

Figure 7.6: Illustration of analysis progression through potential crack points $a, a+1, a+2$ and crack spacing for a section of reservoir (pattern continues around reservoir circumference).

In the case that a crack does form at point a , the crack length, ℓ_a , and crack width, w_a , are calculated, incorporating a realization of $\theta_{cw,a}$. The crack is broken up into a number of segments, n_b . A sample is then drawn from the same quantile value for each crack width range's θ_{Q0} distribution, as illustrated by Figure 7.2 and 7.3. Similarly for each of the crack width ranges for the θ_{0d7d} , θ_{3d8d} , θ_{7d14d} and θ_{14d21d} distributions. The leakage through each segment is calculated for half of the crack length and doubled, based on symmetry, in order to reduce the required computation time. The sum of the leakage through the whole crack is calculated and added to the total reservoir leakage, after which the analysis progresses to the next potential crack point, $a+1$. A new set of values are generated, $f_{ct,a+1}$ and $\theta_{space,a+1}$ and the distance between point a and $a+1$ is given by $\theta_{space,a} \cdot \ell_{s,mean,a}/2 + \theta_{space,a+1} \cdot \ell_{s,mean,a+1}/2$, as illustrated in Figure 7.6.

This progresses until all the potential crack points around the circumference of the reservoir have been considered. The leakage of all the cracks is accumulated for each of the variants of leakage regimes, θ_{0d7d} , θ_{3d8d} , θ_{7d14d} and θ_{14d21d} . The predicted leakage (L_p) from each reservoir is evaluated against its respective allowable leakage value (L_{al}). This part of the analysis is repeated a number of times, until the p_f of the reservoir converges (See discussion in section 7.7.3). The results of the total leakage and the allowable leakage are stored for each iteration of the same reservoir, which allows for the calculation of the p_f , as well as whether the reservoir is near to failure ($L_p/L_{al} \approx 1$), passes easily ($L_p/L_{al} \ll 1$) or fails notably ($1 \ll L_p/L_{al}$). Once the reservoir has been analysed a suitable number of times for that

value of w_t , the same reservoir is analysed again for a decremented value of w_t , i.e. the next iteration of the green loop. The analysis ends once all the values of w_t have been considered.

7.7 Results and discussion

The results from the single reservoir analysis are detailed and discussed here to gain an understanding of the behaviour of the model, to consider the leakage that transpires and the implications it has for the achieved leakage-related SLS reliability level. A general overview of the analysis output is given first, followed by a more detailed consideration of the individual aspects/parameters.

7.7.1 General model output

Table 7.4 shows typical results obtained from an analysis of reservoir R1, with characteristics and geometry as shown in Table 7.1. One thousand repetitions of the reservoir analysis were run for target crack widths of $w_t = 0.18, 0.16, 0.14$ and 0.12 mm (other crack widths not shown here, for the sake of brevity). See section 7.7.3 with regard to the choice of 1000 repetitions.

Table 7.4: Selected analysis output for reservoir R1 for $n = 1000$ repetitions.

Parameter	Value	Parameter	C_{0d7d}	C_{3d8d}	C_{7d14d}	C_{14d21d}
T_{max} (kN)	754					
w_t	0.18					
A_s (mm ² /m)	2878	μ	7.21	2.56	1.64	0.79
$T_{r,low} / T_{rm}$ (kN)	624 / 734	σ	2.02	0.99	1.36	0.80
ϕ_s (mm)	20	p_f	1	0.99	0.74	0.19
w_t	0.16					
A_s (mm ² /m)	3121	μ	4.28	1.41	0.8	0.37
$T_{r,low} / T_{rm}$ (kN)	631 / 742	σ	1.3	0.58	0.48	0.26
ϕ_s (mm)	20	p_f	1	0.77	0.23	0.03
w_t	0.14					
A_s (mm ² /m)	3974	μ	1.5	0.45	0.22	0.10
$T_{r,low} / T_{rm}$ (kN)	653 / 768	σ	0.52	0.23	0.22	0.13
ϕ_s (mm)	25	p_f	0.88	0.03	0.01	0.00
w_t	0.12					
A_s (mm ² /m)	4451	μ	0.76	0.21	0.09	0.04
$T_{r,low} / T_{rm}$ (kN)	666 / 783	σ	0.29	0.13	0.08	0.04
ϕ_s (mm)	25	p_f	0.15	0.00	0.00	0.00

μ - Mean value of L_p/L_{al} σ - Standard deviation of L_p (kℓ) p_f - Probability of failure

Table 7.4 and Figure 7.7 show how the required A_s increases non-linearly with decreasing w_t . Note that target crack widths < 0.08 mm are not shown, as their required reinforcing was greater than 8042 mm²/m. Conversely, the leakage drops considerably with decreasing w_t , as expected. The most leakage transpires for leakage regime C_{0d7d} , followed by C_{3d8d} and C_{7d14d} , with C_{14d21d} leaking the least. Interestingly, even when $T_{max} < T_{rm}$ (for $w_t = 0.14$ & 0.12), unacceptable leakage still occurs for C_{0d7d} . Conversely, the other flow regimes all achieve $p_f \approx 0.06$ ($\beta \approx 1.5$) when $T_{rm} \approx T_{max}$. Figure 7.7 shows the mean value of leakage for 1000 repetitions, as a function of target crack width for each leakage regime. The allowable leakage is 10.6 kℓ for all leakage regimes, which illustrates how much the target crack width needs to reduce in order to limit the leakage to within-allowable levels when there

is no stabilization period. Note that the jumps in the graph are where the reinforcing bar diameter changes. The probability of failure is also given in Table 7.4 and can be seen to be highly dependent on the target crack width and the duration of the stabilisation period.

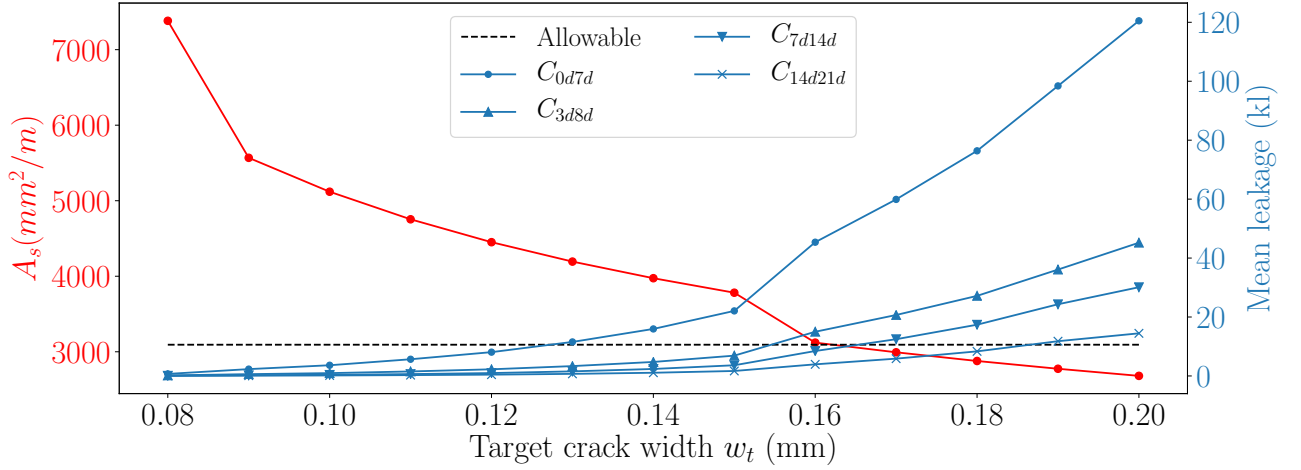


Figure 7.7: Illustration of output from analysis of reservoir R1, showing the relationship between A_s , w_t and the mean of L_p .

7.7.2 Probabilistic model behaviour

The probabilistic model behaviour is considered here. Histograms of the strain difference, crack spacing and crack width are shown, partly to check that the model is giving output as expected but also to consider the distribution of crack widths, compared to the target crack width. Figure 7.8 shows histograms of the strain difference and crack spacing for a single repetition of reservoir R1 with $w_t = 0.2 \text{ mm}$. When considering the strain difference of the cracks around the reservoir, from Equation 6.9, the only parameter that varies from crack to crack is f_{ct} , which is lognormally-distributed (see Appendix A). The lognormal-shaped histogram of the strain difference around the reservoir in Figure 7.8(a) thus indicates that the strain difference is being calculated and applied correctly in the model. A lognormal fit of the distribution is shown in Figure 7.8(a) and later, for ease of distribution visualization.

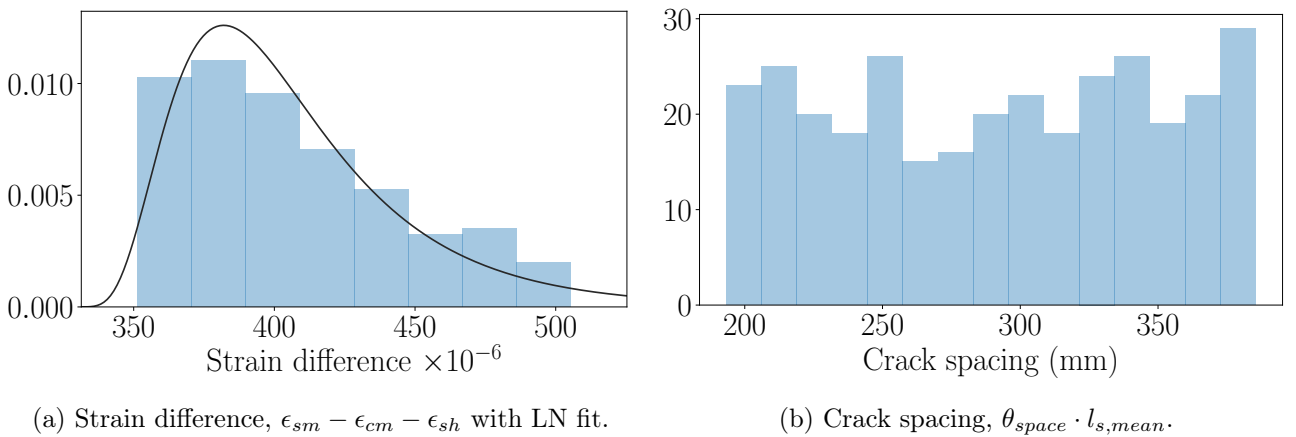


Figure 7.8: Histograms of the strain difference and crack spacing in reservoir R1 for $w_t = 0.2 \text{ mm}$.

The crack spacing, considering the middle part of Equation 7.6, contains probabilistic parameters in θ_{space} and f_{ctm} , which are uniformly and lognormally-distributed, respectively. As θ_{space} has a more dominating effect, one would expect the crack spacing histogram shape to be more uniform than lognormal, as is the case in Figure 7.8(b), indicating that the crack spacing is also being calculated as expected. The histogram shape is more jagged than a uniform distribution, as there were only 320 crack positions around the reservoir in this repetition of the reservoir.

The crack widths calculated according to Equation 7.6 contain the lognormally-distributed θ_{cw} , as well as a combination of the probabilistic parameters from the strain difference and crack spacing. Thus, it contains three instances of lognormally-distributed parameters and one uniformly-distributed, which makes the lognormal shape of the histograms in Figure 7.9 sensible. Figure 7.9(a) shows a histogram of the crack widths for Reservoir R1 for $w_t = 0.2mm$. This figure includes the zero-values that occur as a result of the concrete resistance being greater than the maximum applied tension force at a potential crack point i.e. no crack forms. Figure 7.9(b) shows the same histogram, but excludes the zero values. Figure 7.9(c) shows the same, for a range of w_t values from 0.2 to 0.08 mm. One can see a progressive shift to the left in the histograms as the target crack width decreases. Given the considerable effect that crack width has on the leakage, even small shifts to the left constitute a considerable reduction in leakage.

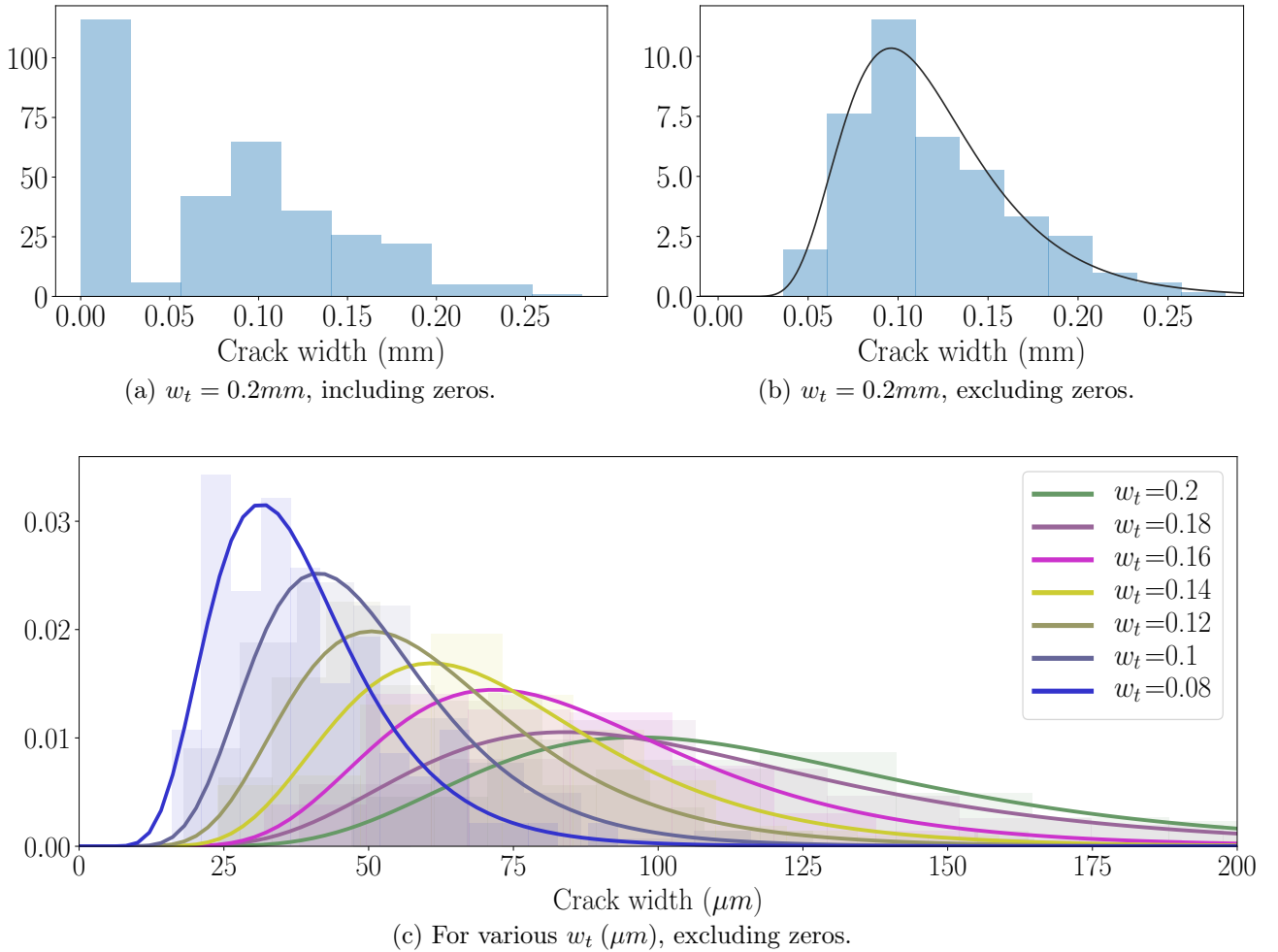


Figure 7.9: Histograms with LN fits of crack widths for a single repetition of reservoir R1 for various target crack widths.

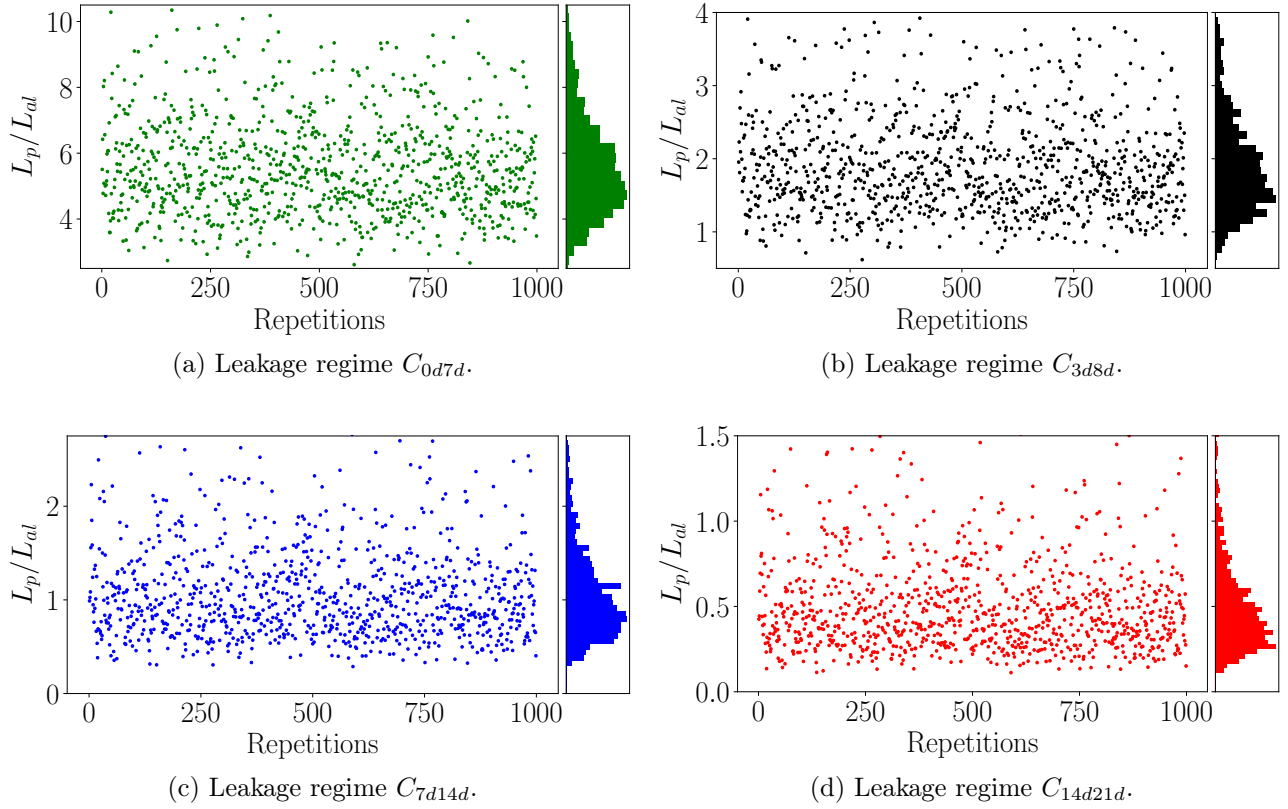
In the development of the crack width equation in EN 1992-1-1/1992-3, the maximum crack width is assumed to be a crack width with a 95% probability of non-exceedance. It was found experimentally that 1.7 times the mean crack width gives a reasonable estimate of the maximum crack width, according to Beeby and Narayanan (2009). MC 2010 uses a more conservative value of 2. Table 7.5 shows the mean, standard deviation and 95th percentile value of crack widths from the analysis, for a range of crack widths for reservoir R1. The results indicate that a value of 1.7 is more appropriate for the range of target crack widths considered than the MC 2010-recommended value of 2. The variation in crack widths is seen to be consistently ≈ 0.4 . Table 7.5 also shows the total number of potential crack points around the circumference of the reservoir and the proportion of those potential crack points where cracks do form, i.e. where $T_r < T_{max}$. As the target crack width is reduced and A_s is increased, the tensile resistance force of the concrete increases and the proportion of points where cracks form reduces, for the same T_{max} . This, in combination with the reduction of the width of cracks that do form, reduces the leakage as illustrated by Figure 7.7.

Table 7.5: Analysis of crack width characteristics, not considering cracks where $T_{max} < T_r$ (uncracked).

w_t (mm)	0.2	0.18	0.16	0.14	0.12	0.1	0.08
A_s (mm ² /m)	2681	2878	3121	3974	4451	5119	7382
Mean w (mm)	0.121	0.103	0.093	0.075	0.063	0.050	0.038
CoV w	0.42	0.35	0.39	0.43	0.40	0.38	0.42
$w_{95\%}$ (mm)	0.207	0.172	0.161	0.126	0.101	0.083	0.062
w_{95}/w_{mean}	1.71	1.67	1.73	1.68	1.60	1.66	1.63
Total num. crack points	326	337	347	347	365	382	394
Prop. points cracked	0.62	0.61	0.55	0.47	0.39	0.40	0.22

The leakage over allowable leakage experienced by reservoir R1 for $w_t = 0.17$ mm is shown in Figure 7.10, for all leakage regimes. One can clearly see that for C_{0d7d} , the L_p/L_{al} ratio is considerably greater than 1. The mean value of 5.65 indicates that the leakage is notably greater than the allowable leakage and in this case, so much so that the probability of failure is 1 ($3.1 < \beta$). Leakage regime C_{3d8d} shows less leakage, with a mean L_p/L_{al} of 1.95 and a $p_f = 0.964$. C_{7d14d} has a mean of 1.18 due to the tail of the distribution extending considerably into failure region. A p_f of just below 0.5 is actually realized, due to the concentration of realizations below 1. As expected, regime C_{14d21d} experiences the least leakage due to it having the longest stabilization period, with a mean of $L_p/L_{al} = 0.55$ and $p_f = 0.09$.

Table 7.6 shows the mean, standard deviation and CoV for reservoir R1. As is expected of concrete cracking applications, the CoV of the leakage over allowable leakage is high. Considering the CoV values, it can be seen that the variation in L_p/L_{al} increases with increasing stabilization period. The CoV is highest for regime C_{14d21d} and lowest for regime C_{0d7d} over all crack widths, which corresponds to the higher variation in θ_{14d21d} and lower variation in θ_{0d7d} . Considering Equations 7.5 and 7.6, the general trend of increasing CoV with decreasing w_t is attributed to the higher variation in θ_{Q0} and θ_{idjd} for smaller crack widths (Table 5.2).

Figure 7.10: L_p/L_{al} for all repetitions and leakage regimes for reservoir R1 and $w_t = 0.17$ mm.Table 7.6: Mean, standard deviation and CoV of L_p/L_{al} for selected target crack widths and leakage regimes for reservoir R1.

w_t (mm)	C_{0d7d}			C_{3d8d}			C_{7d14d}			C_{14d21d}		
	Mean	Std dev	CoV	Mean	Std dev	CoV	Mean	Std dev	CoV	Mean	Std dev	CoV
0.2	11.37	2.66	0.23	4.27	1.3	0.30	2.84	1.52	0.53	1.36	0.84	0.62
0.19	9.28	2.43	0.26	3.41	1.21	0.36	2.29	1.72	0.75	1.11	0.99	0.89
0.18	7.21	2.02	0.28	2.56	0.99	0.39	1.64	1.36	0.83	0.79	0.8	1.01
0.17	5.65	1.62	0.29	1.95	0.76	0.39	1.18	0.82	0.70	0.55	0.45	0.81
0.16	4.28	1.30	0.30	1.41	0.58	0.41	0.80	0.48	0.61	0.37	0.26	0.70
0.15	2.08	0.73	0.35	0.65	0.34	0.52	0.34	0.34	0.99	0.16	0.19	1.20
0.14	1.50	0.52	0.35	0.45	0.23	0.50	0.22	0.22	1.00	0.10	0.13	1.22
0.13	1.09	0.39	0.36	0.32	0.17	0.54	0.15	0.13	0.86	0.07	0.07	1.03
0.12	0.76	0.29	0.38	0.21	0.13	0.61	0.09	0.08	0.88	0.04	0.04	1.07
0.11	0.53	0.21	0.39	0.14	0.09	0.61	0.06	0.05	0.92	0.03	0.03	1.08
0.1	0.34	0.11	0.31	0.09	0.05	0.53	0.04	0.03	0.71	0.02	0.01	0.84
0.09	0.22	0.07	0.31	0.06	0.03	0.51	0.02	0.01	0.58	0.01	0.01	0.63
0.08	0.07	0.02	0.35	0.02	0.01	0.54	0.01	0	0.56	0	0	0.58

7.7.3 Number of analysis repetitions

The probability of failure is closely linked to the target crack width. Small changes in target crack width have a considerable effect on the probability of failure, as seen in Table 7.7. The p_f of reservoir R1 is shown for a selection of crack widths and number of analysis repetitions. It also shows the

execution time of the analysis for each target crack width as a function of the number of analysis repetitions.

Table 7.7: Probability of failure and execution time of the analysis for C_{7d14d} as a function of target crack width and number of analysis repetitions for reservoir R1.

w_t	Number of analysis repetitions							
	10	50	100	500	1000	2500	5000	10000
0.2	1.0	1.00	1.00	0.990	0.992	0.9908	0.9918	0.9921
0.19	0.9	0.92	0.95	0.948	0.947	0.9416	0.9400	0.9419
0.18	0.8	0.78	0.77	0.766	0.771	0.7836	0.7888	0.7824
0.17	0.4	0.34	0.39	0.468	0.486	0.5072	0.4978	0.4997
0.16	0.2	0.26	0.27	0.262	0.247	0.2468	0.2422	0.2408
0.15	0.0	0.00	0.01	0.024	0.025	0.0236	0.0226	0.0218
Time (s)	10	26	45	173	330	835	1668	3300

The previously-mentioned trade-off between analysis result accuracy and time taken to execute the analysis can be seen from Table 7.7. The time taken to execute the analysis increases approximately linearly with the number of repetitions, after 100 repetitions. At a point, increasing the number of repetitions becomes inefficient at improving the accuracy of the analysis, considering the p_f range within which the particular reliability application falls. In the case of reservoirs, the recommended target reliability for irreversible SLS applications is $\beta = 1.5$ or $p_f = 0.067$ for a design life of 50 years, according to both EN 1990 and MC 2010. Given the above, the range of values of interest here is generally $1 \leq \beta \leq 2$ or $0.16 \leq p_f \leq 0.023$.

From the p_f ranges and the required accuracy mentioned above, and by inspection from Table 7.7, $n = 1000$ seems to be an appropriate number of repetitions to balance accuracy with execution time. This also corresponds with the "rule-of-thumb" of using a number of iterations an order of magnitude higher than the desired p_f . The Lemaire *et al.* (2009) approximation from section 2.7.2, repeated below for convenience, is used to verify this. The minimum number of iterations required, n_{min} is dependent on the probability of failure and the CoV of the probability of failure. Choosing a CoV of 0.15 with a desired $p_f = 0.067$ for $\beta = 1.5$, the required n_{min} is 618. Therefore, $n = 1000$ should provide sufficient accuracy for $\beta = 1.5$, as well as satisfactory accuracy for $1.5 < \beta \leq 2$. Probabilities of failure for $2 < \beta$ will be approximate. In some cases where the mean value of L_p/L_{al} is either $\mu \ll 1$ or $1 \ll \mu$ and the p_f is clearly either 0 or 1, respectively, a reduced number of iterations are run, to avoid wasting computational time.

$$CoV = \sqrt{\frac{1 - p_f}{n_{min} \cdot p_f}} \quad (2.20)$$

7.7.4 Target and achieved reliability

One of the chief aims of this research is to determine what the actual, achieved SLS level of reliability is for tension-dominated RC reservoirs considering leakage. Most design codes specify that a certain level of reliability is achieved for irreversible SLS when code guidelines are adhered to, not considering gross human error or construction-related errors. For SLS crack leakage-related applications, however, this has not been proven to any appreciable degree. Code revisions have largely made use of qualitative

performance-over-time as a justification that the level of reliability is near to optimal. Interestingly, the SLS target β values for EN 1992-3 and MC 2010 discussed in section 7.7.3 are given without a means of measuring whether they are achieved or not for WRS; no water tightness test criterion or time periods are specified.

Some probabilistic elements have been included in code provisions, such as the use of an upper-percentile, non-exceedance value for the design crack width but no all-inclusive research on the achieved level of reliability has been conducted to date. Particularly, the beneficial effect of self-sealing on the achieved leakage related reliability has not been considered. Because of this, the specification of design crack widths has thus typically been based on past performance that has deemed-to-satisfy, which has served the industry fairly well. The problem with the specification of deemed-to-satisfy criterion is that it does not have any quantitative basis upon which optimization can be performed. So whether a reservoir is close-to-optimally designed, or is grossly over-designed remains unknown. As a result, potential savings in materials and labour costs can not be realized.

One of the probabilistic elements introduced into modern WRS design codes is the specification of design crack widths based on self-sealing, in EN 1992-3. The recommendations in EN 1992-3 are based directly on research by Edvardsen (1996), and are shown in Figure 7.11, along with research findings by Meichsner (1992) and Lohmeyer (1984). The figure gives the maximum crack width to be designed for, depending on the hydraulic ratio h_D/h (ratio of water pressure head to element thickness, referred to here as h^*/t). Edvardsen's recommendations of crack widths for the hydraulic ratios, as shown in Figure 7.11, specify that cracks should self-seal within 4-to-10 weeks with a 90% probability of non-exceedance, though this is not mentioned in EN 1992-3. This is likely the reason that EN 1992-3 gives no guidance with respect to times for stabilization and water tightness test periods. This is under the assumption that changes in crack width that result from load fluctuations are limited to $\Delta w \leq 10\%$, and that greater Δw lead to extended healing times and reduced probability of sealing. Many designers in Britain, however, feel that particularly the higher h^*/t ratio limits are unnecessarily stringent and are thus uneconomical (Atkinson, 2018).

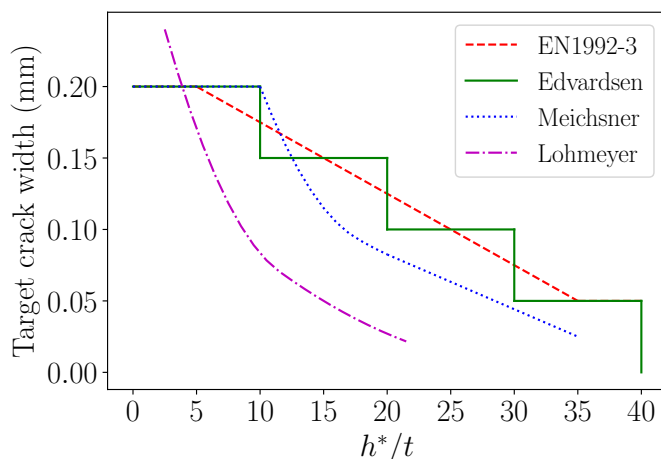


Figure 7.11: Recommendations on limitation of crack width based on self-sealing, according to EN 1992-3, Edvardsen (1996), Meichsner (1992) and Lohmeyer (1984).

Such recommendation of target crack width based on the probability of self-sealing, is progress in the direction of SLS reliability-based design and optimization of WRS. However, adherence to these target crack widths does not necessarily mean that the reservoir will pass the water tightness test in

the allotted time. Nor does the adherence to these target crack widths provide an optimum design. Edvardsen's recommendations specify a period of between 4 and 10 weeks for 90% of the cracks to seal, whereas water tightness tests conclude at 4 weeks at the latest. Thus, without consideration of both the target crack width *and* the quantum of leakage for a specific time period, an accurate assessment of the leakage-related SLS reliability is incomplete.

The analysis output from reservoir R1 (Table 7.8) is compared to the recommendations given in the design codes, to gauge how the reservoir performs. Note that due to the focus around $\beta = 1.5$ and the subsequently-chosen number of analysis repetitions, the maximum reliability "resolution" is $-3.1 < \beta < 3.1$ and values of $\beta < -3.1$ and $3.1 < \beta$ are denoted by $-\infty$ and ∞ , respectively. Even though the crack width design was carried out to MC 2010, the recommended periods from BS 8007 and ACI are considered. The least stringent target crack width limit for tension cracks is 0.2 mm from BS 8007, MC 2010 and EN 1992-3 (for $h^*/t < 5$) which should correspond to an achieved $\beta = 1.5 \approx p_f = 0.067$ according to MC 2010 and EN 1992-3. From Table 7.8, one can see that even with a 7 day test period preceded by a 14 day stabilization period (C_{14d21d}), the target β value is not achieved for $w_t = 0.2\text{ mm}$. A value of $\beta = 1.5$ is only achieved at target crack widths of $w_t \approx 0.16, 0.15, 0.14$ and 0.11 mm for leakage regimes C_{14d21d} to C_{0d7d} , respectively.

Table 7.8: Reservoir R1 p_f , associated β value and mean L_p/L_{al} , for all leakage regimes and all w_t for which $A_s < 8042\text{ mm}^2/m$ (1000 repetitions).

Reservoir R1 $h = 7.5, D = 30, t = 0.25, f_{ctm} = 2.58, h^*/t = 20.4$													
w_t	A_s	C_{0d7d}			C_{3d8d}			C_{7d14d}			C_{14d21d}		
		p_f	β	μ	p_f	β	μ	p_f	β	μ	p_f	β	μ
0.2	2681	1.000	$-\infty$	11.37	1.000	$-\infty$	4.27	0.994	-2.51	2.84	0.617	-0.30	1.36
0.19	2775	1.000	$-\infty$	9.28	1.000	$-\infty$	3.41	0.940	-1.55	2.29	0.391	0.28	1.11
0.18	2878	1.000	$-\infty$	7.21	0.996	-2.65	2.56	0.738	-0.64	1.64	0.186	0.89	0.79
0.17	2993	1.000	$-\infty$	5.65	0.964	-1.80	1.95	0.482	0.05	1.18	0.090	1.34	0.55
0.16	3121	1.000	$-\infty$	4.28	0.773	-0.75	1.41	0.233	0.73	0.80	0.026	1.94	0.37
0.15	3782	0.989	-2.29	2.08	0.106	1.25	0.65	0.025	1.96	0.34	0.006	2.51	0.16
0.14	3974	0.875	-1.15	1.50	0.025	1.96	0.45	0.007	2.46	0.22	0.002	2.88	0.10
0.13	4194	0.504	-0.01	1.09	0.008	2.41	0.32	0.004	2.65	0.15	0.000	∞	0.07
0.12	4451	0.151	1.03	0.76	0.002	2.88	0.21	0.000	∞	0.09	0.000	∞	0.04
0.11	4754	0.030	1.88	0.53	0.001	3.09	0.14	0.000	∞	0.06	0.000	∞	0.03
0.1	5119	0.001	3.09	0.34	0.000	∞	0.09	0.000	∞	0.04	0.000	∞	0.02
0.09	5568	0.000	∞	0.22	0.000	∞	0.06	0.000	∞	0.02	0.000	∞	0.01
0.08	7382	0.000	∞	0.07	0.000	∞	0.02	0.000	∞	0.01	0.000	∞	0.00

w_t (mm) A_s (mm²/m) μ - Mean value of L_p/L_{al}

Considering the guidelines of EN 1992-3, reservoir R1 has a ratio of $h_D/h = h^*/t = 20.4$, for which a target crack width of $w_t = 0.12\text{ mm}$ is recommended. It should be noted that, despite the EN 1992-3 h^*/t ratios extending to 35, values higher than 25 are seldom experienced in practical reservoirs of scale where $T_{r,low} < T_{max}$; reservoir R1 is thus close to this upper limit. The analysis shows that for reservoir R1, the EN 1992-3 recommendation of $w_t = 0.12\text{ mm}$ achieves a satisfactory value of $1.5 < \beta$ for all leakage regimes except C_{0d7d} . It does, however, seem to be too stringent for most of the leakage regimes, necessitating more reinforcing than is required to achieve $\beta = 1.5$.

For the guidelines for water tightness testing given in ACI 350.1-10 (C_{3d8d}), the analysis indicates that an acceptable β value is achieved at a target crack width of $w_t < 0.15 \text{ mm}$. ACI's recommendation of a target crack width of $w_t = 0.1 \text{ mm}$ with a water tightness test of 5 days, preceded by a 3 day stabilization period, seems to be appropriate. It does come at a cost; the A_s required is $\approx 27\%$ higher than for regime C_{14d21d} . Leakage regime C_{0d7d} requires the smallest target crack width by a considerable margin, which illustrates why a stabilization period is highly recommended prior to any water tightness test.

Table 7.8 also shows the A_s required to obtain the respective target crack widths. One can see that increases in A_s become less efficient at reducing the crack width, as the target crack width decreases. A 4% increase in reinforcing is required to reduce the crack width from 0.2 to 0.19mm, whereas a 33% increase is required to reduce the crack width from 0.09 to 0.08 mm. Thus, for smaller crack widths, linear reductions in target crack width constitute disproportionately more expensive reservoirs. This relates to the efficiency parameter investigated by Van Nierop *et al.* (2017), as discussed in section 2.6.1.

7.7.5 Analysis results for reservoirs R2, R3 and R4

The same analyses were carried out on reservoirs R2 to R4, with the results shown in Table 7.9. Similarly to reservoir R1, reservoirs R2 and R4 do not show acceptable reliability levels at $w_t = 0.2 \text{ mm}$, even for leakage regime C_{14d21d} . However, reservoir R3 does achieve acceptable reliability at $w_t = 0.2 \text{ mm}$. According to EN 1992-3, the target crack width for reservoirs R2 to R4 should be $w_t = 0.09, 0.15$ and 0.12 mm , respectively, due to their h^*/t ratios. From Table 7.9, it can be seen that the reservoirs all reach $\beta = 1.5$ at the w_t recommended by EN 1992-3, with the exception of flow regime C_{0d7d} , although perhaps too conservatively for regimes C_{7d14d} and C_{14d21d} .

Table 7.9: p_f , associated β value and mean L_p/L_{al} , for reservoirs Reservoir R2 to R4 for all leakage regimes and all w_t for which $A_s < 8042 \text{ mm}^2/\text{m}$ (1000 repetitions).

Reservoir R2 $h=8, D=24, t=0.225, f_{ctm}=2.53, h^*/t=26.1$													
w_t	A_s	C_{0d7d}			C_{3d8d}			C_{7d14d}			C_{14d21d}		
		p_f	β	μ	p_f	β	μ	p_f	β	μ	p_f	β	μ
0.2	2491	1	$-\infty$	29.19	1	$-\infty$	10.9	1	$-\infty$	7.17	1	$-\infty$	3.43
0.19	2578	1	$-\infty$	23.79	1	$-\infty$	8.73	1	$-\infty$	5.72	0.977	-2.00	2.74
0.18	2674	1	$-\infty$	18.78	1	$-\infty$	6.69	0.999	-3.09	4.28	0.851	-1.04	2.05
0.17	2781	1	$-\infty$	14.86	1	$-\infty$	5.15	0.992	-2.41	3.13	0.619	-0.30	1.48
0.16	2899	1	$-\infty$	11.45	1	$-\infty$	3.84	0.895	-1.25	2.25	0.379	0.31	1.06
0.15	3033	1	$-\infty$	8.68	0.998	-2.88	2.84	0.704	-0.54	1.61	0.192	0.87	0.77
0.14	3695	1	$-\infty$	4.11	0.560	-0.15	1.24	0.13	1.13	0.61	0.026	1.94	0.28
0.13	3899	1	$-\infty$	2.89	0.256	0.66	0.84	0.029	1.90	0.40	0.007	2.46	0.19
0.12	4138	0.998	-2.88	2.04	0.071	1.47	0.57	0.017	2.12	0.25	0.004	2.65	0.11
0.11	4419	0.876	-1.16	1.41	0.015	2.17	0.38	0.004	2.65	0.16	0.002	2.88	0.07
0.1	4757	0.346	0.4	0.95	0.004	2.65	0.25	0.001	3.09	0.10	0	∞	0.04
0.09	5173	0.047	1.67	0.62	0.003	2.75	0.17	0.001	3.09	0.06	0	∞	0.03
0.08	5700	0.004	2.65	0.37	0	∞	0.1	0	∞	0.04	0	∞	0.02
Reservoir R3 $h=7, D=40, t=0.275, f_{ctm}=2.72, h^*/t=15.4$													
0.2	2842	1	$-\infty$	3.87	0.877	-1.16	1.45	0.34	0.41	0.96	0.041	1.74	0.46
0.19	2941	1	$-\infty$	3.18	0.607	-0.27	1.16	0.169	0.96	0.76	0.029	1.90	0.37
0.18	3051	1	$-\infty$	2.43	0.26	0.64	0.86	0.066	1.51	0.54	0.009	2.37	0.26
0.17	3678	0.608	-0.27	1.17	0.013	2.23	0.39	0.008	2.41	0.23	0.001	3.09	0.11
0.16	3837	0.250	0.67	0.87	0.001	3.09	0.28	0.002	2.88	0.15	0.001	3.09	0.07
0.15	4015	0.069	1.48	0.65	0.001	3.09	0.20	0.001	3.09	0.10	0	∞	0.05
0.14	4218	0.009	2.37	0.46	0	∞	0.14	0.001	3.09	0.07	0	∞	0.03
0.13	4452	0.001	3.09	0.32	0	∞	0.09	0	∞	0.04	0	∞	0.02
Reservoir R4 $h=9, D=36, t=0.30, f_{ctm}=2.39, h^*/t=20.4$													
0.2	4105	1	$-\infty$	21.11	1	$-\infty$	7.86	1	$-\infty$	5.24	0.997	-2.75	2.53
0.19	4248	1	$-\infty$	17.12	1	$-\infty$	6.2	1	$-\infty$	3.97	0.954	-1.68	1.9
0.18	4406	1	$-\infty$	13.63	1	$-\infty$	4.79	1	$-\infty$	2.99	0.733	-0.62	1.42
0.17	4581	1	$-\infty$	10.62	1	$-\infty$	3.61	0.989	-2.29	2.16	0.379	0.31	1.02
0.16	4777	1	$-\infty$	8.22	1	$-\infty$	2.71	0.835	-0.97	1.56	0.149	1.04	0.74
0.15	4997	1	$-\infty$	6.22	0.996	-2.65	1.98	0.467	0.08	1.06	0.034	1.83	0.49
0.14	5247	1	$-\infty$	4.59	0.882	-1.19	1.41	0.124	1.16	0.72	0.01	2.33	0.33
0.13	5534	1	$-\infty$	3.31	0.399	0.26	0.97	0.018	2.10	0.46	0.003	2.75	0.21
0.12	7029	0.945	-1.60	1.35	0.004	2.65	0.37	0	∞	0.15	0	∞	0.07
0.11	7507	0.340	0.41	0.96	0	∞	0.26	0	∞	0.1	0	∞	0.05

w_t (mm) A_s (mm²/m) μ - Mean value of L_p/L_{al} Note: Values of w_t with $\beta=\infty$ for all regimes not shown.

Notably, the reservoirs seem to perform based on their h^*/t ratio. Taking regime C_{14d21d} as an example, reservoir R2 has the highest h^*/t ratio and requires the most stringent target crack width ($w=0.14 \text{ mm}$) to achieve $\beta=1.5$. Conversely, reservoir R3 has the lowest h^*/t ratio and requires the least stringent target crack width ($w=0.2 \text{ mm}$). R1 and R4 had the same h^*/t ratio and required similar target crack widths ($w_t=0.16$ and 0.15 mm , respectively). This corresponds to the trend in Edvardsen's recommendations from EN 1992-3, although not with the same magnitude.

The evaluation of the performance of reservoirs R1 to R4, with regard to the irreversible SLS reliability levels of $1.5=\beta$ assumed in design codes, seems to indicate that this reliability level is not often achieved for $w_t=0.2 \text{ mm}$ for the evaluated leakage regimes. This is concerning, as many designers in industry use codes that recommend 0.2 mm as the design crack width. The EN 1992-3 recommendations of w_t based on h^*/t ratio seem to capture the trend of more stringent requirements of target

crack width for higher h^*/t ratios. The ACI recommendations of $w_t = 0.1 \text{ mm}$ associated with C_{3d8d} also seem to achieve reliabilities of $1.5 \leq \beta$ though, perhaps too conservatively.

These four observations of achieved reliability are useful to get insight into the achieved SLS level of reliability in reservoirs and whether they achieve the target SLS $\beta = 1.5$ or not. Four observations, however, are only sufficient to get an indication of whether these reliability levels are achieved or not. As such, a greater number of reservoirs with varying geometrical properties will need to be analysed to get a true representation of the range and mean of β values and to see whether the code-specified level of reliability is satisfied or not. This is further investigated in the following chapter.

7.8 Chapter summary

This chapter further develops the crack-leakage theory from predicting the leakage from a single crack, to the leakage from an entire reservoir, considering the reservoir geometry, crack arrangement and crack shape. It further describes the limit state and the Monte Carlo reliability analysis performed on four reservoirs with varying geometry to determine the achieved level of irreversible, SLS reliability as a result of leakage considerations.

The achieved reliability levels were compared to the target reliability levels specified in various design codes for the leakage regimes considered. From the results of the four reservoirs analysed, it seems that the target reliability is not obtained for some of the design codes and over-achieved for others. The results show a trend of more stringent target crack widths for reservoirs with higher h^*/t ratios, similarly to the recommendations in EN 1992-3. The target crack widths recommended by EN 1992-3 do appear to be conservative, however, a greater number of reservoirs will need to be considered to confirm this. The following chapter therefore analyses a greater number of reservoirs in order to determine the extent of realisation or non-realisation of the target reliability more definitively.

8. Multiple Reservoir Leakage Simulation

Chapter 7 investigated the analysis of four reservoirs and determined the achieved level of reliability. The results indicated that target crack widths of 0.2 mm may not be sufficient to achieve reliability levels of $1.5 \leq \beta$, especially for leakage regimes with short or no stabilization periods. It also found that the recommendations of target crack widths from EN 1992-3 are possibly too stringent, especially for higher h^*/t ratios. This chapter simulates and analyses a greater number of reservoirs in order to investigate this further. A substantial number of reservoirs are simulated to cover a variation of geometries that would be more representative of the spectrum of reservoirs likely to be encountered in practice (that are in the stabilized cracking phase, as defined in section 6.4.1). For each of the reservoirs in the set under consideration, the achieved level of reliability will be determined, for target crack widths in the range $0.05 \leq w_t \leq 0.2 \text{ mm}$. The results are discussed and recommendations of target crack widths will be proposed considering the leakage regime.

8.1 Simulated reservoir geometry considerations

The geometry of the simulated reservoirs needs to be as representative of those in practice as possible. In view of this, constraints were placed on the chosen geometrical parameters so that as wide a range of typical reservoirs as possible are included in the simulation. The reservoir geometries are generated from combinations of randomly sampled values for h and D , from the ranges shown in Table 8.1. The wall thickness is then randomly chosen from the ranges as shown. The process of the evaluation of the suitability of the reservoir continues as per section 7.6 and is constrained to the h^*/t (h_D/h in EN 1992-3), h^2/Dt ratios and the limit on volume, as shown in Table 8.1.

Table 8.1: Geometry constraint sets for the reservoir simulations.

Parameter/ratio	Symbol (unit)	Value/range
Height of retained water	h (m)	6-9
Reservoir diameter	D (m)	20 - 40
Wall thickness ($6 \leq h \leq 8$)	t (mm)	225 - 275
Wall thickness ($8 < h \leq 9$)	t (mm)	275 - 325
Hydraulic ratio	h^*/t	5 - 35
Dimensionless parameter ratio	h^2/Dt	3 - 25
Reservoir volume	V (Mℓ)	$1 < V < 10$
Base restraint		Hinged
Top of wall restraint		Free

The h^2/Dt and h^*/t ratios are a means by which the reservoirs are constrained to exclude combinations of geometry that are not cost-effective and are thus unlikely to be used in practice. They are also used to ensure that unrealistic combinations of high water pressure and thin wall sections are not realised. The volume is constrained to be greater than $1 M\ell$, as reservoirs smaller than this are often constructed using catalogue designs, without design calculations to any specific code. For larger reservoir volumes, the cost effectiveness of reinforced concrete begins to decline and at some point, post-tensioned concrete becomes more cost effective for use in round reservoirs. The point at which this happens is a debated topic, but it is usually accepted as being between 5 and $10M\ell$. The upper volume limit of $10 M\ell$ is included, in light of this.

The reservoir diameter is limited, as beyond $\approx 40 m$ the walls have notably less curvature, whereby the circular restraining tension in the walls becomes ineffective and the walls effectively behave as a cantilever and are governed by flexure and not tension. The wall thickness is constrained to be in increments of $25 mm$ in the ranges shown in Table 8.1. The lower limit is instituted for a number of reasons: to ensure that the four layers of reinforcing can fit into the wall section; so that there is adequate spacing between reinforcing bars to facilitate easy fixing of the steel; to avoid the aggregate from becoming lodged between the reinforcing bars; and for considerations of shear resistance at the base. The maximum thickness is imposed based on a practical, economic section used for reservoirs at the upper limits of the constrained values.

In round, reinforced concrete reservoirs, the base restraint is either considered fixed or pinned, but is typically designed as being pinned. This is due to the thinner wall sections, which make a fixed reinforcing arrangement difficult and more expensive to achieve. The base restraint is therefore considered to be pinned.

8.2 Simulation progression

The simulation follows the same progression as discussed in section 7.6, with an initial, deterministic design of A_s considering a design life of 50 years (long-term), followed by a probabilistic consideration of the leakage that transpires at the water-tightness testing stage (short-term). The details of the probabilistic parameters are shown in Table 7.3. Only reservoirs that are in the stabilized cracking stage as defined in section 6.4.1 are considered. The limit state equation remains unchanged from Equation 7.7.

8.3 Results

8.3.1 Simulated reservoirs characteristics

Given the constraints placed on the randomized geometry of the reservoirs from Table 8.1, a range of reservoir characteristics are realised for the 235 reservoirs that were analysed. Histograms of the reservoir diameter, wall height, wall thickness, volume, h^2/Dt and h^*/t ratios, and mean concrete tensile strength are shown in Figure 8.1

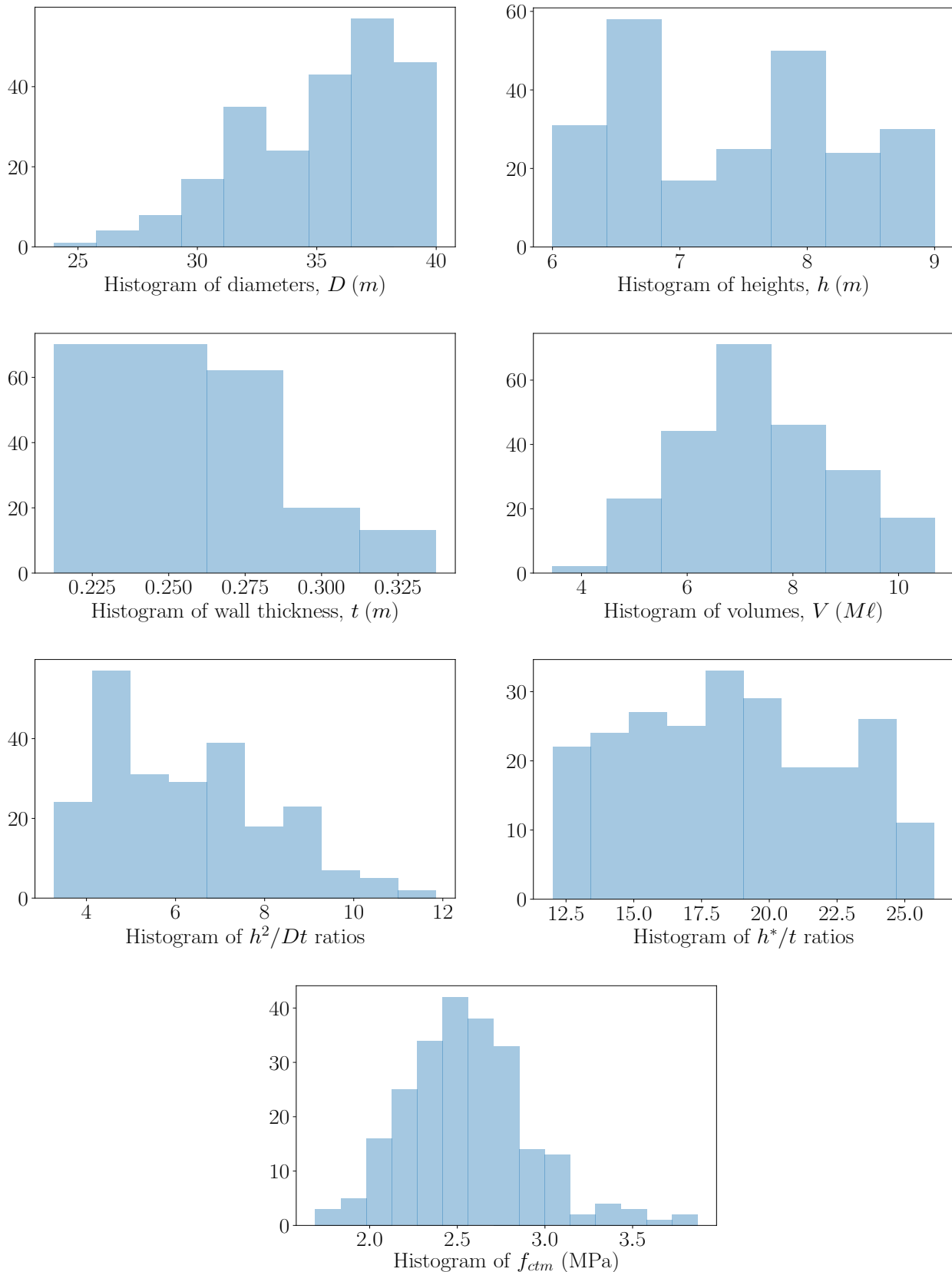


Figure 8.1: Histograms of reservoir characteristics from all analysed reservoirs.

The main constraint that determined the reservoir characteristics as shown in Figure 8.1 is the requirement that the reservoir be in the stabilized cracking stage. For a considerable proportion of the

sampled reservoirs, the stabilized cracking stage was not reached at the maximum applied hoop tension, even though this research considers a requirement that is lower than is typically considered for the stabilized cracking stage ($T_{r,low} < T_{max}$, as opposed to $T_{r,m} < T_{max}$, with reference to Figure 6.6). Fewer than 10% of the total number of randomized reservoir geometries actually reached the stabilized cracking stage. In order to obtain the 235 reservoirs that were in the stabilized cracking stage, over 2500 reservoir geometries were sampled.

From the histogram of the reservoir volumes, one can see that the reservoirs that reached the stabilized cracking stage are predominantly on the larger side of the allowed range ($\approx 7 M\ell$). Similarly, the histogram of the reservoir diameters shows a concentration towards the upper limit of the diameter. The histogram of reservoir f_{ctm} values shows that most of the reservoirs in the stabilized cracking stage have realizations of f_{ctm} lower than the deterministic design value of $2.9 MPa$. This is unsurprising, as the realization of a value of $f_{ctm} < 2.9 MPa$ means that the resulting concrete tensile resistance force will be lower than the intended design tensile resistance and the reservoir will thus be more likely to be in the stabilized cracking stage.

The wall thickness is shown to be predominantly toward the lower end of the imposed limit, as thinner wall sections have a lower concrete tensile resistance force. The h^2/Dt ratios are most commonly in the range of 3–9, corresponding to the considerable proportion of higher diameters. A relatively uniform spread of h^*/t ratio gives a good platform with which to compare the Edvardsen (1996)/EN 1992-3 recommendations of w_t to. The full range of $5 < h^*/t < 35$ could not be investigated due to reservoirs with ratios higher than ≈ 26 and lower than ≈ 12 either not being in the stabilized cracking range, or having unrealistic or uneconomical geometries.

8.3.2 Target crack width, achieved reliability & required area of reinforcing

One of the most important aims of this research is to determine the level of reliability of round, reinforced concrete reservoirs for the case of SLS leakage by means of evaluating the result of the water tightness test. This section presents the results of the achieved level of reliability as a function of target crack width and other reservoir parameters.

Each reservoir was analysed for w_t values from 0.20 to 0.05 mm, with 1000 repetitions for each w_t value. Each w_t has an associated area of reinforcing and achieved level of reliability. Table 8.2 shows the typical summarized output of the analysis of one reservoir. The $-\infty$ and ∞ signs appear for $\beta < -3.1$ and $3.1 < \beta$. If the number of repetitions was increased to a number greater than 1000, more detailed values of these ranges would be realized, however, these ranges are not of importance in this research. Sample output for a subset of reservoirs is shown in Appendix G.

Table 8.2: Typical, summarized reservoir analysis output. Example of reservoir 57.

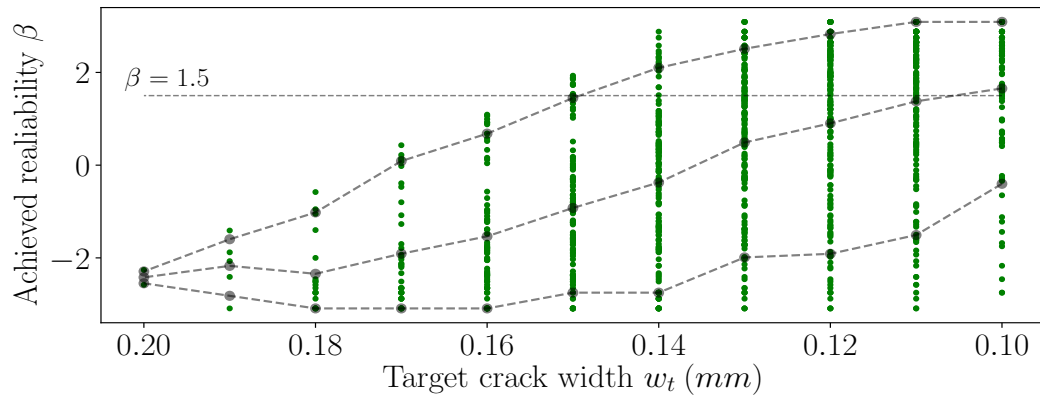
Reservoir 57																
D	h	t	f_{ctm}	h^*/t	$f_{ct,low}$	T_{max}	θ_{HR}									
38	6.5	0.25	2.25	15.3	1.91	715	0.83	w_t	A_s	T_r	$T_{r,low}$	p_f	C_{0d7d}	C_{3d8d}	C_{7d14d}	C_{14d21d}
			β	μ	p_f	β	μ	p_f	β	μ	p_f	β	μ	p_f	β	μ
0.2	2569	632	537	1	$-\infty$	11.98	1	$-\infty$	4.67	1	$-\infty$	3.35	0.812	-0.89	1.63	
0.19	2659	634	539	1	$-\infty$	9.70	1	$-\infty$	3.65	0.997	-2.75	2.46	0.543	-0.11	1.18	
0.18	2759	637	541	1	$-\infty$	7.95	1	$-\infty$	2.93	0.952	-1.66	1.92	0.318	0.47	0.92	
0.17	2869	640	544	1	$-\infty$	6.12	0.999	-3.09	2.18	0.725	-0.60	1.38	0.112	1.22	0.66	
0.16	2992	643	547	1	$-\infty$	4.77	0.962	-1.77	1.64	0.368	0.34	1.00	0.046	1.68	0.47	
0.15	3130	647	550	1	$-\infty$	3.61	0.683	-0.48	1.20	0.119	1.18	0.70	0.018	2.10	0.33	
0.14	3803	665	565	0.99	-2.33	1.76	0.027	1.93	0.54	0.012	2.26	0.28	0.002	2.88	0.13	
0.13	4015	671	570	0.811	-0.88	1.27	0.003	2.75	0.37	0.003	2.75	0.18	0	∞	0.08	
0.12	4261	678	576	0.273	0.60	0.90	0.001	3.09	0.26	0.001	3.09	0.12	0	∞	0.05	
0.11	4553	685	582	0.024	1.98	0.63	0.001	3.09	0.17	0	∞	0.07	0	∞	0.03	
0.1	4904	695	591	0.001	3.09	0.43	0	∞	0.11	0	∞	0.05	0	∞	0.02	
0.09	5336	707	601	0	∞	0.28	0	∞	0.07	0	∞	0.03	0	∞	0.01	
0.08	7068	753	640	0	∞	0.10	0	∞	0.03	0	∞	0.01	0	∞	0	
0.07	7976	778	661	0	∞	0.06	0	∞	0.01	0	∞	0.01	0	∞	0	
0.06	9247										N/A					
0.05	11168										N/A					

μ - Mean value of predicted leakage over allowable leakage (L_p/L_{al}); $T_r, T_{r,low}, T_{max}$ (kN); $f_{ctm}, f_{ct,low}$ (MPa); D, h, t (m); A_s in (mm^2/m); w_t in (mm).

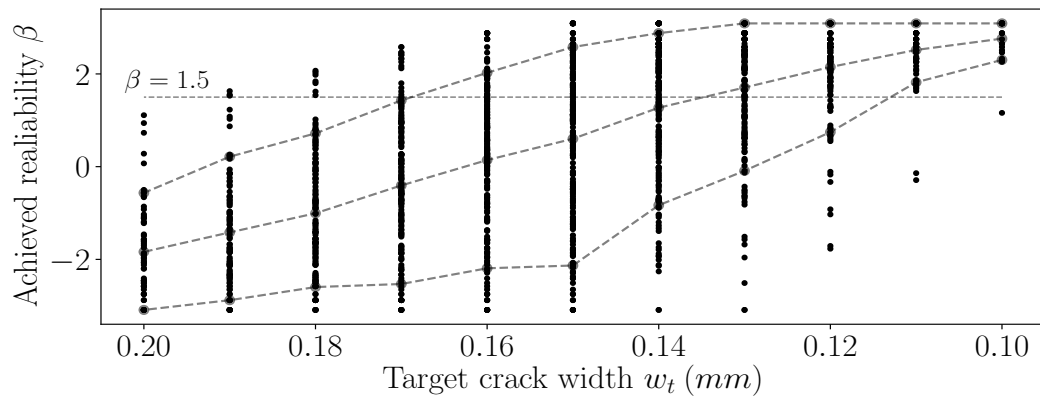
Table 8.2 shows the general reservoir characteristics on top and a summary of the output for each value of w_t below. Table 8.2 also shows the maximum applied load, T_{max} , the mean concrete tensile resistance, $T_{r,m}$ and the lower threshold of concrete tensile resistance, $T_{r,low}$. The reservoir is shown to be in the stabilized cracking stage as discussed in section 6.4.1; $T_{r,low} < T_{max}$ for all w_t values. The w_t values for which $8042 mm^2 < A_s$ are blocked out as N/A, indicating that the sections have an impractical amount of reinforcing and are not considered.

The results of the analysis of all 235 reservoirs are shown in the following series of graphs. Figure 8.2 shows realizations of the achieved β values for each chosen value of w_t from all reservoirs. The cases where the β value was reported as being $-\infty, \infty$ or N/A were not included in the figure. As such, some values of w_t will not be as densely populated, as only a few realizations occur. This can be seen, for example, in Figure 8.2(a) for $w_t = 0.2$ and $w_t = 0.19 mm$, where the reliability is very low; most realizations will have $\beta = -\infty$. Similarly, because the reliability in Figure 8.2(d) is so high at $w_t = 0.1 mm$, most realizations are $\beta = \infty$. Additionally, the graphs only show from $0.2 mm$ down to $w_t = 0.1 mm$, instead of all the way down to $0.05 mm$. This is due to the large proportion of A_s values that are greater than $8042 mm^2/m$, which were not analysed.

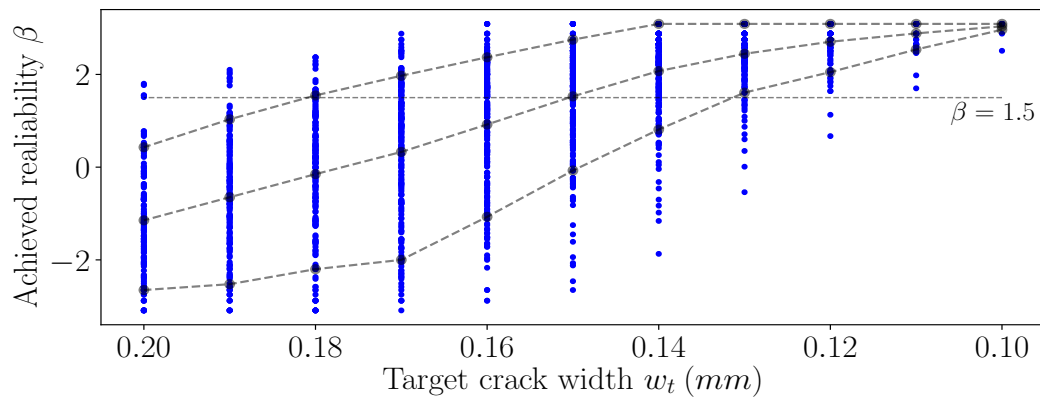
The three sets of broken lines in Figure 8.2 indicate the 10th percentile, mean value and 90th percentile, to indicate the variation in the achieved reliability for different reservoir geometries. The data can be seen to contain considerable variation, as has been common throughout this research, even when the mean reliability is above 1.5. The variation can be seen to reduce with decreasing target crack width. The $\beta = 1.5$ level is indicated to gauge at approximately which value of w_t the leakage regime attains the standard target irreversible SLS reliability.



(a) Leakage regime C_{0d7d}



(b) Leakage regime C_{3d8d}



(c) Leakage regime C_{7d14d}

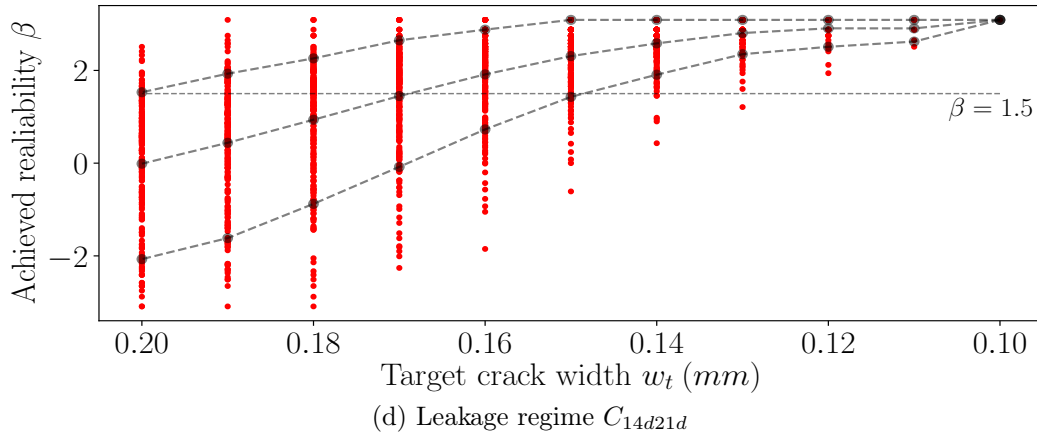


Figure 8.2: Analysis realizations of achieved reliability vs target crack width for all leakage regimes. 10^{th} percentile, mean and 90^{th} percentile shown in broken lines.

Figure 8.2 shows a clear trend of reducing w_t to achieve $\beta = 1.5$, with increasing stabilization period, as expected. The effect is most pronounced from C_{0d7d} to C_{3d8d} and diminishes with increasing stabilization period. Figure 8.3 illustrates the mean achieved reliability, β_m , for a given target crack width for each leakage regime. As each reservoir has its own value of A_s for each w_t due to the differences in applied tension force and reinforcing ratio, the mean A_s value for each target crack width (corresponding to β_m) is calculated and is shown in Figure 8.4. One can see the unreasonable amount of reinforcing ($\approx 5500 \text{ mm}^2/\text{m}$) required to achieve a β value of 1.5 for the C_{0d7d} leakage regime (no stabilization period). Almost 25% less reinforcing is required for regime C_{3d8d} . Reductions in required reinforcing of 30% and 37% are realized from regime C_{0d7d} to C_{7d14d} and C_{14d21d} , respectively. Figure 8.5 shows the mean A_s value calculated for each target crack width, showing the decreasing efficiency of reinforcing with reducing crack width.

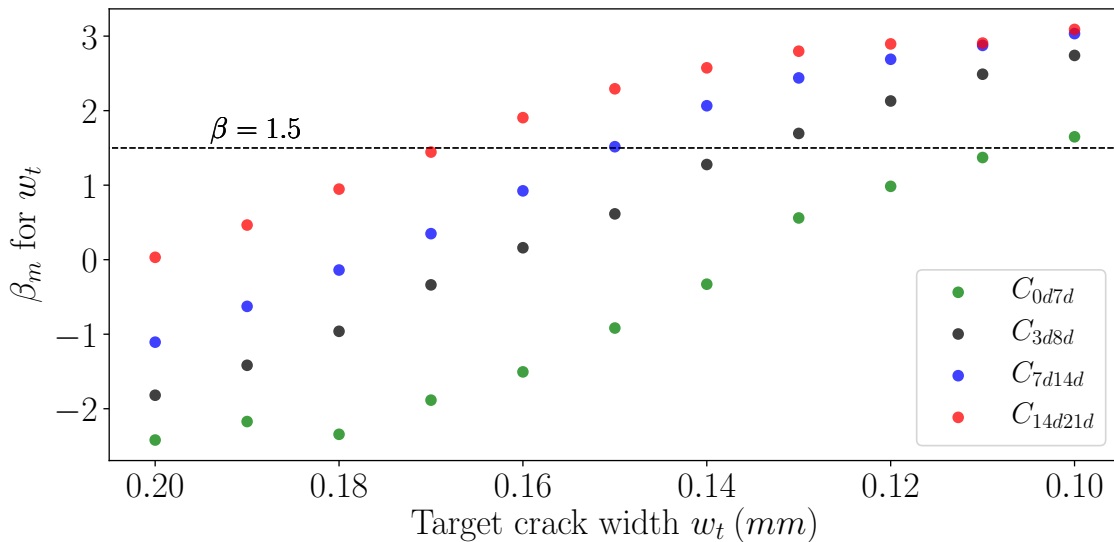


Figure 8.3: Mean achieved reliability vs target crack width for all leakage regimes.

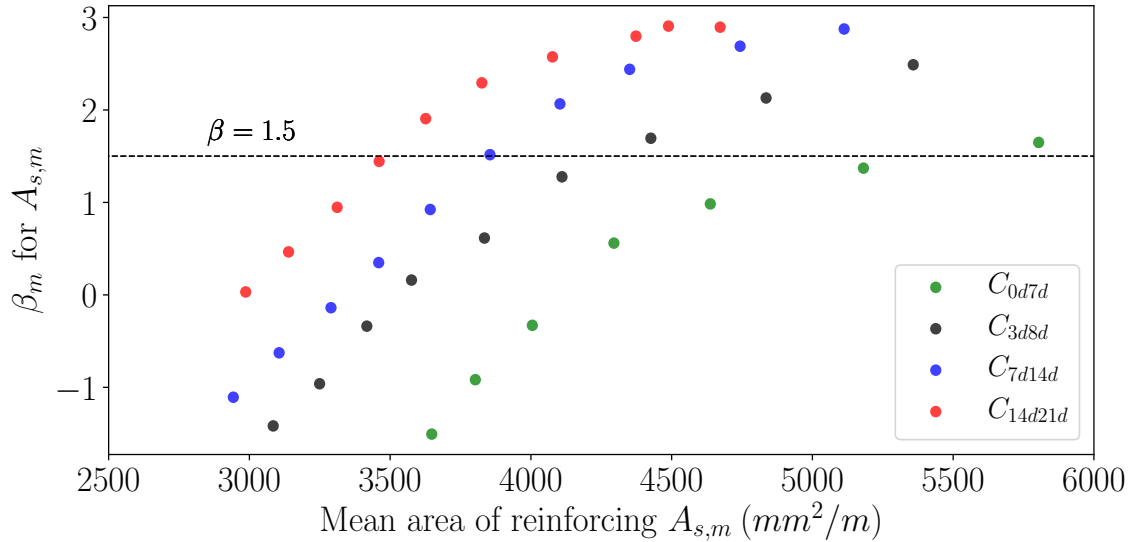


Figure 8.4: Mean achieved reliability vs area of reinforcing for all leakage regimes.

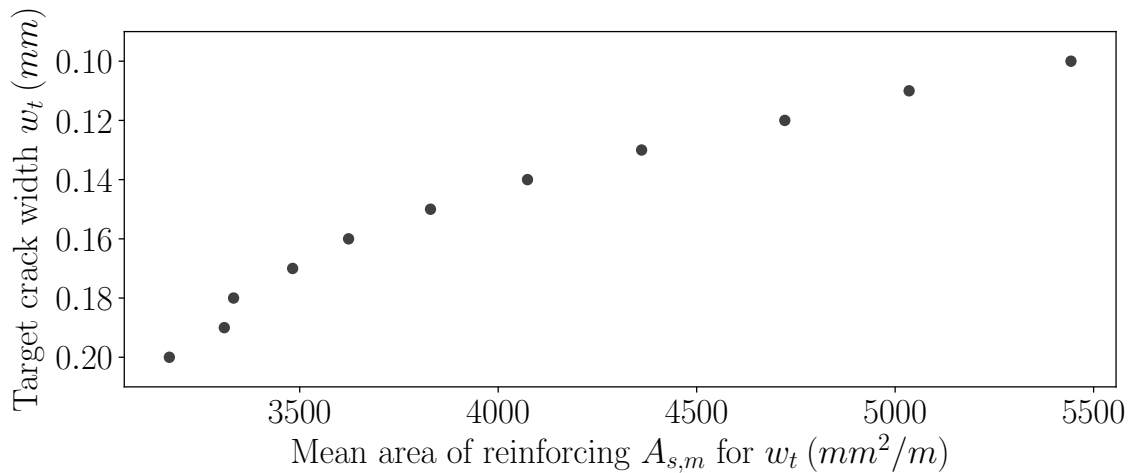


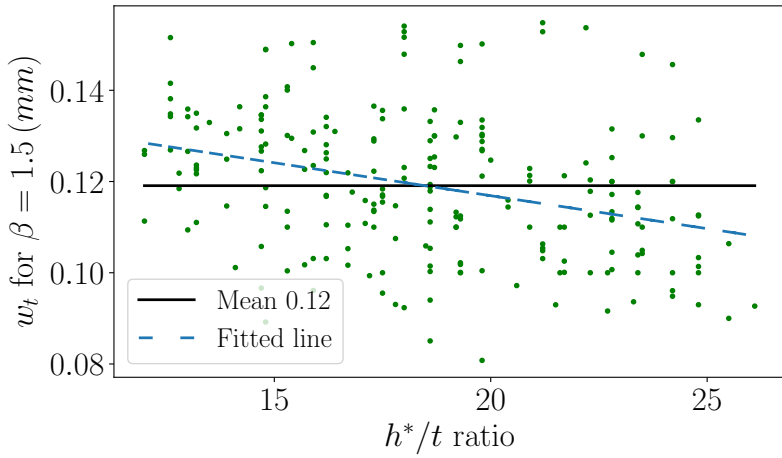
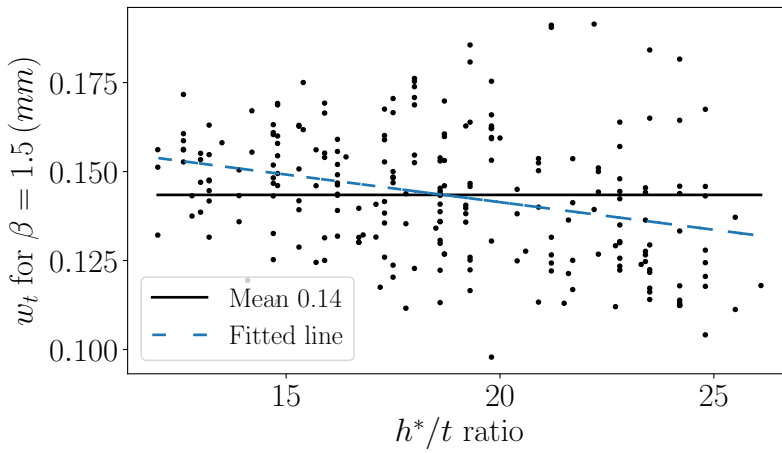
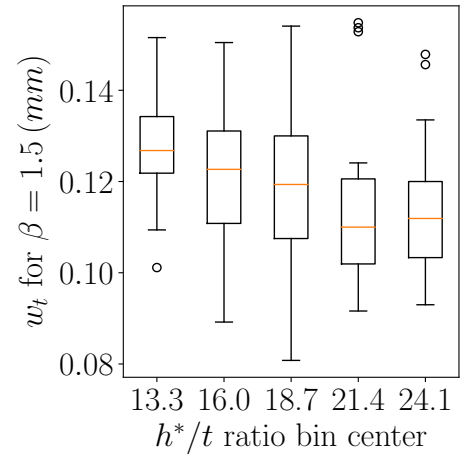
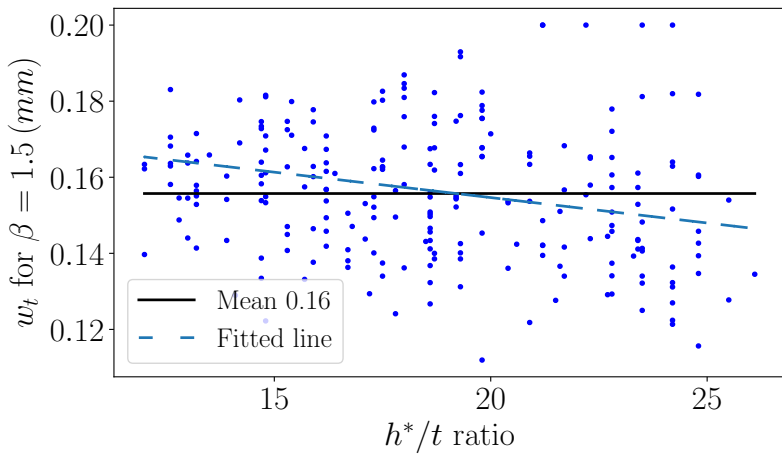
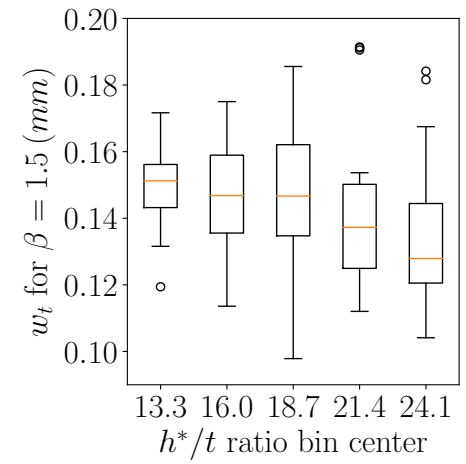
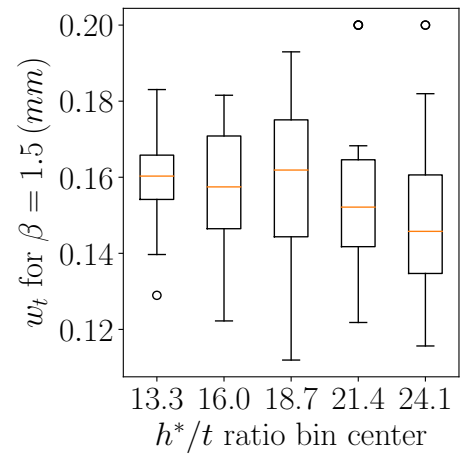
Figure 8.5: Target crack width vs mean area of reinforcing over all leakage regimes. Note that "kinks" in the graph are caused by increases in bar diameter.

8.3.3 Target crack width vs h^*/t ratio

A more detailed consideration is given to the w_t value at which the reservoirs attain a reliability level of $\beta = 1.5$. Figure 8.6 shows the w_t value at which each reservoir attains $\beta = 1.5$, plotted against the reservoir's h^*/t ratio for each leakage regime. The mean w_t value is indicated for each leakage regime, as well as a linear least-squares regression line to indicate any trends in the data with respect to the h^*/t ratio. The mean w_t values for $\beta = 1.5$ for leakage regime C_{0d7d} to C_{14d21d} are 0.12, 0.14, 0.16 and 0.17 mm, respectively.

From the fitted lines in Figure 8.6, it can be seen that there is a weak trend of linearly-decreasing w_t with increasing h^*/t ratio. The box and whisker diagrams on the right hand side of the figure group the data into 5 bins of h^*/t ratio, and further confirm the trend in the data. This trend stems from the effect that the combination of the water pressure head and wall thickness has on the self-sealing potential of the concrete. It can be seen from the trends in Figure 8.6 that the reduction in the efficiency and efficacy of self-sealing and greater resulting leakage for higher h^*/t ratios result in more

stringent w_t values required to achieve $\beta = 1.5$. The variation in w_t for $\beta = 1.5$ shown in the figures, however, overshadows the trend somewhat.

(a) Leakage regime C_{0d7d} (b) Leakage regime C_{3d8d} (c) Leakage regime C_{7d14d} 

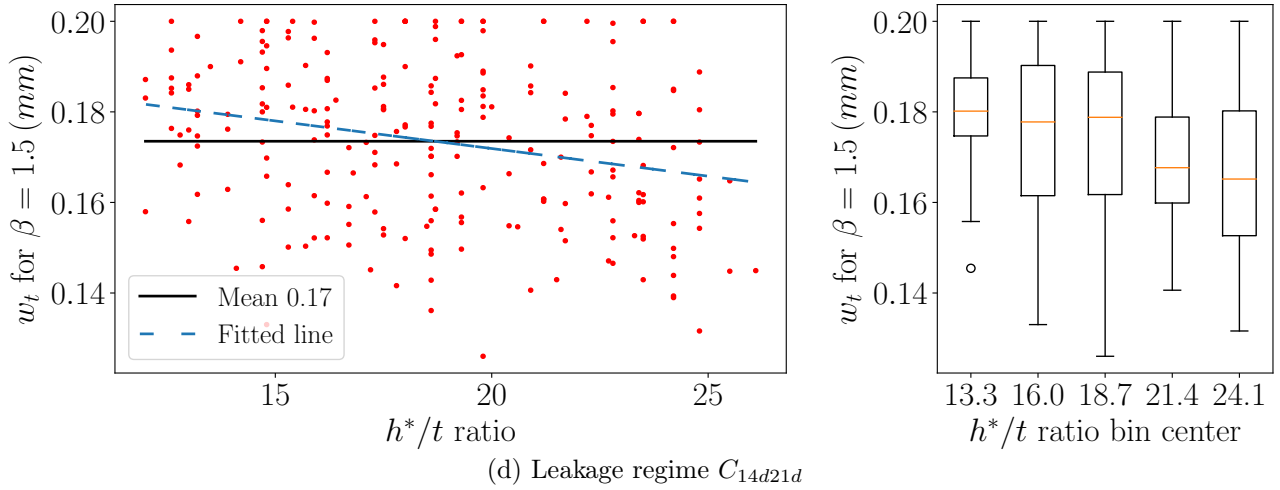


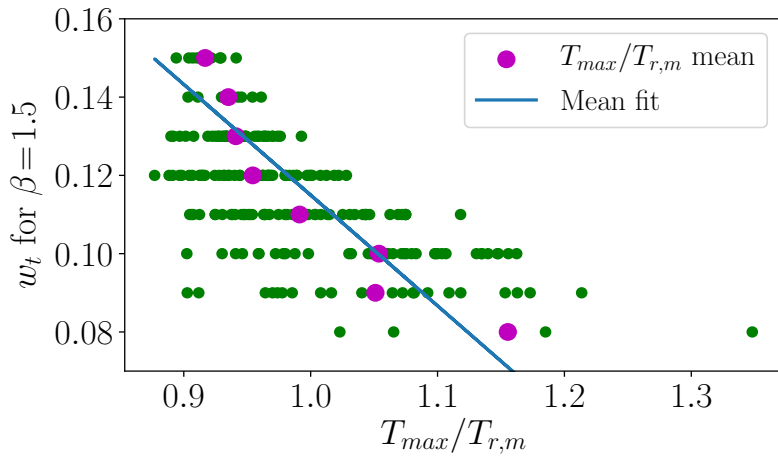
Figure 8.6: Target crack width for $\beta = 1.5$ vs h^*/t ratio for all leakage regimes. Graphs on the right show box and whisker diagrams of w_t for $\beta = 1.5$ for 5 bins of h^*/t ratio.

8.3.4 Target crack width vs $T_{max}/T_{r,m}$ ratio

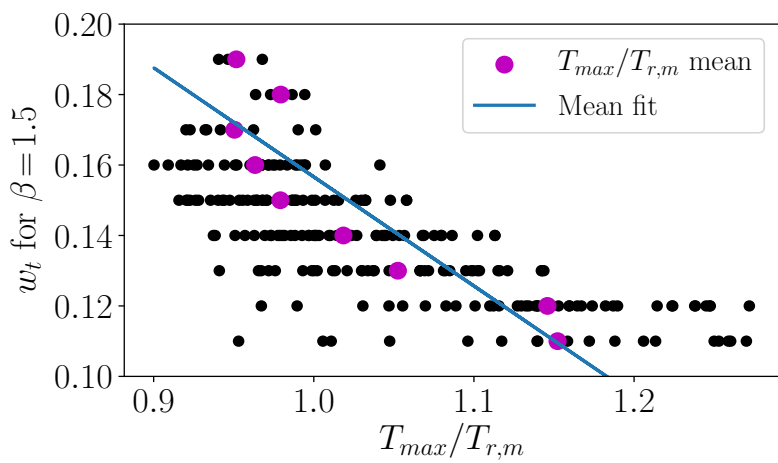
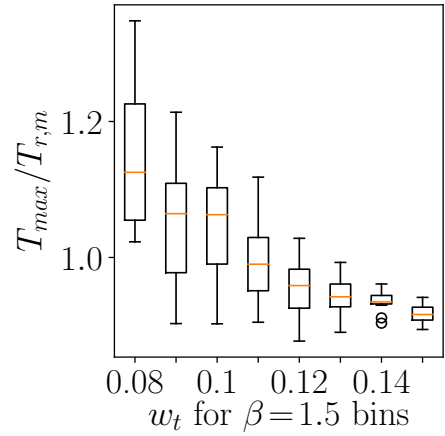
Due to the relatively weak trend in w_t for $\beta = 1.5$ with h^*/t ratio, other trends were investigated. When considering T_{max} , h , D and A_s , none of these parameters were found to have any discernible trend with w_t for $\beta = 1.5$. A trend was identified, however, between the ratio of the maximum applied hoop tension in the wall to the mean concrete tensile resistance force of the wall ($T_{max}/T_{r,m}$), and w_t value for $\beta = 1.5$.

Figure 8.7 shows this trend for all leakage regimes. It can be seen that there is a clear link between $T_{max}/T_{r,m}$ and w_t , with increasing $T_{max}/T_{r,m}$ requiring more stringent w_t values. The fit is performed to the mean value of $T_{max}/T_{r,m}$ for each w_t value (purple dots in Figure 8.7), so as to give each w_t equal weight. From the box and whisker plots on the right, the variation in $T_{max}/T_{r,m}$ with w_t is also seen to be less than the variation in w_t with h^*/t ratio. The variation reduces progressively as the $T_{max}/T_{r,m}$ ratio reduces. The trend in $T_{max}/T_{r,m}$ with w_t is based on the fact that the more the mean concrete tensile resistance exceeds the applied tensile load, the fewer cracks form. Figure 8.8 illustrates this, in that the variation in f_{ct} varies the concrete tensile resistance of the wall. In the case of $T_{max} < T_{r,m}$, a far smaller proportion of cracks form and leak than when $T_{r,m} < T_{max}$.

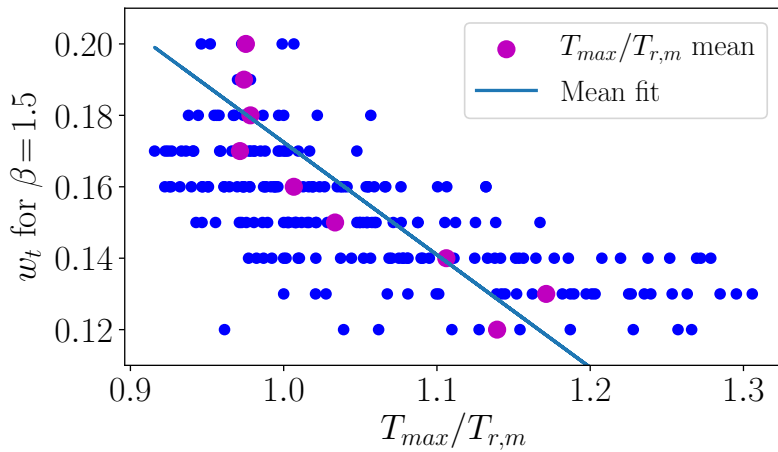
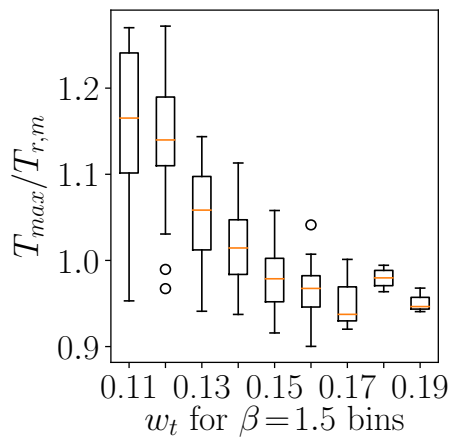
The trend appears to be mostly linear though on the left hand side graphs of Figure 8.7, the w_t mean values start to follow a different trend. The figures show that where the concrete tension resistance force exceeds the applied tension force ($T_{max}/T_{r,m} < 1$), the target crack width reduces quickly for small reductions in $T_{max}/T_{r,m}$ ratio. The trend could not be investigated lower than $T_{max}/T_{r,m} < \approx 0.925$, however, as this ventures into the crack formation phase. The presence of the trend in quickly-reducing w_t for $T_{max}/T_{r,m} < 1$ may be an indication that as reservoirs tend towards the crack formation phase, the requirements for target crack width become exponentially less stringent. This, however, requires further research to confirm. In WRS, increasing the amount of reinforcing is typically thought to be more cost-effective at reducing crack widths than increasing the concrete wall thickness. This identified trend indicates that a small increase in wall thickness and concrete cost to increase $T_{r,m}$ could be more effective at increasing the achieved reliability, than increasing the area of reinforcing, in some cases. This optimization of reliability, based on cost of reinforcing vs cost of concrete is left to future research.



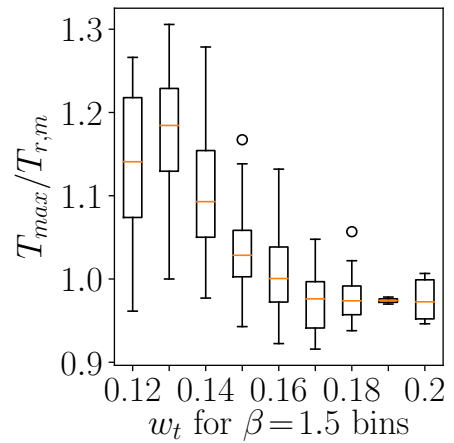
(a) Leakage regime C_{0d7d}



(b) Leakage regime C_{3d8d}



(c) Leakage regime C_{7d14d}



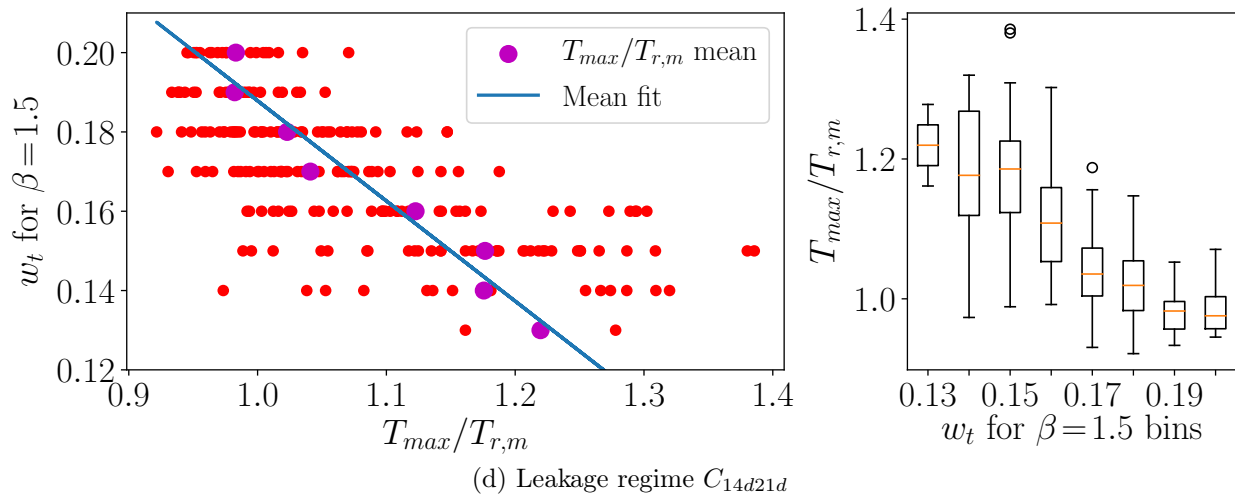
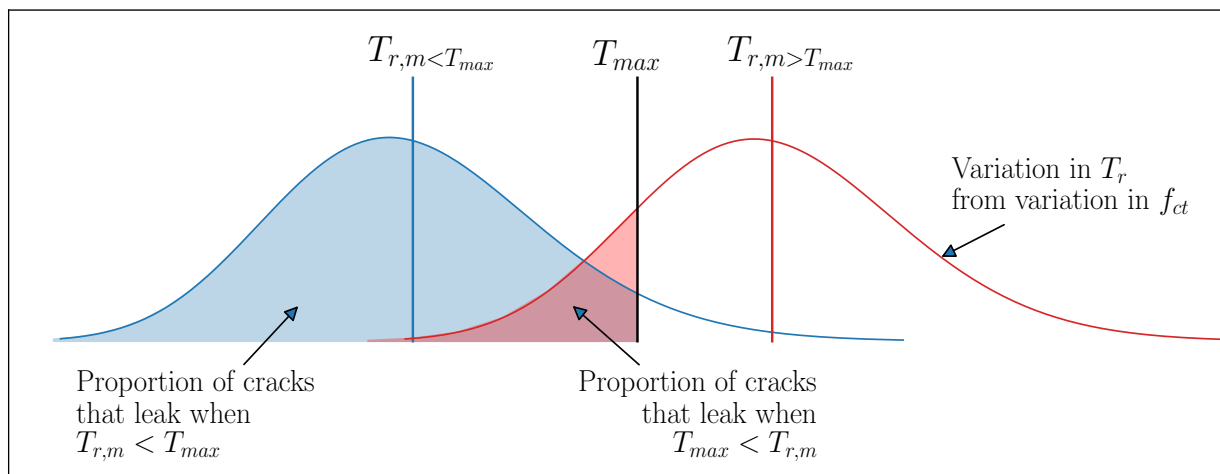


Figure 8.7: Target crack width for $\beta = 1.5$ vs $T_{max}/T_{r,m}$ ratio for all leakage regimes.



Tension force and resistance (kN)

Figure 8.8: Illustration of how mean concrete tensile resistance affects the proportion of cracks that form and leak.

8.4 Discussion

8.4.1 Comparison of results of w_t with h^*/t , with EN 1992-3 and MC 2010

While they have the same practical aim, the outcomes of this research with regard to changes in w_t with h^*/t ratio, and the EN 1992-3 recommendations (based on Edvardsen (1996)) are fundamentally different. The EN 1992-3 recommendations consider self-sealing in tension-cracked concrete and use it as the basis with which to prescribe w_t values based on the probability of self-sealing, but it does not consider the quantum of leakage during the sealing period. It gives w_t values for a tension crack that will completely self-seal in 4-10 weeks with a 90% probability of non exceedance ($\beta=1.28$), on a single crack level. This research on the other hand, considers the effect of self-sealing, but also takes into account the leakage that a reservoir experiences. The findings of this research give w_t values that are given to ensure that unacceptable leakage does not occur in a reservoir at the end of the SLS water tightness test, with a non exceedance probability of 93.4% ($\beta=1.5$). Regardless, each provide a useful

perspective on designing reservoirs that do not leak unacceptably and as such, they are compared to one another.

Figure 8.9 shows the trends in w_t for $\beta_m = 1.5$ from the fits in Figure 8.6 and compares them to the recommendations in EN 1992-3. One can see that in the EN 1992-3 recommendations, w_t decreases more sharply with h^*/d ratio than it does in this research. This is due to the difference between the aim of achieving complete self-sealing within 4-10 weeks for a single, isolated crack, vs the aim of achieving acceptable leakage for the water tightness test (≤ 3 weeks) for an entire reservoir of cracks. It is sensible that the requirement for complete self-sealing on a single crack level is more sensitive to the water pressure head, and thus h^*/t ratio, than it is on reservoir-level for the consideration of acceptable leakage. On a single crack level, more stringent target crack widths are therefore required than for achieving acceptable leakage on a reservoir level (where a small amount of residual leakage after the end of the test is deemed to be acceptable). Thus considering SLS reliability from the perspective of allowable leakage, it is seen that the EN 1992-3 recommendations of w_t with h^*/t ratio for stabilized cracking are more conservative for three of the four leakage regimes. The EN 1992-3 recommendations prescribe values of w_t that are more stringent, and thus consistently obtain values of $1.5 < \beta$ if evaluated from a total leakage perspective, with reference to Figures 8.9 and 8.3 and later in Table 8.4. The exception to this is for a band of lower h^*/t ratios with leakage regime C_{0d7d} , which is not likely to be specified in practice.

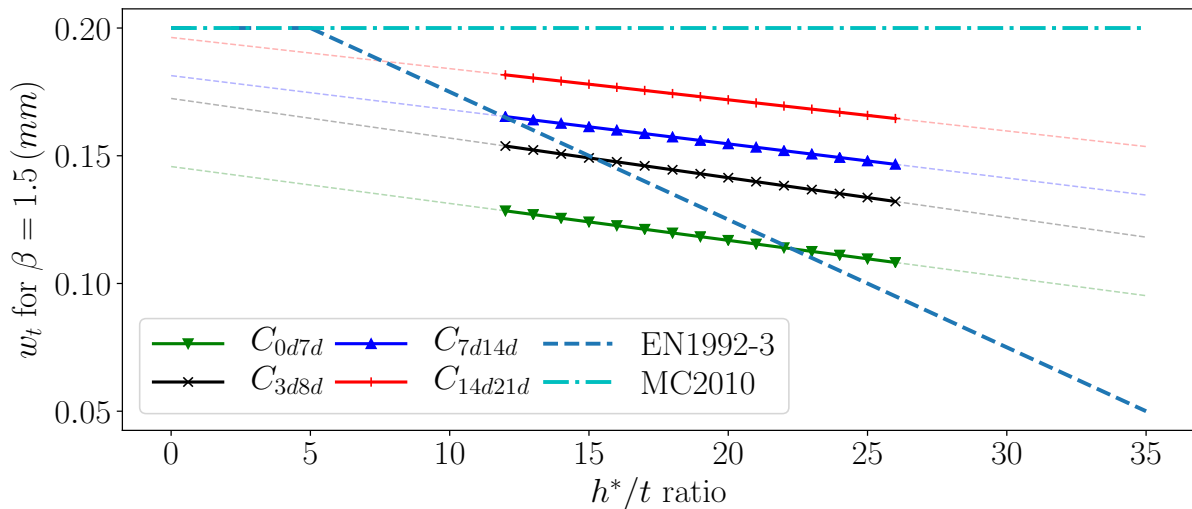


Figure 8.9: Comparison of recommended target crack width for $\beta = 1.5$ vs h^*/t for $12 \leq h^*/t < 27$ from this research with EN 1992-3 and MC 2010.

As the hydraulic ratio could only be varied from $h^*/t \approx 12 \rightarrow 26$, due to the stabilized cracking requirement in this research, the entire h^*/t range of EN 1992-3 could not be analysed. The range of reservoirs where $h^*/t < 12$ are almost exclusively in the crack formation stage, as the lower h values in combination with reasonable values of diameter ($D \leq 40$), do not develop enough applied tension force to exceed the concrete tensile resistance. As such, the trends in w_t are not likely to continue in the same linear trend for $h^*/t < 12$. As progressively fewer cracks form and leak as reservoirs tend towards being uncracked, it is likely that the w_t values will increase more sharply with decreasing h^*/t ratio, than if the linear trend were extended for $h^*/t < 12$ in Figure 8.9 (decreasing-stringency in requirement of crack width). At a point, minimum reinforcing will begin to govern the design and the specification of crack widths is no longer an appropriate design measure. For $h^*/t < 12$, Edvardsen's recommendations may be more appropriate. The consideration of reservoir behaviour in the crack formation stage is out of the scope of this research however, and should be considered in future research. Although they

are unlikely to occur due to the impractical combinations of h and D required, reservoirs in the range of $26 < h^*/t \leq 35$ will increasingly be in the stabilized cracking stage. As such, the linear trend of decreasing w_t with increasing h^*/t ratio is likely to follow the same trend as for the analysed range.

Table 8.3 shows the numeric ranges and values for recommended w_t values for each leakage regime. It also gives equations by which w_t values can be obtained for intermediate values of h^*/t . Consider the trend lines of the analysed h^*/t range in this research and the extensions of these, either side of the analysed h^*/t range in Figure 8.9. The EN 1992-3 recommendations would be less stringent for $h^*/t < 8$ and would be more or less stringent than the recommendations from this research for $8 < h^*/t < 15$, depending on the chosen leakage regime. For $15 < h^*/t$, the recommendations are less stringent than those from EN 1992-3, for all classes except leakage regime C_{0d7d} . From Figure 8.9, the EN 1992-3 recommendations are shown to be more conservative for stabilized cracking stage ($12 \leq h^*/t$) for the more likely-to-be-specified leakage regimes (C_{3d8d} to C_{14d21d}).

The limit of $w_t = 0.2 \text{ mm}$ in MC 2010 is given for "cracks that self-seal" and does not consider the effect of the h^*/t ratio. Neither does it consider any probabilistic measure of self-sealing. This limit is given based on satisfactory performance over time, and is assumed to achieve $\beta = 1.5$, but has not been proven. From Table 8.4, the MC 2010 requirements are shown to be inadequate to obtain $\beta = 1.5$ for tension cracking in reservoirs in the stabilized cracking stage, for any of the leakage regimes considered.

Table 8.3: Summary and comparison of recommendations of target crack width for round reservoirs in the stabilized cracking stage, from this research, EN 1992-3 and MC 2010.

Leak. regime	Stab. period	W.t test beg./end	h^*/t range	w_t (mm)	w_t (mm) interp. [†]	Basis
This research - Allowable leakage: 0.2% of reservoir volume						
C_{0d7d}	0	0 / 7	12 → 26	0.13 → 0.11	$0.145 - 0.05 \cdot \frac{x}{35}$	$\beta_m = 1.5$ for w.t. test
C_{3d8d}	3	3 / 8	12 → 26	0.155 → 0.13	$0.17 - 0.05 \cdot \frac{x}{35}$	$\beta_m = 1.5$ for w.t. test
C_{7d14d}	7	7 / 14	12 → 26	0.165 → 0.145	$0.18 - 0.045 \cdot \frac{x}{35}$	$\beta_m = 1.5$ for w.t. test
C_{14d21d}	14	14 / 21	12 → 26	0.18 → 0.165	$0.2 - 0.045 \cdot \frac{x}{35}$	$\beta_m = 1.5$ for w.t. test
EN 1992-3 - No water tightness test criteria given						
None prescribed			0 → 5	0.20	N/A	$\beta = 1.28$ for cracks to self-seal in 4-10 weeks
None prescribed			5 → 35	0.20 → 0.05	$0.2 - 0.15 \cdot \frac{x-5}{30}$	
None prescribed			35 <	0.05	N/A	
MC 2010 - No water tightness test criteria given						
None prescribed			Any	0.20	N/A	General irreversible $\beta_{SLS} = 1.5$

[†]For interpolation; x refers to the desired h^*/t ratio. w.t - water tightness Stabilization period and w.t. test beginning/end given in days.

Figure 8.10 shows the distribution of the achieved β values for all analysed reservoirs, using the target crack widths recommended by EN 1992-3, MC 2010 and from this research. Table 8.4 gives the mean and standard deviation of each recommendation for each leakage regime. From Figure 8.10, it can be seen that the recommendations of w_t as a function of h^*/t ratio from this research achieve a value of $\beta = 1.5$ (broken lines) most consistently, with the least variation. Due to the "resolution" of β value

of the analyses ($-3.1 < \beta < 3.1$), the EN 1992-3 results give an impression of low standard deviation, however, this is only because many realizations achieve the "ceiling" β value of 3.1. If a greater number of analysis simulations were run, a better approximation of the true mean and standard deviation would be obtained but this is outside of the scope of this research. The results from Table 8.4 confirm that the EN 1992-3 recommendations achieve $1.5 \leq \beta$ for all leakage regimes except C_{0d7d} . It shows that the β values are considerably higher than the required $\beta = 1.5$ for C_{7d14d} and C_{14d21d} . It also confirms that the MC 2010 target crack width of $w_t = 0.2 \text{ mm}$ is inadequate to achieve $1.5 \leq \beta$ for any of the leakage regimes.

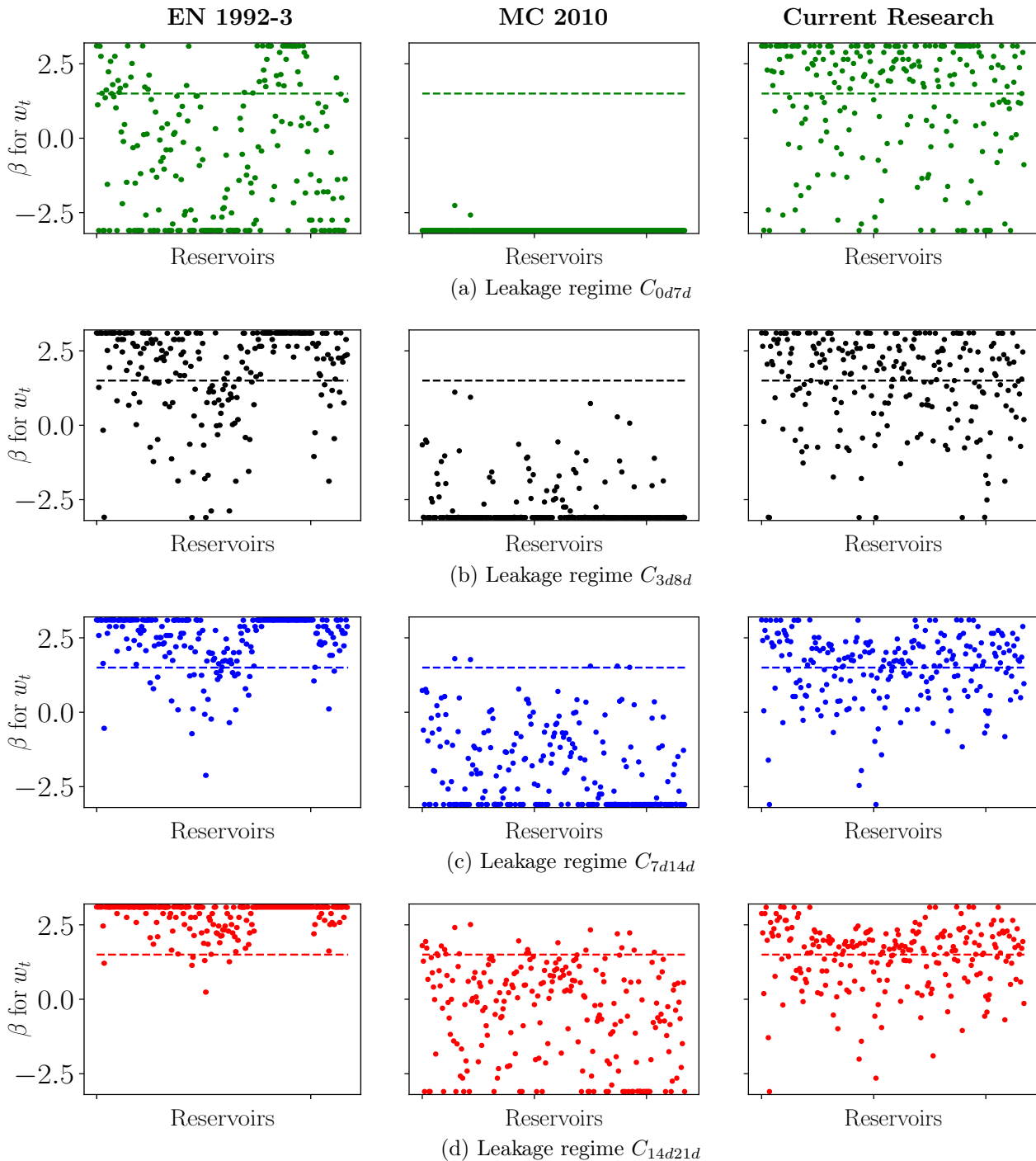


Figure 8.10: Distribution of β achieved for the w_t recommendations from EN 1992-3, MC 2010 and from this research for h^*/t ratio, if applicable, for each reservoir analysed.

Table 8.4: Achieved reliability for SLS leakage and stabilized cracking using the target crack width recommendations of EN 1992-3, MC 2010 and this research for h^*/t ratio, if applicable.

Source	Property	Leakage regime			
		C_{0d7d}	C_{3d8d}	C_{7d14d}	C_{14d21d}
EN 1992-3	Mean β	-0.65	1.93	2.45	2.84
	Std. dev.	2.23	1.47	0.90	0.48
MC 2010	Mean	-3.09	-2.75	-1.91	-0.46
	Std. dev.	0.06	0.79	1.33	1.63
Current Research	Mean	1.25	1.49	1.51	1.45
	Std. dev.	2.00	1.51	1.15	1.08

8.4.2 Proposal of target crack width vs $T_{max}/T_{r,m}$ ratio

The proposal of w_t based on $T_{max}/T_{r,m}$ ratio is indirectly linked to the h^*/t ratio. Practical reservoirs with high $T_{max}/T_{r,m}$ ratios will also have higher h^*/t ratios. The maximum applied hoop tension force, T_{max} , is strongly influenced by the h of the reservoir and thus higher h values result in reservoirs where T_{max} is high. Thus, reservoirs with higher h^*/t ratios generally have a greater probability of having higher $T_{max}/T_{r,m}$ ratios, too. Thus, the prescription of w_t based on $T_{max}/T_{r,m}$ ratio to achieve $\beta=1.5$ in this research simultaneously considers the effect of the h^*/t ratio on the extent and efficiency of self-sealing, as well as the quantum of leakage. Table 8.5 and Figure 8.11 give and illustrate these recommendations, respectively.

Table 8.5: Recommendations of target crack width for $\beta=1.5$ as a function of $T_{max}/T_{r,m}$ ratio.

Leak. regime	Stab. period	W.t test beg./end	$T_{max}/T_{r,m}$ range	w_t (mm)	w_t (mm) interp [†]
C_{0d7d}	0	0 / 7	0.925 → 1.25	0.135 → 0.05	$0.135 - 0.262 \cdot (x - 0.925)$
C_{3d8d}	3	3 / 8	0.925 → 1.25	0.180 → 0.08	$0.18 - 0.308 \cdot (x - 0.925)$
C_{7d14d}	7	7 / 14	0.925 → 1.25	0.190 → 0.10	$0.19 - 0.277 \cdot (x - 0.925)$
C_{14d21d}	14	14 / 21	0.925 → 1.25	0.200 → 0.13	$0.2 - 0.215 \cdot (x - 0.925)$

[†]For interpolation; x refers to the desired $T_{max}/T_{r,m}$ ratio. w.t - water tightness
Stabilization period and w.t. test beginning/end given in days.

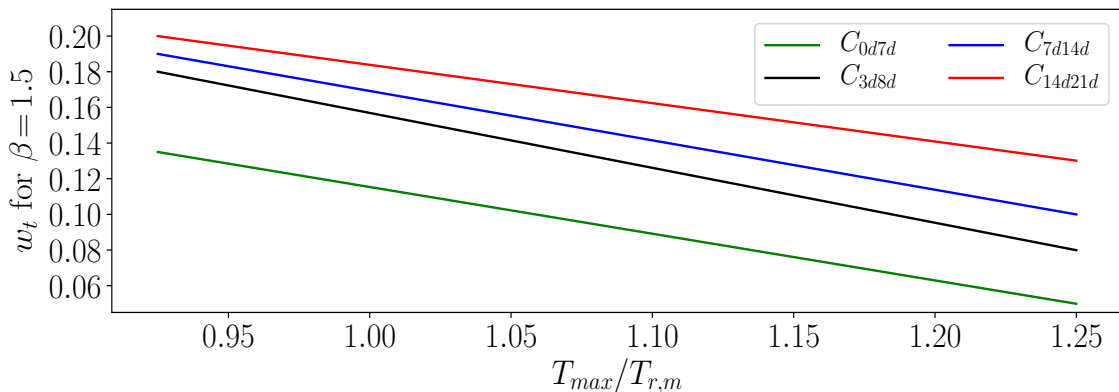
Figure 8.11: Recommended target crack width for $\beta = 1.5$ vs $T_{max}/T_{r,m}$ for the stabilized cracking stage and $12 \leq h^*/t \leq 26$.

Figure 8.12 shows the distribution of the achieved β values for all analysed reservoirs, using the recommendations of w_t as a function of $T_{max}/T_{r,m}$. Table 8.6 gives the mean and standard deviation of the achieved β value for each leakage regime. When compared to Figure 8.10 and Table 8.4, it is clear that the recommendations of w_t based on $T_{max}/T_{r,m}$ more consistently achieve β values near to 1.5, with less variation than any of the recommendations of w_t as a function of h^*/t ratio.

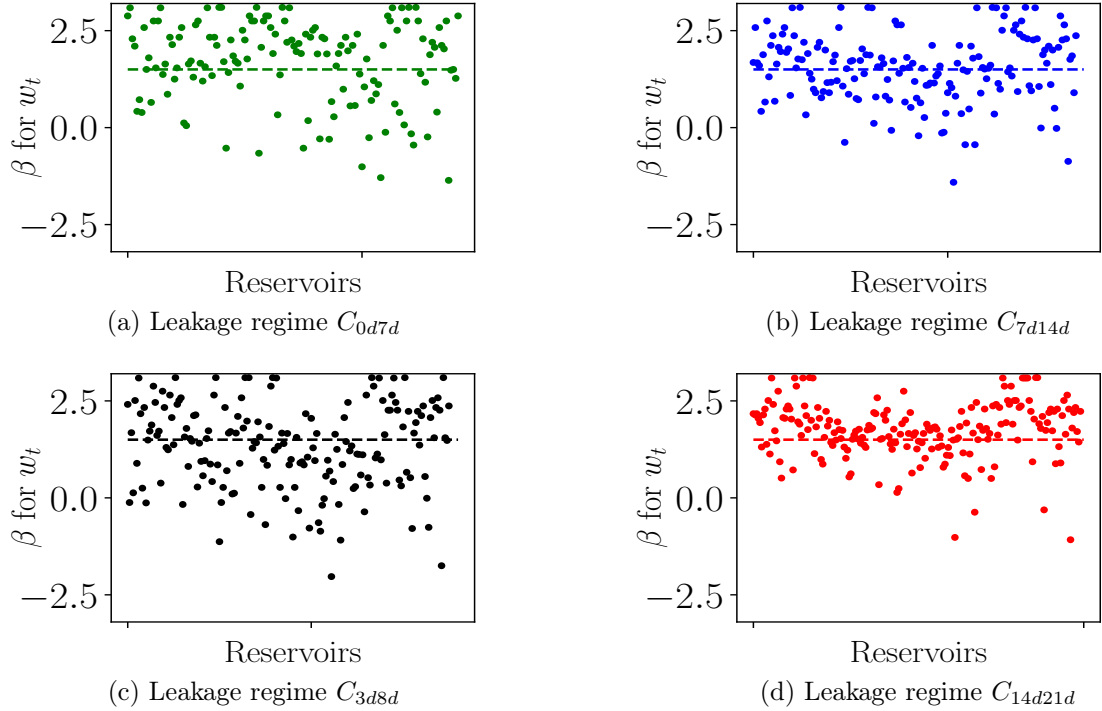


Figure 8.12: Distribution of achieved β , based on recommendations of w_t as a function of $T_{max}/T_{r,m}$ from this research.

Table 8.6: Achieved reliability for SLS leakage and stabilized cracking using the proposed recommendations of w_t as a function of the $T_{max}/T_{r,m}$ ratio from this research.

Source	Property	Leakage regime			
		C_{0d7d}	C_{3d8d}	C_{7d14d}	C_{14d21d}
Current Research	Mean β	1.70	1.32	1.53	1.75
	Std. dev.	1.07	1.09	0.88	0.72

The recommendations of w_t with h^*/t and w_t with $T_{max}/T_{r,m}$ are both given for a target reliability of $\beta = 1.5$. Though, the recommendations of w_t with $T_{max}/T_{r,m}$ are seen to result in less variation in achieved β and should result in an achieved reliability closer to the target reliability more consistently than the alternative. The specification of w_t for $T_{max}/T_{r,m}$ does, however, require an iterative process. An initial value of A_s is specified, after which $T_{r,m}$, T_{max} and the achieved crack width are calculated. The ratio and achieved crack width are then compared to Figure 8.11. If unsatisfactory, A_s is increased, which increases $T_{r,m}$, and the process is repeated until the achieved crack width is below the target crack width from Figure 8.11.

Finally, the recommendations of w_t in this research are clear and are formulated to be "designer-friendly". The given w_t values are specific to set leakage regimes and give a simple, unambiguous,

quantitative means of determining whether the leakage through the reservoir is within the maximum allowable leakage or not. The set stabilization periods and water tightness test durations are clearly laid out with associated w_t values, which gives designers structured choice. This enables the designer to choose between a shorter stabilization period and water tightness test combined with a more stringent target crack width, or a longer stabilization period and water tightness test combined with a less stringent target crack width. This allows the designer the flexibility to potentially save on construction overhead costs and avoid delay penalties at the expense of greater reinforcing costs, or vice versa, depending on the scale and specific costs of the project. The full recommendation from this research is given in Appendix E.

8.4.3 Discussion of implications of analysis assumptions & potential "disconnects" with practice

In the development of the analyses, assumptions were made to simplify the model to a point where meaningful output was attainable. Some of these assumptions will, however, affect the validity of the recommendations and are discussed here. Additionally, the qualitative satisfactory performance over time in reservoirs in practice, given by the crack width limits of $w_t = 0.2 \text{ mm}$ in BS 8007 and MC 2010 cannot be ignored. This fact has led to the disillusionment of practising engineers with the notably-more-stringent EN 1992-3 recommendations of target crack widths, based on h^*/t (h_D/h) ratios. This section thus also serves to comment on potential "disconnects" between the theoretical probabilistic analysis of this research and the realization of the perceived satisfactory, or near-satisfactory, performance of target crack widths of $w_t = 0.2 \text{ mm}$ in practice.

Wall-base connection fixity

The fixity between the reservoir wall and base in round reservoirs is most commonly considered pinned when considering the design of the reinforcing for hoop tension. In reality though, the fixity is somewhere in between fixed and pinned. It will never be truly fixed, as the quantity and complexity of reinforcing required to ensure a fixed connection is difficult to achieve. Additionally, the combination of wall foundation and underlying material are not typically stiff enough to provide enough restraint against rotation to be considered fixed. It will not be entirely pinned either, as the thickness of the concrete wall section and the vertical reinforcing bars that extend up from the foundation will certainly provide some restraint against moment and rotation. Figure 8.13 shows the applied hoop tension as a function of the distance down the height of the wall for two h^2/Dt ratios on the outer parts of the range of analysed reservoirs.

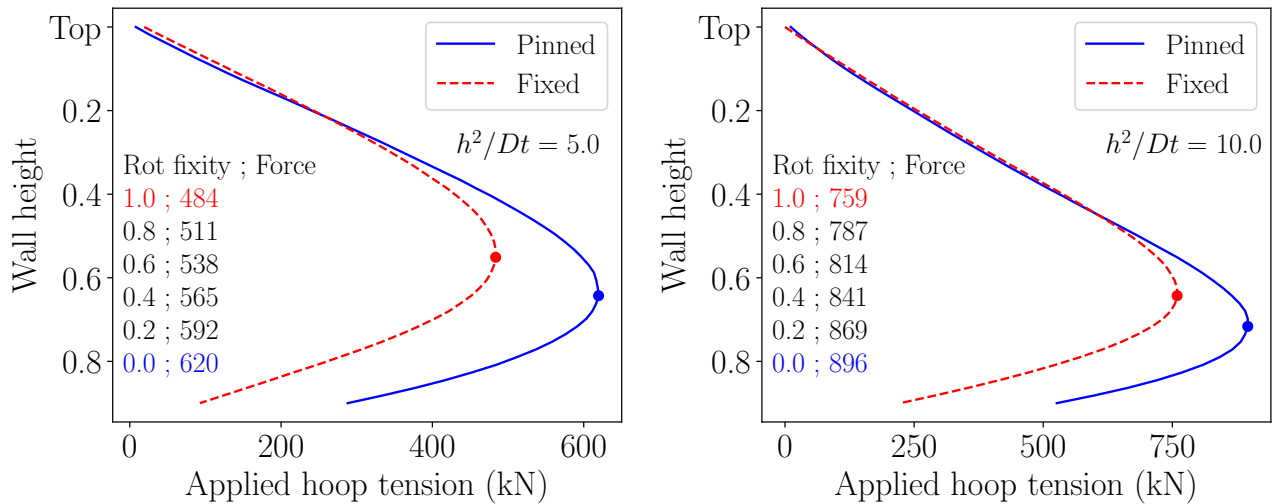


Figure 8.13: Illustration of the effect of wall-base connection fixity on the resulting maximum hoop tension force.

The maximum applied hoop tension, T_{max} , is shown by the red and blue dots and colour-coded to correspond to the rotational fixity, on the left of each graph in Figure 8.13. The wall-base rotational fixity is given as a fraction, with 1 indicating a fixed condition and 0 indicating a pinned condition. The T_{max} value varies from $\approx 10-25\%$ between the fixed and pinned conditions, depending on the h^2/Dt ratio. As such, when a pinned condition is assumed in design, T_{max} is generally over-estimated, which will lead to more reinforcing being specified than is actually required to achieve the target crack width. Additionally, the actual position of T_{max} is slightly higher up along the wall than if it were completely pinned; the actual h^* is thus lower than if it were completely pinned. The design h^*/t ratio will thus be higher than it actually is, also leading to a more stringent target crack width. As such, some conservatism is introduced as a result of the typical assumption that the wall-base connection as pinned.

Choice of reinforcing quantity and spacing

In this research, the exact area of reinforcing required for the target crack width was used in the probabilistic analysis. In a design situation, however, the area of reinforcing specified is constrained by the available reinforcing bar diameters and bar spacings. The centre-to-centre spacing of reinforcing bars generally varies in increments of 25 mm . The table in Appendix C shows the reinforcing areas based on the bar diameters commercially available in Britain and South Africa and the centre to centre (c/c) spacing. As the reinforcing spacing affects the spacing and width of the cracks, smaller spacings and bar diameters are preferred in reservoirs. Spacings smaller than 100 mm tend to lead to steel congestion and thus, spacings typically range between 100 and 200 mm c/c . When an area of reinforcing is specified to achieve a target crack width, a designer will need to choose a combination of bar diameter and spacing that is above, but as close to the required area as possible to avoid excess reinforcing. For smaller reinforcing quantities, achieving this is easy with little excess but for larger quantities ($2500\text{ mm}^2/\text{m} < A_s$), it becomes more difficult and typically, more reinforcing is specified than is required. The realised crack widths will therefore actually be below the target crack widths.

A simple analysis of this was performed to investigate what quantum of excess reinforcing may occur. In this analysis, one thousand random required reinforcing areas were sampled from a uniform distribution with bounds of $2500-5500\text{ mm}^2/\text{m}$ and the nearest, but greater than, area of reinforcing was obtained from the available bar diameters and spacings, as detailed above. From this an excess reinforcing

factor was obtained, defined as the reinforcing selected over the reinforcing required. The analysis indicated that the mean selected area of reinforcing was ≈ 1.07 times the required area. As such, the potential over-specification of reinforcing will increase the $T_{r,m}$ of the concrete and also add a measure of conservatism to the recommendations of target crack width.

Presence of roof and/or backfill

The analysis assumes that either no roof is present, or if there is a roof, that it is not structurally connected to the wall and does not provide restraint to the wall. Roofs are most often simply supported by bearing pads on the walls, so that the roof is free to elongate or contract when temperature differentials occur. Occasionally, the roof is pin-connected to the walls through lower-yield reinforcing bars that are able to withstand the dynamic, fatigue-inducing axial contraction and elongation in the roof. In a case where the roof is connected to the wall by reinforcing, the applied hoop tension in the wall will be lower than assumed in the analysis in this research and this will also add an element of conservatism. The analyses assume that no soil is backfilled before the end of the water tightness test. If backfill is placed around the reservoir walls after the water tightness test is finished, the soil pressure will serve to add a compression force that counteracts the applied tension force on the walls to a degree. This will reduce crack widths, thereby introducing conservatism in the long term leakage performance, however, the long-term is not considered in the recommendations.

Dynamic cracks

The analysis only considers self-sealing in static cracks, which is acceptable for the purposes of determining the reliability of the reservoir at the water tightness test. After the water tightness test, the water level will fluctuate with time and the cracks that have not completely sealed will take on a dynamic nature, which will reduce the effectiveness of the self-sealing. Thus, the long-term behaviour of the reservoir is not considered in the recommendations of this research. It is, however, reasonable to assume from the results in this research, that the remaining leakage through cracks after the water tightness test will not be noteworthy and thus will not contribute notable leakage after the water tightness test. This can be seen from the *Leakage fraction* column in Tables 5.5 to 5.7. After the water tightness test for C_{0d7d} ($w_t < 0.15$, for all h^*/t as per recommendations - see Figure 8.9), 93% of the total leakage has already transpired by 7 days. Similarly for the other regimes; all are above $\approx 90\%$ of the total leakage by the end of the water tightness test.

Time to fill reservoir

Another small consideration is the time that it takes to fill the reservoir, with respect to the days' worth of stabilization time. Reservoirs are filled at a maximum of 2 m of water height per day, which means that some of the cracks that form will have more of a stabilization period than is actually specified. This can also contribute to conservatism of the recommended target crack widths.

Interpretation of h^*/t (h_D/h) ratio

The implementation of the h^*/t ratio from EN 1992-3 is often misunderstood in round reservoirs. Many understand it to mean the total head of water in the reservoir divided by the wall thickness, which is not correct. In the case of *rectangular* reservoirs with cantilevered retaining wall action, the maximum moment is at the base. The most likely point of cracking is thus at the base of the wall and the assumption of h^* as the height of the wall is correct. In *round* reservoirs, however, this is not the case, as the position of h^* is not at the base but rather a distance up the wall.

The derivation of the w_t values that vary with h^*/t ratio by Edvardsen (1996) were based on self-sealing in tension-cracked concrete samples with a specific water pressure head acting on the crack (as discussed in chapters 4 and 5). In a reservoir, the water pressure head translates to the height of water *above the position where cracks occur*. Cracks are most likely to occur where the applied hoop tension is at a maximum and not at the base of the reservoir wall. The height of water above T_{max} is h^* . The hydraulic ratio is thus defined as the water pressure head above the position of cracks, divided by the wall thickness, h^*/t .

Two example reservoirs are shown in Table 8.7. Example 1 (bigger than average) gives a misunderstood h^*/t ratio of $8/0.25 = 32$, which constitutes $w_t = 0.06 \text{ mm}$, according to EN 1992-3. In reality, however, a reservoir with these dimensions experiences T_{max} at $\approx 0.72h$ down from the top of the wall (where cracks are most likely to form), giving $h^* = 5.7 \text{ m}$ and $h^*/t = 22.4$, which gives $w_t = 0.11 \text{ mm}$. The difference in reinforcing required for $w_t = 0.06$ and $w_t = 0.11 \text{ mm}$ is considerable. Example 2 shows a smaller reservoir and shows a similar, notable difference.

Table 8.7: Examples of correct and incorrect interpretation of h^*/t (h_D/h) ratio.

Example reservoir 1				Example reservoir 2			
D	25	Incorrect h^*/t	32	D	20	Incorrect h^*/t	25
h	8	Correct h^*/t	23.04	h	5	Correct h^*/t	16.5
t	0.25	Incorrect w_t	0.06	t	0.2	Incorrect w_t	0.1
h^2/Dt ratio	10.24	Correct w_t	0.11	h^2/Dt ratio	6.25	Correct w_t	0.15
T_{max} height (h^*)	0.72h			T_{max} height (h^*)	0.66h		

Considering this, if used incorrectly, the EN 1992-3 recommendations lead to excess reinforcing requirements which will cause the validity thereof to be doubted by practising engineers. A correct interpretation of the h^*/t ratio is imperative to the correct use of the recommendations of both EN 1992-3 and this research, as well as to reinforce confidence in the need for consideration of the h^*/t ratio altogether. A table of h^* values are therefore given, as a function of h^2/Dt ratio in Appendix D, in order to facilitate the correct use of h^*/t ratio and associated w_t value from the recommendations of this research. The use of the $T_{max}/T_{r,m}$ recommendations would avoid this incorrect interpretation altogether.

Assumption of stabilized cracking

In this research, it was noted that the vast majority of round reservoirs do not enter the stabilized cracking stage at the maximum applied hoop tension. The design crack width equations in EN 1992-3 and MC 2010 both assume a state of stabilized cracking in terms of the strain difference and crack spacing equations. In the case of stabilized cracking, the applied tension is greater than the concrete tensile resistance on average, whereas in the crack formation stage, the applied tension is less than the concrete tensile resistance (with reference to Figure 6.6). As such, in the crack formation stage, a greater proportion of the cracks will not actually form and will thus not leak. The use of stabilized cracking theory for reservoirs in the crack formation stage is thus also a source of conservatism that will affect the vast majority of reservoirs designed according to EN 1992-3 and MC 2010.

Assumption of constant reinforcing up wall height

For simplicity, it was assumed in the analysis that the same reinforcing to resist the applied hoop tension would be used for the whole wall. In reality though, the reinforcing will be reduced in steps away from

the point of T_{max} , where A_s will be at a maximum. This tiered reinforcing layout is illustrated in Figure 8.14. The blue bars show the A_s required to satisfy a target crack width of $w_t = 0.2 \text{ mm}$. The red line shows the practical A_s that is typically specified; the number and spacing of tiers may differ, depending on the geometry of the reservoir.

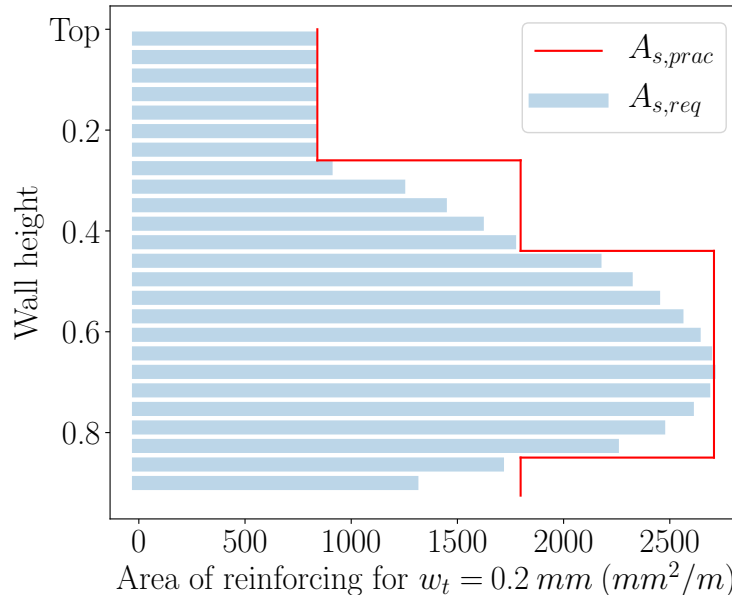


Figure 8.14: Practical, tiered reinforcing layout in a reservoir wall.

The analysis assumes that cracks form at the point of T_{max} and propagate above and below T_{max} until $T_{r,a} = T_{max}$. From Figure 8.14, it can be seen that the only other possible points where significant cracking may occur is where the reinforcing tiers down from the maximum A_s . At these points however, the applied tension is rapidly reducing. Also, at these points, the maximum A_s still contributes to the T_r , with reducing effect, as one moves away from the tier-down point. Therefore if cracks were to form, they would have limited length through which to contribute significant leakage. Additionally, the h^*/t ratio would be lower if the cracks formed higher up the wall, reducing the initial leakage and increasing the extent and effectiveness of self-sealing.

The combination of the above-mentioned factors result in the introduction of a degree of conservatism into the recommendations of this research that is difficult to quantify. Though, this conservatism is similarly present in many semi-probabilistic ULS applications that are governed by reliability criterion. The conservatism should not therefore disqualify it from being considered as a viable tool with which to design round reservoirs that adhere to a reliability level of $\beta = 1.5$.

8.4.4 Discussion on SLS target reliability

In this research, an irreversible SLS level of reliability of $\beta = 1.5$ was used as the target reliability for the case of leakage. This is given in most codes as the reliability level for general irreversible SLS. In the case of WRS, where the design is governed by SLS considerations, however, it is unclear whether this limit is appropriate or not. The assumption of irreversible SLS is sensible, as a failed water tightness test would result in the need for external intervention (repair), in order to restore the structure to proper service. Even within the irreversible SLS category, one umbrella- β value for all cases may not

be appropriate.

Following from the discussion in section 2.6.1, the consequences of failure at the end time of each specified leakage regime vs the cost of increasing safety may be notably different. In the case of specifying regime C_{14d21d} for example, the consequences of failure of significant overhead or project delay costs may overshadow the cost of supplying extra reinforcing to increase safety, and as such, a higher target β would be appropriate. Conversely, if C_{3d8d} is specified, the consequences of failure may be lower and a lower target β value would apply. This should be investigated further in future research.

8.5 Chapter summary

This chapter serves to analyse a large number of round tension-governed reservoirs, to determine the achieved level of SLS leakage-related reliability, given a range of target crack widths and reservoir geometries. The long term deterministic design approach of MC 2010 was used to determine the required area of reinforcing for each target crack width in the range $0.05 - 0.2\text{ mm}$ for each of the 235 simulated reservoir geometries. Subsequently, a probabilistic analysis was carried out for all target crack widths in each reservoir, and the level of reliability was determined for each leakage regime. This was achieved by comparing the short term predicted leakage to the allowable leakage after the specified stabilization period and water tightness test duration.

The results indicate high variation in the achieved reliability for each target crack width. They also indicated that the commonly-used target crack width of 0.2 mm is not sufficient to achieve a mean level of reliability of $\beta_m = 1.5$. The target crack width required to achieve $\beta_m = 1.5$ for flow regimes C_{0d7d} to C_{14d21d} were found to be $0.12, 0.14, 0.16$ and 0.17 mm , respectively. Furthermore it was shown that there is a weak trend of target crack widths linearly increasing in stringency, with increasing h^*/t ratio for all leakage regimes.

The trend of increasing w_t stringency with increasing h^*/t ratio for a reliability level of $\beta = 1.5$ was investigated for the h^*/t range of $12 - 26$ that was analysed. It is clear that for the case of leakage related SLS, the h^*/t ratio has less of an effect on the required w_t than the EN 1992-3 recommendations of w_t suggest. It was shown that overall, the EN 1992-3 recommendations for w_t were more stringent than those from this research and achieved β values considerably higher than 1.5 for leakage regimes C_{7d14d} and C_{14d21d} . The recommendations from this research are tabulated in the form of a range of w_t values, depending on the chosen leakage regime and h^*/t ratio.

A clear trend of decreasing w_t with increasing $T_{max}/T_{r,m}$ ratio was identified from the analyses. While still containing some variation, this trend showed less variation than the trend in w_t vs h^*/t . Furthermore, the trend indirectly takes into account the effect of the h^*/t ratio on the degree and efficiency of self-sealing and the resulting effect on w_t . Recommendations of w_t with $T_{max}/T_{r,m}$ are given for each leakage regime.

Finally, the practicalities of the analysis and the effect that the model assumptions may have on the achieved reliability were discussed. Commentary was also given with regard to where the analysis assumptions may differ from typical reservoir design practice and the conservatism that these deviations may introduce into the model.

9. Final Summary and Conclusions

This research set out to determine the achieved level of serviceability limit state (SLS) reliability in tension-governed, reinforced concrete water retaining structures (WRS), considering the effect of self-sealing. It also aimed at determining whether the achieved reliability is in line with current structural design codes that are used to design water retaining structures or not. The SLS design of WRS is usually governed by the limitation of crack widths, in order to keep the leakage of the stored liquids to within acceptable levels. The design code-specified target crack widths are thus the main driver behind the design of WRS and the achieved reliability that results from the use thereof gives an indication of whether these are satisfactory or not.

9.1 Summary of reviewed literature

The reviewed literature was split into two chapters. Chapter 2 considers risk and reliability in structural engineering applications, and chapter 3 reviews WRS in general and the advancements in the self-sealing of cracks in concrete.

Chapter 2 introduces the concepts of risk and reliability and the need for them in structural engineering. The fundamental concepts of risk and reliability are introduced, along with uncertainties in loading, material resistance and target reliability for both ULS and SLS applications. It also considers the cost of safety in terms of the trade-off between a higher cost and increased reliability, or lower cost and reduced reliability. The two reliability analysis methods, FORM and Monte Carlo simulations, that are used in chapters 7 and 8 are detailed. An overview of the probabilistic distributions that are frequently used in this research are also given.

Chapter 3 introduces a background to WRS and self-sealing and self-healing in concrete. It considers the two typical choices of geometry in WRS, round and rectangular, and the failure mechanisms that govern the designs of each - tension and flexure, respectively. Cracking in concrete structures is then considered, with a focus on the models that are most commonly used to calculate the crack widths in WRS that form as a result of mechanical loading. The three models that are considered and compared to one another are those from EN 1992-1-1, the *fib* Model Code 2010 (MC 2010) and BS 8007. The models are considered in terms of their strain formulation and crack spacing, as well as the uncertainty associated with their use.

The concept of leakage in WRS is introduced through a review of the liquid tightness classes, allowable leakage, post-construction water tightness test criterion and crack width limits imposed by prominent structural design codes. The theory in the calculation of water flow through cracked concrete is introduced, and is shown to be primarily dependent on the water pressure head above the crack, the thickness of section parallel to the direction of flow, crack width, crack length and the flow reduction

factor. The flow of water through cracks in WRS constitutes leakage, which is to be kept to a minimum, as defined by water tightness test criterion. The reduction of flow through concrete over time from self-sealing in the cracks is highly desirable. A review of the current state of autogenous and autonomous self-sealing in concrete was presented therefore.

This research focusses on autogenous self-sealing as a means of reducing the leakage in reinforced concrete WRS over time. It is clear that a number of structural design codes rely on the occurrence of autogenous self-sealing as a means of achieving a reservoir that has a small degree of initial leakage, but that stops within a short period of time. A number of research projects were reviewed that investigated leakage through tension cracks in ordinary concrete or mortar and the subsequent self-sealing that takes place. The most influential parameters on self-sealing were identified as the crack width and the hydraulic ratio, h^*/t . Bigger cracks with higher hydraulic ratios showed notably reduced self-sealing efficiency and efficacy than those with smaller crack widths and lower hydraulic ratios.

This research thus focusses on the effect that autogenous self-sealing has on the achieved level of reliability in round, reinforced concrete WRS.

9.2 Model databases and probabilistic modelling

In order to determine the effect that autogenous self-sealing has on the achieved reliability in WRS, a quantitative measure of self-sealing in tension cracked concrete is required. To this end, chapters 4 and 5 detail two databases compiled from existing literature and the characterization of data from each.

The initial flow of leakage through a crack is determined before the reduction in leakage over time can be considered. Ideal flow through two frictionless, parallel plates was used as the basis and adapted further to be able to probabilistically predict initial leakage. A database of experimental samples with measured initial flow, crack width, crack length, concrete section thickness and water pressure head was compiled from published literature. The experimental samples all had concrete mix constituents similar to those found in practical WRS. The flow reduction factor, ζ , was characterized using the initial flow prediction database of experimental samples and found to have a mean value of 0.11. The variation in the prediction of initial flow is introduced through an initial flow prediction model factor, θ_{Q0} . The θ_{Q0} model factor was characterized for three crack width ranges ($w \leq 0.15 \text{ mm}$, $0.15 < w \leq 0.25 \text{ mm}$ and $0.25 < w \leq 0.35 \text{ mm}$) using a 2-parameter Weibull distribution and confirmed statistically and visually using KS tests and Weibull plots, respectively. The initial flow through a single tension crack can thus be predicted with a measure of uncertainty.

The second database consists of experimental data of tension cracked concrete samples with flow over time data that exhibits self-sealing, compiled from published literature. As before, the experimental data has concrete mix constituents, quantities and exposure conditions similar to that in practical WRS. The data was used to characterize a leakage accumulation factor, θ_{ijd} , that describes the normalized leakage that flows through a crack between a start and end time (in days), i and j , respectively, as a function of the initial flow out of the crack. The θ_{ijd} factor is characterized for four different start and end times, C_{ijd} , referred to as leakage regimes. The leakage regimes correspond generally to recommendations of stabilization periods, followed by water tightness tests, from BS 8007 and ACI 350. The θ_{ijd} factor is characterized for the three crack width ranges, as for the initial flow prediction model factor. The effect of the hydraulic ratio, h^*/t (or h_D/h in EN 1992-3), on self-sealing is

taken into account by the hydraulic ratio factor, θ_{HR} . The θ_{HR} ratio is characterized and used to semi-probabilistically vary the leakage, depending on the h^*/t ratio of the crack, relative to $h^*/t=20$.

The probabilistic prediction of initial flow and leakage over time are then combined, in order to predict the total leakage that transpires through a tension crack in reinforced concrete for a given leakage regime with a measure of uncertainty. The total leakage was found to be significantly dependent on the crack width and leakage regime and to a lesser extent on the hydraulic ratio. Greater crack widths were found to exponentially increase the initial leakage, as well as decrease the extent and efficiency of self-sealing.

9.3 SLS reliability analyses for leakage in reservoirs

As WRS (reservoirs) are governed by the SLS design of limiting crack widths to code-defined values in order to keep leakage to an acceptable level, the SLS leakage-related reliability is determined by the evaluation of leakage through a reservoir at the end of the water tightness test. The predicted leakage is compared to the allowable leakage and the reliability is determined. In order to determine the SLS leakage-related reliability in a reservoir, the probabilistic prediction of the total leakage through a single crack needed to be adapted to be applicable to numerous cracks in the context of a reservoir. Chapter 6 details this process.

A description of the typical design process used to determine the tension forces that act on a round, reinforced concrete reservoir with a pinned base and a simply-supported roof is given. Assumptions are made with respect to physical reservoir parameters, so as to limit the scope to a manageable level. As it has been shown to best predict crack widths most consistently overall, the MC 2010 crack width model is chosen as the basis for the calculation of crack widths in this research. The critical parameters within the MC 2010 crack width model are considered probabilistically to obtain a mean crack width, rather than a maximum crack width. Distributions are assigned to those parameters that are likely to contribute variation to the crack width, based on research by others.

This research only considers the stabilized cracking stage, although the requirement for stabilized cracking is altered slightly. A model factor, θ_{cw} , based on previous research (McLeod, 2019), is used to account for the uncertainty in the prediction of crack widths using the MC 2010 model. A limit state equation was developed, defined as the difference between the allowable leakage and the predicted leakage. The allowable leakage is based on the BS 8007 requirements of 0.2% of the reservoir volume (drop in water depth of $h/500$).

A simplified sensitivity analysis was performed on the adapted mean crack width model. It investigated the model behaviour and upper and lower bound reliability limits were determined, based on the assumed crack spacing of 1 or 2 times the transfer length, respectively. From the results of the sensitivity analysis, it was found that the concrete cover, the reinforcing bar diameter and the mean concrete-reinforcing bond strength (c , ϕ_s and τ_{bms}) contribute little variation to the limit state, and were replaced by deterministic mean values.

Chapter 7 details and performs a Monte Carlo analysis on four entire reservoirs to determine the achieved level of reliability for each leakage regime. The limit state is extended to that of an entire reservoir and further considers the shape of the cracks and the way that the cracks form around the reservoir. Each reservoir is analysed for target crack widths from 0.05–0.2mm. The analysis determines

the amount of reinforcing required to satisfy the current crack width, according to the deterministic design process in MC 2010 for the long-term. The reservoir is then analysed probabilistically, considering the reservoir at water tightness test stage, which is assumed to be at ≈ 28 days (short-term). The analysis is repeated 1000 times, so that the p_f converges for an irreversible SLS β of 1.5.

The results of the analyses indicate that the EN 1992-3 maximum crack width (5% exceedance) that was experimentally-determined as being 1.7 times the mean crack width, is more appropriate for target crack widths in the range of $0.05 < w_t < 0.2 \text{ mm}$, than the MC 2010 recommendation of 2 times the mean crack width. The results also indicate that the MC 2010 recommendation of a target crack width of $w_t = 0.2 \text{ mm}$ is not adequate to achieve $\beta = 1.5$. The ACI recommendation of $w_t = 0.1 \text{ mm}$ seemed too stringent for $\beta = 1.5$. While the trend of increasing w_t stringency with increasing h^*/t ratio from EN 1992-3 was also present in the analysis results, the EN 1992-3 recommendations also appeared too stringent for $\beta = 1.5$. The results also indicate that the stabilization- and water tightness test-times specified have a considerable effect on the achieved reliability.

In chapter 8, a reliability analysis on a far greater number of reservoirs is performed to confirm the indications from chapter 7. The group of 235 simulated reservoirs have h^2/Dt ratios ranging from 3 to 12 and a range of h^*/t values from 12 to 26. The majority of reservoirs do not experience the stabilized cracking state, as is assumed in the crack prediction models. More than 2500 reservoirs were sampled, to obtain 235 reservoirs that experienced stabilized cracking. The analyses showed considerable variation in the results of the achieved reliability for each target crack width. As expected, leakage regimes with longer stabilization periods require less stringent crack widths, due to the extended duration of self-sealing that takes place. This translates to a reduction in required reinforcing of ≈ 25 , 30 and 37 percent from leakage regime C_{0d7d} to C_{3d8d} , C_{7d14d} and C_{14d21d} , respectively. The mean w_t value for $\beta = 1.5$ for leakage regimes C_{0d7d} to C_{14d21d} were shown to be $w_t = 0.12$, 0.14, 0.16 and 0.17 mm, respectively, all of which are below the typically-specified $w_t = 0.2 \text{ mm}$. This shows the necessity for structural design codes to prescribe set stabilization- and water tightness test-times and give guidance as to the effect that these have on the target crack width.

The results confirmed a trend of linearly increasing stringency in w_t for $\beta = 1.5$ (tighter target crack widths) with increasing h^*/t ratio. The analysed h^*/t ratio range was limited to $12 \leq h^*/t \leq 26$ due to the requirement of stabilized cracking. The effect of decreasing w_t with increasing h^*/t ratio was shown to be less stringent than the recommendations in EN 1992-3 for the considered h^*/t ratio range, with the exception of leakage regime C_{0d7d} (which is unlikely to be specified in practice). The recommendations of w_t vs h^*/t in EN 1992-3 were thus found to be too conservative for a reliability level of $\beta = 1.5$ for stabilized cracking for three of the four leakage regimes considered. The conservatism in the EN 1992-3 recommendations of target crack width is likely due to the purpose for which the recommendations were developed. They were given from the perspective of prescribing w_t values that ensure self-sealing in any single tension crack of known width, with a probability of non-exceedance of 90% ($\beta = 1.28$) within 4-10 weeks. They do not consider the uncertainty associated with the prediction of crack widths. In comparison, this research accounts for the uncertainty in the predicted crack width, as well as leakage volume and self-sealing. It recommends values of w_t vs h^*/t to specifically limit leakage to acceptable levels at the end of the water tightness test on reservoir level with a reliability level of $\beta = 1.5$.

The MC 2010 recommendation of $w_t = 0.2 \text{ mm}$ for a typical reservoir is given irrespective of h^*/t ratio and only qualitatively mentions the effect of self-sealing. The analysis results show that a target crack

width of $w_t = 0.2 \text{ mm}$ is not sufficient to obtain a value of $\beta = 1.5$ for stabilized cracking, for any of the leakage regimes considered. If the simplicity of a single-value w_t is desired, the above-mentioned mean values of w_t for $\beta = 1.5$ for each leakage regime should be used instead. The variation in achieved β from the recommendations of w_t as a function of h^*/t was found to be considerable and that the variation overshadows the trend. A summary of the recommendations, listed by flow regime, are shown in Table 9.1.

Table 9.1: Summary of recommendations of target crack widths for round, reinforced concrete reservoirs in the stabilized cracking stage as a function of hydraulic ratio, h^*/t , for $\beta = 1.5$.

Leakage regime	Stabiliz. period ⁺	W. t. test beg./end ⁺	Allow. leakage	h^*/t^\dagger range	w_t (mm)	w_t (mm) interp. [‡]
C_{0d7d}	0	0 / 7	0.2% Vol	12 → 26	0.13 → 0.11	$0.145 - 0.05 \cdot \frac{x}{35}$
C_{3d8d}	3	3 / 8		12 → 26	0.155 → 0.13	$0.17 - 0.05 \cdot \frac{x}{35}$
C_{7d14d}	7	7 / 14		12 → 26	0.165 → 0.145	$0.18 - 0.045 \cdot \frac{x}{35}$
C_{14d21d}	14	14 / 21		12 → 26	0.18 → 0.165	$0.2 - 0.045 \cdot \frac{x}{35}$

[†]See Appendix D for h^* values. [‡]For interpolation; x refers to the desired h^*/t ratio. W.t - Water tightness.
⁺Stabilization period and w.t. test beginning/end given in days.

A trend in w_t as a function of the maximum applied hoop tension to the mean concrete tensile resistance force in the wall, $T_{max}/T_{r,m}$, was identified as another ratio by which target crack widths may be specified. It was found that increasing values of $T_{max}/T_{r,m}$ required stricter target crack widths in order to achieve $\beta = 1.5$. Compared to the trend in w_t vs h^*/t , this trend showed reduced variation in achieved β , and progressively less variation at lower values of $T_{max}/T_{r,m}$. The change in recommended w_t with $T_{max}/T_{r,m}$ ratio indirectly considers the h^*/t ratio and its effects on the extent and efficiency of self-sealing. A summary of the recommendations, listed by flow regime, are shown in Table 9.2. A more detailed summary of both sets of recommendations is given in Appendix E.

Table 9.2: Summary of recommendations of target crack widths for round, reinforced concrete reservoirs in the stabilized cracking stage as a function of $T_{max}/T_{r,m}$ ratio for $\beta = 1.5$.

Leakage regime	Stabiliz. period ⁺	W. t. test beg./end ⁺	Allow. leakage	$T_{max}/T_{r,m}$ range	w_t (mm)	w_t (mm) interp. [†]
C_{0d7d}	0	0 / 7	0.2% Vol	0.925 → 1.25	0.135 → 0.05	$0.135 - 0.262 \cdot (x - 0.925)$
C_{3d8d}	3	3 / 8		0.925 → 1.25	0.180 → 0.08	$0.18 - 0.308 \cdot (x - 0.925)$
C_{7d14d}	7	7 / 14		0.925 → 1.25	0.190 → 0.10	$0.19 - 0.277 \cdot (x - 0.925)$
C_{14d21d}	14	14 / 21		0.925 → 1.25	0.200 → 0.13	$0.20 - 0.215 \cdot (x - 0.925)$

[†]For interpolation; x refers to the desired $T_{max}/T_{r,m}$ ratio. W.t - Water tightness.
⁺Stabilization period and w.t. test beginning/end given in days.

The recommendations made for w_t as a function of leakage regimes are advantageous for a number of reasons. Firstly, in WRS design codes, the specification of leakage regimes and water tightness test criteria are essential to be able to evaluate the level of achieved SLS leakage-related reliability. Thus, this research proposes these in a clear, unambiguous way, giving designers a choice in terms of a quicker (or no) stabilization and water tightness test period combined with a higher material cost, or a longer stabilization and water tightness test period combined with a lower material cost. The water tightness test is simple and the allowable leakage is a quantitative measure, making the judgement of compliance or non-compliance straightforward. The recommendations consider the effect of autogenous self-sealing

in concrete, as well as the quantum of leakage that transpires during the water tightness test. The results show that while there may be some residual leakage after the water tightness test, more than 90% of the total leakage that would transpire through a crack will already have taken place by the end of the water tightness test.

This research and its recommendations bridge the gap between theoretical reliability and achieved reliability in the SLS consideration of leakage in tension-governed reservoirs. Through novel probabilistic analyses considering the effect of self-sealing in ordinary reinforced concrete, the achieved level of reliability of reservoirs is quantified, providing a basis by which the cost-optimization of reservoirs can be conducted. Recommendations of optimal target crack width are given, in order to ensure that the reservoir performs according to design code SLS specifications, i.e. achieves a reliability level of $\beta = 1.5$.

9.4 Limitations of the research

This research is conducted assuming that the stabilized cracking stage in reservoirs is reached, as do the structural design code crack width models. As such, the reservoirs considered here are on the larger side of those in practice. Reservoirs smaller than $\approx 3 M\ell$ are almost exclusively in the crack formation stage and not in the stabilized cracking stage. This research therefore provides a potentially conservative estimate of the target crack widths for such reservoirs. This research also makes assumptions with regard to reservoir geometry and analysis considerations which do not consider the entire range of round tension-governed reservoirs found in practice.

The sample size of the $0.25 < w \leq 0.35 \text{ mm}$ crack width range is rather limited and while this range is actually very infrequently used for the range of target crack widths considered in this research, a greater number of samples would be required if target crack widths $> 0.2 \text{ mm}$ were to be considered. Furthermore, this research does not apply to prestressed concrete reservoirs, nor does it apply to flexure-governed reservoirs. This research is concerned with the achieved SLS reliability at the end of the water tightness test and, while the results show that leakage beyond this point is likely to be minimal, the long-term performance of reservoir is not guaranteed. Some of the assumptions made in this research do introduce a small, difficult-to-quantify measure of conservatism into the recommendations. Due to this, and the occurrence of gross human error in design and construction defects that are not considered in this research, the actual achieved reliability may be different from the results presented here.

9.5 Recommendations for future research

Through the determination of the achieved leakage-related SLS reliability in tension-governed reservoirs in this research, the need for further research into particular elements outside the scope of this study was identified. This section details these potential areas for further research.

- **Stage of cracking.** In this research, only the stabilized cracking stage was considered (although slightly amended to include a more diverse range of h^*/t ratios), following the same assumption being made in the crack width prediction models in the codes used to design reservoirs. It was found that most reservoirs do not, in fact, reach the stabilized cracking stage and are actually in the crack formation phase. This is particularly prevalent for reservoirs in the range $h^*/t < \approx 12$. Future research into the reliability of SLS-related leakage in reservoirs should consider analysing reservoirs in the crack formation stage, as well as those in the stabilized cracking stage.

- **Flexural cracking.** This research only considers tension-governed WRS. While research has shown that the probability of leakage is higher in tension-governed WRS, the potential for leakage in flexure governed WRS still exists, particularly in WRS where the walls can cyclically flex inwards and outwards. The determination of the achieved reliability in flexure governed WRS would allow for optimization in these structures.
- **Probabilistic consideration of shrinkage.** Drying and autogenous shrinkage are considered deterministically in this research. The prediction of shrinkage naturally contains variation and possibly bias and a probabilistic characterization of this would be useful in further identifying sources of uncertainty in WRS. The long-term effects of shrinkage are of particular interest and could affect the long-term reliability considerably.
- **Dynamic cracks and long term effects.** The effect of dynamic, cyclic cracks on self-sealing, particularly in terms of flow reduction over time, has received little research attention even though it can have a notable impact on the long-term performance of reservoirs. The characterization of the effect of dynamic cracks on self-sealing and leakage would provide meaningful insight into the achieved long-term reliability. Additionally, the effects of concrete deterioration, cyclic loading and chloride ingress on the long-term reliability should be investigated.
- **Optimum β from cost optimization.** While this research considers the optimum target crack widths required to satisfy the SLS level of reliability of $\beta = 1.5$, whether this level of reliability is at an optimum level or not remains unknown. This research provides a means by which to determine the achieved level of reliability; a full cost-optimization of reservoirs based on the cost of providing safety vs the cost and consequences of failure now becomes a possibility. This should also incorporate a consideration of stabilization- and water tightness-test time periods, the consequences of failure at these times and their dynamic effect on the reliability.
- **Application to prestressed concrete reservoirs.** Prestressed concrete reservoirs have been growing in popularity due to the maturity of the technology and the realization of reservoir sizes that significantly exceed those possible using reinforced concrete. This study does not consider prestressed concrete reservoirs, but the same probabilistic principles apply to them. Inherent variation in concrete and prestressing tendon material properties, strength and loading will lead to variations in the realized resistance, which can lead to leakage. Thus, a reliability analysis using the number of prestressing tendons and/or strands and/or tendon layout in combination with concrete wall thickness as decision parameters would provide insight as to the achieved level of reliability in prestressed concrete reservoirs.

Bibliography

- [1] ACI (2001). *Control of cracking in concrete structures (ACI 224R01)*. American Concrete Institute, Mississippi, U.S.A.
- [2] ACI (2011). *Specification for Tightness Testing of Environmental Engineering Concrete Containment Structures (ACI 350.1-10) and Commentary*. American Concrete Institute, Mississippi, U.S.A.
- [3] Akhavan, A., Shafaatian, S. and Rajabipour, F. (2012). *Quantifying the effects of crack width, tortuosity, and roughness on water permeability of cracked mortars*. In: *Cement and Concrete Research*, Vol 42, Issue 2, pp. 313–320.
- [4] Aldea, C., Song, W., Popovics, J. and Shah, S. (2000). *Extent of healing of cracked normal strength concrete*. In: *Journal of materials in civil engineering* Vol 12(1), pp.92-96.
- [5] Alexander, M. (2014). *Aggregates and their properties in concrete*. In *Proceedings: Materials for modern concrete seminar (ConSem)*, Concrete Society of Southern Africa, Cape Town, South Africa.
- [6] Alfanda, A.M. and Farouk, A.I. (2017). *Comparative analysis of circular and rectangular reinforced concrete tanks based on economical design perspective*. In: *American Journal of Applied Scientific Research*. Vol. 3, No. 2, 2017, pp. 14-20.
- [7] Anchor, R.D. (1992). *Design of liquid retaining structures*. McGraw-Hill.
- [8] Angelucci, M., Beushausen, H., Alexander, M.G. and Mackechnie, J. (2017). *Specifying cement content for concrete durability: why less is more*. In: *Concrete Beton*, Volume 150, pp 12-17, September 2017.
- [9] AS3735 (2001). *Concrete structures for retaining liquids*. Standards Australia International, Sydney, Australia.
- [10] Atkinson, R. (2018). Session 4: Crack models and standardization. In: *Seminar on the design and construction of liquid retaining structures. Presented at Stellenbosch University, 16-17th April 2018*.
- [11] Azarsa, P., Gupta, R. and Biparva, A. (2018). *Crystalline Waterproofing Admixtures Effects on Self-healing and Permeability of Concrete*. In: *1st International Conference on New Horizons in Green Civil Engineering*, Victoria, Canada.
- [12] Balázs, G. and Borosnyói, A. (2005). Models for flexural cracking in concrete: the state of the art. *Structural Concrete*, vol. 6, no. 2, pp. 53–62.
- [13] Balázs, G.L. (1993). Cracking analysis based on slip and bond stresses. *ACI materials journal*, vol. 90, no. 4, pp. 340–348.
- [14] Balázs, G.L. (2013). Design for SLS according to fib Model Code 2010. *Structural Concrete*, vol. 14, no. 2, pp. 99–123.
- [15] Bamforth, P. (2007). CIRIA C660. *Early-age thermal crack control in concrete*. CIRIA, Classic House London.

- [16] Base, G.D., Read, J.B., Beeby, A.W. and Taylor, H.P.J. (1966). An investigation of the crack control characteristics of various types of bar in reinforced concrete beams. Research Report, Cement and Concrete Association.
- [17] Beeby, A.W. and Narayanan, R.S. (2009). *Designers' guide to EN1992-1-1 and EN1992-1-2 Eurocode 2: Design of concrete structures*. General rules and rules for buildings and structural fire design. Thomas Telford Publishing, Heron Quay, London, United Kingdom.
- [18] Benard, A. and Bosi-Levenbach, E.C. (1953). *The plotting of observations on probability paper*. Statistica Neerlandica, Vol 7, pp. 163-173.
- [19] BIS (2004). *IS: 3370-4:1967 (R2004): Code of Practice for Concrete Structures for the Storage of Liquids - Part 4: Design Tables*. Bureau of Indian Standards, New Delhi, India, 2004.
- [20] Blight, G. and Alexander, M. (2011). *Alkali-aggregate reaction and structural damage to concrete*. CRC Press, Taylor and Francis group, Florida, United States.
- [21] Bomhard, H. (1986). *Concrete Tanks for Water Storage- A Conceptual Approach*. In Proceedings: Tenth International Congress of the FIP, pp. 55-77.
- [22] Borg, R.P., Cuenca, E., Brac, E.M.G. and Ferrara, L. (2018). *Crack sealing capacity in chloride-rich environments of mortars containing different cement substitutes and crystalline admixtures*. In: Journal of Sustainable Cement-Based Materials, Vol 7:3, pp. 141-159.
- [23] Bozorgzadeh, S. (2012). *Investigation of Water Leakage Through Direct Tension Cracks in Reinforced Concrete Panels*. Masters Thesis. Ryerson University, Ontario, Canada.
- [24] BSI (1987). *British Standard code of practice for Design of concrete structures for retaining aqueous liquids (BS8007)*. British Standards Institution (BSI). London, United Kingdom.
- [25] BSI (2003). *Eurocode 2: Design of concrete structures Part 1-1: Part 3: Liquid retaining and containment structures (BS EN 1992-3:2006)*. British Standards Institution (BSI). London, United Kingdom.
- [26] BSI (2004). *Eurocode 2: Design of concrete structures Part 1-1: General rules and rules for buildings (BS EN 1992-1-1:2004)*. British Standards Institution (BSI). London, United Kingdom.
- [27] BSI (2006). *UK National Annex to Eurocode 2: Design of concrete structures Part 1-1: Part 3: Liquid retaining and containment structures (BS EN 1992-3:2006)*. British Standards Institution (BSI). London, United Kingdom.
- [28] Cailleux, E. and Pollet, V. (2009). *Investigations on the development of self-healing properties in protective coatings for concrete and repair mortars*. In Proceedings: 2nd International Conference on Self Healing Materials, Chicago, IL, USA.
- [29] Caldentey, A. (2017). Proposal of new crack width formulas in Eurocode 2, background and experiments. In: *Crack width calculation methods for large concrete structures*. Workshop proceedings No. 12 from a Nordic Miniseminar, Oslo, Norway. The Nordic Concrete Federation.
- [30] Caramelli, S., Croce, P., Salvatore, W. and Sanpaolesi, L. (1997). *Partial safety factors for resistance of steel elements*. University of Pisa. Pisa, Italy.
- [31] CEN (2002). *Eurocode - Basis of structural design (EN 1990:2002)*. Comité Européen de Normalisation (European Committee for Standardization). Rue de Stassart, 36 B-1050, Brussels, Belgium.
- [32] CEN (2002). *Eurocodes: 1990-1998*. Comité Européen de Normalisation (European Committee for Standardization). Rue de Stassart, 36 B-1050, Brussels, Belgium.
- [33] China National Standards, . (2002). *Code for design of concrete structures: GB50010:2002*. National standard of the People's Republic of China, Beijing.

- [34] Choi, H., Inoue, M., Sengoku, R. and Choi, H. (2017). *Strength recovery of concrete exposed to freezing-thawing by self-healing of cementitious materials using synthetic fiber*. In: *Advanced Materials Letters*, Vol 8(10), pp. 993-998.
- [35] CIB (1989). *Report: Publications 115&116 - Actions on Structures: Self-Weight loads & Live loads in buildings*. International Council for research and innovation in building and construction (CIB), Delft, Netherlands.
- [36] CIB (1995). *Report: Draft of CIB W81 Publication - Actions on Structures: Wind Load*. International Council for research and innovation in building and construction (CIB), Delft, Netherlands.
- [37] Cornell, C.A. (1969). *A Probability-Based Structural Code*. *Journal of the American Concrete Institute*, Vol 66(12).
- [38] Cuenca, E., Tejedor, A. and Ferrara, L. (2018). *A methodology to assess crack-sealing effectiveness of crystalline admixtures under repeated cracking-healing cycles*. In: *Construction and Building Materials*, Vol 179, pp. 619–632.
- [39] Daftardar, A., Vichare, S. and Vashi, J. (2017). An analytical solution for hoop tension in liquid storage cylindrical tanks. *International Journal of Engineering and Applied Sciences (IJEAS)*, vol. 4, pp. 99–104.
- [40] de Rooij, M.R., van Tittelboom, K., de Belie, N. and Schlangen, E. (2013). *Self-Healing Phenomena in Cement Based Materials*. State-of-the-Art Report of RILEM TC 221-SHC.
- [41] Debernardi, P.G. and Taliano, M. (2015). *An improvement to Eurocode 2 and b Model Code 2010 methods for calculating crack width in RC structures*. In: *Structural Concrete* 17 (2016), No. 3.
- [42] Diamantidis, D., Holický, M. and Sýkora, M. (2017). *Target Reliability Levels Based on Societal, Economic and Environmental Consequences of Structural Failure*. In *Proceedings: 12th International Conference on Structural Safety & Reliability, ICOSSAR 2017, Vienna, Austria*.
- [43] Dry, C.M. (2000). *Three designs for the internal release of sealants, adhesives, and waterproofing chemicals into concrete to reduce permeability*. In: *Cement and Concrete Research*, Vol 30, pp. 1969–1977.
- [44] Edvardsen, C. (1996). *Wasserdurchlässigkeit und Selbstheilung von Trennrissen in Beton (Water Permeability and Autogenous Healing of Tension Cracks in Concrete)*. Institute of Building Materials Research, University of Technology, Aachen. Deutscher Ausschuss für Stahlbeton, Booklet 455, Berlin. (in German).
- [45] Edvardsen, C. (1999). *Water Permeability and Autogenous Healing of Cracks in Concrete*. In: *ACI Materials Journal*, Vol. 96, July-August.
- [46] Esgandani, M. (2017). *Role of binder, permeability- reducing admixtures and cracking in the watertightness of concrete structures*. Doctoral thesis, Faculty of Engineering and Information Technology, School of Civil and Environmental Engineering University of Technology Sydney, Australia.
- [47] Fajkus, M., Holický, M., Rozlívka, L. and Vorlíček, M. (1999). *Random Properties of Steel Elements Produced in Czech Republic*. Eurosteel, Praha 1999, pp. 657-660.
- [48] Fédération internationale du béton, . (2013). *fib Model Code for Concrete Structures 2010*. Case Postale 88 CH-1015, Lausanne, Switzerland. Wiley: Ernst & Sohn.
- [49] Ferrara, L., Cuenca, E., Tejedor, A. and Brac, E.G. (2018). *Performance of concrete with and without crystalline admixtures under repeated cracking/healing cycles*. In *Proceedings: International Conference on Concrete Repair, Rehabilitation and Retrofitting (ICCRRR)*, MATEC Web Conferences, Vol 199.
- [50] Fischer, K., Viljoen, C., Köhler, J. and Faber, M.H. (2018). *Optimal and acceptable reliabilities for structural design*. In: *Structural Safety*, Vol 76, pp 149-161, Elsevier.

- [51] Gautam, B. (2018). *Bacteria Based Self Healing Concrete – A Bacterial Approach*. In: The International Journal of Engineering and Science (IJES): Recent Innovation & Challenges in Civil Engineering, pp. 57-61.
- [52] Gulvanessian, H., Calgaro, J. and Holický, M. (2002). *Designers' guide to EN 1990. Eurocode: Basis of structural design*. Thomas Telford, London, United Kingdom.
- [53] Gwon, S., Ahn, E. and Shin, M. (2019). *Self-healing of modified sulfur composites with calcium sulfoaluminate cement and superabsorbent polymer*. In: Composites Part B Engineering, Vol 162, pp. 469-483.
- [54] Hackl, J. (2018). PyRe (Python Reliability): Python module for structural reliability analysis. Available at: <http://github.com/hackl/pyre>
- [55] Hasofer, A.M. and Lind, N.C. (1974). *An Exact and Invariant First Order Reliability Format*. ACI-Journal, Vol. 66, pp. 974-985.
- [56] Hendy, C.R. and Smith, D.A. (2013). *Designers' guide to EN 1992-2 Eurocode 2: Design of concrete structures*. Part 2: Concrete Bridges. ICE Publishing, Westminster, London, United Kingdom.
- [57] Holický, M. (2009). *Reliability analysis for structural design*. Sun Press, SUN MeDIA, Stellenbosch, South Africa.
- [58] Holický, M., Diamantidis, D. and Sýkora, M. (2015). *Determination of Target Safety for Structures*. 12th International Conference on Applications of Statistics and Probability in Civil Engineering, ICASP12, Vancouver, Canada.
- [59] Holický, M. and Marková, J. (2000). *Verification of load factors for concrete components by reliability and optimization analysis: Background documents for implementing Eurocodes*. Progress in Structural Engineering and Materials, Vol. 2 No. 4, pp. 502-507.
- [60] Holický, M., Retief, J. and Wium, J. (2009). *Probabilistic Design for Cracking of Concrete Structures*. In Proceedings: 7th International Probabilistic Workshop, Delft, Netherlands.
- [61] Holický, M., Retief, J.V. and Sýkora, M. (2016). Assessment of model uncertainties for structural resistance. *Probabilistic Eng. Mech.*, 45, 188–197.
- [62] Holický, M., Sýkora, M., Viljoen, C., Mensah, .K. and Retief, J.V. (2013). *Model uncertainties in reliability analysis of reinforced concrete structures*. SEMC: 5th International Conference on Structural Engineering, Mechanics and Computation, Cape Town, South Africa.
- [63] Hosoda, A., Komatsu, S., Ahn, T., Kishi, T., Ikeno, S. and Kobayashi, K. (2008). *Self healing properties with various crack widths under continuous water leakage*. In Proceedings: 2nd International Conference on Concrete Repair, Rehabilitation and Retrofitting, ICCRRR-2, Cape Town, South Africa.
- [64] Huaco, D.R., Bowders, J.J. and Loehr, J.E. (2012). *Method to develop target levels of reliability for design using LRFD*. 91st Annual Meeting of the Transportation Research Board. Washington DC, United States.
- [65] Hussain, I. and Gupta, S.C. (2018). Analytical solution for hoop tension and bending moment coefficient for long cylinders by beam on elastic foundation. *International Journal of Research in Advent Technology*, vol. 6, pp. 791–796.
- [66] Ikoma, H., Kishi, T., Sakai, Y. and Kayondo, M. (2015). *Elucidation of rapid reduction of water flow through concrete crack regarded as self-healing phenomenon*. In: Journal of Ceramic Processing Research. Vol. 16, Special. 1, pp. s22-s27.
- [67] ISO (1998). *ISO 2394:1998 - General principles on reliability for structures*. International Organization for Standardization (ISO). Geneva, Switzerland.

- [68] ISO (2014). *ISO 2394:2014 - General principles on reliability for structures*. International Organization for Standardization (ISO). Geneva, Switzerland.
- [69] Jaroenratanapirom, D. and Sahamitmongkol, R. (2011). *Self-Crack closing ability of mortar with different additives*. In: *Journal of Metals, Materials and Minerals*, Vol 21 (1), pp. 9-17.
- [70] Jin, X., Hou, C., Fan, X., Lu, C., Yang, H., Shu, X. and Wang, Z. (2017). *Quasi-static and dynamic experimental studies on the tensile strength and failure pattern of concrete and mortar discs*. In: *Scientific Reports*, Vol 7, Article number: 15305.
- [71] Joint Committee for Structural Safety (JCSS), . (2001). *Probabilistic Model Code*. Working materials, (available on web pages: <http://www.jcss.ethz.ch/>).
- [72] Jonkers, H.M. (2011). *Bacteria-based self-healing concrete*. In: *Heron Journal*, vol 56, pp. 1-12.
- [73] Juenger, M., Provis, J.L., Elsen, J., Matthes, W., Hooton, R.D., Duchesne, J., Courard, L., He, H., Michel, F., Snellings, R. and N De. Belie (2012). *Supplementary Cementitious Materials for Concrete: Characterization Needs*. Materials Research Society Symposium Proceedings, Vol 1488, Materials Research Society.
- [74] Lapi, M., Orlando, M. and Spinelli, P. (2018). A review of literature and code formulations for cracking in r/c members. *Structural Concrete*, vol. 19, no. 5, pp. 1481–1503.
- [75] Lee, H.X.D., Wong, H.S. and Buenfeld, N. (2010). *Self-sealing cement-based materials using superabsorbent polymers*. In *Proceedings: International RILEM Conference on Use of Superabsorbent Polymers and Other New Additives in Concrete*, Technical University of Denmark, Lyngby, Denmark.
- [76] Lemaire, M., Chateaufneuf, A. and Mitteau, J.-C. (2009). *Structural reliability*. Wiley Online Library.
- [77] Li, V.C. and Yang, E. (2007). *Self Healing in Concrete Materials*. Self Healing Materials: An Alternative Approach to 20 Centuries of Materials Science, in *Self Healing Materials: An Alternative Approach to 20 Centuries of Materials Science*, Springer, pp. 161-193.
- [78] Lohmeyer, G. (1984). Wasserundurchlässige Betonbauwerke; Gegenmassnahmen bei Durchfeuchtungen (waterproof concrete structures; countermeasures against moisture penetration.). *Beton 34 (1984), Nr 2, pp 57-60 (in German)*.
- [79] Lv, Z., Chen, H. and Yuan, H. (2011). *Quantitative solution on dosage of repair agent for healing of cracks in materials: short capsule model vs. two-dimensional crack pattern*. In: *Science and Engineering of Composite Materials*, Vol 18, pp. 13–19.
- [80] Madsen, H.O. and Egeland, T. (1989). Structural reliability: Models and applications. *International Statistical Review / Revue Internationale de Statistique*, vol. 57, no. 3, pp. 185–203.
- [81] Maes, M. (2015). *Combined Effects of Chlorides and Sulphates on Cracked and Self-Healing Concrete in Marine Environments*. Doctoral thesis, Magnel Laboratory for Concrete Research, Department of Structural Engineering Faculty of Engineering and Architecture, Ghent University, Belgium.
- [82] Manoj, N.R. (2016). First-order reliability method: Concepts and application. Tech. Report, Faculty of Civil Engineering and Geosciences (CiTG). Delft University of Technology.
- [83] McLeod, C.H. (2013). *Investigation into Cracking in Reinforced Concrete Water-retaining Structures*. Master's thesis, Stellenbosch University, Stellenbosch, South Africa.
- [84] McLeod, C.H. (2019). *Model uncertainty in the prediction of crack widths in reinforced concrete structures and reliability implications*. Ph.D. thesis, Stellenbosch: Stellenbosch University.

- [85] McLeod, C.H., Viljoen, C. and Retief, J.V. (2017). *Determining model uncertainty associated with concrete crack models for members in flexure*. Conference: 15th International Probabilistic Workshop/10th Dresden Probabilistic Workshop 2017, Dresden, Germany.
- [86] Meichsner, H. (1992). *Über die Selbstdichtung von Trennrissen in Beton (On the self-sealing of tension cracks in concrete)*. In: Beton- und Stahlbetonbau 4/92, pp 95–99. Ernst & Sohn, Wiley-VCH.
- [87] Meichsner, H. and Röhling, S. (2015). Die selbstdichtung von trennrissen – ein risiko in der WU-Richtlinie (The self sealing of tension cracks - a risk in the WU guidelines). *Der Bausachverständige*, vol. 5, pp. 9–13.
- [88] Mlčoch, J., Marková, J. and Sýkora, M. (2017). *Uncertainty in crack width estimates according to fib Model Code 2010*. Transactions of the VŠB – Technical University of Ostrava, Civil Engineering Series, Vol. 17, No. 1. Ostrava, Czech Republic.
- [89] Montgomery, D.C. and Runger, G.C. (2003). *Applied Statistics and Probability for Engineers*. 3rd Ed. John Wiley & Sons, New York, USA.
- [90] Nanayakkara, S.M.A. (2003). *Self-healing of cracks in concrete subjected to water pressure*. In: New Technologies for Urban Safety of Mega Cities in Asia, Tokyo, Japan.
- [91] Nanayakkara, S.M.A. and Elakneshwaran, E. (2005). *Self-healing of cracks in concrete with Portland limestone cement*. In Proceedings: Cement Combinations for Durable Concrete, University of Dundee, Scotland, UK, 5–7 July.
- [92] Nathwani, J.S., Lind, N.C. and Pandey, M.D. (1997). *Affordable safety by choice: the life quality method*. Institute for Risk Research, University of Waterloo, Canada.
- [93] Palin, D., Wiktor, V. and Jonkers, H. (2015). *Autogenous healing of marine exposed concrete: Characterization and quantification through visual crack closure*. In: Cement and Concrete Research, Vol 73 (2015), pp. 17–24.
- [94] Palin, D., Wiktor, V. and Jonkers, H. (2017). *A Bacteria-Based Self-Healing Cementitious Composite for Application in Low-Temperature Marine Environments*. In: Biomimetics, 2(3), 13.
- [95] PCA (1943). *Circular concrete tanks without prestressing*. Portland Cement Association, Illinois, USA.
- [96] Pillai, S. and Menon, D. (2003). *Reinforced Concrete Design*. 3rd edn. Tata McGraw-Hill Education. 7 West Patel Nagar, New Delhi, India.
- [97] Quan, Q. and Gengwei, Z. (2002). Calibration of reliability index of RC beams for serviceability limit state of maximum crack width. *Reliability Engineering and System Safety*, vol. 75, pp. 359–366.
- [98] Rackwitz, R. (2000). *Optimization - the basis of codemaking and reliability verification*. In: Structural Safety, Vol 22, pp 27-60, Elsevier.
- [99] Ramm, W. and Biscopig, M. (1997). *Selbsteheilung und Bewehrungskorrosion bei wasserdurchströmten Trennrissen in bewehrtem Beton (Autogenous healing and reinforcement corrosion of water-penetrated tension cracks in reinforced concrete)*. Dissertation, University of Kaiserslautern, Germany.
- [100] Ramm, W. and Biscopig, M. (1998). *Autogenous healing and reinforcement corrosion of water-penetrated separation cracks in reinforced concrete*. University of Kaiserslautern. In: Nuclear Engineering and Design 179, pp. 191–200.
- [101] Ratnayake, K. and Nanayakkara, S. (2018). *Effect of Fly Ash on Self-healing of Cracks in Concrete*. In Proceedings: 4th International Multidisciplinary Engineering Research Conference, University of Moratuwa, Sri Lanka.

- [102] Reinhardt, H. and Jooss, M. (2003). *Permeability and self-healing of cracked concrete as a function of temperature and crack width*. In: Cement and Concrete Research 33 (2003) pp. 981–985.
- [103] Ripphausen, B. (1989). *Untersuchungen zur Wasserdurchlässigkeit und Sanierung von Stahlbetonbauteilen mit Trennrissen (Investigations on water permeability and rehabilitation of reinforced concrete components with tension cracks)*. Dissertation, RWTH-Aachen.
- [104] Roig-Flores, M., Moscato, S., Serna, P. and Ferrara, L. (2015). *Self-healing capability of concrete containing crystalline admixtures in different exposure conditions*. In: Concrete – Innovation and Design, fib Symposium, Copenhagen, Denmark.
- [105] Roig-Flores, M., Pirritano, F., Serna, P. and Ferrara, L. (2016). *Effect of crystalline admixtures on the self-healing capability of early-age concrete studied by means of permeability and crack closing tests*. In: Construction and Building Materials 114, pp. 447–457.
- [106] Sahmaran, M., Yildirim, G. and Erdem, T.K. (2013). *Self-healing capability of cementitious composites incorporating different supplementary cementitious materials*. In: Cement & Concrete Composites 35, pp. 89–101. Elsevier.
- [107] Shaikh, F.U.A. (2011). *Effect of Cracking on Corrosion of Steel in Concrete*. In: International Journal of Concrete Structures and Materials. Springer Singapore.
- [108] Sisomphon, K. and Copuroglu, O. (2011). *Self healing mortars by using different cementitious materials*. In Proceeding: International Conference on advances in construction materials through science and engineering, Hong Kong, China.
- [109] Sisomphon, K., Copuroglu, O. and Koenders, E.A.B. (2011). *Surface crack self healing behaviour of mortars with expansive additives*. In Proceedings: 3rd International Conference on Self-Healing Materials Bath, UK.
- [110] Snoeck, D., Van Tittelboom, K., Steuperaert, S., Dubruel, P. and De Belie, N. (2012). *Self-healing cementitious materials by the combination of microfibres and superabsorbent polymers*. In: Journal of Intelligent Material Systems and Structures, Vol 25(1), pp. 13-24.
- [111] Sørensen, J., Hansen, S. and Nielsen, T. (2001). *Partial Safety Factors and Target Reliability Level in Danish Codes*. Safety, Risk, and Reliability. IABSE, Malta, pp. 179-184.
- [112] Suleiman, A. and Nehdi, M. (2013). *Effect of environmental exposure on autogenous self-healing of cracked cement-based materials*. In: Cement and Concrete Research, Vol 111, pp. 197-208.
- [113] Tan, R., Eileraas, K., Opkvitne, O., Žirgulis, G., Hendriks, M.A., Geiker, M., Brekke, D.-E. and Kanstad, T. (2018). Experimental and theoretical investigation of crack width calculation methods for RC ties. *Structural Concrete*, vol. 19, no. 5, pp. 1436–1447.
- [114] Tan, R., Hendriks, M. and Kanstad, T. (2017). *Evaluation of current crack width calculation methods according to Eurocode 2 and Model Code 2010*. In: High Tech Concrete: Where Technology and Engineering Meet: Proceedings of the 2017 fib Symposium, held in Maastricht, Netherlands.
- [115] Tat, L. (1991). *Statistical analysis of reinforcing steel properties*. Master’s thesis, University of Canterbury, Christchurch, New Zealand.
- [116] Teal, O.R. (2016). *Crack closure and enhanced autogenous healing of structural concrete using shape memory polymers*. Doctoral thesis, School of Engineering, Cardiff University, Wales.
- [117] Van Coile, R., Hopkin, D., Bisby, L. and Caspeepe, R. (2017). *The meaning of Beta: background and applicability of the target reliability index for normal conditions to structural fire engineering*. In Proceedings: 6th International Workshop on Performance, Protection & Strengthening of Structures under Extreme Loading, PROTECT2017, 11-12 December 2017, Guangzhou (Canton), China.

- [118] Van Mullem, T., Gruyaert, E., Debbaut, B., Caspeepe, R. and De Belie, N. (2019). *Novel active crack width control technique to reduce the variation on water permeability results for self-healing concrete*. In: Construction and Building Materials, Volume 203, pp. 541-551. Elsevier.
- [119] van Tittelboom, K. and De Belie, N. (2013). *Self-Healing in Cementitious Materials—A Review*. In: Materials - Journal of Materials Science, Vol 6. MDPI, Basel, Switzerland.
- [120] Tran, N.L. and Graubner, C. (2018). *Uncertainties of concrete parameters in shear capacity calculation of RC members without shear reinforcement*. In: Extended Abstracts of the 16th International Probabilistic Workshop.
- [121] Van Nierop, S. (2017). *Target Reliability of Concrete Structures Governed by Serviceability Limit State Design*. Master's thesis, Stellenbosch University, Stellenbosch, South Africa.
- [122] Van Nierop, S., Viljoen, C. and Lenner, R. (2017). *Target Reliability of Concrete Structures Governed by Serviceability Limit State Design*. In Proceedings: 15th International Probabilistic Workshop, Dresden.
- [123] van Tittelboom, K., Gruyaert, E., Rahier, H. and De Belie, N. (2012). *Influence of mix composition on the extent of autogenous crack healing by continued hydration or calcium carbonate formation*. In: Construction and Building Materials, Vol. 37, pp. 349-359.
- [124] Viljoen, C. and Retief, J.V. (2017). *Design guidance on T1 and T2 for South African conditions and concretes*. WRC Project K5/2514/1 for the South African Water Research Commission (WRC). Lead Organisation: Stellenbosch University.
- [125] Vrouwenvelder, T. (2001). *JCSS Probabilistic Model Code*. In Proceedings: Safety, Risk, and Reliability. IABSE, Malta, pp. 65-70.
- [126] West-Russel, A., Viljoen, C. and van der Klashorst, E. (2018). *An assessment of the inherent reliability of SANS 10162-2 for cold-formed steel columns using the Direct Strength Method*. In Proceedings: 6th International Symposium on Life-Cycle Civil Engineering (IALCCE), Ghent, Belgium.
- [127] Wium, J. (2007). The development and calibration of South Africa's National Standards for water retaining structures. Tech. Report, for the South African Water Research Commission (WRC) Project Number K5/1764. Lead Organisation: Stellenbosch University.
- [128] Zemskov, S.V., Jonkers, H.M. and Vermolen, F.J. (2011). *Two analytical models for the probability characteristics of a crack hitting encapsulated particles: Application to self-healing materials*. In: Computational Material Sciences, Vol 50, pp. 3323-3333.
- [129] Zięba, J., Buda-Ożóg, L. and Skrzypczac, I. (2020). Probabilistic method and fem analysis in the design and analysis of cracks widths. *Engineering Structures*, vol. 209, p. 110022.

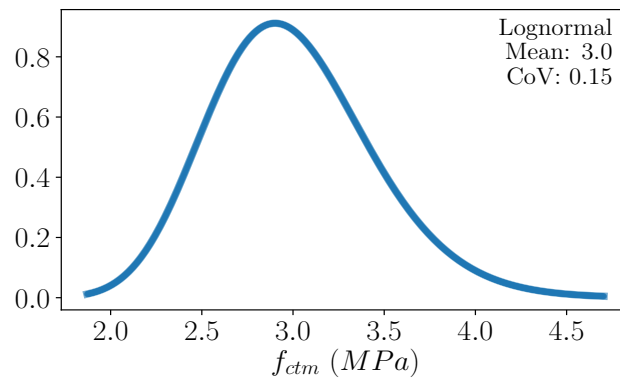
Appendices

A. Appendix A

A.1 Probabilistic distributions

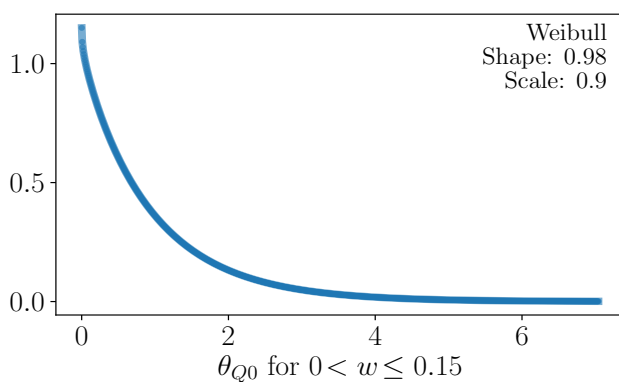
This appendix gives probability density functions for the probabilistic parameters in this research. Note that uniform distributions are not shown, as their densities are trivially constant between the bounds.

Mean concrete axial tensile strength f_{ctm}

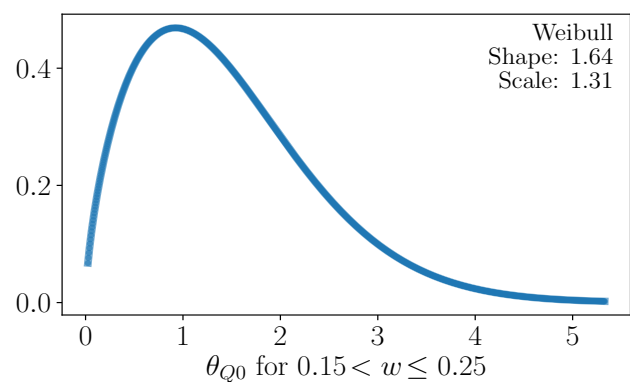


PDF of f_{ctm} distribution (MPa).

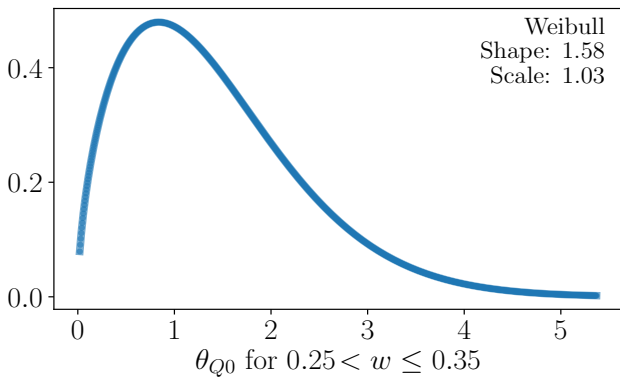
Initial flow prediction model factor θ_{Q0}



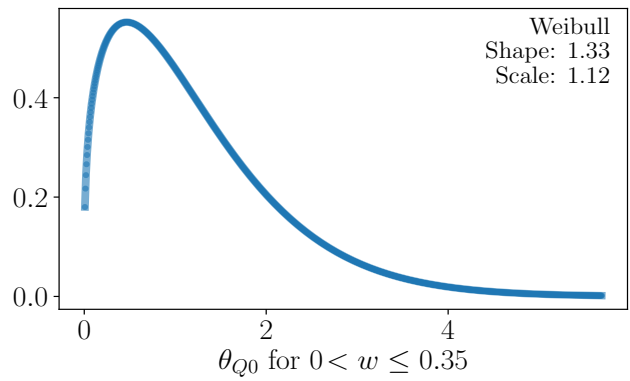
PDF of θ_{Q0} for $0 < w \leq 0.15mm$.



PDF of θ_{Q0} for $0.15 < w \leq 0.25mm$.

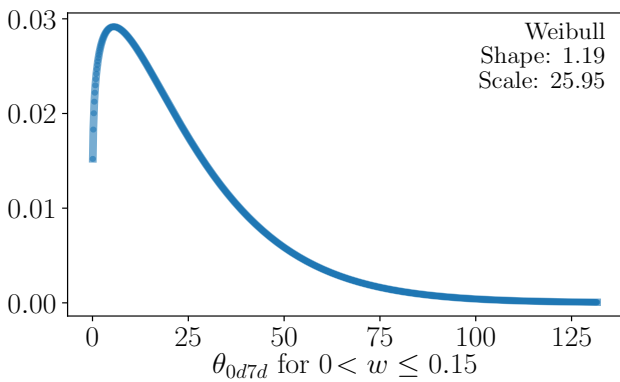


PDF of θ_{Q0} for $0.25 < w \leq 0.35mm$.

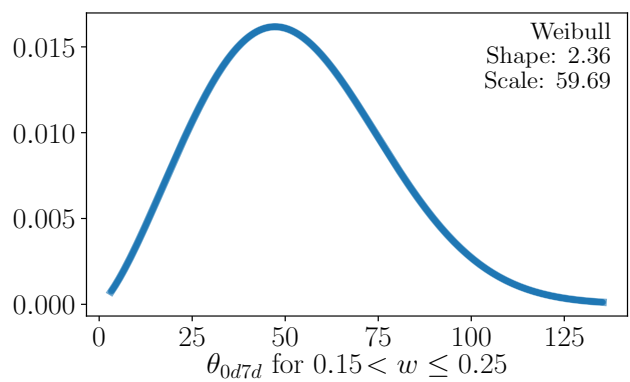


PDF of θ_{Q0} for $0 < w \leq 0.35mm$.

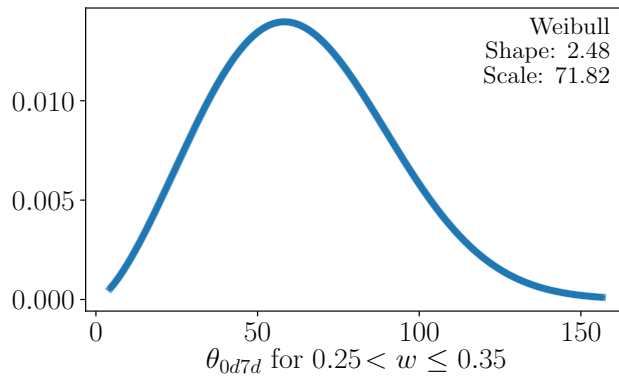
Leakage accumulation factor - θ_{0d7d}



PDF of θ_{0d7d} for $0 < w \leq 0.15mm$ (hrs).

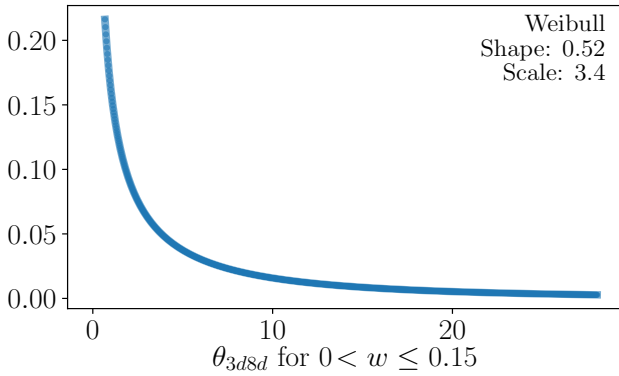


PDF of θ_{0d7d} for $0.15 < w \leq 0.25mm$ (hrs).

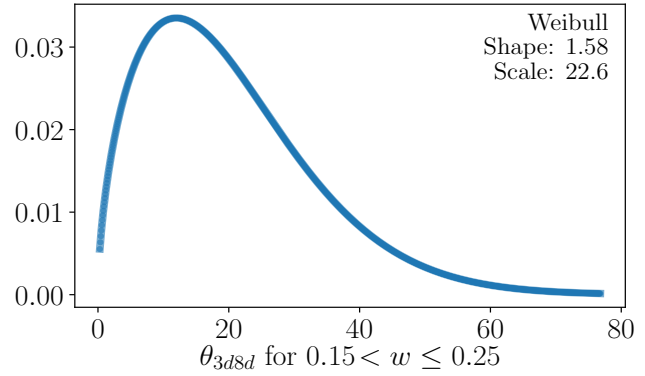


PDF of θ_{0d7d} for $0.25 < w \leq 0.35mm$ (hrs).

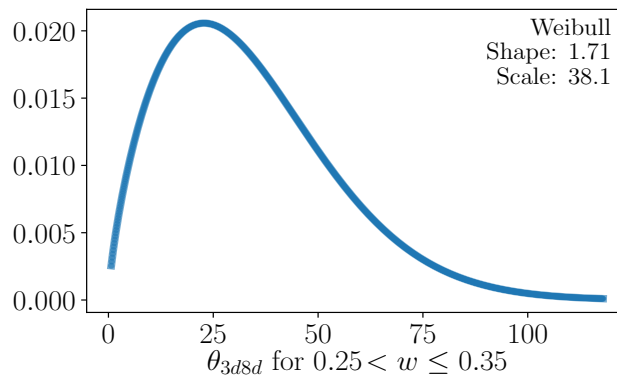
Leakage accumulation factor - θ_{3d8d}



PDF of θ_{3d8d} for $0 < w \leq 0.15mm$ (hrs).

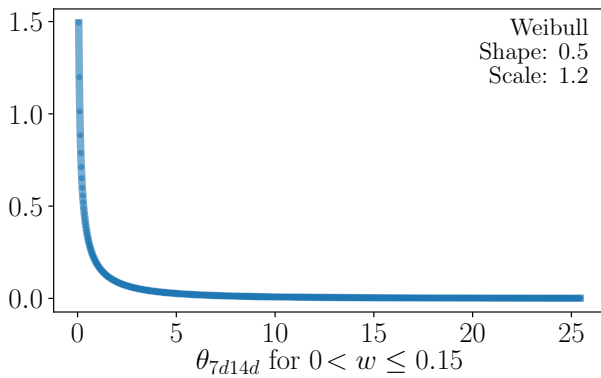


PDF of θ_{3d8d} for $0.15 < w \leq 0.25mm$ (hrs).

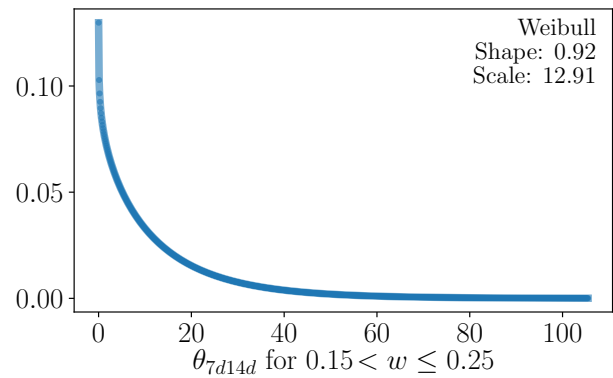


PDF of θ_{3d8d} for $0.25 < w \leq 0.35mm$ (hrs).

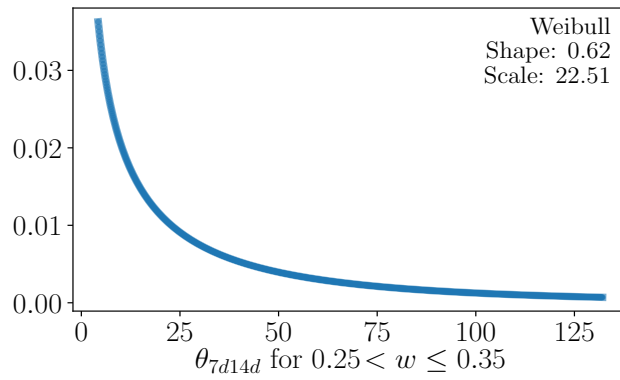
Leakage accumulation factor - θ_{7d14d}



PDF of θ_{7d14d} for $0 < w \leq 0.15mm$ (hrs).

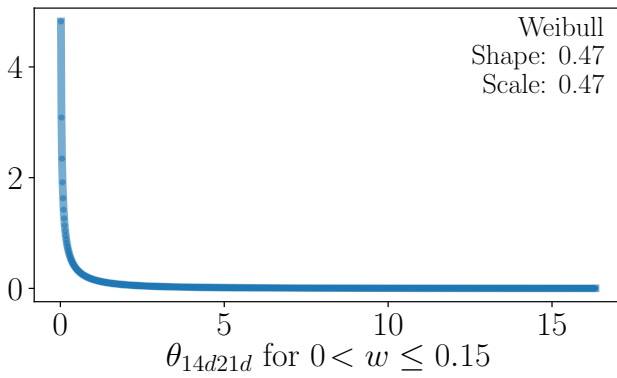


PDF of θ_{7d14d} for $0.15 < w \leq 0.25mm$ (hrs).

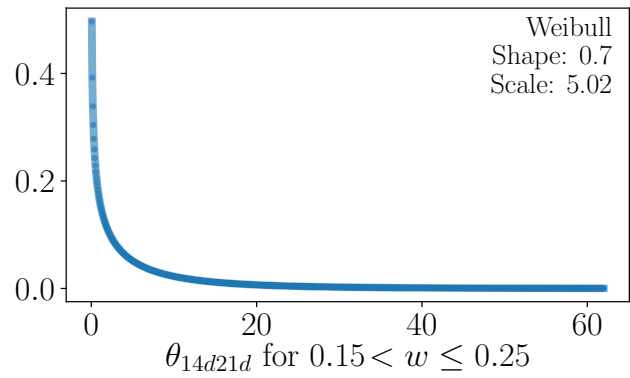


PDF of θ_{7d14d} for $0.25 < w \leq 0.35mm$ (hrs).

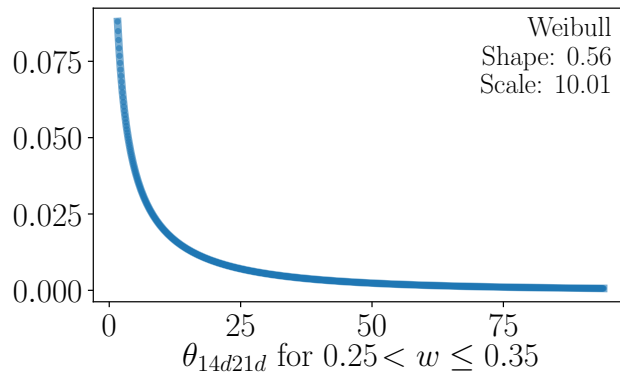
Leakage accumulation factor - θ_{14d21d}



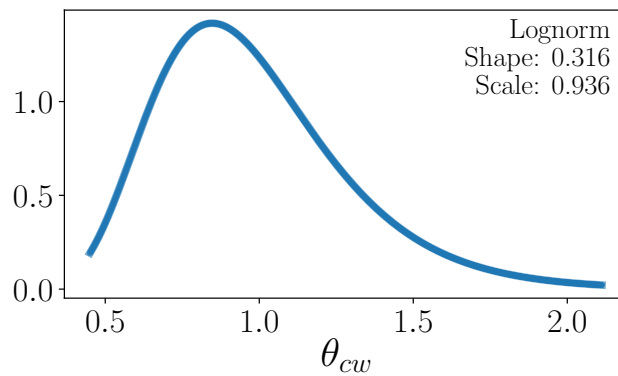
PDF of θ_{14d21d} for $0 < w \leq 0.15mm$ (hrs).



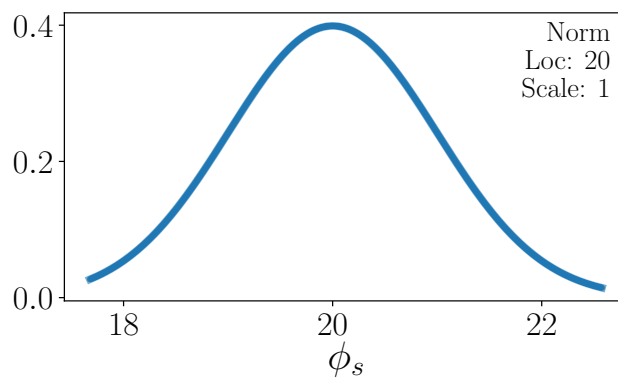
PDF of θ_{14d21d} for $0.15 < w \leq 0.25mm$ (hrs).



PDF of θ_{14d21d} for $0.25 < w \leq 0.35mm$ (hrs).

MC 2010 Crack width prediction model factor - θ_{cw} from McLeod (2019)

PDF of θ_{cw} to account for the uncertainty in predicting crack widths using the MC 2010 crack model.

Distribution of bar diameter for sensitivity analysis - ϕ_s 

PDF of ϕ_s for use in the sensitivity analysis (mm - later replaced with a deterministic value).

B. Appendix B

B.1 Hoop tension coefficients

Pinned/hinged

Hoop tension coefficients (C_t) for circular reservoirs walls with a pinned/hinged base, free top and a hydrostatic load only, as a function of reservoir height. Top of wall at $h = 0$. From Daftardar *et al.* (2017).

h	h^2/Dt														
	0.1	0.2	0.4	0.6	0.8	1	1.2	1.4	1.6	1.8	2	3	4	5	
0.000	0.499	0.495	0.48	0.456	0.426	0.391	0.354	0.315	0.278	0.242	0.209	0.085	0.021	0.007	
0.037	0.48	0.477	0.464	0.444	0.418	0.388	0.355	0.322	0.29	0.259	0.23	0.122	0.065	0.045	
0.073	0.462	0.459	0.449	0.432	0.41	0.385	0.357	0.329	0.302	0.276	0.252	0.159	0.108	0.085	
0.110	0.444	0.442	0.433	0.419	0.402	0.381	0.359	0.337	0.314	0.293	0.273	0.195	0.151	0.127	
0.147	0.426	0.424	0.417	0.407	0.393	0.378	0.361	0.344	0.326	0.309	0.294	0.232	0.194	0.172	
0.184	0.408	0.407	0.402	0.395	0.385	0.374	0.362	0.35	0.338	0.326	0.314	0.268	0.237	0.218	
0.220	0.39	0.389	0.386	0.382	0.376	0.37	0.363	0.355	0.348	0.341	0.334	0.303	0.28	0.263	
0.257	0.371	0.371	0.37	0.369	0.368	0.366	0.362	0.359	0.356	0.355	0.353	0.337	0.323	0.307	
0.294	0.353	0.353	0.354	0.356	0.358	0.361	0.361	0.362	0.364	0.369	0.37	0.37	0.362	0.35	
0.331	0.335	0.336	0.338	0.343	0.348	0.355	0.36	0.366	0.372	0.38	0.385	0.4	0.397	0.393	
0.367	0.317	0.318	0.322	0.329	0.338	0.348	0.359	0.369	0.379	0.39	0.399	0.428	0.428	0.435	
0.404	0.298	0.3	0.306	0.315	0.327	0.341	0.355	0.37	0.384	0.398	0.41	0.454	0.464	0.474	
0.441	0.28	0.282	0.289	0.301	0.315	0.332	0.35	0.368	0.386	0.403	0.418	0.475	0.508	0.51	
0.478	0.262	0.264	0.272	0.286	0.302	0.322	0.343	0.364	0.385	0.405	0.423	0.493	0.55	0.543	
0.514	0.244	0.246	0.255	0.27	0.289	0.31	0.333	0.357	0.381	0.403	0.424	0.505	0.575	0.571	
0.551	0.225	0.228	0.238	0.254	0.274	0.297	0.322	0.348	0.374	0.398	0.421	0.512	0.58	0.594	
0.588	0.207	0.21	0.22	0.237	0.258	0.282	0.309	0.336	0.363	0.389	0.414	0.513	0.576	0.61	
0.624	0.189	0.191	0.202	0.219	0.24	0.266	0.293	0.321	0.349	0.376	0.402	0.506	0.57	0.616	
0.661	0.17	0.173	0.184	0.2	0.222	0.247	0.275	0.303	0.331	0.359	0.385	0.493	0.563	0.614	
0.698	0.152	0.155	0.165	0.181	0.202	0.227	0.254	0.281	0.309	0.336	0.362	0.471	0.547	0.601	
0.735	0.133	0.136	0.146	0.161	0.181	0.205	0.23	0.257	0.283	0.31	0.335	0.441	0.518	0.575	
0.771	0.115	0.117	0.126	0.141	0.159	0.181	0.204	0.229	0.254	0.278	0.302	0.403	0.478	0.536	
0.808	0.097	0.099	0.107	0.119	0.136	0.155	0.176	0.198	0.221	0.243	0.264	0.356	0.427	0.483	
0.845	0.078	0.08	0.087	0.098	0.112	0.128	0.146	0.165	0.184	0.203	0.221	0.302	0.365	0.416	
0.882	0.06	0.061	0.066	0.075	0.086	0.099	0.114	0.129	0.144	0.159	0.174	0.239	0.291	0.334	
0.900	0.05	0.052	0.056	0.064	0.073	0.084	0.097	0.11	0.123	0.136	0.148	0.205	0.25	0.288	

continued...

h	h^2/Dt													
	6	7	8	9	10	11	12	13	14	16	18	20	22	24
0.000	0.016	0.018	0.016	0.012	0.009	0.006	0.004	0.002	0.001	0	0.001	0.001	0	0
0.037	0.044	0.042	0.04	0.039	0.038	0.037	0.037	0.036	0.036	0.036	0.037	0.037	0.037	0.037
0.073	0.077	0.072	0.071	0.07	0.07	0.07	0.071	0.071	0.072	0.073	0.073	0.073	0.074	0.074
0.110	0.115	0.108	0.106	0.105	0.105	0.106	0.106	0.107	0.108	0.109	0.109	0.11	0.11	0.11
0.147	0.158	0.15	0.146	0.144	0.143	0.143	0.143	0.143	0.144	0.145	0.146	0.146	0.146	0.147
0.184	0.204	0.195	0.189	0.185	0.183	0.182	0.181	0.181	0.181	0.181	0.182	0.182	0.183	0.183
0.220	0.25	0.24	0.232	0.227	0.223	0.221	0.219	0.218	0.217	0.217	0.218	0.219	0.219	0.22
0.257	0.294	0.284	0.275	0.269	0.263	0.26	0.257	0.256	0.255	0.254	0.254	0.255	0.255	0.256
0.294	0.339	0.328	0.318	0.311	0.305	0.3	0.297	0.295	0.293	0.291	0.291	0.291	0.291	0.292
0.331	0.383	0.372	0.362	0.353	0.347	0.342	0.338	0.335	0.332	0.329	0.328	0.328	0.328	0.328
0.367	0.426	0.417	0.407	0.396	0.391	0.385	0.38	0.376	0.373	0.368	0.366	0.365	0.364	0.364
0.404	0.469	0.461	0.452	0.44	0.436	0.429	0.423	0.419	0.415	0.409	0.405	0.403	0.402	0.401
0.441	0.509	0.504	0.497	0.486	0.481	0.475	0.468	0.463	0.458	0.451	0.446	0.443	0.44	0.439
0.478	0.547	0.545	0.54	0.533	0.527	0.521	0.515	0.509	0.504	0.495	0.489	0.484	0.48	0.478
0.514	0.58	0.583	0.581	0.577	0.572	0.567	0.561	0.556	0.55	0.541	0.534	0.528	0.523	0.519
0.551	0.609	0.616	0.619	0.619	0.616	0.612	0.608	0.603	0.598	0.589	0.581	0.574	0.568	0.563
0.588	0.631	0.644	0.651	0.655	0.655	0.654	0.652	0.649	0.645	0.637	0.629	0.622	0.616	0.61
0.624	0.645	0.663	0.676	0.684	0.688	0.69	0.691	0.69	0.689	0.684	0.678	0.671	0.665	0.659
0.661	0.649	0.674	0.692	0.705	0.714	0.721	0.725	0.728	0.729	0.728	0.725	0.721	0.716	0.711
0.698	0.641	0.671	0.695	0.713	0.727	0.738	0.747	0.753	0.758	0.763	0.765	0.764	0.762	0.759
0.735	0.619	0.654	0.682	0.705	0.724	0.74	0.753	0.764	0.772	0.785	0.794	0.799	0.802	0.803
0.771	0.582	0.621	0.653	0.68	0.704	0.724	0.742	0.757	0.77	0.791	0.807	0.82	0.829	0.835
0.808	0.529	0.568	0.602	0.632	0.658	0.681	0.701	0.72	0.736	0.764	0.786	0.804	0.819	0.831
0.845	0.459	0.496	0.53	0.559	0.586	0.61	0.631	0.651	0.669	0.7	0.727	0.75	0.769	0.785
0.882	0.372	0.405	0.435	0.462	0.487	0.51	0.531	0.55	0.569	0.602	0.631	0.656	0.679	0.7
0.900	0.322	0.352	0.379	0.404	0.428	0.449	0.469	0.488	0.506	0.539	0.568	0.595	0.62	0.642

continued...

h	h^2/Dt												
	26	28	30	32	34	36	38	40	42	44	46	48	50
0.000	0	0	0	0	0	0	0	0	0	0	0	0	0
0.037	0.037	0.037	0.037	0.037	0.037	0.037	0.037	0.037	0.037	0.037	0.037	0.037	0.037
0.073	0.074	0.073	0.073	0.073	0.073	0.073	0.073	0.073	0.073	0.073	0.073	0.073	0.073
0.110	0.11	0.11	0.11	0.11	0.11	0.11	0.11	0.11	0.11	0.11	0.11	0.11	0.11
0.147	0.147	0.147	0.147	0.147	0.147	0.147	0.147	0.147	0.147	0.147	0.147	0.147	0.147
0.184	0.183	0.184	0.184	0.184	0.184	0.184	0.184	0.184	0.184	0.184	0.184	0.184	0.184
0.220	0.22	0.22	0.22	0.22	0.22	0.22	0.221	0.221	0.22	0.22	0.22	0.22	0.22
0.257	0.256	0.257	0.257	0.257	0.257	0.257	0.257	0.257	0.257	0.257	0.257	0.257	0.257
0.294	0.292	0.293	0.293	0.293	0.294	0.294	0.294	0.294	0.294	0.294	0.294	0.294	0.294
0.331	0.329	0.329	0.329	0.33	0.33	0.33	0.33	0.33	0.331	0.331	0.331	0.331	0.331
0.367	0.365	0.365	0.365	0.365	0.366	0.366	0.367	0.367	0.367	0.367	0.367	0.367	0.367
0.404	0.401	0.401	0.402	0.402	0.402	0.403	0.403	0.403	0.403	0.404	0.404	0.404	0.404
0.441	0.438	0.438	0.438	0.438	0.438	0.439	0.439	0.439	0.439	0.44	0.44	0.44	0.44
0.478	0.476	0.475	0.475	0.474	0.474	0.475	0.475	0.475	0.475	0.476	0.476	0.476	0.476
0.514	0.517	0.515	0.513	0.512	0.512	0.512	0.511	0.511	0.512	0.512	0.512	0.512	0.512
0.551	0.559	0.556	0.554	0.552	0.551	0.55	0.549	0.548	0.548	0.548	0.548	0.548	0.548
0.588	0.605	0.601	0.597	0.594	0.592	0.59	0.588	0.587	0.587	0.586	0.585	0.585	0.585
0.624	0.654	0.649	0.644	0.64	0.637	0.634	0.632	0.63	0.628	0.626	0.625	0.624	0.623
0.661	0.705	0.7	0.695	0.69	0.686	0.682	0.679	0.675	0.673	0.67	0.668	0.666	0.664
0.698	0.755	0.751	0.747	0.743	0.738	0.735	0.731	0.727	0.724	0.721	0.718	0.715	0.713
0.735	0.802	0.801	0.799	0.797	0.794	0.792	0.789	0.786	0.783	0.78	0.777	0.775	0.772
0.771	0.84	0.843	0.845	0.846	0.847	0.846	0.845	0.844	0.843	0.841	0.839	0.837	0.834
0.808	0.84	0.848	0.854	0.859	0.863	0.866	0.868	0.869	0.87	0.87	0.87	0.87	0.869
0.845	0.8	0.812	0.823	0.832	0.84	0.846	0.852	0.857	0.862	0.865	0.869	0.871	0.874
0.882	0.718	0.735	0.75	0.764	0.777	0.788	0.799	0.809	0.818	0.826	0.833	0.84	0.847
0.900	0.662	0.681	0.699	0.715	0.731	0.745	0.758	0.77	0.782	0.793	0.803	0.813	0.822

Fixed

Hoop tension coefficients (C_t) for circular reservoirs walls with a fixed base, free top and a hydrostatic load only, as a function of reservoir height. Top of wall at $h=0$. From Hussain and Gupta (2018).

h	h^2/Dt													
	0.4	0.8	1.2	1.6	2	3	4	5	6	8	10	12	14	16
0.000	0.152	0.059	0.05	0.027	0.041	0.042	0.029	0.019	0.009	0	0	0	0	0
0.037	0.134	0.024	0.046	0.056	0.074	0.08	0.07	0.059	0.05	0.039	0.036	0.061	0.036	0.036
0.073	0.117	0.008	0.052	0.083	0.105	0.118	0.11	0.1	0.09	0.078	0.074	0.109	0.072	0.072
0.110	0.102	0.007	0.066	0.109	0.134	0.154	0.15	0.141	0.131	0.118	0.112	0.147	0.108	0.108
0.147	0.087	0.015	0.085	0.132	0.161	0.189	0.189	0.183	0.172	0.158	0.151	0.178	0.145	0.145
0.184	0.074	0.028	0.103	0.153	0.186	0.222	0.227	0.223	0.214	0.2	0.19	0.207	0.182	0.181
0.220	0.061	0.041	0.12	0.172	0.208	0.253	0.264	0.263	0.255	0.241	0.23	0.237	0.22	0.219
0.257	0.05	0.051	0.132	0.187	0.227	0.28	0.299	0.301	0.296	0.284	0.271	0.27	0.259	0.257
0.294	0.04	0.06	0.142	0.2	0.244	0.305	0.332	0.337	0.336	0.326	0.313	0.307	0.299	0.296
0.331	0.031	0.067	0.149	0.21	0.257	0.327	0.361	0.371	0.375	0.368	0.355	0.347	0.34	0.335
0.367	0.023	0.072	0.154	0.217	0.267	0.344	0.387	0.402	0.411	0.408	0.398	0.389	0.382	0.375
0.404	0.015	0.076	0.157	0.221	0.272	0.357	0.408	0.43	0.443	0.447	0.441	0.433	0.425	0.418
0.441	0.008	0.079	0.158	0.222	0.274	0.366	0.424	0.453	0.472	0.484	0.482	0.476	0.468	0.462
0.478	0.004	0.079	0.156	0.219	0.272	0.369	0.435	0.47	0.495	0.517	0.521	0.519	0.512	0.508
0.514	0.002	0.074	0.151	0.213	0.266	0.366	0.439	0.48	0.512	0.544	0.556	0.558	0.554	0.552
0.551	0.003	0.066	0.144	0.204	0.256	0.358	0.436	0.482	0.521	0.563	0.585	0.593	0.594	0.594
0.588	0.005	0.057	0.135	0.192	0.242	0.344	0.425	0.476	0.521	0.574	0.606	0.621	0.629	0.631
0.624	0.007	0.053	0.123	0.177	0.225	0.324	0.407	0.461	0.511	0.574	0.617	0.641	0.656	0.664
0.661	0.007	0.052	0.111	0.159	0.204	0.299	0.381	0.436	0.49	0.561	0.614	0.647	0.67	0.686
0.698	0.007	0.051	0.097	0.139	0.179	0.268	0.347	0.402	0.457	0.534	0.595	0.636	0.668	0.691
0.735	0.006	0.046	0.082	0.118	0.153	0.232	0.305	0.358	0.412	0.491	0.556	0.604	0.644	0.673
0.771	0.006	0.037	0.066	0.096	0.126	0.193	0.258	0.306	0.356	0.433	0.5	0.551	0.597	0.63
0.808	0.005	0.027	0.051	0.074	0.098	0.152	0.206	0.248	0.292	0.362	0.426	0.478	0.526	0.561
0.845	0.004	0.017	0.036	0.053	0.071	0.111	0.153	0.186	0.223	0.282	0.338	0.385	0.431	0.465
0.882	0.003	0.011	0.023	0.034	0.046	0.072	0.101	0.124	0.151	0.193	0.237	0.274	0.312	0.342
0.900	0.002	0.009	0.017	0.025	0.034	0.054	0.076	0.093	0.114	0.147	0.182	0.212	0.242	0.269

continued...

h	h^2/Dt						
	20	25	30	35	40	45	50
0.000	0	0	0	0	0	0	0
0.037	0.037	0.037	0.037	0.037	0.037	0.037	0.037
0.073	0.073	0.074	0.073	0.073	0.073	0.073	0.073
0.110	0.109	0.11	0.11	0.11	0.11	0.11	0.11
0.147	0.145	0.147	0.147	0.147	0.147	0.147	0.147
0.184	0.182	0.183	0.184	0.184	0.184	0.184	0.184
0.220	0.218	0.219	0.22	0.22	0.22	0.22	0.22
0.257	0.255	0.256	0.257	0.257	0.257	0.257	0.257
0.294	0.293	0.292	0.293	0.293	0.294	0.294	0.294
0.331	0.33	0.328	0.329	0.329	0.33	0.33	0.331
0.367	0.369	0.365	0.365	0.366	0.367	0.367	0.368
0.404	0.408	0.403	0.402	0.402	0.403	0.403	0.404
0.441	0.45	0.442	0.44	0.439	0.439	0.439	0.44
0.478	0.493	0.483	0.478	0.476	0.476	0.476	0.476
0.514	0.537	0.526	0.519	0.515	0.514	0.512	0.512
0.551	0.583	0.571	0.562	0.556	0.553	0.55	0.55
0.588	0.627	0.617	0.607	0.6	0.594	0.59	0.589
0.624	0.668	0.663	0.655	0.647	0.64	0.633	0.63
0.661	0.701	0.705	0.701	0.694	0.687	0.68	0.675
0.698	0.72	0.737	0.741	0.74	0.735	0.729	0.724
0.735	0.719	0.751	0.768	0.777	0.779	0.779	0.777
0.771	0.692	0.74	0.772	0.793	0.805	0.814	0.818
0.808	0.634	0.696	0.74	0.774	0.796	0.816	0.827
0.845	0.541	0.609	0.662	0.705	0.736	0.766	0.787
0.882	0.406	0.471	0.525	0.572	0.609	0.647	0.676
0.900	0.322	0.38	0.431	0.477	0.515	0.555	0.589

C. Appendix C

C.1 Table of reinforcing areas

Table of reinforcing areas (mm^2/m), based on bar diameter and c/c spacings.

Bar Spacing (mm)	Bar Diameter (mm)				
	12	16	20	25	32
250	452	804	1257	1963	3217
225	503	894	1396	2182	3574
200	565	1005	1571	2454	4021
175	646	1149	1795	2805	4596
150	754	1340	2094	3272	5362
125	905	1608	2513	3927	6434
100	1131	2011	3142	4909	8042
75	1508	2681	4189	6545	10723

D. Appendix D

D.1 Values of h^*

The table below gives values of h^* (or h_D) for use in the hydraulic ratio, (h^*/t) (or h_D/h), as a function of the h^2/Dt ratio of the reservoir. Values are given for either a pinned/hinged or a fixed base restraint condition and free at the top of the wall. The h^* value is given as a fraction of the wall height, down from the top of the wall. The h^* value is given, assuming that most cracks will form at the point of maximum hoop tension and that the height of retained water and the total wall height are synonymous.

Values of h^* , as a fraction of the wall height, down from the top of the wall. Given for various h^2/Dt ratios for pinned or fixed wall base restraint conditions.

h^2/Dt	h^* from top of wall		h^2/Dt	h^* from top of wall	
	Pinned	Fixed		Pinned	Fixed
1	0	0.478	17	0.771	0.698
2	0.514	0.459	18	0.771	0.698
3	0.588	0.478	19	0.771	0.716
4	0.551	0.514	20	0.771	0.716
5	0.643	0.551	21	0.771	0.716
6	0.661	0.569	22	0.79	0.716
7	0.68	0.588	23	0.79	0.735
8	0.698	0.606	24	0.79	0.735
9	0.698	0.624	25	0.79	0.735
10	0.716	0.643	26	0.79	0.753
11	0.716	0.643	27	0.79	0.753
12	0.735	0.661	28	0.79	0.753
13	0.735	0.68	29	0.79	0.753
14	0.753	0.68	30	0.79	0.753
15	0.753	0.68	31	0.808	0.753
16	0.753	0.698	32-50	0.808	0.771

E. Appendix E

E.1 Recommendations of target crack width

A complete recommendation of the results from this research are presented here in a concise form. Two sets of recommendations are presented: Recommendations of target crack width, w_t , as a function of hydraulic ratio, h^*/t (h_D/h in EN 1992-3), and recommendations of w_t as a function of the ratio between the maximum applied tension force and the mean concrete tensile resistance force in the reservoir wall, $T_{max}/T_{r,m}$.

Both of these recommendations are based on a probabilistic analysis of SLS leakage in typical above-ground, round, tension-governed reservoirs that retain potable water, sewage or a similar water-based substance that facilitates self-sealing in concrete. The analysis assumes a pinned connection between the wall and the foundation, and assumes no structural connection to the roof (no restraint at the top). It does not consider the presence of backfill on the walls. The analysis is based on the Model Code 2010 crack prediction model and uses the long term (50 year) design procedure in MC 2010 to calculate reinforcing to satisfy the specified target crack widths ranging from $0.05 - 0.2\text{mm}$. Furthermore, it only assesses reservoirs that are in the stabilized cracking state. It performs numerous Monte Carlo analyses of the reservoirs, considering a short term (28 day) state of cracking (at water tightness test stage). It defines reliability in terms of the leakage experienced at the end of a water tightness test performed soon after construction, compared to the allowable leakage, as specified in the recommendations. It assumes a target, irreversible SLS reliability level of $\beta = 1.5$, which corresponds to a reservoir that does not experience unacceptable leakage, with a mean non-exceedance probability of 93.4%.

The recommendations consider the autogenous self-sealing that occurs in the concrete and the effect it has on the reduction of crack widths and the subsequent reduction in leakage over time. It does not consider the state of the reservoir in the long term, nor does it consider the effect of dynamic cracks. However, from the results, $> 90\%$ of the total leakage from the cracks takes place by the end of the water tightness test, which gives confidence that the recommendations are appropriate for long performance as well.

E.1.1 Leakage regimes and water tightness test criterion

The specification of the various leakage regimes and water tightness test criteria are applicable to both sets of recommendations. Designers have a choice between four leakage regimes, varying in stabilization period and water tightness test duration, C_{0d7d} to C_{14d21d} . Quicker water tightness tests require more stringent w_t values, whereas longer ones require less strict w_t values, due to the increased time available for self-sealing and flow reduction to take place. In projects where time is of the essence, or where preliminary and general costs are high, the cost savings of a shorter stabilization period and water tightness test may outweigh the extra costs incurred in providing extra reinforcing to satisfy

a more stringent crack width. In projects where time is not a concern or where passing the water tightness test is not on the critical path of a project, a longer leakage regime will provide material savings in reinforcement.

Each leakage regime has an initial stabilization period where the concrete is given the chance to absorb water and for self-sealing to occur. Leakage is only measured from the start of the water tightness test. All leakage regimes have an acceptable leakage of 0.2% of the reservoir volume, which corresponds to the BS 8007 criterion of $d/500$, where d is the depth of retained water. If the leakage experienced by the reservoir is less than the allowable leakage at the end of the water tightness test, then the reservoir is deemed to be "water tight", and conversely as not water tight if the leakage is greater than the allowable. The stabilization period, water tightness test times and allowable leakage criterion are shown in the table below:

Leakage regime, stabilization period and water tightness test criterion.

Leakage regime	Stabilization period		Water tightness test		Allowable leakage
	Start (day)	End (day)	Start (day)	End (day)	
C_{0d7d}	0	0	0	7	0.2% of volume
C_{3d8d}	0	3	3	8	
C_{7d14d}	0	7	7	14	
C_{14d21d}	0	14	14	21	

E.1.2 Recommendations of w_t as a function of h^*/t

The recommendations of w_t as a function of h^*/t from this research are shown in the table below. The analysis was performed for an h^*/d range of 12-26. Ratios other than this were unable to be realised, as reservoirs with ratios of $h^*/t < \approx 12$ did not reach the stabilized cracking stage and ratios over 26 were realised, given the choice of constraints placed on reservoir geometries to ensure sensible only geometries were realised. Thus, the results are only valid for $12 \leq h^*/t \leq 26$. The results of the analysis of w_t vs $T_{max}/T_{r,m}$ give an indication that the extrapolation of these recommendations to the $h^*/t < 12$ range would give conservative w_t values, however, the use thereof is left up to the discretion of the reader.

Table E.1: Summary of recommendations of target crack widths for round, reinforced concrete reservoirs in the stabilized cracking stage as a function of hydraulic ratio, h^*/t , for $\beta=1.5$.

Leakage regime	h^*/t^\dagger range	w_t (mm)	w_t (mm) interp. [‡]
C_{0d7d}	12 → 26	0.13 → 0.11	$0.145 - 0.05 \cdot \frac{x}{35}$
C_{3d8d}	12 → 26	0.155 → 0.13	$0.17 - 0.05 \cdot \frac{x}{35}$
C_{7d14d}	12 → 26	0.165 → 0.145	$0.18 - 0.045 \cdot \frac{x}{35}$
C_{14d21d}	12 → 26	0.18 → 0.165	$0.2 - 0.045 \cdot \frac{x}{35}$

[†]See Appendix D for h^* values.

[‡]For interpolation; x refers to the desired h^*/t ratio.

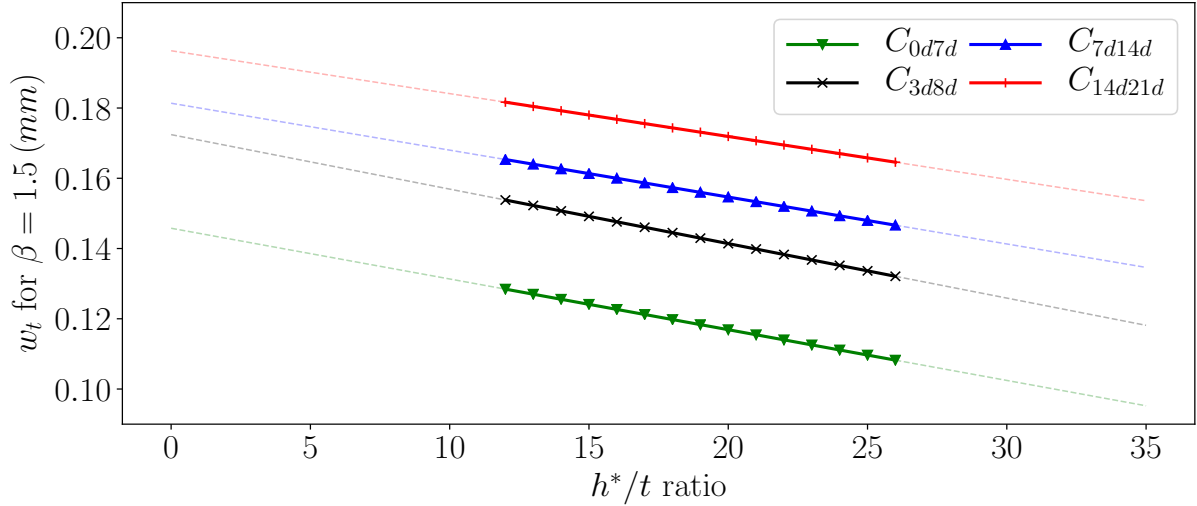


Figure E.1: Recommended target crack width for $\beta=1.5$ vs h^*/t for $12 \leq h^*/t < 27$.

E.1.3 Recommendations of w_t as a function of $T_{max}/T_{r,m}$

An alternative specification of w_t is in relation to the $T_{max}/T_{r,m}$ ratio. As the maximum applied tension in the wall progressively exceeds the mean tensile resistance force of the concrete, more cracks form and their lengths increase and subsequently, leak. Conversely, as T_{max} reduces below $T_{r,m}$, fewer and fewer cracks form. The $T_{max}/T_{r,m}$ ratio is indirectly linked to the h^*/t ratio, as both are dependent on the height of retained water in the reservoir. The recommendations are shown in the table below and are similarly valid for range of $12 \leq h^*/t \leq 26$.

Table E.2: Summary of recommendations of target crack widths for round, reinforced concrete reservoirs in the stabilized cracking stage as a function of $T_{max}/T_{r,m}$ ratio, for $\beta=1.5$

Leakage regime	$T_{max}/T_{r,m}$	w_t (mm)	w_t (mm) interp [†]
C_{0d7d}	0.925 → 1.25	0.135 → 0.05	$0.135 - 0.262 \cdot (x - 0.925)$
C_{3d8d}	0.925 → 1.25	0.180 → 0.08	$0.18 - 0.308 \cdot (x - 0.925)$
C_{7d14d}	0.925 → 1.25	0.190 → 0.10	$0.19 - 0.277 \cdot (x - 0.925)$
C_{14d21d}	0.925 → 1.25	0.200 → 0.13	$0.2 - 0.215 \cdot (x - 0.925)$

[†]For interpolation; x refers to the desired $T_{max}/T_{r,m}$ ratio.

The recommendations are both given for $\beta=1.5$ and should give the same mean achieved reliability, over a range of reservoirs, however, the recommendations of w_t vs $T_{max}/T_{r,m}$ were shown to have less variation than those for w_t vs h^*/t . The reliability obtained through the use of the former will more consistently be closer to $\beta=1.5$.

F. Appendix F

This appendix details the experimental samples compiled from various researchers for the characterization of the initial flow prediction model factor and the leakage accumulation factor. Note that initial flow rate is given in $m\ell/min$ and crack widths are given in mm .

F.1 Initial flow prediction database

Roig-Flores *et al.* (2016)

Init-Flow	w	$\Delta p(m)$	$\ell (mm)$	$d (m)$	Init-Flow	w	$\Delta p(m)$	$\ell (mm)$	$d (m)$
59.16	0.10	20.50	75.00	0.15	23.72	0.10	20.50	75.00	0.15
55.58	0.12	20.50	75.00	0.15	29.32	0.10	20.50	75.00	0.15
39.38	0.09	20.50	75.00	0.15	164.72	0.12	20.50	75.00	0.15
60.32	0.11	20.50	75.00	0.15	84.76	0.09	20.50	75.00	0.15
546.66	0.18	20.50	75.00	0.15	34.88	0.08	20.50	75.00	0.15
18.56	0.16	20.50	75.00	0.15	178.68	0.10	20.50	75.00	0.15
328.92	0.15	20.50	75.00	0.15	19.60	0.13	20.50	75.00	0.15
208.66	0.16	20.50	75.00	0.15	23.48	0.09	20.50	75.00	0.15
42.12	0.11	20.50	75.00	0.15	77.78	0.13	20.50	75.00	0.15
38.22	0.11	20.50	75.00	0.15	51.22	0.10	20.50	75.00	0.15
5.76	0.11	20.50	75.00	0.15	79.10	0.09	20.50	75.00	0.15
40.16	0.07	20.50	75.00	0.15	1082	0.239	20.50	75.00	0.15
48.62	0.09	20.50	75.00	0.15	767	0.165	20.50	75.00	0.15
39	0.097	20.50	75.00	0.15	505	0.116	20.50	75.00	0.15
90	0.121	20.50	75.00	0.15	642	0.165	20.50	75.00	0.15
945	0.347	20.50	75.00	0.15	39	0.099	20.50	75.00	0.15
448	0.425	20.50	75.00	0.15	72	0.101	20.50	75.00	0.15
76	0.106	20.50	75.00	0.15	1104	0.302	20.50	75.00	0.15
47	0.106	20.50	75.00	0.15	324	0.171	20.50	75.00	0.15
690	0.207	20.50	75.00	0.15	359	0.168	20.50	75.00	0.15
389	0.228	20.50	75.00	0.15	818	0.207	20.50	75.00	0.15
928	0.246	20.50	75.00	0.15	837	0.205	20.50	75.00	0.15
1250	0.324	20.50	75.00	0.15	2433	0.309	20.50	75.00	0.15
9	0.078	20.50	75.00	0.15	1694	0.302	20.50	75.00	0.15
543	0.264	20.50	75.00	0.15	1120	0.244	20.50	75.00	0.15
237	0.259	20.50	75.00	0.15	238	0.185	20.50	75.00	0.15
302	0.336	20.50	75.00	0.15	29	0.114	20.50	75.00	0.15
229	0.130	20.50	75.00	0.15	278	0.161	20.50	75.00	0.15
471	0.223	20.50	75.00	0.15	316	0.186	20.50	75.00	0.15
4231	0.336	20.50	75.00	0.15	319	0.158	20.50	75.00	0.15
420	0.213	20.50	75.00	0.15	857	0.204	20.50	75.00	0.15
398	0.164	20.50	75.00	0.15	1241	0.218	20.50	75.00	0.15
43	0.109	20.50	75.00	0.15	75	0.148	20.50	75.00	0.15
92	0.096	20.50	75.00	0.15	158	0.160	20.50	75.00	0.15
534	0.230	20.50	75.00	0.15	498	0.195	20.50	75.00	0.15
1395	0.229	20.50	75.00	0.15	33	0.085	20.50	75.00	0.15
742	0.224	20.50	75.00	0.15	878	0.226	20.50	75.00	0.15

630	0.195	20.50	75.00	0.15	308	0.260	20.50	75.00	0.15
1380	0.317	20.50	75.00	0.15	34	0.094	20.50	75.00	0.15
328	0.168	20.50	75.00	0.15	231	0.148	20.50	75.00	0.15
98	0.207	20.50	75.00	0.15	43	0.111	20.50	75.00	0.15
1116	0.249	20.50	75.00	0.15	33	0.110	20.50	75.00	0.15
2454	0.303	20.50	75.00	0.15	622	0.170	20.50	75.00	0.15
47	0.112	20.50	75.00	0.15	1165	0.333	20.50	75.00	0.15
329	0.178	20.50	75.00	0.15	109	0.145	20.50	75.00	0.15
846	0.211	20.50	75.00	0.15	131	0.152	20.50	75.00	0.15
174	0.197	20.50	75.00	0.15	173	0.141	20.50	75.00	0.15
44	0.099	20.50	75.00	0.15	481	0.184	20.50	75.00	0.15
801	0.194	20.50	75.00	0.15	471	0.140	20.50	75.00	0.15
296	0.126	20.50	75.00	0.15	958	0.191	20.50	75.00	0.15
220	0.145	20.50	75.00	0.15	2096	0.304	20.50	75.00	0.15
340	0.160	20.50	75.00	0.15	324	0.259	20.50	75.00	0.15
457	0.170	20.50	75.00	0.15	949	0.207	20.50	75.00	0.15
504	0.141	20.50	75.00	0.15	529	0.310	20.50	75.00	0.15
406	0.269	20.50	75.00	0.15	277	0.161	20.50	75.00	0.15
1396	0.240	20.50	75.00	0.15	424	0.179	20.50	75.00	0.15
1633	0.210	20.50	75.00	0.15	517	0.187	20.50	75.00	0.15
1255	0.233	20.50	75.00	0.15	3546	0.447	20.50	75.00	0.15
851	0.276	20.50	75.00	0.15	597	0.208	20.50	75.00	0.15
724	0.224	20.50	75.00	0.15	776	0.168	20.50	75.00	0.15
334	0.200	20.50	75.00	0.15	803	0.336	20.50	75.00	0.15
1047	0.224	20.50	75.00	0.15	288	0.112	20.50	75.00	0.15
323	0.160	20.50	75.00	0.15	290	0.211	20.50	75.00	0.15
1747	0.325	20.50	75.00	0.15	972	0.251	20.50	75.00	0.15
184	0.143	20.50	75.00	0.15	3719	0.506	20.50	75.00	0.15
1172	0.346	20.50	75.00	0.15	1241	0.340	20.50	75.00	0.15
479	0.297	20.50	75.00	0.15	76	0.163	20.50	75.00	0.15
417	0.183	20.50	75.00	0.15	712	0.411	20.50	75.00	0.15
55	0.169	20.50	75.00	0.15	45	0.121	20.50	75.00	0.15
165	0.164	20.50	75.00	0.15	452	0.288	20.50	75.00	0.15
442	0.239	20.50	75.00	0.15	506	0.177	20.50	75.00	0.15
1624	0.301	20.50	75.00	0.15	257	0.135	20.50	75.00	0.15
505	0.180	20.50	75.00	0.15	1871	0.333	20.50	75.00	0.15
731	0.203	20.50	75.00	0.15	586	0.214	20.50	75.00	0.15
1875	0.382	20.50	75.00	0.15	100	0.119	20.50	75.00	0.15
3739	0.384	20.50	75.00	0.15	240	0.231	20.50	75.00	0.15
1679	0.299	20.50	75.00	0.15	242	0.135	20.50	75.00	0.15
621	0.150	20.50	75.00	0.15	215	0.126	20.50	75.00	0.15
264	0.162	20.50	75.00	0.15	430	0.167	20.50	75.00	0.15
860	0.316	20.50	75.00	0.15	679	0.190	20.50	75.00	0.15
224	0.166	20.50	75.00	0.15	485	0.251	20.50	75.00	0.15
260	0.125	20.50	75.00	0.15	350	0.209	20.50	75.00	0.15
368	0.180	20.50	75.00	0.15	1078	0.240	20.50	75.00	0.15
74	0.134	20.50	75.00	0.15	604	0.19	20.50	75.00	0.15

Ramm and Biscopig (1997)

Init-Flow	w	$\Delta p(m)$	$\ell (m)$	$d (m)$	Init-Flow	w	$\Delta p(m)$	$\ell (m)$	$d (m)$
3.2	0.090	2.5	0.3	1	6033.3	0.203	12	0.18	1
21.7	0.100	12	0.6	1	189.2	0.210	2.5	0.3	1
138.3	0.100	12	0.3	1	399.3	0.210	12	0.6	1
27.0	0.100	12	0.6	1	114.7	0.210	2.5	0.6	1
4.3	0.110	2.5	0.3	1	688.2	0.211	12	0.3	1
3.2	0.110	2.5	0.6	1	676.7	0.220	12	0.3	1
104.0	0.111	12	0.3	1	89.8	0.220	2.5	0.6	1
5.2	0.120	2.5	0.3	1	724.4	0.220	12	0.6	1
112.2	0.120	12	0.3	1	748.3	0.230	12	0.3	1
2.2	0.120	2.5	0.6	1	2023.2	0.299	2.5	0.18	1
3.2	0.120	2.5	0.6	1	7966.7	0.300	12	0.18	1
70.0	0.130	12	0.6	1	3333.3	0.300	2.5	0.18	1
181.7	0.181	2.5	0.3	1	2033.3	0.301	2.5	0.18	1
130.5	0.190	2.5	0.3	1	8766.7	0.301	12	0.18	1
101.2	0.190	2.5	0.6	1	11466	0.302	12	0.18	1
228.3	0.190	12	0.6	1	3250.0	0.380	2.5	0.3	1
8950.0	0.198	12	0.18	1	1990.4	0.390	2.5	0.3	1
1466.7	0.199	2.5	0.18	1	2924.5	0.399	2.5	0.18	1
1900.0	0.201	2.5	0.18	1	4133.3	0.400	2.5	0.18	1
4233.3	0.201	12	0.18	1	2839.2	0.400	2.5	0.3	1
1193.3	0.202	2.5	0.18	1	3266.7	0.401	2.5	0.18	1

Note: Results reported in flow per meter crack.

Palin *et al.* (2015) and Palin *et al.* (2017)

Init-Flow	w	$\Delta p(m)$	$\ell (m)$	$d (m)$	Init-Flow	w	$\Delta p(m)$	$\ell (m)$	$d (m)$
27.5	0.201	1	0.034	0.06	158.1	0.398	1	0.034	0.06
80.3	0.201	1	0.034	0.06	212.5	0.398	1	0.034	0.06
60.7	0.201	1	0.034	0.06	169.5	0.398	1	0.034	0.06
17.4	0.203	1	0.034	0.06	181.5	0.398	1	0.034	0.06
41.3	0.201	1	0.034	0.06	164.4	0.401	1	0.034	0.06
64.9	0.201	1	0.034	0.06	173.8	0.401	1	0.034	0.06
14.5	0.206	1	0.034	0.06	223.0	0.401	1	0.034	0.06
21.1	0.201	1	0.034	0.06	269.6	0.401	1	0.034	0.06
152.3	0.399	1	0.034	0.06	125.9	0.401	1	0.034	0.06
192.1	0.399	1	0.034	0.06	152.0	0.401	1	0.034	0.06
163.6	0.400	1	0.034	0.06	196.8	0.401	1	0.034	0.06
227.2	0.398	1	0.034	0.06	151.8	0.401	1	0.034	0.06

Azarsa *et al.* (2018)

Init-Flow	w	$\Delta p(m)$	$\ell(m)$	$d(m)$
69.6	0.258	1.5	0.1	0.2
189.1	0.28	1.5	0.1	0.15
25	0.195	1.5	0.15	0.175
57.5	0.242	1.5	0.1	0.2
193	0.303	1.5	0.1	0.15
29	0.191	1.5	0.15	0.175

Bozorgzadeh (2012)

Init-Flow	w	$\Delta p(m)$	$\ell(m)$	$d(m)$	InitFlow	w	$\Delta p(m)$	$\ell(m)$	$d(m)$
10	0.074	2.34	1.11	0.25	321	0.123	7.18	1.11	0.25
20	0.085	2.34	1.11	0.25	540	0.143	7.18	1.11	0.25
80	0.103	2.34	1.11	0.25	805	0.164	7.18	1.11	0.25
190	0.123	2.34	1.11	0.25	1130	0.182	7.18	1.11	0.25
330	0.143	2.34	1.11	0.25	1560	0.207	7.18	1.11	0.25
540	0.164	2.34	1.11	0.25	1901	0.224	7.18	1.11	0.25
850	0.182	2.34	1.11	0.25	8	0.056	2.34	1.06	0.20
1194	0.207	2.34	1.11	0.25	23	0.088	2.34	1.06	0.20
1600	0.224	2.34	1.11	0.25	67	0.168	2.34	1.06	0.20
10	0.074	4.48	1.11	0.25	312	0.245	2.34	1.06	0.20
34	0.085	4.48	1.11	0.25	832	0.314	2.34	1.06	0.20
110	0.103	4.48	1.11	0.25	14	0.057	4.48	1.06	0.20
256	0.123	4.48	1.11	0.25	25	0.089	4.48	1.06	0.20
400	0.143	4.48	1.11	0.25	119	0.169	4.48	1.06	0.20
652	0.164	4.48	1.11	0.25	428	0.246	4.48	1.06	0.20
1030	0.182	4.48	1.11	0.25	886	0.315	4.48	1.06	0.20
1377	0.207	4.48	1.11	0.25	20	0.058	7.18	1.06	0.20
1710	0.224	4.48	1.11	0.25	28	0.090	7.18	1.06	0.20
10	0.074	7.18	1.11	0.25	180	0.170	7.18	1.06	0.20
47	0.085	7.18	1.11	0.25	636	0.247	7.18	1.06	0.20
140	0.103	7.18	1.11	0.25	1243	0.316	7.18	1.06	0.20

Esgandani (2017)

Init-Flow	w	$\Delta p(m)$	$\ell(m)$	$d(m)$	Init-Flow	w	$\Delta p(m)$	$\ell(m)$	$d(m)$
18.6	0.09	40	0.161	0.05	12600	0.29	40	0.165	0.049
14.4	0.11	40	0.156	0.051	15000	0.33	40	0.164	0.0485
12.6	0.110	40	0.152	0.05	9000	0.28	40	0.174	0.0505
20.4	0.090	40	0.162	0.0495	13200	0.31	40	0.169	0.051
21	0.110	40	0.156	0.048	8400	0.32	40	0.156	0.0505
15	0.110	40	0.153	0.051	13800	0.3	40	0.168	0.0495
1380	0.21	40	0.165	0.049	66000	0.38	40	0.166	0.051
1860	0.23	40	0.159	0.0495	48000	0.39	40	0.167	0.0485
1200	0.19	40	0.168	0.0505	60000	0.4	40	0.159	0.048
1740	0.18	40	0.154	0.0485	84000	0.43	40	0.171	0.05
1980	0.220	40	0.159	0.051	54000	0.401	40	0.166	0.049
1680	0.190	40	0.16	0.050	66000	0.41	40	0.156	0.0505

Edvardsen (1996)

Init-Flow	w	$\Delta p(m)$	$\ell(m)$	$d(m)$	Init-Flow	w	$\Delta p(m)$	$\ell(m)$	$d(m)$
5.84	0.100	2.5	0.12	0.4	482.5	0.301	5	0.12	0.4
19.16	0.101	2.5	0.12	0.4	354.16	0.300	5	0.12	0.4
39	0.100	5	0.12	0.4	222.16	0.300	5	0.12	0.4
0.24	0.101	5	0.12	0.4	180.5	0.300	5	0.12	0.4
0.28	0.100	5	0.12	0.4	701.34	0.300	10	0.12	0.4
3	0.100	5	0.12	0.4	763.84	0.300	10	0.12	0.4
2.78	0.100	10	0.12	0.4	812.5	0.300	10	0.12	0.2
133.34	0.100	10	0.12	0.4	3.3	0.101	5	0.12	0.4
20.82	0.101	10	0.12	0.2	21.66	0.101	5	0.12	0.4
20.84	0.100	10	0.12	0.2	148.66	0.201	5	0.12	0.4
2	0.101	10	0.12	0.2	107	0.200	5	0.12	0.4
52.84	0.200	10	0.12	0.4	98.66	0.201	5	0.12	0.4
126.34	0.200	2.5	0.12	0.4	60.34	0.200	5	0.12	0.4
76.34	0.200	2.5	0.12	0.4	63.84	0.201	10	0.12	0.4
101.84	0.201	5	0.12	0.4	308.34	0.301	2.5	0.12	0.4
179.16	0.201	5	0.12	0.4	314.66	0.300	2.5	0.12	0.4
180.5	0.201	5	0.12	0.4	45.34	0.101	10	0.12	0.2
45.16	0.201	5	0.12	0.4	100	0.201	2.5	0.12	0.4
2.84	0.200	5	0.12	0.4	79.16	0.201	2.5	0.12	0.4
212.5	0.200	10	0.12	0.4	68.66	0.201	2.5	0.12	0.4
223	0.200	10	0.12	0.2	58.34	0.200	2.5	0.12	0.4
654.54	0.201	10	0.12	0.2	732.66	0.200	15	0.12	0.2
277.84	0.201	10	0.12	0.4	388.84	0.300	2.5	0.12	0.4
354.16	0.201	10	0.12	0.2	272.16	0.301	2.5	0.12	0.4
129.84	0.201	10	0.12	0.4	143	0.300	2.5	0.12	0.4
166.66	0.201	15	0.12	0.2	8.34	0.100	5	0.12	0.4
81.26	0.300	2.5	0.12	0.4	73.66	0.200	5	0.12	0.4
416.66	0.300	2.5	0.12	0.4	161.16	0.201	10	0.12	0.4
741.66	0.301	5	0.12	0.4	166.66	0.201	15	0.12	0.4

F.2 Flow reduction database

The data in this database is given in relative flow with time, $Q(t)/Q_0$, and is therefore unit-less. Crack widths are given in *mm*. The descriptions relate to the nomenclature given to each sample by the researcher and can be ignored.

Nanayakkara and Elakneshwaran (2005)

Time (hrs)	Relative flow	w	Description	h^*/t	Time (hrs)	Relative flow	w	Description	h^*/t
0	1.000	0.073	Sample A1	10	0	1.000	0.086	Sample B1	10
12	0.524	0.073	Sample A1	10	12	0.348	0.086	Sample B1	10
24	0.238	0.073	Sample A1	10	24	0.174	0.086	Sample B1	10
36	0.190	0.073	Sample A1	10	36	0.087	0.086	Sample B1	10
48	0.143	0.073	Sample A1	10	48	0.065	0.086	Sample B1	10
72	0.095	0.073	Sample A1	10	72	0.043	0.086	Sample B1	10
96	0.048	0.073	Sample A1	10	96	0.022	0.086	Sample B1	10
144	0.024	0.073	Sample A1	10	144	0.001	0.086	Sample B1	10
240	0.000	0.073	Sample A1	10	510	0.000	0.086	Sample B1	10
510	0.000	0.073	Sample A1	10					
					0	1.000	0.136	Sample B2	10
0	1.000	0.109	Sample A2	10	12	0.229	0.136	Sample B2	10
12	0.375	0.109	Sample A2	10	24	0.125	0.136	Sample B2	10
24	0.167	0.109	Sample A2	10	36	0.042	0.136	Sample B2	10
36	0.063	0.109	Sample A2	10	48	0.042	0.136	Sample B2	10
48	0.063	0.109	Sample A2	10	72	0.042	0.136	Sample B2	10
72	0.042	0.109	Sample A2	10	96	0.042	0.136	Sample B2	10
96	0.033	0.109	Sample A2	10	144	0.021	0.136	Sample B2	10
144	0.000	0.109	Sample A2	10	240	0.011	0.136	Sample B2	10
510	0.000	0.109	Sample A2	10	510	0.000	0.136	Sample B2	10
0	1.000	0.082	Sample A3	10	0	1.000	0.132	Sample B3	10
12	0.333	0.082	Sample A3	10	12	0.400	0.132	Sample B3	10
24	0.250	0.082	Sample A3	10	24	0.180	0.132	Sample B3	10
36	0.146	0.082	Sample A3	10	36	0.160	0.132	Sample B3	10
48	0.115	0.082	Sample A3	10	48	0.140	0.132	Sample B3	10
72	0.063	0.082	Sample A3	10	72	0.080	0.132	Sample B3	10
96	0.042	0.082	Sample A3	10	96	0.060	0.132	Sample B3	10
144	0.031	0.082	Sample A3	10	144	0.020	0.132	Sample B3	10
240	0.012	0.082	Sample A3	10	240	0.011	0.132	Sample B3	10
510	0.000	0.082	Sample A3	10	510	0.000	0.132	Sample B3	10
0	1.000	0.123	Sample A4	10	0	1.000	0.068	Sample B4	10
12	0.229	0.123	Sample A4	10	12	0.769	0.068	Sample B4	10
24	0.125	0.123	Sample A4	10	24	0.577	0.068	Sample B4	10
36	0.083	0.123	Sample A4	10	36	0.462	0.068	Sample B4	10
48	0.067	0.123	Sample A4	10	48	0.385	0.068	Sample B4	10
72	0.042	0.123	Sample A4	10	72	0.231	0.068	Sample B4	10
96	0.033	0.123	Sample A4	10	96	0.154	0.068	Sample B4	10
144	0.025	0.123	Sample A4	10	144	0.135	0.068	Sample B4	10
240	0.010	0.123	Sample A4	10	240	0.121	0.068	Sample B4	10
510	0.000	0.123	Sample A4	10	510	0.060	0.068	Sample B4	10

Ratnayake and Nanayakkara (2018)

Time (hours)	Relative Flow	w	Description	h^*/t	Time (hours)	Relative Flow	w	Description	h^*/t
0.00	1.000	0.12	0A-0FA	10	0.00	1.000	0.131	3B-30FA	10

0.24	0.946	0.12	0A-0FA	10	0.19	1.000	0.131	3B-30FA	10
0.24	0.885	0.12	0A-0FA	10	0.34	0.976	0.131	3B-30FA	10
0.41	0.843	0.12	0A-0FA	10	0.50	0.959	0.131	3B-30FA	10
0.60	0.800	0.12	0A-0FA	10	0.68	0.937	0.131	3B-30FA	10
0.75	0.757	0.12	0A-0FA	10	0.84	0.941	0.131	3B-30FA	10
0.92	0.732	0.12	0A-0FA	10	1.02	0.926	0.131	3B-30FA	10
1.10	0.591	0.12	0A-0FA	10	1.18	0.942	0.131	3B-30FA	10
1.28	0.686	0.12	0A-0FA	10	1.37	0.890	0.131	3B-30FA	10
1.45	0.657	0.12	0A-0FA	10	1.55	0.939	0.131	3B-30FA	10
1.62	0.645	0.12	0A-0FA	10	1.72	0.907	0.131	3B-30FA	10
1.78	0.627	0.12	0A-0FA	10	1.88	0.898	0.131	3B-30FA	10
1.95	0.611	0.12	0A-0FA	10	2.05	0.874	0.131	3B-30FA	10
2.12	0.581	0.12	0A-0FA	10	2.22	0.888	0.131	3B-30FA	10
2.29	0.622	0.12	0A-0FA	10	2.39	0.877	0.131	3B-30FA	10
3.13	0.518	0.12	0A-0FA	10	2.56	0.906	0.131	3B-30FA	10
3.33	0.507	0.12	0A-0FA	10	3.40	0.855	0.131	3B-30FA	10
3.53	0.470	0.12	0A-0FA	10	3.60	0.810	0.131	3B-30FA	10
3.93	0.469	0.12	0A-0FA	10	3.80	0.767	0.131	3B-30FA	10
4.12	0.467	0.12	0A-0FA	10	4.00	0.814	0.131	3B-30FA	10
4.32	0.445	0.12	0A-0FA	10	4.19	0.819	0.131	3B-30FA	10
20.13	0.191	0.12	0A-0FA	10	4.38	0.803	0.131	3B-30FA	10
42.02	0.081	0.12	0A-0FA	10	4.58	0.805	0.131	3B-30FA	10
47.17	0.067	0.12	0A-0FA	10	20.12	0.670	0.131	3B-30FA	10
67.66	0.014	0.12	0A-0FA	10	20.34	0.661	0.131	3B-30FA	10
94.32	0.001	0.12	0A-0FA	10	42.03	0.213	0.131	3B-30FA	10
510.00	0.000	0.12	0A-0FA	10	47.13	0.140	0.131	3B-30FA	10
					67.57	0.021	0.131	3B-30FA	10
0.00	1.000	0.20	2A-20FA	10	93.77	0.002	0.131	3B-30FA	10
0.24	0.948	0.20	2A-20FA	10	510.00	0.000	0.131	3B-30FA	10
0.35	0.939	0.20	2A-20FA	10					
0.49	0.911	0.20	2A-20FA	10	0.00	1.000	0.129	3C-30FA	10
0.65	0.880	0.20	2A-20FA	10	0.45	0.942	0.129	3C-30FA	10
0.83	0.859	0.20	2A-20FA	10	0.81	0.955	0.129	3C-30FA	10
0.99	0.831	0.20	2A-20FA	10	1.04	0.935	0.129	3C-30FA	10
1.17	0.846	0.20	2A-20FA	10	1.20	0.931	0.129	3C-30FA	10
1.33	0.840	0.20	2A-20FA	10	1.38	0.909	0.129	3C-30FA	10
1.52	0.837	0.20	2A-20FA	10	1.54	0.840	0.129	3C-30FA	10
1.70	0.836	0.20	2A-20FA	10	1.72	0.840	0.129	3C-30FA	10
1.87	0.833	0.20	2A-20FA	10	1.88	0.882	0.129	3C-30FA	10
2.03	0.810	0.20	2A-20FA	10	2.07	0.873	0.129	3C-30FA	10
2.20	0.837	0.20	2A-20FA	10	2.25	0.860	0.129	3C-30FA	10
2.37	0.821	0.20	2A-20FA	10	2.42	0.857	0.129	3C-30FA	10
2.54	0.815	0.20	2A-20FA	10	2.58	0.854	0.129	3C-30FA	10
2.71	0.866	0.20	2A-20FA	10	2.75	0.843	0.129	3C-30FA	10
3.55	0.800	0.20	2A-20FA	10	2.92	0.839	0.129	3C-30FA	10
3.75	0.788	0.20	2A-20FA	10	3.09	0.830	0.129	3C-30FA	10
3.95	0.785	0.20	2A-20FA	10	3.26	0.894	0.129	3C-30FA	10
4.15	0.774	0.20	2A-20FA	10	4.10	0.788	0.129	3C-30FA	10
4.34	0.784	0.20	2A-20FA	10	4.30	0.759	0.129	3C-30FA	10
4.53	0.775	0.20	2A-20FA	10	4.50	0.752	0.129	3C-30FA	10
4.73	0.778	0.20	2A-20FA	10	4.70	0.745	0.129	3C-30FA	10
20.12	0.696	0.20	2A-20FA	10	4.89	0.740	0.129	3C-30FA	10
20.34	0.718	0.20	2A-20FA	10	5.08	0.748	0.129	3C-30FA	10
41.48	0.583	0.20	2A-20FA	10	5.28	0.726	0.129	3C-30FA	10
46.70	0.550	0.20	2A-20FA	10	20.12	0.518	0.129	3C-30FA	10
47.56	0.545	0.20	2A-20FA	10	20.34	0.483	0.129	3C-30FA	10
66.86	0.509	0.20	2A-20FA	10	42.03	0.095	0.129	3C-30FA	10
67.17	0.512	0.20	2A-20FA	10	47.13	0.060	0.129	3C-30FA	10
93.19	0.459	0.20	2A-20FA	10	67.58	0.009	0.129	3C-30FA	10
112.92	0.425	0.20	2A-20FA	10	94.31	0.001	0.129	3C-30FA	10
116.57	0.410	0.20	2A-20FA	10	510.00	0.000	0.129	3C-30FA	10
138.10	0.372	0.20	2A-20FA	10					
143.01	0.360	0.20	2A-20FA	10	0.00	1.000	0.098	4A-40FA	10
162.81	0.343	0.20	2A-20FA	10	0.24	0.963	0.098	4A-40FA	10
165.49	0.336	0.20	2A-20FA	10	0.43	0.973	0.098	4A-40FA	10
189.53	0.281	0.20	2A-20FA	10	0.68	0.959	0.098	4A-40FA	10

215.78	0.220	0.20	2A-20FA	10	1.08	0.981	0.098	4A-40FA	10
237.26	0.171	0.20	2A-20FA	10	1.24	0.970	0.098	4A-40FA	10
286.62	0.100	0.20	2A-20FA	10	1.41	0.937	0.098	4A-40FA	10
331.40	0.049	0.20	2A-20FA	10	1.57	0.974	0.098	4A-40FA	10
357.63	0.037	0.20	2A-20FA	10	1.75	0.960	0.098	4A-40FA	10
405.54	0.022	0.20	2A-20FA	10	1.92	0.953	0.098	4A-40FA	10
455.22	0.013	0.20	2A-20FA	10	2.10	0.948	0.098	4A-40FA	10
523.59	0.009	0.20	2A-20FA	10	2.28	0.945	0.098	4A-40FA	10
					2.45	0.957	0.098	4A-40FA	10
0.00	1.000	0.13	2B-20FA	10	2.62	0.943	0.098	4A-40FA	10
0.45	0.932	0.13	2B-20FA	10	2.78	0.932	0.098	4A-40FA	10
0.81	0.914	0.13	2B-20FA	10	2.95	0.952	0.098	4A-40FA	10
0.89	0.876	0.13	2B-20FA	10	3.13	0.924	0.098	4A-40FA	10
1.05	0.857	0.13	2B-20FA	10	3.29	0.973	0.098	4A-40FA	10
1.23	0.840	0.13	2B-20FA	10	3.47	0.907	0.098	4A-40FA	10
1.39	0.838	0.13	2B-20FA	10	3.67	0.906	0.098	4A-40FA	10
1.57	0.842	0.13	2B-20FA	10	3.87	0.903	0.098	4A-40FA	10
1.73	0.844	0.13	2B-20FA	10	4.07	0.892	0.098	4A-40FA	10
1.92	0.838	0.13	2B-20FA	10	4.27	0.831	0.098	4A-40FA	10
2.10	0.807	0.13	2B-20FA	10	4.47	0.888	0.098	4A-40FA	10
2.27	0.824	0.13	2B-20FA	10	4.67	0.874	0.098	4A-40FA	10
2.43	0.838	0.13	2B-20FA	10	20.12	0.766	0.098	4A-40FA	10
2.60	0.795	0.13	2B-20FA	10	20.34	0.730	0.098	4A-40FA	10
2.77	0.829	0.13	2B-20FA	10	41.48	0.448	0.098	4A-40FA	10
2.94	0.809	0.13	2B-20FA	10	46.88	0.408	0.098	4A-40FA	10
3.11	0.868	0.13	2B-20FA	10	47.56	0.400	0.098	4A-40FA	10
3.95	0.806	0.13	2B-20FA	10	67.06	0.376	0.098	4A-40FA	10
4.15	0.784	0.13	2B-20FA	10	93.35	0.310	0.098	4A-40FA	10
4.35	0.787	0.13	2B-20FA	10	112.92	0.248	0.098	4A-40FA	10
4.55	0.762	0.13	2B-20FA	10	116.90	0.229	0.098	4A-40FA	10
4.74	0.767	0.13	2B-20FA	10	138.10	0.166	0.098	4A-40FA	10
4.93	0.787	0.13	2B-20FA	10	143.01	0.155	0.098	4A-40FA	10
5.13	0.743	0.13	2B-20FA	10	162.81	0.101	0.098	4A-40FA	10
20.12	0.555	0.13	2B-20FA	10	165.66	0.091	0.098	4A-40FA	10
20.34	0.535	0.13	2B-20FA	10	190.43	0.036	0.098	4A-40FA	10
42.02	0.100	0.13	2B-20FA	10	226.12	0.007	0.098	4A-40FA	10
47.17	0.071	0.13	2B-20FA	10	350.00	0.002	0.098	4A-40FA	10
67.66	0.024	0.13	2B-20FA	10	510.00	0.000	0.098	4A-40FA	10
94.34	0.001	0.13	2B-20FA	10					
510.00	0.000	0.13	2B-20FA	10	0.00	1.000	0.111	4B-40FA	10
					0.30	0.951	0.111	4B-40FA	10
0.00	1.000	0.11	2C-20FA	10	0.53	0.902	0.111	4B-40FA	10
0.19	1.000	0.11	2C-20FA	10	0.78	0.881	0.111	4B-40FA	10
0.43	0.962	0.11	2C-20FA	10	1.14	0.754	0.111	4B-40FA	10
0.70	0.761	0.11	2C-20FA	10	1.43	0.864	0.111	4B-40FA	10
1.08	0.916	0.11	2C-20FA	10	1.59	0.797	0.111	4B-40FA	10
1.41	0.967	0.11	2C-20FA	10	1.76	0.823	0.111	4B-40FA	10
1.57	0.934	0.11	2C-20FA	10	1.92	0.796	0.111	4B-40FA	10
1.74	0.913	0.11	2C-20FA	10	2.10	0.803	0.111	4B-40FA	10
1.90	0.860	0.11	2C-20FA	10	2.27	0.791	0.111	4B-40FA	10
2.08	0.852	0.11	2C-20FA	10	2.45	0.720	0.111	4B-40FA	10
2.25	0.800	0.11	2C-20FA	10	2.63	0.791	0.111	4B-40FA	10
2.43	0.870	0.11	2C-20FA	10	2.80	0.766	0.111	4B-40FA	10
2.62	0.804	0.11	2C-20FA	10	2.97	0.769	0.111	4B-40FA	10
2.78	0.781	0.11	2C-20FA	10	3.13	0.774	0.111	4B-40FA	10
2.95	0.777	0.11	2C-20FA	10	3.30	0.759	0.111	4B-40FA	10
3.12	0.791	0.11	2C-20FA	10	3.48	0.773	0.111	4B-40FA	10
3.28	0.766	0.11	2C-20FA	10	3.64	0.816	0.111	4B-40FA	10
3.46	0.799	0.11	2C-20FA	10	3.82	0.755	0.111	4B-40FA	10
3.63	0.870	0.11	2C-20FA	10	4.02	0.721	0.111	4B-40FA	10
4.47	0.827	0.11	2C-20FA	10	4.22	0.706	0.111	4B-40FA	10
4.67	0.694	0.11	2C-20FA	10	4.42	0.718	0.111	4B-40FA	10
4.87	0.734	0.11	2C-20FA	10	4.61	0.719	0.111	4B-40FA	10
5.07	0.694	0.11	2C-20FA	10	4.80	0.705	0.111	4B-40FA	10
5.26	0.818	0.11	2C-20FA	10	5.00	0.697	0.111	4B-40FA	10
5.45	0.690	0.11	2C-20FA	10	20.12	0.428	0.111	4B-40FA	10

5.65	0.696	0.11	2C-20FA	10	20.34	0.150	0.111	4B-40FA	10
20.12	0.573	0.11	2C-20FA	10	42.03	0.079	0.111	4B-40FA	10
20.34	0.515	0.11	2C-20FA	10	47.13	0.057	0.111	4B-40FA	10
42.02	0.114	0.11	2C-20FA	10	67.58	0.017	0.111	4B-40FA	10
67.66	0.031	0.11	2C-20FA	10	94.27	0.003	0.111	4B-40FA	10
94.34	0.001	0.11	2C-20FA	10	510.00	0.000	0.111	4B-40FA	10
510.00	0.000	0.11	2C-20FA	10					
					0.00	1.000	0.26	4C-40FA	10
0.00	1.000	0.1	3A-30FA	10	0.25	0.861	0.26	4C-40FA	10
0.24	0.973	0.1	3A-30FA	10	0.39	0.853	0.26	4C-40FA	10
0.41	0.972	0.1	3A-30FA	10	0.68	0.848	0.26	4C-40FA	10
0.56	0.945	0.1	3A-30FA	10	0.87	0.841	0.26	4C-40FA	10
0.75	0.987	0.1	3A-30FA	10	1.22	0.942	0.26	4C-40FA	10
0.92	0.983	0.1	3A-30FA	10	1.40	0.977	0.26	4C-40FA	10
1.10	0.989	0.1	3A-30FA	10	1.58	0.919	0.26	4C-40FA	10
1.28	0.982	0.1	3A-30FA	10	1.75	0.957	0.26	4C-40FA	10
1.45	0.976	0.1	3A-30FA	10	1.92	0.972	0.26	4C-40FA	10
1.62	0.975	0.1	3A-30FA	10	2.08	0.903	0.26	4C-40FA	10
1.78	0.971	0.1	3A-30FA	10	2.25	0.915	0.26	4C-40FA	10
1.95	0.970	0.1	3A-30FA	10	2.43	0.953	0.26	4C-40FA	10
2.12	0.965	0.1	3A-30FA	10	2.59	0.964	0.26	4C-40FA	10
2.29	1.048	0.1	3A-30FA	10	3.43	0.907	0.26	4C-40FA	10
3.13	0.966	0.1	3A-30FA	10	3.63	0.939	0.26	4C-40FA	10
3.33	0.851	0.1	3A-30FA	10	3.83	0.887	0.26	4C-40FA	10
3.53	0.849	0.1	3A-30FA	10	4.03	0.918	0.26	4C-40FA	10
3.73	0.839	0.1	3A-30FA	10	4.23	0.910	0.26	4C-40FA	10
3.93	0.837	0.1	3A-30FA	10	4.42	0.890	0.26	4C-40FA	10
4.12	0.858	0.1	3A-30FA	10	4.62	0.923	0.26	4C-40FA	10
4.32	0.812	0.1	3A-30FA	10	20.12	0.913	0.26	4C-40FA	10
20.12	0.678	0.1	3A-30FA	10	20.34	0.893	0.26	4C-40FA	10
20.34	0.632	0.1	3A-30FA	10	47.55	0.769	0.26	4C-40FA	10
42.03	0.227	0.1	3A-30FA	10	66.79	0.732	0.26	4C-40FA	10
47.13	0.200	0.1	3A-30FA	10	67.28	0.698	0.26	4C-40FA	10
67.41	0.109	0.1	3A-30FA	10	93.13	0.643	0.26	4C-40FA	10
94.26	0.029	0.1	3A-30FA	10	113.06	0.640	0.26	4C-40FA	10
114.64	0.018	0.1	3A-30FA	10	116.53	0.655	0.26	4C-40FA	10
118.42	0.016	0.1	3A-30FA	10	142.93	0.580	0.26	4C-40FA	10
129.50	0.014	0.1	3A-30FA	10	162.77	0.602	0.26	4C-40FA	10
141.26	0.011	0.1	3A-30FA	10	165.49	0.590	0.26	4C-40FA	10
152.87	0.010	0.1	3A-30FA	10	189.51	0.586	0.26	4C-40FA	10
176.06	0.007	0.1	3A-30FA	10	215.78	0.555	0.26	4C-40FA	10
510.00	0.000	0.1	3A-30FA	10	237.15	0.531	0.26	4C-40FA	10
					238.44	0.477	0.26	4C-40FA	10
					238.63	0.473	0.26	4C-40FA	10
					331.33	0.388	0.26	4C-40FA	10
					356.59	0.360	0.26	4C-40FA	10
					405.38	0.342	0.26	4C-40FA	10
					454.80	0.327	0.26	4C-40FA	10
					523.39	0.301	0.26	4C-40FA	10
					619.45	0.250	0.26	4C-40FA	10
					716.63	0.194	0.26	4C-40FA	10
					793.36	0.075	0.26	4C-40FA	10
					836.92	0.014	0.26	4C-40FA	10
					836.94	0.014	0.26	4C-40FA	10
					861.97	0.016	0.26	4C-40FA	10
					1005.4	0.012	0.26	4C-40FA	10
					1026.8	0.004	0.26	4C-40FA	10

Ramm and Biscopig (1997)

Time (hours)	Relative Flow	w	Description	h^*/t	Time (hours)	Relative Flow	w	Description	h^*/t
0.0	1.000	0.201	V18 PH7 WH2.5	14	0.0	1.000	0.120	V30 PH5.2 WH12	40
0.9	0.897	0.201	V18 PH7 WH2.5	14	1.0	0.574	0.120	V30 PH5.2 WH12	40
2.0	0.825	0.201	V18 PH7 WH2.5	14	2.0	0.497	0.120	V30 PH5.2 WH12	40
2.9	0.772	0.201	V18 PH7 WH2.5	14	9.1	0.478	0.120	V30 PH5.2 WH12	40
3.9	0.724	0.201	V18 PH7 WH2.5	14	26.4	0.250	0.120	V30 PH5.2 WH12	40
26.3	0.309	0.201	V18 PH7 WH2.5	14	201.6	0.005	0.120	V30 PH5.2 WH12	40
87.3	0.067	0.201	V18 PH7 WH2.5	14	510.0	0.000	0.120	V30 PH5.2 WH12	40
300.7	0.007	0.201	V18 PH7 WH2.5	14					
510.0	0.000	0.201	V18 PH7 WH2.5	14	0.0	1.000	0.210	V30 PH7 WH2.5	8
					0.9	0.559	0.210	V30 PH7 WH2.5	8
0.0	1.000	0.199	V18 PH6.1 WH2.5	14	1.9	0.391	0.210	V30 PH7 WH2.5	8
1.0	0.785	0.199	V18 PH6.1 WH2.5	14	2.9	0.282	0.210	V30 PH7 WH2.5	8
2.0	0.709	0.199	V18 PH6.1 WH2.5	14	4.9	0.280	0.210	V30 PH7 WH2.5	8
6.0	0.378	0.199	V18 PH6.1 WH2.5	14	26.0	0.278	0.210	V30 PH7 WH2.5	8
25.2	0.194	0.199	V18 PH6.1 WH2.5	14	84.2	0.153	0.210	V30 PH7 WH2.5	8
29.3	0.079	0.199	V18 PH6.1 WH2.5	14	482.2	0.003	0.210	V30 PH7 WH2.5	8
113.1	0.030	0.199	V18 PH6.1 WH2.5	14	510.0	0.000	0.210	V30 PH7 WH2.5	8
672.0	0.011	0.199	V18 PH6.1 WH2.5	14					
					0.0	1.000	0.181	V30 PH6.1 WH2.5	8
0.0	1.000	0.202	V18 PH5.2 WH2.5	14	0.9	0.509	0.181	V30 PH6.1 WH2.5	8
0.9	0.793	0.202	V18 PH5.2 WH2.5	14	1.9	0.507	0.181	V30 PH6.1 WH2.5	8
2.0	0.732	0.202	V18 PH5.2 WH2.5	14	6.0	0.220	0.181	V30 PH6.1 WH2.5	8
2.9	0.638	0.202	V18 PH5.2 WH2.5	14	25.2	0.057	0.181	V30 PH6.1 WH2.5	8
3.9	0.563	0.202	V18 PH5.2 WH2.5	14	29.2	0.045	0.181	V30 PH6.1 WH2.5	8
5.0	0.500	0.202	V18 PH5.2 WH2.5	14	163.5	0.028	0.181	V30 PH6.1 WH2.5	8
21.1	0.376	0.202	V18 PH5.2 WH2.5	14	672.0	0.009	0.181	V30 PH6.1 WH2.5	8
22.1	0.375	0.202	V18 PH5.2 WH2.5	14					
25.1	0.359	0.202	V18 PH5.2 WH2.5	14	0.0	1.000	0.190	V30 PH5.2 WH2.5	8
88.2	0.190	0.202	V18 PH5.2 WH2.5	14	1.0	0.515	0.190	V30 PH5.2 WH2.5	8
173.0	0.003	0.202	V18 PH5.2 WH2.5	14	2.0	0.259	0.190	V30 PH5.2 WH2.5	8
510.0	0.000	0.202	V18 PH5.2 WH2.5	14	3.0	0.230	0.190	V30 PH5.2 WH2.5	8
					6.1	0.201	0.190	V30 PH5.2 WH2.5	8
0.0	1.000	0.198	V18 PH7 WH12	67	25.4	0.039	0.190	V30 PH5.2 WH2.5	8
1.0	0.864	0.198	V18 PH7 WH12	67	336.0	0.009	0.190	V30 PH5.2 WH2.5	8
2.0	0.813	0.198	V18 PH7 WH12	67	450.0	0.003	0.190	V30 PH5.2 WH2.5	8
3.0	0.778	0.198	V18 PH7 WH12	67	510.0	0.000	0.190	V30 PH5.2 WH2.5	8
3.9	0.738	0.198	V18 PH7 WH12	67					
5.9	0.707	0.198	V18 PH7 WH12	67	0.0	1.000	0.22	V30 PH7 WH12	40
19.0	0.617	0.198	V18 PH7 WH12	67	0.9	1.000	0.22	V30 PH7 WH12	40
20.0	0.570	0.198	V18 PH7 WH12	67	1.9	1.000	0.22	V30 PH7 WH12	40
21.0	0.625	0.198	V18 PH7 WH12	67	2.9	1.000	0.22	V30 PH7 WH12	40
22.0	0.588	0.198	V18 PH7 WH12	67	4.0	1.000	0.22	V30 PH7 WH12	40
24.0	0.512	0.198	V18 PH7 WH12	67	6.0	1.000	0.22	V30 PH7 WH12	40
154.0	0.199	0.198	V18 PH7 WH12	67	18.2	1.000	0.22	V30 PH7 WH12	40
323.8	0.067	0.198	V18 PH7 WH12	67	19.2	0.998	0.22	V30 PH7 WH12	40
496.9	0.035	0.198	V18 PH7 WH12	67	20.2	0.870	0.22	V30 PH7 WH12	40
670.4	0.019	0.198	V18 PH7 WH12	67	21.2	0.894	0.22	V30 PH7 WH12	40
1345.3	0.016	0.198	V18 PH7 WH12	67	22.2	0.855	0.22	V30 PH7 WH12	40
					24.3	0.760	0.22	V30 PH7 WH12	40
					80.0	0.300	0.22	V30 PH7 WH12	40
					150.1	0.008	0.22	V30 PH7 WH12	40
					250.0	0.002	0.22	V30 PH7 WH12	40
					510.0	0.000	0.22	V30 PH7 WH12	40
0.0	1.000	0.203	V18 PH6.1 WH12	67					
1.0	0.801	0.203	V18 PH6.1 WH12	67	0.0	1.000	0.23	V30 PH6.1 WH12	40
2.0	0.761	0.203	V18 PH6.1 WH12	67	0.9	0.870	0.23	V30 PH6.1 WH12	40
4.0	0.524	0.203	V18 PH6.1 WH12	67	1.9	0.654	0.23	V30 PH6.1 WH12	40
5.0	0.463	0.203	V18 PH6.1 WH12	67	2.9	0.647	0.23	V30 PH6.1 WH12	40
6.0	0.398	0.203	V18 PH6.1 WH12	67	5.9	0.631	0.23	V30 PH6.1 WH12	40
10.1	0.384	0.203	V18 PH6.1 WH12	67	22.2	0.417	0.23	V30 PH6.1 WH12	40
23.3	0.348	0.203	V18 PH6.1 WH12	67	24.2	0.374	0.23	V30 PH6.1 WH12	40
24.3	0.320	0.203	V18 PH6.1 WH12	67					

28.4	0.312	0.203	V18 PH6.1 WH12	67	28.3	0.281	0.23	V30 PH6.1 WH12	40
195.0	0.119	0.203	V18 PH6.1 WH12	67	85.0	0.084	0.23	V30 PH6.1 WH12	40
365.6	0.007	0.203	V18 PH6.1 WH12	67	173.0	0.006	0.23	V30 PH6.1 WH12	40
450.0	0.002	0.203	V18 PH6.1 WH12	67	510.0	0.000	0.23	V30 PH6.1 WH12	40
510.0	0.000	0.203	V18 PH6.1 WH12	67					
					0.0	0.920	0.211	V30 PH5.2 WH12	40
0.0	1.000	0.201	V18 PH5.2 WH12	67	1.0	0.699	0.211	V30 PH5.2 WH12	40
1.0	0.816	0.201	V18 PH5.2 WH12	67	5.0	0.522	0.211	V30 PH5.2 WH12	40
5.0	0.488	0.201	V18 PH5.2 WH12	67	9.0	0.463	0.211	V30 PH5.2 WH12	40
9.1	0.401	0.201	V18 PH5.2 WH12	67	26.3	0.341	0.211	V30 PH5.2 WH12	40
22.3	0.332	0.201	V18 PH5.2 WH12	67	85.0	0.103	0.211	V30 PH5.2 WH12	40
28.4	0.228	0.201	V18 PH5.2 WH12	67	156.6	0.002	0.211	V30 PH5.2 WH12	40
150.3	0.001	0.201	V18 PH5.2 WH12	67	510.0	0.000	0.211	V30 PH5.2 WH12	40
510.0	0.000	0.201	V18 PH5.2 WH12	67					
					0.0	1.000	0.38	V30 PH7 WH2.5	8
0.0	1.000	0.3	V18 PH7 WH2.5	14	1.0	0.424	0.38	V30 PH7 WH2.5	8
0.9	0.803	0.3	V18 PH7 WH2.5	14	2.0	0.373	0.38	V30 PH7 WH2.5	8
1.9	0.788	0.3	V18 PH7 WH2.5	14	2.9	0.315	0.38	V30 PH7 WH2.5	8
2.9	0.703	0.3	V18 PH7 WH2.5	14	4.0	0.289	0.38	V30 PH7 WH2.5	8
4.0	0.642	0.3	V18 PH7 WH2.5	14	26.4	0.109	0.38	V30 PH7 WH2.5	8
26.3	0.401	0.3	V18 PH7 WH2.5	14	61.2	0.043	0.38	V30 PH7 WH2.5	8
487.2	0.003	0.3	V18 PH7 WH2.5	14	105.2	0.000	0.38	V30 PH7 WH2.5	8
510.0	0.000	0.3	V18 PH7 WH2.5	14	510.0	0.000	0.38	V30 PH7 WH2.5	8
					0.0	1.000	0.39	V30 PH6.1 WH2.5	8
0.0	1.000	0.301	V18 PH6.1 WH2.5	14	1.0	0.609	0.39	V30 PH6.1 WH2.5	8
1.0	0.614	0.301	V18 PH6.1 WH2.5	14	2.0	0.522	0.39	V30 PH6.1 WH2.5	8
2.0	0.531	0.301	V18 PH6.1 WH2.5	14	6.0	0.307	0.39	V30 PH6.1 WH2.5	8
6.0	0.531	0.301	V18 PH6.1 WH2.5	14	25.2	0.046	0.39	V30 PH6.1 WH2.5	8
25.2	0.409	0.301	V18 PH6.1 WH2.5	14	29.3	0.042	0.39	V30 PH6.1 WH2.5	8
29.2	0.312	0.301	V18 PH6.1 WH2.5	14	53.0	0.021	0.39	V30 PH6.1 WH2.5	8
243.2	0.081	0.301	V18 PH6.1 WH2.5	14	163.3	0.005	0.39	V30 PH6.1 WH2.5	8
638.4	0.011	0.301	V18 PH6.1 WH2.5	14	510.0	0.000	0.39	V30 PH6.1 WH2.5	8
					0.0	1.000	0.400	V30 PH5.2 WH2.5	8
0.0	1.000	0.299	V18 PH5.2 WH2.5	14	0.9	0.591	0.400	V30 PH5.2 WH2.5	8
1.0	0.660	0.299	V18 PH5.2 WH2.5	14	1.9	0.462	0.400	V30 PH5.2 WH2.5	8
2.0	0.605	0.299	V18 PH5.2 WH2.5	14	2.9	0.389	0.400	V30 PH5.2 WH2.5	8
2.9	0.496	0.299	V18 PH5.2 WH2.5	14	3.9	0.188	0.400	V30 PH5.2 WH2.5	8
25.1	0.248	0.299	V18 PH5.2 WH2.5	14	5.0	0.114	0.400	V30 PH5.2 WH2.5	8
173.0	0.003	0.299	V18 PH5.2 WH2.5	14	22.1	0.033	0.400	V30 PH5.2 WH2.5	8
510.0	0.000	0.299	V18 PH5.2 WH2.5	14	30.2	0.026	0.400	V30 PH5.2 WH2.5	8
					57.0	0.005	0.400	V30 PH5.2 WH2.5	8
0.0	1.000	0.302	V18 PH7 WH12	67	85.3	0.000	0.400	V30 PH5.2 WH2.5	8
1.0	0.779	0.302	V18 PH7 WH12	67	510.0	0.000	0.400	V30 PH5.2 WH2.5	8
2.0	0.666	0.302	V18 PH7 WH12	67					
3.0	0.666	0.302	V18 PH7 WH12	67					
3.9	0.621	0.302	V18 PH7 WH12	67	0.0	1.000	0.120	V60 PH7 WH2.5	4
5.9	0.643	0.302	V18 PH7 WH12	67	1.0	0.385	0.120	V60 PH7 WH2.5	4
18.0	0.542	0.302	V18 PH7 WH12	67	2.0	0.000	0.120	V60 PH7 WH2.5	4
19.0	0.581	0.302	V18 PH7 WH12	67	510.0	0.000	0.120	V60 PH7 WH2.5	4
20.0	0.563	0.302	V18 PH7 WH12	67					
21.0	0.601	0.302	V18 PH7 WH12	67					
22.0	0.558	0.302	V18 PH7 WH12	67	0.0	1.000	0.120	V60 PH6.1 WH2.5	4
24.0	0.518	0.302	V18 PH7 WH12	67	1.0	0.526	0.120	V60 PH6.1 WH2.5	4
154.7	0.283	0.302	V18 PH7 WH12	67	2.0	0.158	0.120	V60 PH6.1 WH2.5	4
340.2	0.094	0.302	V18 PH7 WH12	67	6.0	0.053	0.120	V60 PH6.1 WH2.5	4
503.5	0.051	0.302	V18 PH7 WH12	67	25.2	0.000	0.120	V60 PH6.1 WH2.5	4
676.9	0.038	0.302	V18 PH7 WH12	67	510.0	0.000	0.120	V60 PH6.1 WH2.5	4
847.7	0.023	0.302	V18 PH7 WH12	67					
1345.2	0.018	0.302	V18 PH7 WH12	67	0.0	1.000	0.110	V60 PH5.2 WH2.5	4
					0.9	0.474	0.110	V60 PH5.2 WH2.5	4
					1.9	0.234	0.110	V60 PH5.2 WH2.5	4
					2.9	0.154	0.110	V60 PH5.2 WH2.5	4
					23.5	0.000	0.110	V60 PH5.2 WH2.5	4
					672.0	0.000	0.110	V60 PH5.2 WH2.5	4
0.0	1.000	0.301	V18 PH6.1 WH12	67					

1.0	0.969	0.301	V18 PH6.1 WH12	67						
2.0	0.870	0.301	V18 PH6.1 WH12	67	0.0	1.000	0.100	V60 PH7 WH12	20	
4.0	0.783	0.301	V18 PH6.1 WH12	67	1.0	1.324	0.100	V60 PH7 WH12	20	
5.0	0.697	0.301	V18 PH6.1 WH12	67	2.0	1.027	0.100	V60 PH7 WH12	20	
6.1	0.605	0.301	V18 PH6.1 WH12	67	3.0	0.814	0.100	V60 PH7 WH12	20	
10.1	0.609	0.301	V18 PH6.1 WH12	67	22.3	0.458	0.100	V60 PH7 WH12	20	
23.3	0.586	0.301	V18 PH6.1 WH12	67	24.4	0.331	0.100	V60 PH7 WH12	20	
24.3	0.518	0.301	V18 PH6.1 WH12	67	146.2	0.175	0.100	V60 PH7 WH12	20	
28.4	0.498	0.301	V18 PH6.1 WH12	67	354.5	0.120	0.100	V60 PH7 WH12	20	
157.2	0.317	0.301	V18 PH6.1 WH12	67	505.1	0.083	0.100	V60 PH7 WH12	20	
359.0	0.087	0.301	V18 PH6.1 WH12	67	656.5	0.048	0.100	V60 PH7 WH12	20	
1172.0	0.001	0.301	V18 PH6.1 WH12	67						
					0.0	1.000	0.130	V60 PH6.1 WH12	20	
0.0	1.000	0.299	V18 PH5.2 WH12	67	1.0	0.591	0.130	V60 PH6.1 WH12	20	
2.9	0.702	0.299	V18 PH5.2 WH12	67	2.0	0.494	0.130	V60 PH6.1 WH12	20	
5.0	0.591	0.299	V18 PH5.2 WH12	67	3.0	0.459	0.130	V60 PH6.1 WH12	20	
9.0	0.510	0.299	V18 PH5.2 WH12	67	6.0	0.419	0.130	V60 PH6.1 WH12	20	
21.2	0.475	0.299	V18 PH5.2 WH12	67	22.2	0.240	0.130	V60 PH6.1 WH12	20	
28.4	0.432	0.299	V18 PH5.2 WH12	67	24.2	0.217	0.130	V60 PH6.1 WH12	20	
151.5	0.001	0.299	V18 PH5.2 WH12	67	28.3	0.079	0.130	V60 PH6.1 WH12	20	
510.0	0.000	0.299	V18 PH5.2 WH12	67	159.8	0.019	0.130	V60 PH6.1 WH12	20	
					189.3	0.008	0.130	V60 PH6.1 WH12	20	
					240.3	0.000	0.130	V60 PH6.1 WH12	20	
0.0	1.000	0.4	V18 PH7 WH2.5	14	510.0	0.000	0.130	V60 PH6.1 WH12	20	
0.9	0.682	0.4	V18 PH7 WH2.5	14						
1.9	0.588	0.4	V18 PH7 WH2.5	14	0.0	1.000	0.099	V60 PH5.2 WH12	20	
2.9	0.544	0.4	V18 PH7 WH2.5	14	3.0	0.752	0.099	V60 PH5.2 WH12	20	
4.0	0.508	0.4	V18 PH7 WH2.5	14	26.4	0.257	0.099	V60 PH5.2 WH12	20	
26.4	0.260	0.4	V18 PH7 WH2.5	14	189.1	0.041	0.099	V60 PH5.2 WH12	20	
482.2	0.003	0.4	V18 PH7 WH2.5	14	366.8	0.023	0.099	V60 PH5.2 WH12	20	
510.0	0.000	0.4	V18 PH7 WH2.5	14	435.2	0.005	0.099	V60 PH5.2 WH12	20	
					510.0	0.000	0.099	V60 PH5.2 WH12	20	
0.0	1.000	0.401	V18 PH6.1 WH2.5	14						
1.0	0.540	0.401	V18 PH6.1 WH2.5	14	0.0	1.000	0.190	V60 PH7 WH2.5	4	
2.0	0.444	0.401	V18 PH6.1 WH2.5	14	0.9	0.553	0.190	V60 PH7 WH2.5	4	
6.0	0.239	0.401	V18 PH6.1 WH2.5	14	1.9	0.332	0.190	V60 PH7 WH2.5	4	
25.2	0.144	0.401	V18 PH6.1 WH2.5	14	2.9	0.334	0.190	V60 PH7 WH2.5	4	
29.2	0.140	0.401	V18 PH6.1 WH2.5	14	26.0	0.218	0.190	V60 PH7 WH2.5	4	
95.8	0.022	0.401	V18 PH6.1 WH2.5	14	134.2	0.090	0.190	V60 PH7 WH2.5	4	
672.0	0.009	0.401	V18 PH6.1 WH2.5	14	257.3	0.003	0.190	V60 PH7 WH2.5	4	
					660.2	0.000	0.190	V60 PH7 WH2.5	4	
0.0	1.000	0.399	V18 PH5.2 WH2.5	14						
0.9	0.622	0.399	V18 PH5.2 WH2.5	14	0.0	1.000	0.210	V60 PH6.1 WH2.5	4	
1.9	0.558	0.399	V18 PH5.2 WH2.5	14	0.9	0.712	0.210	V60 PH6.1 WH2.5	4	
2.9	0.551	0.399	V18 PH5.2 WH2.5	14	2.0	0.564	0.210	V60 PH6.1 WH2.5	4	
3.9	0.533	0.399	V18 PH5.2 WH2.5	14	6.0	0.517	0.210	V60 PH6.1 WH2.5	4	
4.9	0.458	0.399	V18 PH5.2 WH2.5	14	25.1	0.448	0.210	V60 PH6.1 WH2.5	4	
21.1	0.428	0.399	V18 PH5.2 WH2.5	14	29.2	0.327	0.210	V60 PH6.1 WH2.5	4	
22.1	0.395	0.399	V18 PH5.2 WH2.5	14	113.1	0.178	0.210	V60 PH6.1 WH2.5	4	
25.1	0.390	0.399	V18 PH5.2 WH2.5	14	350.6	0.104	0.210	V60 PH6.1 WH2.5	4	
131.6	0.005	0.399	V18 PH5.2 WH2.5	14	672.0	0.036	0.210	V60 PH6.1 WH2.5	4	
350.0	0.000	0.399	V18 PH5.2 WH2.5	14	2016.0	0.018	0.210	V60 PH6.1 WH2.5	4	
510.0	0.000	0.399	V18 PH5.2 WH2.5	14						
0.0	1.000	0.09	V30 PH7 WH2.5	8						
1.0	0.526	0.09	V30 PH7 WH2.5	8						
2.0	0.000	0.09	V30 PH7 WH2.5	8	0.0	1.000	0.220	V60 PH5.2 WH2.5	4	
510.0	0.000	0.09	V30 PH7 WH2.5	8	1.0	0.724	0.220	V60 PH5.2 WH2.5	4	
					2.0	0.377	0.220	V60 PH5.2 WH2.5	4	
					3.0	0.335	0.220	V60 PH5.2 WH2.5	4	
0.0	1.000	0.11	V30 PH6.1 WH2.5	8	6.1	0.291	0.220	V60 PH5.2 WH2.5	4	
1.0	0.577	0.11	V30 PH6.1 WH2.5	8	25.4	0.057	0.220	V60 PH5.2 WH2.5	4	
2.0	0.423	0.11	V30 PH6.1 WH2.5	8	78.3	0.021	0.220	V60 PH5.2 WH2.5	4	
6.0	0.192	0.11	V30 PH6.1 WH2.5	8	336.0	0.009	0.220	V60 PH5.2 WH2.5	4	
25.2	0.385	0.11	V30 PH6.1 WH2.5	8	510.0	0.000	0.220	V60 PH5.2 WH2.5	4	

29.3	0.000	0.11	V30 PH6.1 WH2.5	8						
510.0	0.000	0.11	V30 PH6.1 WH2.5	8	0.0	1.000	0.2100	V60 PH7 WH12	20	
					1.0	1.000	0.2100	V60 PH7 WH12	20	
0.0	1.192	0.12	V30 PH5.2 WH2.5	8	2.0	1.000	0.2100	V60 PH7 WH12	20	
0.9	0.385	0.12	V30 PH5.2 WH2.5	8	3.0	0.905	0.2100	V60 PH7 WH12	20	
1.9	0.385	0.12	V30 PH5.2 WH2.5	8	4.0	0.856	0.2100	V60 PH7 WH12	20	
5.6	0.230	0.12	V30 PH5.2 WH2.5	8	6.0	0.753	0.2100	V60 PH7 WH12	20	
15.0	0.130	0.12	V30 PH5.2 WH2.5	8	18.2	0.640	0.210	V60 PH7 WH12	20	
24.0	0.000	0.12	V30 PH5.2 WH2.5	8	19.2	0.637	0.210	V60 PH7 WH12	20	
672.0	0.000	0.12	V30 PH5.2 WH2.5	8	20.2	0.643	0.210	V60 PH7 WH12	20	
					21.3	0.633	0.210	V60 PH7 WH12	20	
0.0	1.000	0.111	V30 PH7 WH12	40	22.3	0.626	0.210	V60 PH7 WH12	20	
1.0	1.394	0.111	V30 PH7 WH12	40	24.4	0.629	0.210	V60 PH7 WH12	20	
2.0	1.331	0.111	V30 PH7 WH12	40	85.2	0.231	0.210	V60 PH7 WH12	20	
3.0	1.146	0.111	V30 PH7 WH12	40	145.6	0.016	0.210	V60 PH7 WH12	20	
4.0	1.033	0.111	V30 PH7 WH12	40	481.3	0.013	0.210	V60 PH7 WH12	20	
6.0	0.891	0.111	V30 PH7 WH12	40	510.0	0.000	0.210	V60 PH7 WH12	20	
18.2	1.034	0.111	V30 PH7 WH12	40						
19.2	0.936	0.111	V30 PH7 WH12	40	0.0	1.000	0.190	V60 PH6.1 WH12	20	
20.3	0.894	0.111	V30 PH7 WH12	40	1.0	0.809	0.190	V60 PH6.1 WH12	20	
21.3	0.950	0.111	V30 PH7 WH12	40	2.0	0.725	0.190	V60 PH6.1 WH12	20	
22.3	0.965	0.111	V30 PH7 WH12	40	3.0	0.704	0.190	V60 PH6.1 WH12	20	
24.3	0.881	0.111	V30 PH7 WH12	40	6.0	0.673	0.190	V60 PH6.1 WH12	20	
169.7	0.039	0.111	V30 PH7 WH12	40	22.2	0.580	0.190	V60 PH6.1 WH12	20	
538.2	0.019	0.111	V30 PH7 WH12	40	24.2	0.587	0.190	V60 PH6.1 WH12	20	
					28.3	0.503	0.190	V60 PH6.1 WH12	20	
0.0	1.000	0.1	V30 PH6.1 WH12	40	75.3	0.102	0.190	V60 PH6.1 WH12	20	
1.0	0.779	0.1	V30 PH6.1 WH12	40	165.8	0.027	0.190	V60 PH6.1 WH12	20	
2.0	0.825	0.1	V30 PH6.1 WH12	40	475.2	0.007	0.190	V60 PH6.1 WH12	20	
3.0	0.662	0.1	V30 PH6.1 WH12	40	1323.1	0.004	0.190	V60 PH6.1 WH12	20	
6.0	0.586	0.1	V30 PH6.1 WH12	40						
22.2	0.444	0.1	V30 PH6.1 WH12	40	0.0	1.000	0.220	V60 PH5.2 WH12	20	
24.2	0.412	0.1	V30 PH6.1 WH12	40	1.0	0.800	0.220	V60 PH5.2 WH12	20	
28.3	0.281	0.1	V30 PH6.1 WH12	40	2.0	0.696	0.220	V60 PH5.2 WH12	20	
153.9	0.012	0.1	V30 PH6.1 WH12	40	3.0	0.753	0.220	V60 PH5.2 WH12	20	
185.0	0.070	0.1	V30 PH6.1 WH12	40	9.1	0.538	0.220	V60 PH5.2 WH12	20	
300.0	0.000	0.1	V30 PH6.1 WH12	40	26.4	0.415	0.220	V60 PH5.2 WH12	20	
510.0	0.000	0.1	V30 PH6.1 WH12	40	86.0	0.102	0.220	V60 PH5.2 WH12	20	
					156.6	0.001	0.220	V60 PH5.2 WH12	20	
					510.0	0.000	0.220	V60 PH5.2 WH12	20	

Edwardsen (1996)

Time (hrs)	Rel. Flow	w	Description	h^*/t	Time (hrs)	Rel. Flow	w	Description	h^*/t
0.0	1.000	0.200	4.10-Aach 1-0.5Bar	25	0.0	1.000	0.201	4.12-Hoz-0.5Bar	25
26.3	0.812	0.200	4.10-Aach 1-0.5Bar	25	10.6	0.806	0.201	4.12-Hoz-0.5Bar	25
37.8	0.673	0.200	4.10-Aach 1-0.5Bar	25	24.6	0.587	0.201	4.12-Hoz-0.5Bar	25
37.8	0.673	0.200	4.10-Aach 1-0.5Bar	25	41.8	0.377	0.201	4.12-Hoz-0.5Bar	25
76.7	0.547	0.200	4.10-Aach 1-0.5Bar	25	67.1	0.313	0.201	4.12-Hoz-0.5Bar	25
98.9	0.469	0.200	4.10-Aach 1-0.5Bar	25	99.8	0.254	0.201	4.12-Hoz-0.5Bar	25
137.9	0.295	0.200	4.10-Aach 1-0.5Bar	25	138.0	0.234	0.201	4.12-Hoz-0.5Bar	25
192.8	0.291	0.200	4.10-Aach 1-0.5Bar	25	160.6	0.186	0.201	4.12-Hoz-0.5Bar	25
276.2	0.228	0.200	4.10-Aach 1-0.5Bar	25	200.4	0.141	0.201	4.12-Hoz-0.5Bar	25
328.1	0.204	0.200	4.10-Aach 1-0.5Bar	25	219.2	0.025	0.201	4.12-Hoz-0.5Bar	25
422.7	0.151	0.200	4.10-Aach 1-0.5Bar	25	259.6	0.000	0.201	4.12-Hoz-0.5Bar	25
544.0	0.000	0.200	4.10-Aach 1-0.5Bar	25	400.5	0.000	0.201	4.12-Hoz-0.5Bar	25
600.0	0.000	0.200	4.10-Aach 1-0.5Bar	25	507.0	0.000	0.201	4.12-Hoz-0.5Bar	25
					600.0	0.000	0.201	4.12-Hoz-0.5Bar	25
0.0	1.000	0.200	4.10-Esch1-0.5Bar	25	0.0	1.000	0.180	4.12-Poz-0.5Bar	25
19.5	0.652	0.200	4.10-Esch1-0.5Bar	25	21.3	0.629	0.180	4.12-Poz-0.5Bar	25
26.0	0.522	0.200	4.10-Esch1-0.5Bar	25	40.9	0.407	0.180	4.12-Poz-0.5Bar	25
51.0	0.310	0.200	4.10-Esch1-0.5Bar	25	71.6	0.181	0.180	4.12-Poz-0.5Bar	25
100.4	0.207	0.200	4.10-Esch1-0.5Bar	25	118.8	0.107	0.180	4.12-Poz-0.5Bar	25
154.9	0.203	0.200	4.10-Esch1-0.5Bar	25	160.8	0.076	0.180	4.12-Poz-0.5Bar	25
212.1	0.193	0.200	4.10-Esch1-0.5Bar	25	239.8	0.074	0.180	4.12-Poz-0.5Bar	25
317.5	0.177	0.200	4.10-Esch1-0.5Bar	25	356.5	0.069	0.180	4.12-Poz-0.5Bar	25
413.9	0.156	0.200	4.10-Esch1-0.5Bar	25	501.4	0.061	0.180	4.12-Poz-0.5Bar	25
489.2	0.145	0.200	4.10-Esch1-0.5Bar	25	601.6	0.057	0.180	4.12-Poz-0.5Bar	25
671.3	0.030	0.200	4.10-Esch1-0.5Bar	25	701.0	0.037	0.180	4.12-Poz-0.5Bar	25
837.1	0.026	0.200	4.10-Esch1-0.5Bar	25	751.3	0.001	0.180	4.12-Poz-0.5Bar	25
1010.3	0.013	0.200	4.10-Esch1-0.5Bar	25					
0.0	1.000	0.190	4.10-Aach2-0.5Bar	25	0.0	1.000	0.201	4.13-Kalk-0.5Bar	25
32.4	0.581	0.190	4.10-Aach2-0.5Bar	25	19.1	0.829	0.201	4.13-Kalk-0.5Bar	25
49.7	0.457	0.190	4.10-Aach2-0.5Bar	25	48.2	0.706	0.201	4.13-Kalk-0.5Bar	25
102.6	0.304	0.190	4.10-Aach2-0.5Bar	25	84.2	0.607	0.201	4.13-Kalk-0.5Bar	25
172.2	0.177	0.190	4.10-Aach2-0.5Bar	25	109.4	0.227	0.201	4.13-Kalk-0.5Bar	25
247.5	0.147	0.190	4.10-Aach2-0.5Bar	25	144.1	0.151	0.201	4.13-Kalk-0.5Bar	25
308.5	0.060	0.190	4.10-Aach2-0.5Bar	25	277.9	0.129	0.201	4.13-Kalk-0.5Bar	25
426.2	0.037	0.190	4.10-Aach2-0.5Bar	25	348.5	0.119	0.201	4.13-Kalk-0.5Bar	25
540.0	0.000	0.190	4.10-Aach2-0.5Bar	25	401.0	0.034	0.201	4.13-Kalk-0.5Bar	25
600.0	0.000	0.190	4.10-Aach2-0.5Bar	25	500.0	0.026	0.201	4.13-Kalk-0.5Bar	25
					600.9	0.023	0.201	4.13-Kalk-0.5Bar	25
0.0	1.000	0.190	4.10-Esch2-0.5Bar	25	0.0	1.000	0.190	4.13-Qua-0.5Bar	25
17.8	0.833	0.190	4.10-Esch2-0.5Bar	25	12.1	0.765	0.190	4.13-Qua-0.5Bar	25
37.4	0.582	0.190	4.10-Esch2-0.5Bar	25	32.6	0.659	0.190	4.13-Qua-0.5Bar	25
59.4	0.344	0.190	4.10-Esch2-0.5Bar	25	52.0	0.481	0.190	4.13-Qua-0.5Bar	25
78.8	0.219	0.190	4.10-Esch2-0.5Bar	25	87.0	0.350	0.190	4.13-Qua-0.5Bar	25
126.8	0.122	0.190	4.10-Esch2-0.5Bar	25	124.6	0.205	0.190	4.13-Qua-0.5Bar	25
183.5	0.108	0.190	4.10-Esch2-0.5Bar	25	150.2	0.186	0.190	4.13-Qua-0.5Bar	25
269.0	0.054	0.190	4.10-Esch2-0.5Bar	25	213.2	0.130	0.190	4.13-Qua-0.5Bar	25
368.9	0.026	0.190	4.10-Esch2-0.5Bar	25	263.5	0.117	0.190	4.13-Qua-0.5Bar	25
675.0	0.008	0.190	4.10-Esch2-0.5Bar	25	350.1	0.040	0.190	4.13-Qua-0.5Bar	25
					600.0	0.022	0.190	4.13-Qua-0.5Bar	25
0.0	1.000	0.200	4.11-Aach1-0.5Bar	25	0.0	1.000	0.190	4.13-Bas-0.5Bar	25
9.2	0.885	0.200	4.11-Aach1-0.5Bar	25	35.0	0.600	0.190	4.13-Bas-0.5Bar	25
19.4	0.814	0.200	4.11-Aach1-0.5Bar	25	57.1	0.322	0.190	4.13-Bas-0.5Bar	25
28.3	0.703	0.200	4.11-Aach1-0.5Bar	25	110.2	0.223	0.190	4.13-Bas-0.5Bar	25
40.0	0.639	0.200	4.11-Aach1-0.5Bar	25	139.5	0.098	0.190	4.13-Bas-0.5Bar	25
55.1	0.517	0.200	4.11-Aach1-0.5Bar	25	182.4	0.077	0.190	4.13-Bas-0.5Bar	25
81.7	0.453	0.200	4.11-Aach1-0.5Bar	25	259.9	0.020	0.190	4.13-Bas-0.5Bar	25
107.4	0.319	0.200	4.11-Aach1-0.5Bar	25	400.4	0.007	0.190	4.13-Bas-0.5Bar	25
131.8	0.217	0.200	4.11-Aach1-0.5Bar	25	600.0	0.006	0.190	4.13-Bas-0.5Bar	25
175.4	0.123	0.200	4.11-Aach1-0.5Bar	25					
234.4	0.096	0.200	4.11-Aach1-0.5Bar	25					

340.7	0.054	0.200	4.11-Aach1-0.5Bar	25						
390.3	0.035	0.200	4.11-Aach1-0.5Bar	25	0.0	1.000	0.201	4.14-Qua-0.5Bar	25	
504.5	0.032	0.200	4.11-Aach1-0.5Bar	25	10.9	0.873	0.201	4.14-Qua-0.5Bar	25	
600.0	0.032	0.200	4.11-Aach1-0.5Bar	25	21.4	0.814	0.201	4.14-Qua-0.5Bar	25	
					40.3	0.663	0.201	4.14-Qua-0.5Bar	25	
0.0	1.000	0.200	4.11-Aach2-0.5Bar	25	72.2	0.496	0.201	4.14-Qua-0.5Bar	25	
9.1	0.888	0.200	4.11-Aach2-0.5Bar	25	138.4	0.118	0.201	4.14-Qua-0.5Bar	25	
28.9	0.703	0.200	4.11-Aach2-0.5Bar	25	200.2	0.090	0.201	4.14-Qua-0.5Bar	25	
35.4	0.647	0.200	4.11-Aach2-0.5Bar	25	349.5	0.042	0.201	4.14-Qua-0.5Bar	25	
59.6	0.503	0.200	4.11-Aach2-0.5Bar	25	516.8	0.039	0.201	4.14-Qua-0.5Bar	25	
88.7	0.321	0.200	4.11-Aach2-0.5Bar	25	600.0	0.039	0.201	4.14-Qua-0.5Bar	25	
101.5	0.259	0.200	4.11-Aach2-0.5Bar	25						
132.9	0.180	0.200	4.11-Aach2-0.5Bar	25	0.0	1.000	0.190	4.14-Kalk-0.5Bar	25	
179.7	0.112	0.200	4.11-Aach2-0.5Bar	25	38.6	0.489	0.190	4.14-Kalk-0.5Bar	25	
234.4	0.079	0.200	4.11-Aach2-0.5Bar	25	58.3	0.396	0.190	4.14-Kalk-0.5Bar	25	
301.3	0.046	0.200	4.11-Aach2-0.5Bar	25	105.8	0.364	0.190	4.14-Kalk-0.5Bar	25	
390.5	0.031	0.200	4.11-Aach2-0.5Bar	25	121.0	0.294	0.190	4.14-Kalk-0.5Bar	25	
505.0	0.033	0.200	4.11-Aach2-0.5Bar	25	197.9	0.234	0.190	4.14-Kalk-0.5Bar	25	
600.0	0.033	0.200	4.11-Aach2-0.5Bar	25	259.9	0.095	0.190	4.14-Kalk-0.5Bar	25	
					400.3	0.085	0.190	4.14-Kalk-0.5Bar	25	
0.0	1.000	0.201	4.11-Esch1-0.5Bar	25	550.9	0.082	0.190	4.14-Kalk-0.5Bar	25	
9.6	0.854	0.201	4.11-Esch1-0.5Bar	25	600.0	0.082	0.190	4.14-Kalk-0.5Bar	25	
20.2	0.717	0.201	4.11-Esch1-0.5Bar	25						
32.8	0.655	0.201	4.11-Esch1-0.5Bar	25	0.0	1.000	0.201	4.18-AVG1Bar	50	
39.0	0.533	0.201	4.11-Esch1-0.5Bar	25	20.1	0.928	0.201	4.18-AVG1Bar	50	
47.6	0.443	0.201	4.11-Esch1-0.5Bar	25	39.3	0.790	0.201	4.18-AVG1Bar	50	
63.0	0.344	0.201	4.11-Esch1-0.5Bar	25	79.3	0.647	0.201	4.18-AVG1Bar	50	
89.5	0.234	0.201	4.11-Esch1-0.5Bar	25	138.6	0.401	0.201	4.18-AVG1Bar	50	
117.4	0.178	0.201	4.11-Esch1-0.5Bar	25	240.8	0.258	0.201	4.18-AVG1Bar	50	
152.9	0.143	0.201	4.11-Esch1-0.5Bar	25	300.1	0.200	0.201	4.18-AVG1Bar	50	
187.5	0.109	0.201	4.11-Esch1-0.5Bar	25	402.0	0.178	0.201	4.18-AVG1Bar	50	
246.8	0.083	0.201	4.11-Esch1-0.5Bar	25	450.7	0.155	0.201	4.18-AVG1Bar	50	
304.0	0.070	0.201	4.11-Esch1-0.5Bar	25	601.7	0.155	0.201	4.18-AVG1Bar	50	
376.8	0.011	0.201	4.11-Esch1-0.5Bar	25	800.9	0.155	0.201	4.18-AVG1Bar	50	
449.5	0.005	0.201	4.11-Esch1-0.5Bar	25						
510.0	0.005	0.201	4.11-Esch1-0.5Bar	25	0.0	1.000	0.201	4.18-AVG0.5Bar	25	
600.0	0.000	0.201	4.11-Esch1-0.5Bar	25	12.7	0.822	0.201	4.18-AVG0.5Bar	25	
					32.4	0.759	0.201	4.18-AVG0.5Bar	25	
0.0	1.000	0.201	4.11-Esch2-0.5Bar	25	54.6	0.525	0.201	4.18-AVG0.5Bar	25	
25.0	0.719	0.201	4.11-Esch2-0.5Bar	25	87.6	0.476	0.201	4.18-AVG0.5Bar	25	
34.5	0.658	0.201	4.11-Esch2-0.5Bar	25	101.2	0.352	0.201	4.18-AVG0.5Bar	25	
50.5	0.486	0.201	4.11-Esch2-0.5Bar	25	121.8	0.263	0.201	4.18-AVG0.5Bar	25	
61.0	0.402	0.201	4.11-Esch2-0.5Bar	25	142.4	0.219	0.201	4.18-AVG0.5Bar	25	
70.0	0.340	0.201	4.11-Esch2-0.5Bar	25	221.3	0.179	0.201	4.18-AVG0.5Bar	25	
91.2	0.267	0.201	4.11-Esch2-0.5Bar	25	302.3	0.158	0.201	4.18-AVG0.5Bar	25	
106.6	0.224	0.201	4.11-Esch2-0.5Bar	25	454.3	0.119	0.201	4.18-AVG0.5Bar	25	
147.0	0.164	0.201	4.11-Esch2-0.5Bar	25	553.5	0.115	0.201	4.18-AVG0.5Bar	25	
179.6	0.131	0.201	4.11-Esch2-0.5Bar	25	753.7	0.110	0.201	4.18-AVG0.5Bar	25	
219.7	0.124	0.201	4.11-Esch2-0.5Bar	25						
258.2	0.117	0.201	4.11-Esch2-0.5Bar	25	0.0	1.000	0.201	4.18-AVG0.25Bar	12.5	
300.0	0.106	0.201	4.11-Esch2-0.5Bar	25	18.5	0.631	0.201	4.18-AVG0.25Bar	12.5	
357.0	0.097	0.201	4.11-Esch2-0.5Bar	25	39.6	0.472	0.201	4.18-AVG0.25Bar	12.5	
427.0	0.028	0.201	4.11-Esch2-0.5Bar	25	90.3	0.206	0.201	4.18-AVG0.25Bar	12.5	
510.0	0.005	0.201	4.11-Esch2-0.5Bar	25	160.3	0.117	0.201	4.18-AVG0.25Bar	12.5	
600.0	0.000	0.201	4.11-Esch2-0.5Bar	25	239.4	0.070	0.201	4.18-AVG0.25Bar	12.5	
					350.5	0.056	0.201	4.18-AVG0.25Bar	12.5	
0.0	1.000	0.190	4.12-HozL-0.5Bar	25	449.8	0.034	0.201	4.18-AVG0.25Bar	12.5	
10.2	0.856	0.190	4.12-HozL-0.5Bar	25	550.5	0.028	0.201	4.18-AVG0.25Bar	12.5	
31.3	0.638	0.190	4.12-HozL-0.5Bar	25	651.8	0.025	0.201	4.18-AVG0.25Bar	12.5	
60.5	0.406	0.190	4.12-HozL-0.5Bar	25	800.0	0.000	0.201	4.18-AVG0.25Bar	12.5	
88.5	0.235	0.190	4.12-HozL-0.5Bar	25						
143.8	0.190	0.190	4.12-HozL-0.5Bar	25						
219.9	0.129	0.190	4.12-HozL-0.5Bar	25						
304.8	0.122	0.190	4.12-HozL-0.5Bar	25						
351.4	0.100	0.190	4.12-HozL-0.5Bar	25						
376.9	0.067	0.190	4.12-HozL-0.5Bar	25						

401.0	0.001	0.190	4.12-HozL-0.5Bar	25
510.2	0.000	0.190	4.12-HozL-0.5Bar	25
600.0	0.000	0.190	4.12-HozL-0.5Bar	25

G. Appendix G

G.1 Sample of reservoir analyses outputs

A small sample of the summarized output of the reservoir analyses is shown below, for the sake of brevity. The full output can be requested from the author, if desired (Andrew.way@live.co.za / Acway@sun.ac.za). Note that only analyses for w_t where $A_s < 8042 \text{ mm}^2/\text{m}$ are shown. The mean leakage over allowable leakage, probability of failure and achieved reliability index are shown for each leakage regime starting with C_{0d7d} on the left and progressing to C_{14d21d} on the right. The reservoirs parameters are denoted as follows:

- D, h, t Reservoir diameter, height and wall thickness. (m)
- $f_{ctm}, f_{ct,low}$ Mean concrete tensile strength, lower concrete tensile strength. (MPa)
- ENw_t Target crack width as prescribed by EN 1992-3. (mm)
- h^*/t Hydraulic ratio of the height of water pressure head above a crack, over the concrete wall thickness.
- θ_{HR}, w_t, A_s Hydraulic ratio factor, target crack width, area of reinforcing. ($n/a, mm, mm^2/m$)
- $T_{r,low}, T_r, T_{max}$ Lower concrete tensile resistance force, mean concrete tensile resistance force, maximum applied tension force. (kN)
- $\mu_{L_p/L_{al}}, p_f, \beta$ Mean leakage over allowable leakage, probability of failure, reliability index.

		C_{0d7d}			C_{3d8d}			C_{7d214d}			C_{14d21d}					
Reservoir 0.0																
D/h/t	40/7/0.25		$f_{ctm}/ENw_t/(h^*/t)$ 3.02/0.13/18						$f_{ct,low}/\theta_{HR}$			2.57/0.93				
w_t	A_s	$T_{r,low}$	T_r	T_{max}	$\mu_{L_p/L_{al}}$	p_f	β	$\mu_{L_p/L_{al}}$	p_f	β	$\mu_{L_p/L_{al}}$	p_f	β	$\mu_{L_p/L_{al}}$	p_f	β
0.2	2915	731.9	861	840	3.64	1	-inf	1.3	0.744	-0.66	0.83	0.234	0.73	0.4	0.036	1.8
0.19	3017	734.4	864	840	2.88	1	-inf	1	0.408	0.23	0.63	0.098	1.29	0.3	0.015	2.17
0.18	3130	737.8	868	840	2.28	0.998	-2.88	0.78	0.174	0.94	0.48	0.046	1.68	0.23	0.009	2.37
0.17	3777	758.2	892	840	1.04	0.47	0.08	0.33	0.008	2.41	0.18	0.007	2.46	0.08	0.002	2.88
0.16	3939	763.3	898	840	0.78	0.162	0.99	0.24	0.002	2.88	0.13	0.002	2.88	0.06	0.002	2.88
0.15	4122	768.4	904	840	0.56	0.032	1.85	0.16	0	inf	0.08	0	inf	0.04	0	inf
0.14	4330	775.2	912	840	0.4	0.002	2.88	0.11	0	inf	0.05	0	inf	0.02	0	inf
0.13	4569	782.9	921	840	0.29	0	inf	0.08	0	inf	0.03	0	inf	0.02	0	inf
0.12	4847	791.4	931	840	0.19	0	inf	0.05	0	inf	0.02	0	inf	0.01	0	inf
0.11	5175	801.6	943	840	0.13	0	inf	0.03	0	inf	0.01	0	inf	0.01	0	inf
0.1	5570	813.4	957	840	0.09	0	inf	0.02	0	inf	0.01	0	inf	0	0	inf
0.09	7271	866.2	1019	840	0.02	0	inf	0.01	0	inf	0	0	inf	0	0	inf
0.08	8034	889.1	1046	840	0.01	0	inf	0	0	inf	0	0	inf	0	0	inf
Reservoir 1.0																
D/h/t	40/8.5/0.3		$f_{ctm}/ENw_t/(h^*/t)$ 2.91/0.13/18.7						$f_{ct,low}/\theta_{HR}$			2.47/0.95				

w_t	A_s	$T_{r,low}$	T_r	T_{max}	$\mu_{L_p/L_{al}}$	p_f	β	$\mu_{L_p/L_{al}}$	p_f	β	$\mu_{L_p/L_{al}}$	p_f	β	$\mu_{L_p/L_{al}}$	p_f	β
0.2	4096	888.2	1045	1083	5.96	1	-inf	2.13	0.999	-3.09	1.36	0.727	-0.6	0.65	0.101	1.28
0.19	4240	893.4	1051	1083	4.57	1	-inf	1.57	0.94	-1.55	0.96	0.335	0.43	0.45	0.034	1.83
0.18	4397	898.4	1057	1083	3.6	1	-inf	1.21	0.693	-0.5	0.72	0.13	1.13	0.34	0.016	2.14
0.17	4572	905.2	1065	1083	2.77	1	-inf	0.91	0.306	0.51	0.52	0.039	1.76	0.24	0.013	2.23
0.16	4767	912	1073	1083	2.04	1	-inf	0.64	0.068	1.49	0.35	0.014	2.2	0.16	0.003	2.75
0.15	4987	919.7	1082	1083	1.55	0.953	-1.67	0.47	0.017	2.12	0.25	0.008	2.41	0.11	0.002	2.88
0.14	5237	928.2	1092	1083	1.13	0.598	-0.25	0.33	0.004	2.65	0.17	0.004	2.65	0.08	0.002	2.88
0.13	5523	938.4	1104	1083	0.78	0.132	1.12	0.22	0.001	3.09	0.1	0.001	3.09	0.05	0	inf
0.12	7015	992	1167	1083	0.26	0	inf	0.07	0	inf	0.03	0	inf	0.01	0	inf
0.11	7492	1009	1187	1083	0.16	0	inf	0.04	0	inf	0.02	0	inf	0.01	0	inf

Reservoir 2.0

D/h/t	32/8/0.25			$f_{ctm}/ENw_t/(h^*/t)$			2.37/0.12/21.7			$f_{ct,low}/\theta_{HR}$			2.01/1.1			
w_t	A_s	$T_{r,low}$	T_r	T_{max}	$\mu_{L_p/L_{al}}$	p_f	β	$\mu_{L_p/L_{al}}$	p_f	β	$\mu_{L_p/L_{al}}$	p_f	β	$\mu_{L_p/L_{al}}$	p_f	β
0.2	3000	576.3	678	872	32.84	1	-inf	12.53	1	-inf	8.6	1	-inf	4.1	1	-inf
0.19	3105	578.8	681	872	26.33	1	-inf	9.75	1	-inf	6.47	1	-inf	3.1	1	-inf
0.18	3739	594.1	699	872	14.28	1	-inf	5	1	-inf	3.11	0.999	-3.09	1.48	0.729	-0.61
0.17	3889	597.6	703	872	11.34	1	-inf	3.84	1	-inf	2.29	0.979	-2.03	1.07	0.425	0.19
0.16	4056	601.8	708	872	8.56	1	-inf	2.79	1	-inf	1.58	0.817	-0.9	0.74	0.172	0.95
0.15	4244	606	713	872	6.53	1	-inf	2.05	0.989	-2.29	1.11	0.479	0.05	0.52	0.055	1.6
0.14	4458	611.2	719	872	4.87	1	-inf	1.47	0.849	-1.03	0.75	0.176	0.93	0.34	0.015	2.17
0.13	4704	617.1	726	872	3.5	1	-inf	1.01	0.454	0.12	0.48	0.03	1.88	0.22	0.002	2.88
0.12	4989	623.9	734	872	2.55	1	-inf	0.71	0.102	1.27	0.31	0.005	2.58	0.14	0	inf
0.11	5327	632.4	744	872	1.76	0.999	-3.09	0.47	0.023	2	0.2	0.004	2.65	0.09	0	inf
0.1	6871	669.8	788	872	0.73	0.062	1.54	0.19	0	inf	0.08	0	inf	0.03	0	inf
0.09	7485	684.2	805	872	0.47	0.001	3.09	0.12	0	inf	0.05	0	inf	0.02	0	inf

Reservoir 3.0

D/h/t	38/7/0.25			$f_{ctm}/ENw_t/(h^*/t)$			2.96/0.13/18			$f_{ct,low}/\theta_{HR}$			2.52/0.93			
w_t	A_s	$T_{r,low}$	T_r	T_{max}	$\mu_{L_p/L_{al}}$	p_f	β	$\mu_{L_p/L_{al}}$	p_f	β	$\mu_{L_p/L_{al}}$	p_f	β	$\mu_{L_p/L_{al}}$	p_f	β
0.2	2838	714.8	841	811	3.53	1	-inf	1.26	0.692	-0.5	0.81	0.222	0.77	0.39	0.026	1.94
0.19	2937	717.4	844	811	2.87	1	-inf	1.01	0.413	0.22	0.63	0.12	1.17	0.3	0.02	2.05
0.18	3046	720.8	848	811	2.26	0.997	-2.75	0.77	0.2	0.84	0.48	0.047	1.67	0.23	0.01	2.33
0.17	3673	739.5	870	811	1.02	0.441	0.15	0.32	0.012	2.26	0.17	0.006	2.51	0.08	0.002	2.88
0.16	3831	744.6	876	811	0.78	0.179	0.92	0.24	0.003	2.75	0.13	0.002	2.88	0.06	0.001	3.09
0.15	4009	749.7	882	811	0.57	0.042	1.73	0.17	0.003	2.75	0.09	0.003	2.75	0.04	0	inf
0.14	4212	756.5	890	811	0.41	0.011	2.29	0.12	0	inf	0.05	0	inf	0.02	0	inf
0.13	4445	763.3	898	811	0.29	0.001	3.09	0.08	0	inf	0.03	0	inf	0.02	0	inf
0.12	4716	771.8	908	811	0.19	0	inf	0.05	0	inf	0.02	0	inf	0.01	0	inf
0.11	5036	781.2	919	811	0.14	0	inf	0.04	0	inf	0.02	0	inf	0.01	0	inf
0.1	5421	793	933	811	0.09	0	inf	0.02	0	inf	0.01	0	inf	0	0	inf
0.09	7074	842.4	991	811	0.02	0	inf	0.01	0	inf	0	0	inf	0	0	inf
0.08	7819	865.3	1018	811	0.01	0	inf	0	0	inf	0	0	inf	0	0	inf

Reservoir 4.0

D/h/t	34/7.5/0.25			$f_{ctm}/ENw_t/(h^*/t)$			3.06/0.13/19.8			$f_{ct,low}/\theta_{HR}$			2.6/0.99			
w_t	A_s	$T_{r,low}$	T_r	T_{max}	$\mu_{L_p/L_{al}}$	p_f	β	$\mu_{L_p/L_{al}}$	p_f	β	$\mu_{L_p/L_{al}}$	p_f	β	$\mu_{L_p/L_{al}}$	p_f	β
0.2	2889	740.4	871	830	3.72	1	-inf	1.34	0.717	-0.57	0.86	0.253	0.67	0.41	0.043	1.72
0.19	2990	743.8	875	830	2.93	1	-inf	1.03	0.433	0.17	0.66	0.119	1.18	0.32	0.026	1.94
0.18	3101	747.2	879	830	2.32	0.994	-2.51	0.79	0.215	0.79	0.46	0.055	1.6	0.22	0.007	2.46
0.17	3741	766.7	902	830	1	0.411	0.22	0.31	0.01	2.33	0.17	0.005	2.58	0.08	0.001	3.09
0.16	3902	771.8	908	830	0.77	0.19	0.88	0.23	0.002	2.88	0.12	0.002	2.88	0.05	0	inf
0.15	4083	777.8	915	830	0.59	0.065	1.51	0.18	0.001	3.09	0.09	0.001	3.09	0.04	0	inf
0.14	4290	784.6	923	830	0.4	0.018	2.1	0.11	0.001	3.09	0.05	0.001	3.09	0.02	0	inf
0.13	4526	791.4	931	830	0.28	0.003	2.75	0.08	0	inf	0.03	0	inf	0.01	0	inf
0.12	4802	799.8	941	830	0.19	0	inf	0.05	0	inf	0.02	0	inf	0.01	0	inf
0.11	5128	810.1	953	830	0.13	0	inf	0.03	0	inf	0.01	0	inf	0.01	0	inf
0.1	5518	822.8	968	830	0.09	0	inf	0.02	0	inf	0.01	0	inf	0	0	inf
0.09	7204	875.5	1030	830	0.02	0	inf	0	0	inf	0	0	inf	0	0	inf
0.08	7960	898.4	1057	830	0.01	0	inf	0	0	inf	0	0	inf	0	0	inf

Reservoir 5.0

D/h/t	30/9/0.3			$f_{ctm}/ENw_t/(h^*/t)$			2.71/0.12/20.9			$f_{ct,low}/\theta_{HR}$			2.3/1.05			
w_t	A_s	$T_{r,low}$	T_r	T_{max}	$\mu_{L_p/L_{al}}$	p_f	β	$\mu_{L_p/L_{al}}$	p_f	β	$\mu_{L_p/L_{al}}$	p_f	β	$\mu_{L_p/L_{al}}$	p_f	β
0.2	3699	813.4	957	943	7.49	1	-inf	2.73	1	-inf	1.77	0.831	-0.96	0.84	0.25	0.67

0.19	3829	817.7	962	943	5.81	1	-inf	2.05	0.975	-1.96	1.27	0.588	-0.22	0.6	0.095	1.31	
0.18	3972	822.8	968	943	4.6	1	-inf	1.58	0.845	-1.02	0.96	0.336	0.42	0.45	0.05	1.64	
0.17	4130	827.9	974	943	3.44	1	-inf	1.15	0.546	-0.12	0.68	0.138	1.09	0.32	0.024	1.98	
0.16	4307	833.9	981	943	2.57	1	-inf	0.82	0.238	0.71	0.45	0.044	1.71	0.21	0.006	2.51	
0.15	4507	840.6	989	943	1.87	0.975	-1.96	0.57	0.064	1.52	0.29	0.006	2.51	0.13	0.005	2.58	
0.14	4733	848.3	998	943	1.39	0.792	-0.81	0.42	0.02	2.05	0.21	0.007	2.46	0.1	0.001	3.09	
0.13	4993	856.8	1008	943	0.94	0.337	0.42	0.27	0.001	3.09	0.12	0.001	3.09	0.06	0.001	3.09	
0.12	5295	867	1020	943	0.65	0.065	1.51	0.18	0.001	3.09	0.08	0.001	3.09	0.04	0	inf	
0.11	5652	878.9	1034	943	0.44	0.011	2.29	0.12	0	inf	0.05	0	inf	0.02	0	inf	
0.1	7295	933.3	1098	943	0.13	0	inf	0.04	0	inf	0.01	0	inf	0.01	0	inf	
0.09	7942	954.6	1123	943	0.08	0	inf	0.02	0	inf	0.01	0	inf	0	0	inf	
Reservoir 6.0																	
D/h/t	32/9/0.3				$f_{ctm}/ENw_t/(h^*/t)$					2.08/0.12/20.9			$f_{ct,low}/\theta_{HR}$			1.77/1.05	
w_t	A_s	$T_{r,low}$	T_r	T_{max}	$\mu_{L_p/L_{al}}$	p_f	β	$\mu_{L_p/L_{al}}$	p_f	β	$\mu_{L_p/L_{al}}$	p_f	β	$\mu_{L_p/L_{al}}$	p_f	β	
0.2	3842	628.2	739	992	33.27	1	-inf	12.79	1	-inf	9.13	1	-inf	4.45	1	-inf	
0.19	3976	631.6	743	992	27.61	1	-inf	10.39	1	-inf	7.24	1	-inf	3.52	1	-inf	
0.18	4124	635.8	748	992	21.87	1	-inf	7.93	1	-inf	5.16	1	-inf	2.47	0.992	-2.41	
0.17	4289	639.2	752	992	17.3	1	-inf	6.09	1	-inf	3.87	1	-inf	1.84	0.902	-1.29	
0.16	4472	644.3	758	992	13.19	1	-inf	4.44	1	-inf	2.63	0.998	-2.88	1.24	0.578	-0.2	
0.15	4679	649.4	764	992	9.93	1	-inf	3.23	1	-inf	1.81	0.946	-1.61	0.84	0.231	0.74	
0.14	4913	655.3	771	992	7.4	1	-inf	2.31	0.999	-3.09	1.23	0.626	-0.32	0.57	0.06	1.55	
0.13	5183	662.2	779	992	5.34	1	-inf	1.59	0.934	-1.51	0.79	0.191	0.87	0.36	0.016	2.14	
0.12	5496	670.6	789	992	3.85	1	-inf	1.12	0.566	-0.17	0.53	0.05	1.64	0.24	0.007	2.46	
0.11	7029	709.8	835	992	1.58	0.992	-2.41	0.43	0.01	2.33	0.18	0.004	2.65	0.08	0	inf	
0.1	7572	723.4	851	992	1.1	0.617	-0.3	0.29	0.001	3.09	0.12	0.002	2.88	0.05	0	inf	
Reservoir 7.0																	
D/h/t	32/7.5/0.25				$f_{ctm}/ENw_t/(h^*/t)$					1.72/0.13/19.8			$f_{ct,low}/\theta_{HR}$			1.46/0.99	
w_t	A_s	$T_{r,low}$	T_r	T_{max}	$\mu_{L_p/L_{al}}$	p_f	β	$\mu_{L_p/L_{al}}$	p_f	β	$\mu_{L_p/L_{al}}$	p_f	β	$\mu_{L_p/L_{al}}$	p_f	β	
0.2	2792	414.8	488	794	68.6	1	-inf	28.43	1	-inf	22.05	1	-inf	10.83	1	-inf	
0.19	2889	416.5	490	794	55.02	1	-inf	21.96	1	-inf	16.27	1	-inf	7.96	1	-inf	
0.18	2997	418.2	492	794	45.92	1	-inf	17.93	1	-inf	12.75	1	-inf	6.18	1	-inf	
0.17	3116	419.9	494	794	35.7	1	-inf	13.49	1	-inf	9.16	1	-inf	4.39	1	-inf	
0.16	3767	431.8	508	794	19.74	1	-inf	7.02	1	-inf	4.43	1	-inf	2.1	0.968	-1.85	
0.15	3942	434.4	511	794	14.83	1	-inf	5.04	1	-inf	2.97	1	-inf	1.4	0.729	-0.61	
0.14	4142	437.8	515	794	11.16	1	-inf	3.66	1	-inf	2.13	0.969	-1.87	1	0.334	0.43	
0.13	4371	442	520	794	8.18	1	-inf	2.58	0.999	-3.09	1.39	0.707	-0.54	0.65	0.113	1.21	
0.12	4638	447.1	526	794	5.72	1	-inf	1.71	0.956	-1.71	0.87	0.25	0.67	0.41	0.026	1.94	
0.11	4953	452.2	532	794	4.03	1	-inf	1.15	0.614	-0.29	0.54	0.045	1.7	0.24	0.006	2.51	
0.1	5332	459	540	794	2.71	1	-inf	0.74	0.124	1.16	0.32	0.006	2.51	0.14	0	inf	
0.09	6956	487.9	574	794	1.19	0.834	-0.97	0.32	0.003	2.75	0.13	0.001	3.09	0.06	0	inf	
0.08	7691	500.6	589	794	0.76	0.044	1.71	0.2	0.001	3.09	0.08	0	inf	0.03	0	inf	
Reservoir 8.0																	
D/h/t	38/9/0.3				$f_{ctm}/ENw_t/(h^*/t)$					3.07/0.13/19.8			$f_{ct,low}/\theta_{HR}$			2.61/0.99	
w_t	A_s	$T_{r,low}$	T_r	T_{max}	$\mu_{L_p/L_{al}}$	p_f	β	$\mu_{L_p/L_{al}}$	p_f	β	$\mu_{L_p/L_{al}}$	p_f	β	$\mu_{L_p/L_{al}}$	p_f	β	
0.2	4231	941.8	1108	1133	5.61	1	-inf	1.97	0.993	-2.46	1.24	0.579	-0.2	0.59	0.081	1.4	
0.19	4379	947.8	1115	1133	4.41	1	-inf	1.51	0.895	-1.25	0.9	0.283	0.57	0.42	0.03	1.88	
0.18	4542	953.7	1122	1133	3.43	1	-inf	1.14	0.603	-0.26	0.67	0.118	1.19	0.31	0.011	2.29	
0.17	4722	960.5	1130	1133	2.57	1	-inf	0.83	0.207	0.82	0.46	0.03	1.88	0.22	0.005	2.58	
0.16	4924	968.1	1139	1133	1.93	0.996	-2.65	0.6	0.046	1.68	0.31	0.009	2.37	0.15	0.003	2.75	
0.15	5151	976.6	1149	1133	1.41	0.899	-1.28	0.42	0.008	2.41	0.21	0.001	3.09	0.1	0.001	3.09	
0.14	5408	986	1160	1133	1.02	0.45	0.13	0.3	0.004	2.65	0.14	0.001	3.09	0.06	0	inf	
0.13	5704	997	1173	1133	0.71	0.087	1.36	0.2	0	inf	0.09	0	inf	0.04	0	inf	
0.12	7245	1054.8	1241	1133	0.23	0	inf	0.06	0	inf	0.02	0	inf	0.01	0	inf	
0.11	7735	1073.6	1263	1133	0.15	0	inf	0.04	0	inf	0.02	0	inf	0.01	0	inf	
Reservoir 9.0																	
D/h/t	30/9/0.3				$f_{ctm}/ENw_t/(h^*/t)$					2.74/0.12/20.9			$f_{ct,low}/\theta_{HR}$			2.33/1.05	
w_t	A_s	$T_{r,low}$	T_r	T_{max}	$\mu_{L_p/L_{al}}$	p_f	β	$\mu_{L_p/L_{al}}$	p_f	β	$\mu_{L_p/L_{al}}$	p_f	β	$\mu_{L_p/L_{al}}$	p_f	β	
0.2	3699	822.8	968	943	6.8	1	-inf	2.47	0.995	-2.58	1.6	0.758	-0.7	0.76	0.186	0.89	
0.19	3829	827	973	943	5.26	1	-inf	1.86	0.928	-1.46	1.18	0.474	0.07	0.56	0.084	1.38	
0.18	3972	832.2	979	943	4.14	1	-inf	1.42	0.763	-0.72	0.86	0.254	0.66	0.41	0.048	1.66	
0.17	4130	837.2	985	943	3.12	1	-inf	1.04	0.449	0.13	0.61	0.092	1.33	0.29	0.013	2.23	
0.16	4307	843.2	992	943	2.37	0.996	-2.65	0.76	0.199	0.85	0.43	0.044	1.71	0.2	0.009	2.37	

0.15	4507	850	1000	943	1.69	0.927	-1.45	0.52	0.044	1.71	0.27	0.01	2.33	0.12	0.002	2.88
0.14	4733	857.6	1009	943	1.22	0.627	-0.32	0.36	0.016	2.14	0.18	0.003	2.75	0.08	0.001	3.09
0.13	4993	866.2	1019	943	0.85	0.236	0.72	0.24	0.003	2.75	0.11	0.002	2.88	0.05	0	inf
0.12	5295	876.4	1031	943	0.6	0.053	1.62	0.17	0.001	3.09	0.07	0.001	3.09	0.03	0	inf
0.11	5652	888.2	1045	943	0.39	0.012	2.26	0.11	0	inf	0.05	0	inf	0.02	0	inf
0.1	7295	943.5	1110	943	0.11	0	inf	0.03	0	inf	0.01	0	inf	0.01	0	inf
0.09	7942	964.8	1135	943	0.06	0	inf	0.02	0	inf	0.01	0	inf	0	0	inf

Reservoir 10.0

D/h/t	40/7.5/0.25			$f_{ctm}/ENw_t/(h^*/t)$ 2.74/0.13/19.3					$f_{ct,low}/\theta_{HR}$ 2.33/0.97							
w_t	A_s	$T_{r,low}$	T_r	T_{max}	$\mu_{L_p/L_{al}}$	p_f	β	$\mu_{L_p/L_{al}}$	p_f	β	$\mu_{L_p/L_{al}}$	p_f	β	$\mu_{L_p/L_{al}}$	p_f	β
0.2	3674	685.1	806	935	9.03	1	-inf	3.21	1	-inf	2.03	0.975	-1.96	0.96	0.34	0.41
0.19	3803	688.5	810	935	7.19	1	-inf	2.48	1	-inf	1.51	0.823	-0.93	0.71	0.144	1.06
0.18	3945	692.8	815	935	5.64	1	-inf	1.88	0.989	-2.29	1.1	0.492	0.02	0.52	0.049	1.65
0.17	4103	697	820	935	4.41	1	-inf	1.43	0.876	-1.16	0.81	0.191	0.87	0.38	0.017	2.12
0.16	4279	702.1	826	935	3.36	1	-inf	1.05	0.526	-0.07	0.57	0.058	1.57	0.26	0.006	2.51
0.15	4477	707.2	832	935	2.51	1	-inf	0.76	0.132	1.12	0.38	0.014	2.2	0.17	0.001	3.09
0.14	4701	714	840	935	1.86	1	-inf	0.54	0.021	2.03	0.26	0.003	2.75	0.12	0.001	3.09
0.13	4960	720.8	848	935	1.38	0.939	-1.55	0.39	0.006	2.51	0.18	0.004	2.65	0.08	0	inf
0.12	5260	729.3	858	935	0.98	0.393	0.27	0.27	0	inf	0.11	0	inf	0.05	0	inf
0.11	5614	739.5	870	935	0.69	0.038	1.77	0.19	0	inf	0.08	0	inf	0.03	0	inf
0.1	7246	784.6	923	935	0.26	0	inf	0.07	0	inf	0.03	0	inf	0.01	0	inf
0.09	7890	802.4	944	935	0.16	0	inf	0.04	0	inf	0.02	0	inf	0.01	0	inf

.....

Reservoir 230.0

D/h/t	38/8/0.275			$f_{ctm}/ENw_t/(h^*/t)$ 2.54/0.13/19.2					$f_{ct,low}/\theta_{HR}$ 2.16/0.97							
w_t	A_s	$T_{r,low}$	T_r	T_{max}	$\mu_{L_p/L_{al}}$	p_f	β	$\mu_{L_p/L_{al}}$	p_f	β	$\mu_{L_p/L_{al}}$	p_f	β	$\mu_{L_p/L_{al}}$	p_f	β
0.2	3781	701.2	825	971	12.32	1	-inf	4.48	1	-inf	2.92	1	-inf	1.4	0.743	-0.65
0.19	3914	705.5	830	971	9.86	1	-inf	3.49	1	-inf	2.19	0.994	-2.51	1.04	0.39	0.28
0.18	4060	709.7	835	971	7.83	1	-inf	2.69	1	-inf	1.65	0.882	-1.19	0.79	0.174	0.94
0.17	4222	714	840	971	6.15	1	-inf	2.05	0.998	-2.88	1.21	0.568	-0.17	0.57	0.066	1.51
0.16	4402	719.1	846	971	4.69	1	-inf	1.5	0.915	-1.37	0.85	0.227	0.75	0.4	0.022	2.01
0.15	4606	725	853	971	3.49	1	-inf	1.08	0.545	-0.11	0.57	0.044	1.71	0.26	0.01	2.33
0.14	4837	731.8	861	971	2.61	1	-inf	0.77	0.148	1.05	0.38	0.014	2.2	0.18	0.001	3.09
0.13	5102	739.5	870	971	1.88	1	-inf	0.53	0.017	2.12	0.24	0.004	2.65	0.11	0	inf
0.12	5411	748	880	971	1.35	0.93	-1.48	0.37	0.005	2.58	0.16	0.002	2.88	0.08	0	inf
0.11	6920	791.3	931	971	0.53	0.009	2.37	0.14	0	inf	0.05	0	inf	0.02	0	inf
0.1	7455	805.8	948	971	0.35	0	inf	0.09	0	inf	0.03	0	inf	0.02	0	inf

Reservoir 231.0

D/h/t	40/8.5/0.3			$f_{ctm}/ENw_t/(h^*/t)$ 2.33/0.13/18.7					$f_{ct,low}/\theta_{HR}$ 1.98/0.95							
w_t	A_s	$T_{r,low}$	T_r	T_{max}	$\mu_{L_p/L_{al}}$	p_f	β	$\mu_{L_p/L_{al}}$	p_f	β	$\mu_{L_p/L_{al}}$	p_f	β	$\mu_{L_p/L_{al}}$	p_f	β
0.2	4096	710.6	836	1083	18.54	1	-inf	6.91	1	-inf	4.67	1	-inf	2.25	0.989	-2.29
0.19	4240	714.9	841	1083	15	1	-inf	5.42	1	-inf	3.52	1	-inf	1.68	0.91	-1.34
0.18	4397	720	847	1083	12.02	1	-inf	4.24	1	-inf	2.67	1	-inf	1.28	0.651	-0.39
0.17	4572	724.2	852	1083	9.42	1	-inf	3.2	1	-inf	1.95	0.976	-1.98	0.92	0.282	0.58
0.16	4767	730.2	859	1083	7.21	1	-inf	2.37	1	-inf	1.37	0.765	-0.72	0.64	0.08	1.41
0.15	4987	736.1	866	1083	5.4	1	-inf	1.7	0.984	-2.14	0.93	0.312	0.49	0.43	0.022	2.01
0.14	5237	743.8	875	1083	4.06	1	-inf	1.23	0.76	-0.71	0.63	0.067	1.5	0.29	0.007	2.46
0.13	5523	751.4	884	1083	2.94	1	-inf	0.86	0.228	0.75	0.42	0.013	2.23	0.19	0.003	2.75
0.12	7015	793.9	934	1083	1.2	0.817	-0.9	0.32	0.001	3.09	0.13	0	inf	0.06	0	inf
0.11	7492	807.5	950	1083	0.84	0.121	1.17	0.22	0	inf	0.09	0	inf	0.04	0	inf

Reservoir 232.0

D/h/t	34/8/0.275			$f_{ctm}/ENw_t/(h^*/t)$ 2.54/0.13/19.2					$f_{ct,low}/\theta_{HR}$ 2.16/0.97							
w_t	A_s	$T_{r,low}$	T_r	T_{max}	$\mu_{L_p/L_{al}}$	p_f	β	$\mu_{L_p/L_{al}}$	p_f	β	$\mu_{L_p/L_{al}}$	p_f	β	$\mu_{L_p/L_{al}}$	p_f	β
0.2	3054	680.8	801	893	15.78	1	-inf	5.98	1	-inf	4.08	1	-inf	1.96	0.932	-1.49
0.19	3672	698.7	822	893	8.1	1	-inf	2.88	1	-inf	1.83	0.898	-1.27	0.87	0.26	0.64
0.18	3809	702.1	826	893	6.35	1	-inf	2.18	0.991	-2.37	1.3	0.662	-0.42	0.61	0.094	1.32
0.17	3961	706.3	831	893	4.97	1	-inf	1.66	0.925	-1.44	0.99	0.34	0.41	0.47	0.044	1.71

0.16	4132	711.4	837	893	3.72	1	-inf	1.19	0.63	-0.33	0.66	0.122	1.17	0.31	0.009	2.37
0.15	4323	716.6	843	893	2.77	1	-inf	0.86	0.259	0.65	0.46	0.032	1.85	0.21	0.007	2.46
0.14	4541	723.3	851	893	2.05	0.998	-2.88	0.61	0.06	1.55	0.31	0.013	2.23	0.14	0.003	2.75
0.13	4791	730.2	859	893	1.47	0.914	-1.37	0.42	0.01	2.33	0.2	0.004	2.65	0.09	0	inf
0.12	5081	738.6	869	893	1.05	0.5	0	0.29	0	inf	0.13	0	inf	0.06	0	inf
0.11	5424	748	880	893	0.72	0.067	1.5	0.19	0	inf	0.08	0	inf	0.04	0	inf
0.1	6998	793	933	893	0.26	0	inf	0.07	0	inf	0.03	0	inf	0.01	0	inf
0.09	7623	810.9	954	893	0.16	0	inf	0.04	0	inf	0.01	0	inf	0.01	0	inf

Reservoir 233.0

D/h/t	32/7.5/0.25			$f_{ctm}/ENw_t/(h^*/t)$ 2.75/0.13/19.8					$f_{ct,low}/\theta_{HR}$ 2.34/0.99							
w_t	A_s	$T_{r,low}$	T_r	T_{max}	$\mu_{L_p/L_{al}}$	p_f	β	$\mu_{L_p/L_{al}}$	p_f	β	$\mu_{L_p/L_{al}}$	p_f	β	$\mu_{L_p/L_{al}}$	p_f	β
0.2	2792	663	780	794	7.97	1	-inf	2.93	0.999	-3.09	1.93	0.899	-1.28	0.93	0.288	0.56
0.19	2889	665.6	783	794	6.26	1	-inf	2.22	0.99	-2.33	1.4	0.662	-0.42	0.66	0.117	1.19
0.18	2997	668.1	786	794	5.07	1	-inf	1.76	0.939	-1.55	1.09	0.424	0.19	0.52	0.075	1.44
0.17	3116	671.5	790	794	3.89	1	-inf	1.31	0.716	-0.57	0.79	0.183	0.9	0.38	0.026	1.94
0.16	3767	690.2	812	794	1.84	0.962	-1.77	0.57	0.07	1.48	0.31	0.013	2.23	0.14	0.001	3.09
0.15	3942	695.3	818	794	1.39	0.79	-0.81	0.42	0.025	1.96	0.21	0.002	2.88	0.1	0.001	3.09
0.14	4142	700.4	824	794	1.02	0.42	0.2	0.3	0.007	2.46	0.14	0.001	3.09	0.07	0	inf
0.13	4371	707.2	832	794	0.7	0.102	1.27	0.19	0.002	2.88	0.09	0	inf	0.04	0	inf
0.12	4638	714.8	841	794	0.51	0.024	1.98	0.14	0	inf	0.06	0	inf	0.03	0	inf
0.11	4953	723.3	851	794	0.34	0.002	2.88	0.09	0	inf	0.04	0	inf	0.02	0	inf
0.1	5332	733.6	863	794	0.22	0	inf	0.06	0	inf	0.02	0	inf	0.01	0	inf
0.09	6956	779.4	917	794	0.07	0	inf	0.02	0	inf	0.01	0	inf	0	0	inf
0.08	7691	799.8	941	794	0.04	0	inf	0.01	0	inf	0	0	inf	0	0	inf

Reservoir 234.0

D/h/t	34/7/0.225			$f_{ctm}/ENw_t/(h^*/t)$ 2.44/0.12/20.6					$f_{ct,low}/\theta_{HR}$ 2.07/1.03							
w_t	A_s	$T_{r,low}$	T_r	T_{max}	$\mu_{L_p/L_{al}}$	p_f	β	$\mu_{L_p/L_{al}}$	p_f	β	$\mu_{L_p/L_{al}}$	p_f	β	$\mu_{L_p/L_{al}}$	p_f	β
0.2	2658	532.9	627	769	23.61	1	-inf	8.95	1	-inf	6.15	1	-inf	2.96	1	-inf
0.19	2751	535.5	630	769	19.3	1	-inf	7.14	1	-inf	4.77	1	-inf	2.29	0.986	-2.2
0.18	2853	538	633	769	15.29	1	-inf	5.49	1	-inf	3.54	1	-inf	1.69	0.863	-1.09
0.17	2967	540.6	636	769	12.05	1	-inf	4.17	1	-inf	2.56	0.998	-2.88	1.21	0.555	-0.14
0.16	3094	544	640	769	9.3	1	-inf	3.13	1	-inf	1.85	0.935	-1.51	0.87	0.258	0.65
0.15	3759	560.2	659	769	4.5	1	-inf	1.39	0.835	-0.97	0.74	0.169	0.96	0.35	0.013	2.23
0.14	3948	565.2	665	769	3.4	1	-inf	1.01	0.426	0.19	0.51	0.047	1.67	0.24	0.007	2.46
0.13	4166	570.4	671	769	2.46	1	-inf	0.7	0.11	1.23	0.33	0.009	2.37	0.15	0.001	3.09
0.12	4420	576.3	678	769	1.76	0.997	-2.75	0.48	0.009	2.37	0.21	0.002	2.88	0.1	0.001	3.09
0.11	4718	584	687	769	1.23	0.813	-0.89	0.33	0.001	3.09	0.13	0	inf	0.06	0	inf
0.1	5078	593.3	698	769	0.85	0.169	0.96	0.22	0.002	2.88	0.09	0	inf	0.04	0	inf
0.09	5519	604.3	711	769	0.56	0.002	2.88	0.15	0	inf	0.06	0	inf	0.02	0	inf
0.08	7324	648.6	763	769	0.19	0	inf	0.05	0	inf	0.02	0	inf	0.01	0	inf